UNIVERSITY OF BIRMINGHAM

Microencapsulation of Phase Change Materials (PCMs) for Cryogenic Energy Storage

By

Abdullah Naseer Mustapha

A thesis submitted to
The University of Birmingham
for the degree of
DOCTOR OF PHILOSOPHY

School of Chemical Engineering
College of Engineering and Physical Sciences
University of Birmingham
November 2021

ABSTRACT

Thermal energy storage (TES) technologies have been copiously garnering a proliferation in attention over the past decade and have been employed to increase renewable energy utilisation and to mitigate the climate change crisis. Phase change materials (PCMs) are a class of organic or inorganic compounds, which have the capability to store and release vast amounts of energy due to their latent heat energy storage (LHES) capabilities, and various melting point ranges that are suitable for an array of applications. A challenge with these PCMs, especially organic PCMs, is their toxicity, flammability, and their tendency to leak during the phase change process. Therefore, the PCMs can be amalgamated within an inert shell, in a process known as 'microencapsulation'.

In this study, volatile cryo-PCMs were encapsulated via the one-step in situ polymerization technique, in which the mechanical and barrier properties were characterized to observe their feasibility to be applied in real world applications. It has been observed that with the one-step in situ polymerization method, the choice of emulsifier used is an imperative consideration, and such emulsifiers greatly affect the microencapsulated PCM (MPCM) properties, such as their mechanical strength, morphology, long term core material retention, payload, yield, and encapsulation efficiency. A range of emulsifiers were employed in this process, which were categorised into two main categories: natural and synthetic emulsifiers. A significant finding in this work is that the functional groups of the emulsifiers predominantly affect the reaction rate, and the order of reactivity was seen to be as follows: carboxyl > amino/amide > hydroxyl.

Additionally, the process optimization of the polymerization process was carried out, in which the Taguchi and ANOVA methods were employed. Various parameters such as reaction time, pH, reaction temperature and homogenization speed were studied. The ANOVA analysis conveyed that the parameters that affect the microcapsule formulation in terms of magnitude are as follows: temperature, reaction time, pH, homogenization speed.

PCMs when amalgamated in a shell material exhibited high levels of supercooling due to the limited crystallization process, and various efforts were made to reduce this phenomenon. Such efforts included increasing the MPCM size, employing nucleating agents, and embedding copper nanoparticles on the MPCM shell to increase the thermal conductivity. Furthermore, di(propylene glycol) methyl ether was used as a carrier fluid for the MPCMs to study the viscosity changes with various MPCM compositions.

DEDICATION

This thesis is dedicated to my beloved parents who have given me a great amount of unconditional love and support over the past few years. Thank you for all the sacrifices you have made so me and my brothers can have a better future.

ACKNOWLEDGEMENTS

I would like to express my sincere gratitude to the almighty Allah for his compassion, the most beneficent, the most merciful.

I would also like to thank the Engineering and Physical Science Research Council (EPSRC) for their sponsorship and funding, enabling me to carry out this work. My appreciation goes out to my supervisors, Prof. Yongliang Li, Prof. Zhibing Zhang and Prof. Yulong Ding. Thank you for your excellent guidance and patience during my work. My gratitude is also extended to Dr. Yan Zhang, who taught me many vital skills during my PhD. I would also like to thank Dr. Mark Taylor for all his technical help during my work, he went out of his way on multiple occasions. A special thanks to all my office mates too, making my time at UoB a pleasure.

My sincere appreciation to my friends and loved ones during this time. Hamza Sheikh for being a motivation to me, and a great friend.

Lastly, I would like to express my upmost gratitude to my family for their patience, love, support, understanding and prayers. My father Dr. Ahmed Mustapha, my mother Mrs. Hafsat Mustapha, and my brothers Haleem and Adam Mustapha. I am proud to call you my family, thank you for everything.

TABLE OF CONTENTS

LIST OF FIGURES

LIST OF TABLES

ABBREVIATIONS

AA:	Alginic Acid
AFM:	Atomic Force Microscope
ANOVA:	Analysis of Variance
BSE:	Back Scattered Electrons
CES:	Cryogenic Energy Storage
CHI:	Chitosan
CMC:	Critical Micelle Concentration
DSC:	Differential Scanning Calorimetry
EE:	Encapsulation Efficiency
FM:	Fluorescence Microscope
FTIR:	Fourier transform Infra-Red
GEL:	Gelatin
GG:	Gellan Gum
GHG:	Green House Gas
HLB:	Hydrophilic Lipophilic Balance
HPLC:	High Performance Liquid Chromatography
IT:	Interfacial Tension
LAES:	Latent Air Energy Storage

LCMS:	Liquid Chromatography-Mass Spectroscopy
LFA:	Laser Flash Analysis
LHES:	Latent Heat Energy Storage
LHF:	Latent Heat Fluid
LHS:	Latent Heat Storage
LHTF:	Latent Heat Thermal Fluid
MC:	Methyl Cellulose
MCAP:	Microencapsulation
MF:	Melamine Formaldehyde
MPCM:	Microencapsulated Phase Change Material
MPCS:	Micro Phase Change Material Slurry
O/W:	Oil in Water
OM:	Optical Microscope
PA:	Palmitic Acid
PAM:	Polyacrylamide
PCM:	Phase Change Material
PEG:	Poly(Ethylene Glycol)
PEI:	Poly(ethylenimine)
PEMA:	Poly(Ethylene-alt-Maleic Anhydride)
PL:	Payload
PMVE:	Poly(Methyl Vinyl Ether)
PUF:	Poly Urea Formaldehyde

S/N:	Signal-to-Noise
SDS:	Sodium Dodecyl Sulphate
SEM:	Scanning Electron Microscope
SLS:	Static Light Scattering
SMA:	Styrene Maleic Anhydride
TEOS:	Tetraethyl Orthosilicate
TES:	Thermal energy storage
TGA:	Thermo Gravimetric Analysis
TGA:	Thermo Gravimetric Analysis
UF:	Urea Formaldehyde
XG:	Xanthan Gum
XRD:	X-Ray Diffraction

NOMENCLATURE

A^*	Interfacial area (m^2)
a_m	Fraction of melted material
c_p	Specific heat capacity ($J.kg^{-1}.K^{-1}$)
C_{uf}	Aqueous pre-polymer concentration
G^*	Interfacial dilatational modulus
H_m	Specific enthalpy of melting material ($J.kg^{-1}$)
k_c	Mass transfer coefficient
k_r	Rate constant for UF particle formation
R_{uf}	Overall condensation reaction rate for the formation of UF particles
SS_{EE}	Encapsulation efficiency sum of squares
SS_k	Sum of squares for parameters
SS_P	Payload sum of squares
SS_T	Total sum of squares
SS_Y	Yield sum of squares
T_m	Melted material temperature (°C)
γ^*	Interfacial tension ($mN.m^{-1}$)
A	Area (m^2)
E	Young's Modulus (MPa)
F	Compressive force ($m.s^{-2}$)
G	Trial run data
k	Mass transfer coefficient
m	Storage media mass (kg)
Q	Amount of stored energy (J)
R	Microcapsule radius
T	Temperature (°C)
t	Time (s)
v	Poisson's ratio
y	Yield
δ	Half the sum of axial compression displacement
ρ	Density ($Kg.m^{-3}$)
ω	Angular velocity (s^{-1})

CHAPTER 1: INTRODUCTION

1.1. BACKGROUND AND MOTIVATION

The paradigm shift in the energy storage sector has been auspiciously leaning towards thermal energy storage (TES) technologies, which have long garnered plentiful attention over the past decade. A motivation for these technologies has been fuelled by the present energy usage, in which current levels are environmentally, economically, and socially unsustainable. In the last 150 years, there has been a radical acceleration of industrialization and global development, which has thus accumulated large amounts of greenhouse gasses (GHGs) into the atmosphere (Anisur *et al.*, 2013; Akeiber *et al.*, 2016). A model prepared by Alexiadis (2007) to measure the anthropogenic activities contributing to the rise in emissions conveyed that CO_2 is the main driving force in global warming. Fundamentally, there must be pivotal actions taken to mitigate this, otherwise the strain on energy security will increase, and the carbon dioxide emissions will double by 2050 (IEA, 2008).

Energy demand diverges in the manufacturing, public, services and transport sectors, often on a daily basis (Dincer and Rosen, 2011). A superlative situation to mitigate this are various energy conversion systems that synergistically match these demands. Peak electricity demand is the most challenging to meet, in terms of supply and cost. Conventionally, these peak energy demands are met by diesel generators or gas turbines, which are reliant on relatively scarce gas and oil reserves. Energy storage thereby provides an exciting alternative method of supplying

energy at these peak periods. There are many forms of energy storage, and many of them are in very early stages of development. There are numerous advantages of energy storage systems, such as an increased process flexibility to meet energy demands, reduced energy consumption, reduced energy costs, and reduced maintenance costs (Dincer and Rosen, 2011). There are several classifications of energy storage methods, as shown in Figure 1.1. Cryogenic energy storage (CES) is a combination of mechanical and thermal energy storage. Biological and magnetic storage do not have extensive research compared to the other various storage methods, and there are very limited papers that investigate this currently. Liquid Air Energy Storage (LAES) is a type of CES, and the storage medium is liquefied nitrogen or air (Ding et al., 2016; Smith, 1977). Cold temperature storage in CES can improve the thermal efficiency by up to 70 % (Ding *et al.*, 2016).

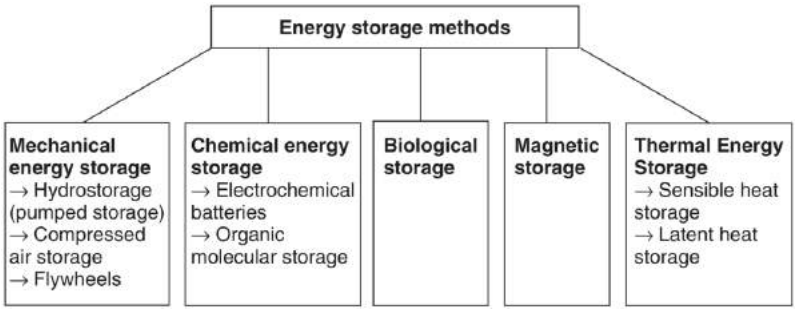

Figure 1.1. Energy storage method classifications (Dincer and Ronsen, 2011).

It is established that substances can hold a certain amount of heat within their system, and this is known as the thermal capacity of the substance (Dincer and Rosen, 2011). Materials can primarily store heat in three main ways, chemical reactions, sensible heat and latent heat (Akeiber *et al.*, 2016). When a liquid is exposed to heat, the heat which the liquid absorbs to raise it to its boiling point is known as 'sensible heat' (Dincer and Rosen, 2011). In sensible heat storage, the principle factors that act as variables in this process are the temperature variations, the mediums' specific heat, and the quantity of the material (Akeiber *et al.*, 2016).

These factors influence the heat storage capacity of sensible heat storage (SHS) and is shown by Equation (1.1).

$$Q = \int_{T_1}^{T_2} mC_p dT = mC_p(T_2 - T_1) \tag{1.1}$$

where Q is the amount of stored energy, T_1 is the initial temperature, T_2 is the final temperature, m is the storage media mass, and C_p is the specific heat capacity.

Conversely, in latent heat storage (LHS), thermal energy is primarily reserved and subsequently released when an energy storage medium changes from one phase to another phase. The stored energy can be defined by Equation (1.2).

$$Q = \int_{T_1}^{T_m} mC_{sp} dT + ma_m \Delta H_m + \int_{T_m}^{T_2} mC_{lp} dT \tag{1.2}$$

where T_m is the melting temperature of the storage medium, a_m is the fraction of melted material, H_m is the specific enthalpy of the melting material, C_{sp} is the specific heat capacity of the solid phase, and C_{lp} is the specific heal capacity of the liquid phase.

Materials commonly used for latent heat storage are known as phase change materials (PCMs). These materials have the characteristics of absorbing and releasing vast quantities of energy during phase changes, and also have negligible volume changes (Akeiber *et al.*, 2016). In cryogenic energy storage, a factor to consider is the storage vessels of the liquid air or liquid nitrogen, and with the utilisation of phase change materials, this can ultimately lead to a reduction in capital cost and higher process efficiency.

A large focus in this field is the encapsulation of PCMs with melting points ranging from −10 to 80 °C, mostly for energy storage applications and for use in building envelopes (Brown *et al*., 2003a; Hawlader, Uddin and Khin, 2003; Jamekhorshid, Sadrameli and Farid, 2014; Sharma *et al*., 2015; Song *et al*., 2019). However, there has been fewer research with more volatile PCMs, such as heptane (Zhang *et al*., 2018; Zhang *et al*., 2019; Zhang, *et al*., 2019b). Volatile PCMs are much more arduous to encapsulate due to their high vapour pressures (~0.13 to ~101.3 kPa at 20°C) resulting in difficulty in the containment of the core material during storage or employment extreme temperature ranges. Nevertheless, the volatile core materials have lower melting points below $-10\,^{\circ}\mathrm{C}$, and are suitable for cryogenic energy storage applications (Zhang, *et al*., 2019).

There are numerous techniques to formulate microcapsules, which include chemical and physical methods. Amongst the chemical methods, in situ polymerization has garnered bounteous attention, due to the excellent mechanical stability that results in the formulated microcapsules (Brown *et al*., 2003a; Bolimowski, Bond and Wass, 2016; Nguon *et al*., 2017). There are two methods of in situ polymerization, namely one-step and two-step methods. The two-step process initiates from a pre-condensate (pre-polymer) aqueous solution, which in this case consists of urea and formaldehyde (UF), prior to the addition of the core material. However, in the one-step process, after the dissolution of the urea monomer species in an acidic environment, the core material can be added and emulsified, with the formaldehyde supplemented during the mechanical stirring (Brown *et al*., 2003a; Fan and Zhou, 2011; Nguon *et al*., 2017). Overall, the one-step method is much more time efficient.

Microcapsules created from formaldehyde and urea/melamine wall materials, termed as 'amino resins', are well recognised for their prodigious properties such as chemical and water resistance, long term stability and storage, excellent loading capacity, and low cost of production (Yuan *et al*., 2006, 2007; Bolimowski, Bond and Wass, 2016; Nguon *et al*., 2017). Even though amino resin microcapsules have been capaciously employed for more than 50 years, to an extent it is an empirical process due to the complexity of the reactions occurring during the polymerization process (Nguon *et al*., 2017). Recent renewed interest in this field has sparked a number of investigations probing the influence of various experimental parameters (Salaün *et al*., 2009; Chuanjie, Juntao and Xiaodong, 2013; Sharma *et al*., 2015). However, a complete understanding of the reaction mechanisms is still lacking, and further research is required achieve a more robust comprehension of this process.

Another issue to be tackled with microencapsulated PCMs (MPCMs) is the supercooling phenomena. Supercooling is a process in which a liquid solidifies at a temperature lower than its freezing point (Al-Shannaq *et al*., 2015; Safari *et al*., 2017). This can limit the use of MPCMs, as more energy input is required to reduce the temperature of the system to induce a phase change. Therefore, it is imperative to understand this process to enhance further the efficiency of MPCM utilisation in various technologies (Alvarado *et al*., 2006a; Al-Shannaq *et al*., 2015; Safari *et al*., 2017). Organic paraffin PCMs do not tend to supercool in their pure form, but when encapsulated, there is severe supercooling observed (Al-Shannaq *et al*., 2015).

Furthermore, MPCMs can be dispersed in a heat transfer fluid (HTF), with the most common being water due to sheer abundance of the resource, to increase the heat transfer rate (Yamagishi *et al*., 1999). Such a mixture in this case is termed as a MPCM slurry, and can also be termed as a Latent Functional Thermal Fluid (LFTF) (Zhang and Zhao, 2011). It is of great importance to study the thermo-physical properties of the MPCM slurry, such as the viscosity of the slurry as a function MPCM mass ratio and temperature (Yamagishi *et al*., 1999; Huang *et al*., 2011; Zhang and Zhao, 2011).

Although generally, people seem to be concerned about the challenges we face with climate change, there is still a discrepancy between those who hold these views and those who proactively engage in attempts to mitigate these challenges. This is a great predicament, and a shift in the mindset of people to a more proactive and exigent approach would significantly contribute to the alleviation of the current crisis we are facing.

1.2. STUDY OBJECTIVES

This PhD research aims to encapsulate PCMs for cryogenic energy storage applications. A well-established chemical microencapsulation technique known as 'in situ polymerization' will be utilised to produce amino resin microcapsules with organic paraffin PCM cores, which have appropriate freeze points. The formulated PCMs will then be characterized in terms of their mechanical and barrier properties, which will convey the feasibility of the shell material retaining the PCM for an extended period of time, both after the formulation period and after being subjected to thermal cycling.

It has been observed that emulsifiers have a significant effect on the successful formulation of microcapsules with appropriate properties, such as mechanical strength to survive the pressure changes after formulation, as the aqueous phase is evaporated. There will also be the study of modifiers added to the formulation, which give the PCM desired properties, such as higher mechanical integrity and water resistance. Subsequently, there will be a mechanistic study that will help screen the best emulsifier candidates, and in this study a mechanism for emulsifier selection will be proposed. There will be further validation experiments to further prove the mechanism, which in turn will make a significant impact on understanding the process of formulating amino resin microcapsules.

The microcapsules will be characterized in terms of their shell thickness, morphology, mechanical, barrier and thermal properties. This includes rupture force, Young's modulus, air release behaviour, heat conductivity and thermal cycling. With the study of these properties, there will be a guidance in formulation provided, as well as an insight into the feasibility of utilising amino resins as shell materials, highlighting both key advantages and issues between choosing this shell material and the intended servicing condition requirements.

The reduction of the supercooling phenomena is also of great importance and will be explored in this work. The influence of microcapsule size, shell thickness, shell roughness, nucleating agents and metallic coating will be investigated. Furthermore, the rheological behaviours of MPCM slurries will be correlated to the PCM composition in a suitable latent heat fluid (LHF).

1.3. THESIS STRUCTURE

Chapter 1 provides an overview of the background and motivation for this current work. The current discourse in the energy storage sector is established, including the current challenges faced, and the potential future technologies in this field. The limitations of previous studies are also highlighted, especially in previous mechanistic studies carried out by various researchers.

Chapter 2 provides a literature review on the microencapsulation of phase change materials for thermal energy storage, not only via the in situ polymerization route, but through other physical and chemical methods. The advantages and disadvantages of such methods are discussed. Furthermore, the role of modifiers in the in situ polymerization process are deliberated, and how such modifiers affect the microcapsule properties. In this chapter, mechanistic studies investigating the one step in situ polymerization process is also conferred, exhibiting the limitations of past work in this field. Finally, the supercooling phenomena is explored, and methods of how to reduce this, as well as the incorporation of PCMs into slurries.

Chapter 3 outlines the detailed experimental methods carried out for this work, as well as the materials and analytical equipment used. This chapter is concerned with the formulation of the MPCMs, as well as the microstructure, chemical and physical characterization.

Chapter 4 delves into the various mechanisms contributing to the chemical reactions occurring in the formulation process. The role of emulsifiers in this process is deliberated, and how such emulsifiers affect the microcapsule properties, and the rate of reaction. Furthermore, the role of modifiers in the encapsulation process is investigated.

Chapter 5 presents the optimization of the one step in situ polymerization process with the use of Taguchi and ANOVA method analysis, to maximise the payload, yield, and encapsulation efficiency of the microcapsules.

Chapter 6 probes the requirement for supercooling reduction to be implemented. With a range of methods implemented to reduce the supercooling, the rheological properties MPCM slurries are examined.

Chapter 7 highlights the conclusions for this study, and furthermore future work in this area is recommended.

1.4. PUBLICATIONS ARISING FROM THIS WORK

Publications as **Main Author**

Abdullah Naseer Mustapha, Yan Zhang, Zhibing Zhang, Yulong Ding, Yongliang Li. (2021) '*A systematic study on the reaction mechanisms for the microencapsulation of a volatile phase change material (PCM) via one-step in situ polymerization*'. **Chemical Engineering Science.** (Under Review).

Abdullah Naseer Mustapha, Yan Zhang, Zhibing Zhang, Yulong Ding, Qingchun Yuan, Yongliang Li. (2021) '*Taguchi and ANOVA analysis for the optimization of the microencapsulation of a volatile phase change material'*. **Journal of Materials Research and Technology.** DOI: 10.1016/j.jmrt.2021.01.025

Abdullah Naseer Mustapha, Helen Onyeaka, Osaze Omoregbe, Yulong Ding, Yongliang Li. (2020) *'Latent heat thermal energy storage: A bibliometric analysis explicating the paradigm from 2000–2019'*. **Journal of Energy Storage.** DOI: 10.1016/j.est.2020.102027

Publications as **Co-Author**

Yan Zhang, **Abdullah Naseer Mustapha,** Xiaotong Zhang, Daniele Baiocco, Gilmore Wellio, Thomas Davies, Zhibing Zhang, Yongliang Li. (2020) '*Improved Volatile Cargo Retention and Mechanical Properties of Capsules via Sediment-Free In Situ Polymerization with Cross-Linked Poly(Vinyl Alcohol) as an Emulsifier'.* **Journal of Colloid and Interface Science.** DOI: 10.1016/j.jcis.2020.01.1115

Yan Zhang, Danielle Baiocco, **Abdullah Naseer Mustapha,** Xiaotong Zhang, Qinghua Yu, Gilmore Wellio, Zhibing Zhang, Yongliang Li. (2019) *'Hydrocolloids: Nova materials assisting encapsulation of volatile phase change materials for cryogenic energy transport and storage'.* **Chemical Engineering Journal.** DOI: 10.1016/j.cej.2019.12302

CHAPTER 2: LITERATURE REVIEW

The work presented in this chapter has been published in the following journal paper: **Abdullah Naseer Mustapha,** Helen Onyeaka, Osaze Omoregbe, Yulong Ding, Yongliang Li. (2020) *'Latent heat thermal energy storage: A bibliometric analysis explicating the paradigm from 2000–2019'*. **Journal of Energy Storage.** DOI: 10.1016/j.est.2020.102027

2.1. OVERVIEW

This chapter concerns the literature survey regarding PCMs and their applications in TES processes. The various types and categories of PCMs are reviewed and deliberated, and their various uses, advantages, and disadvantages. Furthermore, the selection criteria for the various types of PCMs are considered. Organic and inorganic shell material candidates were also reviewed in this section, and their properties in terms of chemical compatibility, mechanical properties, morphological uniformity, thermal conductivity, and structural flexibility. Various microencapsulation methods are also deliberated, reviewing both physical and chemical methods. The effect that emulsifiers have on the encapsulation methods are reviewed also, and especially how this affects the one-step in situ polymerization process, and the various challenges faced within this topic. The supercooling phenomena exhibited by various types of PCMs, as well as how the encapsulation of PCMs further increases the severity of this phenomena is examined. Lastly, the rheological properties of MPCM slurries were reviewed, discussing factors such as volume fraction and temperature affecting the rheological profile.

2.2. PHASE CHANGE MATERIALS

PCMs are a classification of organic or inorganic compounds which have a high latent heat of fusion, and that can store/release a large amount of energy during the solidifying/melting processes (Akeiber *et al.*, 2016). PCMs offer multifaceted properties which can be employed in various fields, such as waste heat recovery systems, solar power and solar cooling plants, space industry, textiles, photovoltaic electricity systems, pharmaceutical and food product preservation, domestic heat water and in the agricultural industry (Fang, Tang and Cao, 2014; Shalaby, Bek and El-Sebaii, 2014; Aydin, Casey and Riffat, 2015; Dhaidan and Khodadadi, 2015; Ma *et al.*, 2015). There have been studies to suggest that PCMs have the advantages of low cost, extensive latent heat storage capacity, high heat storage density, excellent chemical stability, etc. (Fan and Khodadadi, 2011; Khan, Khan and Ghafoor, 2016; Ma *et al.*, 2017; Meng and Zhang, 2017; Yu *et al.*, 2018).

Figure 2.1 conveys the yearly trend of publications and citations within the latent heat transfer energy storage (LHTES) field. As observed, the number of publications had a steady escalation from 2000 – 2010, but there was a pronounced increase in publications during the last decade (2011 – 2019). The citations followed the same trend, conveying the ever-increasing interest in this field.

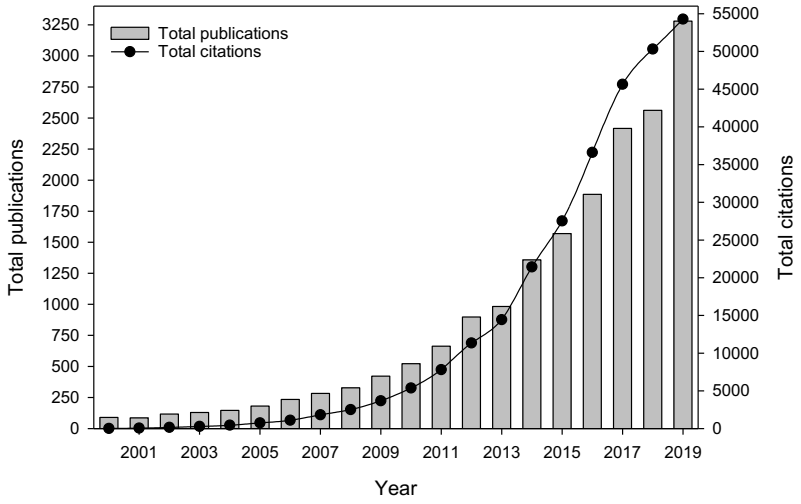

Figure 2.1 – Number of Publications and Citations Regarding LHTES Research During 2000-2019 (Mustapha *et al.*, 2021).

PCMs can be classified into subcategories, depending on the material and phase change mechanism. These categories include solid-solid, solid-liquid and liquid gas transformations, and vice versa (Huang *et al.*, 2019). Solid-liquid PCMs are favourable for TES applications due to the high energy density, low vapour pressure during transition, and high energy density (Peng *et al.*, 2020).

Liu et al. (2015) further categorizes PCMs depending on their material properties, into eutectic, organic and inorganic groups. The classifications are conveyed in Figure 2.2. Eutectic PCMs are a classification of materials that is a mixture of two or more soluble species, in which there is simultaneous solidification and melting, without the separation of the phases (Peng *et al.*, 2020). Inorganic PCMs comprise of molten salts, hydrated salts, metals and alloys (Kumar and Banerjee, 2018). Organic PCMs are classified into paraffin and non-paraffin. Organic PCMs in particular are an attractive group of materials due to appropriate temperature ranges for various applications, stable physical and chemical characteristics, and extremely high latent heat storage capacity (Kumar and Banerjee, 2018).

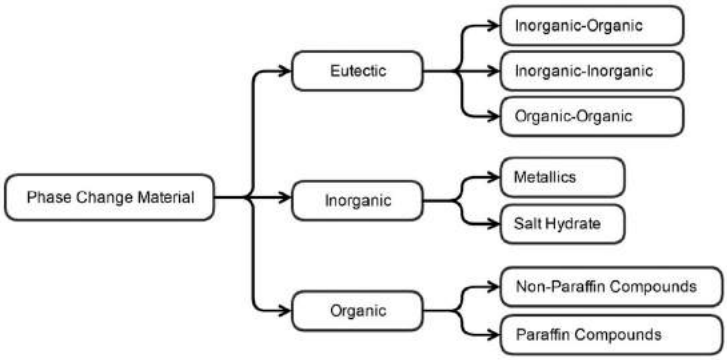

Figure 2.2 - Classification of PCMs (Zhang et al., 2016).

PCMs are also categorized according to their specific phase transition temperatures. High temperature PCMs are classed as PCMs with a melting point of > 420 °C, intermediate PCMs have a melting point of 220 °C to 420 °C, and low temperature PCMs have a melting point of < 220 °C (Peng *et al.*, 2020). Generally, high temperature PCMs fall into the category of metal carbonates, sulphates, chlorides, fluorides, etc (Peng *et al.*, 2020). Many eutectic PCMs fall into the 'intermediate' classification. Organic PCMs, many of which are paraffins, sugar alcohols and fatty acids, fall into the low temperature classification (Peng *et al.*, 2020).

2.3. ORGANIC PCMS

Although organic PCMs cover a wide range of materials, literature has shown that esters, fatty acids and pure n-alkanes are the most utilised and established for their latent heat storage (Farid *et al.*, 2004a). As mentioned, organic PCMs have been gaining the most attention due to their high latent heat storage capabilities, appropriate temperature ranges and stable chemical and physical characteristics (Akeiber *et al.*, 2016). Nevertheless, pure organic PCMs exhibit certain limitations in regard to low thermal conductivity (less than 0.2 $W.m^{-1}.K^{-1}$ for organic PCMs), liquid seepage and high volume variations during the phase change process (Fang *et al.*, 2014). Organic PCMs are further classified to paraffin and non-paraffin.

2.3.1. ORGANIC PARAFFIN PCMS

Paraffins are a class of materials that consist of straight chained alkanes, with a general formula of (C_nH_{2n+2}). An increase in the chain length of the paraffin results in increased latent heat of fusion and melting points (Akeiber *et al.*, 2016). Generally, paraffins are a very exciting category of PCMs due to their high latent heat capability, as well as low cost and high energy density. Various paraffins have been used in literature for various applications, such as dodecane for energy storage, paraffin wax for solar energy storage, and sodium sulphate decahydrate for building envelope applications (El-Kotb *et al.*, 2006; Cui *et al.*, 2017; Darvin *et al.*, 2019). Various properties of paraffins are conveyed in Table 2.1.

Table 2.1. Inorganic Salts and Salt Hydrates Melting Temperature and Heat of Fusion (Mohamed et al., 2017).

Hydrocarbon	Molecular formula	Molar mass ($g.mol^{-1}$)	H_{fus} ($kJ.kg^{-1}$)	$T_{melting}$ (°C)	Density at 20 °C ($g.ml^{-1}$)
n-heptane	C_7H_{16}	100.2	140.0	– 98	0.683
n-octane	C_8H_{18}	114.2	181.9	– 57	0.702
n-nonane	C_9H_{20}	128.2	117.0	– 53	0.719
n-decane	$C_{10}H_{22}$	142.3	201.7	– 30	0.730
n-undecane	$C_{11}H_{24}$	156.3	144.0	– 26	0.740
n-dodecane	$C_{12}H_{26}$	170.3	216.1	–10	0.750
n-tridecane	$C_{13}H_{28}$	184.4	160.1	–5	0.756
n-tetradecane	$C_{14}H_{30}$	198.4	227.0	6	0.760
n-pentadecane	$C_{15}H_{32}$	212.4	205.1	15	0.769
n-hexadecane	$C_{16}H_{34}$	226.4	237.2	18	0.773
n-heptadecane	$C_{17}H_{36}$	240.5	171.3	22	0.777
n-octadecane	$C_{18}H_{38}$	254.5	242.0	28	0.777
n-nonadecane	$C_{19}H_{40}$	268.5	222.3	32	0.785
n-eicosane	$C_{20}H_{42}$	282.5	247.1	37	0.789

However, there are some drawbacks to utilising paraffin as an energy storage medium, such as low thermal conductivity. With a thermal conductivity of below 0.4 $W.m^{-1}.K^{-1}$, this can lead to lower heat retrieval rates, and thus low stored energy utilisation efficiency (Xiao, Zhang and Li, 2013). However, there have been studies combining paraffins and metal foam composite PCMs, which led to vastly increased thermal conductivities. Xiao, Zhang and Li (2013) conveyed that by utilising paraffin/nickel composites, the thermal conductivity was thrice than that of pure paraffin, and paraffin/copper composites produced a thermal conductivity 15 times that of pure paraffin (Xiao, Zhang and Li, 2013). However, with this being said, it was observed that the latent heat capacity for these composites slightly reduced, which should be a factor to consider in the overall process.

2.3.2. Non-paraffin Organic PCMs

Non-Paraffin PCMs have a wider range of inter-varying properties in comparison to the fairly homogenous paraffin PCMs (Akeiber *et al.*, 2016). Fatty acids, alcohols, esters and glycols are the most widely known non-paraffin PCMs (Akeiber *et al.*, 2016). Non-Paraffin PCMs have the largest category for energy storage. Abhat *et al.*, (1981) and Sharma *et al.*, (2009) conducted a study of organic non-paraffin materials that are suitable for energy storage. Within this study, fatty acids were investigated. The formula that characterizes non-paraffin organic PCMs fatty acids is $CH_3(CH_2)_{2n}COOH$. It was seen that fatty acids have a higher heat of fusion in comparison to paraffin based PCMs (Abhat *et al.*, 1981; Sharma *et al.*, 2009). Furthermore, fatty acids conveyed reproducible results of freezing and melting behaviour without the super-cooling phenomena (Sharma *et al.*, 2009). Due to the protected carboxyl group, these PCMs are heat and chemically stable, as well as non-toxic and show low corrosion activity (Rozanna *et al.*, 2005).

Fatty acids have a surface tension in the range of $0.02 – 0.03 \times 10^{-4}$ $N.m^{-1}$ in their liquid phase, which is high enough to be retained in the microencapsulation host material (Rozanna *et al.*, 2005). Furthermore, these materials have high specific heat, and high latent heat of transition. During melting and solidification, only very small volume changes are observed. For example, melting dilatation is around values of $0.1 – 0.2$ $ml.g^{-1}$ (Rozanna *et al.*, 2005).

There have been studies regarding the utilisation of fatty acids for energy storage processes (Sari, 2003; Sari and Kaygusuz, 2006). Sari (2003) investigated the thermal characteristics of the fatty acids, with the use of cylindrical capsules and thermal cycling processes. It was found that as the thermal cycling increased, the melting temperature and latent heat of fusion of the PCMs decreased. However, even after 12000 cycles, the decrease in these values were still under 20 % of the original values.

Sar and Kaygusuz (2003) have studied thermal stabilities of palmitic, myristic, stearic and lauric acid over periodic heating-cooling cycling processes. The studies show that these specific fatty acids exhibit good thermal stability, with values of up to 410 thermal cycles (Sar and Kaygusuz, 2003). It was also perceived that after 910 cycles, lauric and stearic acid presented a decrease in thermal stability, by more than 30 % (Sar and Kaygusuz, 2003). However, for myristic and palmitic acid, there was a lower reduction of thermal stability, with a value of 17 % (Sar and Kaygusuz, 2003). The chemical degradation of PCMs and the effect of impurities may have influenced the thermal stabilities of the acids. However, overall, it was shown that myristic and palmitic acid exhibited better thermal stability results, due to the lower decrease in latent heat in comparison to lauric and stearic acids.

Even though fatty acids have been shown to have exciting potential for energy storage applications, there are certain limitations. PCM storage effectiveness per unit volume is affected by density (Rozanna *et al.*, 2005). With phase transition, there are volume changes in the order of 10 %, which can pose some challenges (Dincer and Rosen, 2011). It was reported that some non-paraffin PCMs including fatty acid experienced volume changes of up to 20 %, while undergoing solid to liquid phase changes (Lane, 1980). It was also shown that more dense fatty acids, such as caprylic acid, is more effective per unit volume (Lane, 1980).

Another drawback to non-paraffin PCMs are the costs. They are approximately 2 – 2.5 times more expensive than the organic paraffin based PCMs, which should be a consideration for large scale applications (Sharma *et al.*, 2009).

2.4. INORGANIC PCMS

When comparing organic and inorganic PCMs, inorganic PCMs have a lower cost, lower flammability and higher heat of fusion per unit mass (Sharma *et al.*, 2009). However, there are shortcomings for inorganic PCMs, such as lack of thermal stability, decomposition, corrosion and phase segregation (Swet, 1980). The issue of phase segregation is the most prevailing hindrance of these groups of materials, due to the reduction in thermal efficiency and potential leaking of the PCMs. Inorganic PCMs can be further classified to salt hydrates and metallic groups.

2.4.1. INORGANIC SALT HYDRATE PCMS

Salt hydrates are represented as water and inorganic salts creating a crystalline solid, with the general formula of $A_xB_y \cdot nH_2O$. The A_xB_y represent metal carbonates, chlorides, acetate, nitrate, phosphate, or sulphite, whereas the n represents the number of water molecules (Mohamed *et al.*, 2017). These groups of materials are ionic compounds in which the number of water molecules are attracted by the ions, and subsequently enclosed within the crystal lattice. During the phase change transition, and when the salt hydrates dissolve and lose part of their water molecules, latent heat is absorbed (S. A. Mohamed *et al.*, 2017). Table 2.2 conveys some salt hydrates and inorganic salts with potential to be used as PCMs.

Table 2.2 - Inorganic Salts and Salt Hydrates Melting Temperature and Heat of Fusion (S. A. Mohamed *et al.*, 2017).

Compound	Melting temperature (°C)	Heat of fusion ($kJ.kg^{-1}$)
Salts		
$AlCl_3$	192	280
$LiNO_3$	250	370
$NaNO_3$	307	172
KNO_3	333	266
KOH	380	150
$KClO_4$	527	1253
LiH	699	2678
$MgCl_2$	714	452
Salt hydrates		
$Na_2P_2O_7.10H_2O$	70	184
$Ba(OH)_2.8H_2O$	78	266
$(NH_4)AL(SO_4)_2.12H_2O$	95	269
$MgCl_2.6H_2O$	117	169
$Mg(NO_3)_2.6H_2O$	89	150

The dehydration and hydration of a salt can be translated to the case of a solid-liquid transformation, and this phenomenon is similar to the melting-freezing process in thermodynamics (Sharma *et al.*, 2009). Anhydrous salt and water or a hydrate with fewer moles of water are obtained at the melting point of the hydrated crystal, which are conveyed by equation (2.1) and (2.2) respectively.

$$AB \cdot nH_2O \rightarrow AB + nH_2O \tag{2.1}$$

$$AB \cdot nH_2O \rightarrow AB \cdot mH_2O \ + (m-n)H_2O \tag{2.2}$$

There are primarily three melting behaviours that are identified in this process, which are identified as congruent, semi-congruent and incongruent melting. Congruent melting occurs when, at the melting temperature, the anhydrous salt is completely soluble in its water of hydration (Sharma *et al.*, 2009). Semi-congruent melting is when the solid and liquid phases in the equilibrium during the phase transition is of a different melting composition, due to the conversion of a hydrate to a lower-hydrated material from the loss of water (Mohamed *et al.*, 2017). Incongruent melting occurs when, at the melting point, the salt is not completely soluble in the water.

Salt hydrates are a widely studied PCM with many advantages in the latent heat energy storage process (Sharma *et al.*, 2009). Salt hydrates have high latent heat of fusion per unit volume, and also have small volume changes upon melting, and have almost double the thermal conductivity of paraffin based PCMs (Sharma *et al.*, 2009). Also, they do not have high levels of toxicity, and are not very corrosive. Salt hydrates are also relatively inexpensive, especially when compared to the more expensive non-paraffin based PCMs.

However, there are some drawbacks from these types of PCMs. An issue with salt hydrate PCMs is the incongruent melting phenomena. In many instances, at the melting point, the moles of water are not sufficient to dissolve the solid phase completely, and thus due to the density difference, the anhydrous salt (or lower hydrate) settles to the bottom of the container. Subsequently, this settled solid does not recombine with the water during the reverse freezing process, resulting in an irreversible process of melting-freezing of the salt hydrate, which decreases with each cycle (Sharma *et al.*, 2009). However, incongruent melting can be tackled by mechanical stirring, the addition of thickening agents that suspend the solid salts and prevent them from settling, using excess water to prevent supersaturated solutions, and by encapsulating the PCMs to reduce the separation process (Biswas, 1977; Telkes, 1980)

Furthermore, salt hydrates do not have good nucleating properties, resulting in super-cooling of the liquid before the initiation of the crystallization process (Sharma *et al.*, 2009). To mitigate this, a nucleating agent can be added to the solution, in which there will be an initiation of a crystal formation.

2.4.2. Inorganic Metallic PCMs

This group of PCMs involves metals and metallic alloys (Sharma *et al.*, 2009). Metallic inorganic PCMs have not been studied to an extent as the previously mentioned species have, due to weight constraints. However, when volume is the key factor to be considered, these PCMs offer a good option as they have high heat of fusion per unit volume (Sharma *et al.*, 2009). Table 2.3 conveys a range of metallic PCMs, along with their heat of fusion and melting temperatures. One stand out feature of the metallic PCMs is their much higher values of thermal conductivity, especially when compared to the organic PCMs (Sharma *et al.*, 2009).

Table 2.3 - Metals and Metal Alloys for PCM Applications (S. A. Mohamed *et al.*, 2017).

Compound	Melting temperature (°C)	Heat of fusion ($kJ.kg^{-1}$)
Pb	328	23
Al	660	397
Cu	1083	193
Mg-Zn (48/52 wt. %)	340	180
Zn-Al (96/4 wt. %)	381	138
Al-Mg-Zn (59/33/6 wt. %)	443	310
Mg-Al (34.65/65.35 wt. %)	497	285
Al-Cu-Mg (60.8/33.2/6 wt. %)	506	365
Al-Si-Cu (68.5/5/26.5 wt. %)	525	364
Al-Cu (66.92/33.08 wt. %)	548	372
Al-Si (87.76/12.24 wt. %)	557	498
Al-Si-Cu (65/5/30 wt. %)	571	422
Al-Si (20/80 wt. %)	585	460
Zn-Cu-Mg (49/45/6 wt. %)	703	176
Cu-Zn-P (69/17/14 wt. %)	720	368
Cu-Zn-Si (74/19/7 wt. %)	765	125
Mg-Ca (84/16 wt. %)	790	272
Mg-Si-Zn (47/38/15 wt. %)	800	314

In comparison to the other aforementioned PCMs, the metallic PCMs have higher thermal conductivity values, thus eliminating the requirement for conductivity enhancement materials, such as fillers (Mohamed *et al.*, 2017). This eliminates the need for extra cost and weight, as the metallic based PCMs are already compromised by weight constraints. Another important property is that in comparison to the other PCMs, metallic PCMs have relatively high thermal stability when undergoing thermal cycling, as well as high heat of fusion per unit volume, low vapour pressure and specific heat (Mohamed *et al.*, 2017).

An issue facing the application of PCMs in the solid-liquid energy storage process is the chemical interactions and activity between the PCMs containers and the molten alloys (Park, Butt and Beard, 2000). A potential remedy to this issue is the encapsulation of the molten phase

PCM, which will thus limit the interaction between the environment and the PCMs. Zang *et al*. (2014) encapsulated copper balls with chromium/nickel layers to prevent environmental interaction. The results showed that between 1050 - 1150 °C, 1000 thermal charge/discharge cycles conveyed no leakage (Zhang *et al.*, 2014).

2.4.3. EUTECTIC PCMS

A eutectic mixture is a combination of two or more components, which have a minimum melting composition, each of which during crystallization congruently melt and freeze to form a mixture of component crystals (Sharma *et al.*, 2009; Akeiber *et al.*, 2016). Eutectics usually melt and freeze without observed segregation, as they freeze to a closely packed structure upon phase change, leaving very little space for the separation of components. Conversely, the components liquefy simultaneously, which again leaves very little opportunity for phase separation. Table 2.4 conveys a selection of eutectic PCM combinations with their melting point and latent heat capacity.

Table 2.4 - Eutectic PCMs and Properties (Sharma et al., 2009) (— is insufficient data)

Compound	Melting temperature (°C)	Heat of fusion ($kJ.kg^{-1}$)
Gallium-gallium antimony eutectic	30	—
Gallium	30	80
Cerrolow eutectic	58	91
Bi-Cd-In eutectic	61	25
Cerrobend eutectic	70	33
Bi-Pd-In eutectic	70	29
Bi-In eutectic	72	25
Bi-Pd-tin eutectic	96	—
Bi-Pd eutectic	125	—

Ge *et al*. (2014) composed a study by preparing composite materials which were based on inorganic salts for high and medium temperature energy storage applications. The composite materials consisted of a eutectic salt of sodium carbonates and lithium as the PCM, and a ceramic material, which proved to produce high thermal conductivity (Ge *et al.*, 2014; Mohamed *et al.*, 2017).

The thermo-chemical behaviour of eutectic PCMs was investigated by Olivares and Edwards (2013). The PCM consisted of a KNO_3-$NaNO_3$-$LiNO_3$ eutectic mixture, and by using DSC-TGA-MC analysis, the data was collected under nitrogen, argon, oxygen, and air (Olivares and Edwards, 2013). During the experimental procedures, the mixture went through solid-solid type endothermic transformation at 87 °C. The melting point of the eutectic PCM was identified at 121°C, while solidification was observed at 98 °C (Olivares and Edwards, 2013). The thermogravimetric analysis (TGA) conveyed that at 500 °C, the high stability of the salts is limited at this temperature, which was further validated by the differential scanning calorimetry (DSC) experiments (Olivares and Edwards, 2013). It has been suggested by Kenisarin (2010) that compositions of double and ternary eutectics are the most promising, especially those with chlorides and fluorides. Furthermore, the chlorides and fluorides salts that are attached with polyatomic ions, such as nitrates, hydroxides and carbonates, have been attracting the highest level of interest in this category (Kenisarin, 2010).

It is to be noted that even though eutectics do not have the issues regarding super-cooling and phase segregation, there is still further improvement required on the utilization of eutectic fatty acids for PCM applications. Challenges facing fatty acid eutectic PCMs include leakage above the thermal transition, and individual fatty acid limited thermal capacity (Atinafu *et al.*, 2018). Based on a report by Cai *et al.* (2012), a matrix composed of poly-ethylene terephthalate

supporting myristic acid-stearic acid composite conveyed a storage capacity that was lower than initially expected (100 – 200 $kJ.kg^{-1}$) (Cai *et al.*, 2012). However, as previously mentioned, binary eutectic PCMs have the advantage of good chemical compatibility and high surface tension. Therefore, it can be stated that the factor to be considered when employing eutectic PCMs depends on the supporting matrix materials to be employed (Atinafu *et al.*, 2018).

2.5. THE USE OF PCMS IN INDUSTRY

The use of PCMs in various industrial applications conveys the wide scope and great potential of these materials. PCMs have been employed in many systems, and one popular application of PCMs has been TES tanks with heat pump systems. Current work in this field is concerned with the integration of solar district heating (SDH) with seasonal thermal energy storage systems (STES) to improve the overall thermal efficiency (Marx, Bauer and Drueck, 2014). Moreno *et al.* (2014) examined the application of PCMs in TES tanks, combined with heat pump systems. It was conveyed that the smaller volume PCM tank stored 35.5 % more cold energy than the conventional water tank. However, a drawback of this was that the charging time was 4.55 times higher. Furthermore, Zou *et al.* (2017) carried out research of an air-source heat pump water heater using a water and paraffin PCM slurry for heat storage, in which a 14 % increase in heat capacity was observed. Furthermore, the PCM exhibited a discharge efficiency of 83.9 %. The usage of PCMs in heat pumps are an exciting prospect, and the STES can be discharged at lower temperatures without as many heat losses, however, the current drawbacks are associated with the charging times, which may increase.

The integration of PCMs in building envelopes is also an area with a high level of interest and is considered a significantly effective approach to reduce energy consumption in buildings. Memon *et al.* (2015) conducted various thermal performance tests for lightweight aggregate concrete (LWAC) containing a macro-encapsulated paraffin lightweight aggregate (LWA) to be imbedded in domestic home walls. The study conveyed that LWA integration reduced the interior room temperature by 4.7 °C, and the environmental evaluation concluded that 465 kg CO_2-eq was saved. Additionally, Tokuç, Başaran and Yesügey (2015) employed experimental and CFD methods to evaluate thermal performances of PCM-concrete layers incorporated in flat roofs in Istanbul, Turkey. Performance tests conveyed that 2 cm was a suitable thickness for the PCM-concrete layer, and a decrease in the heat flux passing through the roof by 36.1 % was observed. However, it was seen that the application of PCMs in building applications offers seasonal advantages in countries exhibiting four seasons, which reduces the overall usability of this system. Furthermore, another issue with the integration of PCMs in building applications is that, should there be any maintenance issues, it is difficult to replace the PCM using a non-destructive method, which is an issue if the PCM degrades over time (Bland *et al.*, 2017).

PCMs have also been employed in an array of solar applications. The temperature decrease of a photovoltaic (PV) system using a paraffin PCM with melting points of 42 – 44 °C was studied by Klugmann-Radziemska and Wcisło-Kucharek (2017). The cell efficiency was increased by more than 5 %, and the surface cell temperature reduced by 7 °C and remained stable for 5 hours at a set temperature. Baygi and Sadrameli (2018) incorporated Polyethylene glycol 1000 (PEG 1000) in a solar panel, and the results shown conveyed that the thermal efficiency of the panel increased by up to 8 %, and the panel temperature reduced by 15 °C compared to the conventional panel. Although the use of PCMs in PV applications offers merits such as increased thermal efficiency, reduced panel surface temperature and higher heat transfer, there

are still prevailing concerns such as flammability of organic PCMs, toxicity of various paraffins, high initial costs of implementation, and corrosion. Nevertheless, the prospect of PCM implementation in PV cells is an exciting foretaste with very auspicious potential.

The application of PCMs in the textile industry is primarily concerned with the thermo-regulation of clothing (Salaün, 2019). Current challenges in this field involve PCM leakage, and thus they must be entrapped or encapsulated in a matrix, with suitable mechanical strength. Moreover, the PCM material must be of a suitable size to integrate into textile materials and allow for thermoregulation. Lu *et al.* (2017) fabricated highly porous Polystyrene fibres and impregnated the pores with Lauric acid as the PCM. A superior melting enthalpy was observed (74 $J.g^{-1}$), as well as a melting transition temperature of 44 °C. However, after 100 cooling/heating cycles, there was a decrease in the enthalpy value to 67 $J.g^{-1}$, which signified relatively decent reusability, however, improvements can be made to increase the cyclic stability further by entrapment in a polymer matrix. Chen, Wang and Huang (2011) produced thermoregulating fibres with PEG as the PCM and explicated that up to 70 wt.% of PEG can be incorporated into the matrix, and the resulting fibre blend exhibited 120 $J.g^{-1}$ of enthalpy storage. However, one issue exhibited by this was that upon water treatment, the enthalpy storage diminished due to the solubility of PEG in water, which often can be the case with soluble PCMs applied in textile applications.

2.6. PCM SELECTION AND EMPLOYMENT IN TES APPLICATIONS

In terms of the phase changes before and after, the PCMs can be further classified into solid-solid, solid-liquid, solid-gas, and liquid-gas PCMs. For energy storage applications, solid-liquid PCMs have a lower volume phase change and higher latent heat capacity compared to the rest (Yu *et al.*, 2018). These factors have consequently lead to organic solid-liquid PCMs being more commonly used for this purpose (Liu *et al.*, 2015).

For a PCM to be used in practical applications, it is important that there is high latent heat capacity, high thermal conductivity, the phase change transition temperature is within the practicable limits, and for it to be thermally and chemically stable (Lin *et al.*, 2018). However, no PCM can fully meet perfect requirements. There are issues such as phase separation, leakage of the core material, super-cooling, low heat transfer rates and performance instability (Lopez *et al.*, 2010; Alva *et al.*, 2017; Sciacovelli, Vecchi and Ding, 2017). It has been studied and shown that organic PCMs possess lower thermal conductivity compared to inorganic PCMs, and hence why thermal conductivity improvements are a significant factor to improve for PCM usage in energy storage (Liu *et al.*, 2015; Lin *et al.*, 2018; Yu *et al.*, 2018).

Concerning the performance of the energy storage systems, the cryogenic temperature is pivotal. Organic PCMs are often employed for CES applications due to low melting points and low supercooling in their pure form, making them suitable for this application. It was suggested by Yu *et al.* (2018) that currently, packed beds are utilised for CES systems. However, in terms of efficiency, capacity and flexibility, there is room for further improvement (Fan and Khodadadi, 2011; Yu *et al.*, 2018). Microencapsulated Phase Change Materials (MPCMs) are a prodigious solution to these gaps. Literature has shown that PCMs are still in their early development stages for use in CES, however the success of this relies on the PCMs being

microencapsulated in an inert material, which can be tested in various conditions, such as repeated pumping, cyclic cooling and heating, as well as long term periodic storage (Yu *et al.*, 2018).

2.7. ENCAPSULATION SHELL MATERIALS

For the effective reduction of leakage of the PCMs during phase transition processes, the surrounding of PCMs with an inert wall material has been an attractive prospect in recent years (Farid *et al.*, 2004b; Alkan and Sari, 2008; Huang *et al.*, 2011). Microencapsulation technology can also provide a larger heat transfer area, relatively constant volume during phase change processes, and enhanced thermal cycling stability (Peng *et al.*, 2020). The shell materials utilised in encapsulation processes play an important role in mechanical properties, thermal properties, barrier properties and morphological characteristics (Peng *et al.*, 2020). Shell materials can be classified into three main categories, namely organic, inorganic and organic-inorganic hybrids (Agyenim et al., 2010). Figure 2.3 conveys these classifications, and examples of such materials. The benefits and drawbacks of each group of shells will be discussed in the following section.

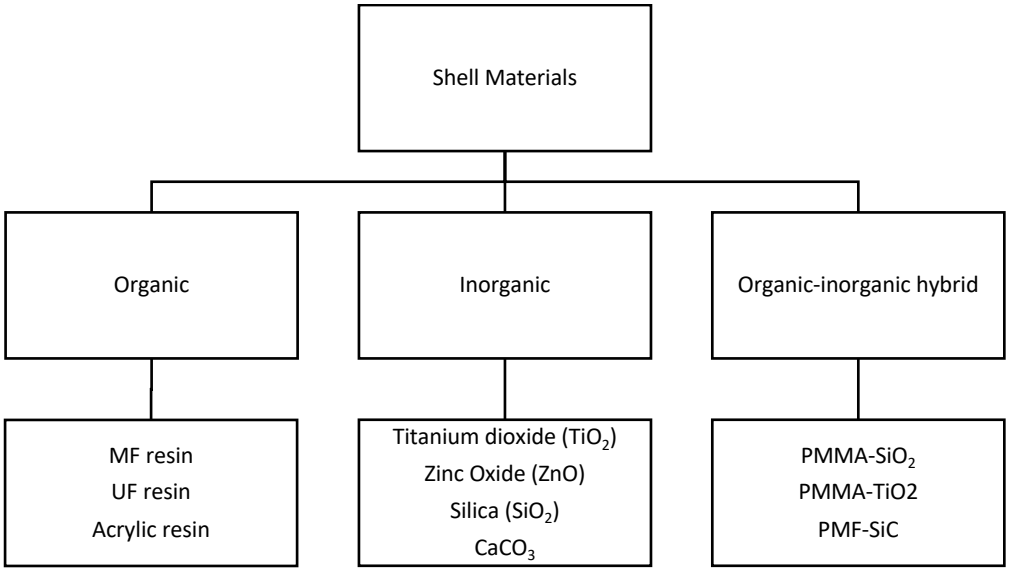

Figure 2.3 - Classifications of shell material for the microencapsulation of PCMs (Peng et al., 2020).

2.7.1. ORGANIC SHELLS

Organic materials can consist of natural and synthetic polymeric materials, which possess virtuous structural flexibility, good sealing properties, and resistance to volume changes during with repeated thermal cycling and phase changes (Peng *et al.*, 2020). However, the drawbacks of organic shells stem from their low thermal conductivity, which is undesirable for TES applications, as well as flammability for some organic materials. Such common organic shell materials include acrylic resin, UF resin, melamine-formaldehyde (MF) resin (Fan *et al.*, 2004; Xing Xiang Zhang *et al.*, 2004; Salaün *et al.*, 2009). MF resins have the advantages of being thermally stable, having low cost, and good chemical compatibility (Peng *et al.*, 2020). However, UF resins are less brittle than their MF counterparts and have a more linear structure, which is beneficial for thermal cycling applications, reducing the chances of buckling (Qin, Dong and Li, 2019).

MF microcapsules and nanocapsules containing n-dodecane were produced by Zhu *et al.* (2012) for applications in heat storage, temperature control and heat transfer. They observed that the physical properties of the microcapsules were largely dependent on the average diameter of the encapsulated PCMs. Thermogravimetric analysis conveyed that the n-dodecane capsules had increased thermal stability with decreases in their diameter. Furthermore, differential scanning calorimetry conveyed that the supercooling degree of n-dodecane in the microcapsules was lower than that in the nanocapsules (Zhu *et al.*, 2012). Microcapsules containing paraffin wax core (Rubitherm® RT-42) and a UF shell were prepared by Silva et al. (2018). Various reaction conditions were investigated, such as the shell/core ratio, the reaction temperature, and the reaction time. It was observed that the optimum reaction time was 2-3 hours, and that the optimum reaction temperature was in between 60 and 70 °C. Furthermore, it was observed that the optimal shell/core ratio was 0.8. With these reaction conditions, microcapsules were produced with high encapsulation efficiency (90.6 wt. %) (Sánchez-Silva *et al.*, 2018).

Amongst the acrylic resin shell materials, copolymers of methacrylate possess the advantageous properties of good thermal stability, excellent chemical resistance and non-toxicity (Peng *et al.*, 2020). Ma et al. (2012) encapsulated butyl stearate and paraffin with a poly(methylmethacralate-co-divinylbenzene) (P(MMA-co-DVB)) shell. The microcapsules exhibited morphological uniformity, and a compact shell. Eicosane PCM microcapsules were prepared by Alkan, Aksoy and Anayurt (2015) with a polymethylmethacrylate (PMMA) shell. The microcapsules exhibited stellar thermal stability after 5000 cycles, which is excellent for long-term TES applications.

2.7.2. INORGANIC SHELLS

Compared with their organic counterparts, inorganic shell materials exhibit higher thermal conductivity, higher mechanical strength, and higher rigidity (Peng *et al.*, 2020). With this being said, a few inorganic shells require pre-cursors to synthesise, which can be a timely and costly procedure, and often precursors can reduce the mechanical strength of the shell. Examples of inorganic shells include titanium dioxide (TiO_2), zinc oxide (ZnO), silica (SiO_2) (Fang, Chen and Li, 2010). Specifically, silica is a commonly used inorganic shell material due to the merits it offers, such as fire resistance and high thermal conductivity (Fang, Chen and Li, 2010). Silica is often employed to encapsulate fatty acids, inorganic hydrated salts and organic paraffin waxes (Peng *et al.*, 2020). The encapsulation of n-octadecane was carried out by Liang *et al.* (2015) to produce nanocapsules. The thermal conductivity of the nanocapsules was measured to be above 0.4 $W.m^{-1}.K^{-1}$, with an encapsulation efficiency of 51.5 % and a melting enthalpy of 109.5 $J.g^{-1}$ (Liang *et al.*, 2015). No leakage was observed after 500 thermal cycles. However, the drawback with silica shell materials is that a precursor is usually needed, such as tetraethoxysilane (TEOS), and the polycondensation and hydrolysis of TEOS may lead to the weakening of the shells mechanical strength (Peng *et al.*, 2020).

In comparison with the silica shells, $CaCO_3$ shells demonstrate improved compactness and enhanced rigidity (Peng *et al.*, 2020). Yu, Wang and Wu (2014) synthesized n-octadecane microcapsules with a CaCO3 shell via the self-assembly method. The microcapsules exhibited good thermal conductivity, anti-osmosis properties, thermal stability and a uniform diameter of around 5 μm (Yu, Wang and Wu, 2014).

Moreover, metal oxides with crystalline structures, such as TiO_2 and ZnO offer multiple properties, such as anti-bacterial, photochemical and catalytic properties (Azizi-Lalabadi *et al.*, 2019). Liu *et al.* (2019) utilised TiO_2 shells to encapsulate n-eicosane via the interfacial polymerisation method, which was followed by the impregnation with ZnO. The capsules exhibited photocatalytic and thermal storage capabilities. The latent heat and melting temperatures were 188.27 $J.g^{-1}$ and 41.76 °C respectively (Liu *et al.*, 2019).

2.7.3. Organic-Inorganic Hybrid Shells

In order to circumvent the shortcomings of organic and inorganic materials, researchers have been crafting organic-inorganic hybrids to synergistically combine their advantageous properties (Peng *et al.*, 2020). In the organic-inorganic hybrid shells, the organic materials offer structural flexibility, while the inorganic materials offer thermal conductivity, stability and mechanical strength (Huang *et al.*, 2020). Microcapsules formulated with polymers such as PMF and PMMA can be doped with TiO_2 or SiO_2 for enhanced properties (Niu *et al.*, 2012).

A PMMA-silica hybrid shell was utilised to encapsulate n-octadecane by Wang *et al*. (2017), via Pickering emulsion polymerization. The microcapsules exhibited 62.55 % encapsulation efficiency and had a size distribution ranging from 5 μm to 15 μm. Furthermore, Wang, Li and Zhao (2018) formulated microcapsules with an n-octadecane core and a poly(MF)/silicon carbide (PMF/SiC) hybrid shell via in situ polymerization. The SiC improved the heat transfer rate of the microcapsules by 7 %, and the thermal conductivity improved by 60.34 %. Zhao *et al.* (2018) formulated n-octadecane microcapsules with PMMA doped with TiO_2. It was established that while the TiO_2 improved the thermal conductivity of the microcapsules, it however led to lower encapsulation efficiency. Furthermore, another drawback of the PMMA-silica shell was that during the synthesis of this shell material, silica formed on the PMMA

surface can aggregate on the shell rather than forming small individual particles. This is an issue for thermal cycling for PCMs due to the additional stress points while the shell flexes during the cycling process, which can lead to collapse or buckling. Therefore, organic-inorganic shell hybrids must have a homogenous shell for TES applications specifically.

2.8. MICROENCAPSULATION OF PCMS

There are many defects in utilising PCMs in the conventional manner, such as surface diffusion and volume changes (Jamekhorshid, Sadrameli and Farid, 2014). Because of this, there is the necessity of utilising heat exchange surfaces or latent heat devices which in turn increases thermal resistance between the environment and the active PCM, as well as increasing the cost of the process. There have been studies carried out on form-stable PCMs, in which the PCM is blended with a supporting material (polymers), and subject to a series of further treatments (Hong, 2000; Song *et al.*, 2010). However, there is still diffusion to the surface and there is shape loss from the PCM (Jamekhorshid, Sadrameli and Farid, 2014).

As discussed, PCMs can be affected by the surrounding stimuli, and to increase their longevity, surrounding them in an inert material can preserve them. Surrounding a core component with a wall material provides the advantage of combining the properties of multiple components within a single construction, as well as protecting the core material from the environment. At the microscale level, this process is known as microencapsulation. Microencapsulation is a versatile and expedient process that segregates the core component from the environment to ensure preservation, controlled release, safety, enhanced handling and processing of a material (Dubey, Shami and Bhasker Rao, 2009; Cui and Hao, 2011; Mishra, 2015).

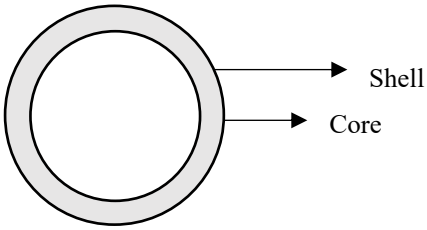

Figure 2.4 - Microcapsule illustration. Adapted from Jamekhorshid *et al.* (2014)

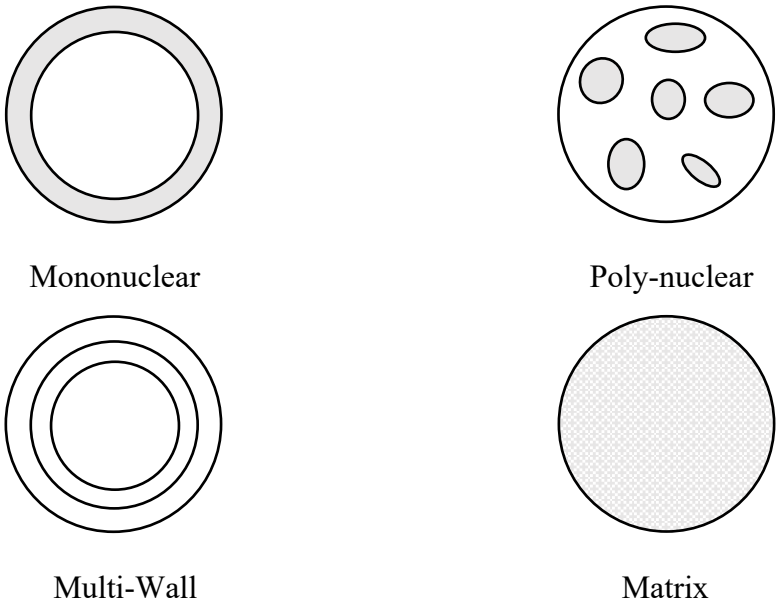

Figure 2.5 - Microcapsule morphology. Adapted from Jamekhorshid *et al.* (2014)

The first application of microencapsulation stems from the production of carbonless copy paper, and since then, many protocols have been investigated and reported (Salaön, 2013). With the utilisation of wall materials such as fats, waxes, organic polymers, and inorganic compounds, a wide range of core materials have been encapsulated (Boh, Knez and Staresinic, 2005).

As shown by Figure 2.4, an active core material is surrounded by an inert shell material. Figure 2.5 conveys the various morphologies that can be achieved with microencapsulation. Microcapsules can have either a regular, or irregular profile, and this mainly depends on the deposition process on the shell and the core material properties (Jamekhorshid, Sadrameli and Farid, 2014; Alva *et al.*, 2017).

During phase change in cold thermal energy storage systems, there is potential for leakage of the PCM to occur, and microencapsulation is the most suitable method to prevent this. Microencapsulation also increases the heat transfer rate, control PCM volume changes, reduces PCM reactivity with the external environment during the phase change process (Jamekhorshid, Sadrameli and Farid, 2014; Alva *et al.*, 2017).

Microencapsulated PCMs may be used in a powder form, or there can be dispersion of the PCM into a carrier fluid, such as water, to increase the heat capacity of the service carrier liquid considerably (Jamekhorshid, Sadrameli and Farid, 2014). This suspension method is known as Microencapsulated Phase Change Materials in Slurry (MPCS) (Jamekhorshid, Sadrameli and Farid, 2014). As there is limited thermal conductivity of PCMs, such as the paraffin-based species, there have been studies carried out to increase the thermal conductivities. Zhang *et al.* (2014) studied the utilisation of nanoparticles into the core system, which improved the thermal conductivity of the microcapsule. However, due to the small size of the nanoparticle, this created agglomeration issues in the nano-fluid, as well as instability in the system (Jamekhorshid, Sadrameli and Farid, 2014).

There are a selection of various methods to encapsulate active core materials, which are primarily split into three groups, namely chemical, physico-chemical and physico-mechanical processes (Jamekhorshid, Sadrameli and Farid, 2014). Various methods are summarised in Table 2.5, with the methods of interest emboldened. The physical methods consist of the microcapsule wall being condensed or mechanically applied to the PCM core, whereas the chemical methods consist of the core being dispersed, then deposition of the wall, followed by recovery (Jamekhorshid, Sadrameli and Farid, 2014).

Table 2.5 – Microencapsulation Methods, Adapted from Bakan (1991).

Chemical Processes	Physico-Chemical Processes	Physico-Mechanical Processes
In Situ Polymerization	**Coacervation and Phase Separation**	Spray Drying and Congealing
Interfacial Polymerization	Sol-Gel Encapsulation	Fluid Bed Coating
Poly Condensation	Supercritical CO_2 Assisted Microencapsulation	Pan Coating
		Solvent Evaporation

2.8.1. COACERVATION AND PHASE SEPARATION

This process is dependent on partial dissolution of a polymer solution into two phases, in which one phase is polymer rich (coacervate) and the other is polymer poor (coacervation medium) (Jamekhorshid, Sadrameli and Farid, 2014). There are two types of coacervation processes, namely simple and complex coacervation, and the differing factor is the phase separation process of the polymer solution.

In the simple coacervation process, the phase separation of the polymer solution can be induced by addition of a non-solvent, salt, polymer, or a change in temperature or pH level of the system. In the presence of water, the polymer rich phase (coacervate) deposits a thin film around the PCM core. Complex coacervation concerns the interaction between two polymers, in which the macromolecules contain opposite charges (Jamekhorshid, Sadrameli and Farid, 2014). The initial step for complex coacervation is the emulsion preparation via core material (usually oil) dispersion, into an aqueous polymer solution. By adding a second polymer with an opposite macromolecular charge, the deposition of the shell onto the core initiates. Thermal treatment or dissolution is the final stage, which stabilises the microcapsules by crosslinking (Jamekhorshid, Sadrameli and Farid, 2014). Figure 2.6 conveys a typical complex coacervation process diagram.

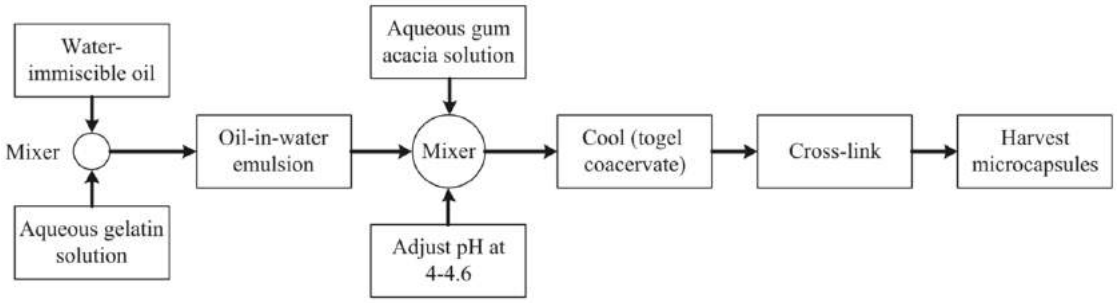

Figure 2.6 - Process Diagram for Complex Coacervation (Jamekhorshid, Sadrameli and Farid, 2014).

In the literature, it has been evident that the term 'coacervation' and 'phase separation' can be interchangeably used, and thus are seen to be synonymous terms. The coacervation microencapsulation technique was investigated by Hawlader, Uddin and Khin (2003). A microencapsulated paraffin wax was prepared, and the core-to-coating influence was studied on the effects of the characteristics of the PCM, as well as the effect on energy storage capacity, hydrophilicity, and size distribution (Hawlader, Uddin and Khin, 2003). The shell material of choice was a gelatine/gum acacia, and there was optimization of the process conditions based on the Response Surface Method (RSM) (Jamekhorshid, Sadrameli and Farid, 2014). The RSM method is a collection of statistical and mathematical techniques to empirically construct an experimental model. In various experimental procedures and simulations, Hawlader, Uddin and Khin (2003) investigated the characteristics of the MPCMs via the complex coacervation microencapsulation technique.

A similar study was carried out by Bayes-Garcia *et al.* (2010) also through the complex coacervation technique. Adding to the Hawlader, Uddin and Khin (2003) technique, Bayes-Garcia *et al.* (2010) utilised two different coacervates for the shell, which consisted of agar-agar/acacia (AA/AG) gum, and sterilized gelatine/acacia gum (SG/AG). The SEM results conveyed that the AA/AG produced smaller capsules than that of the SG/AG coacervates, which produced 12 μm capsules (Bayés-García *et al.*, 2010). The encapsulation ratio was also

studied in the experiment, which is defined as the percentage of the core PCM encapsulated by the coacervate shell material.

Further investigations were carried out by Butstraen and Salatun (2014), in which optimum parameters were established for the coacervation encapsulation process utilising acacia gum/chitosan microcapsules, with a blend of triglycerides. It was observed that the optimum conditions were pH 3.6, a 15 minute emulsification time at 11,000 rpm, and a chitosan to acacia gum ratio of 0.25 (Butstraen and Salaün, 2014).

In section 2.3.2, it was discussed that dense fatty acids, such as caprylic acid, are very effective per unit volume. Konuklu, Unal and Paksoy (2014) investigated the use of the coacervation technique to encapsulate caprylic acid, with use of various shell materials, including melamine/formaldehyde, urea/formaldehyde, and urea-melamine/formaldehyde resins (Konuklu, Unal and Paksoy, 2014). It was concluded that the urea/formaldehyde is the most effective shell material for caprylic acid (Konuklu, Unal and Paksoy, 2014).

Microcapsules were prepared by Huang *et al.* (2007) via the coacervation method, utilising gum Arabic and gelatine. In the microencapsulation process, the formaldehyde cross-linking agent in the gelatin/acacia microcapsules was altered by glycerol in the study. It was shown that there was a decrease of the gelatin/acacia microcapsule yields at any point above or below the optimum pH, and there was indication that the microcapsules were multi-dispersed, as shown by the size distribution. The study also concluded that if the pH of the continuous gelatin phase was altered above the iso-electric point, which created negatively charged gelatine, more mono-dispersed microcapsules were formed. When the pH is altered below the iso-electric point, the gelatine becomes positively charged, and becomes attracted to the negatively charged acacia, which in turn created mono-dispersed microcapsules (Huang *et al.*, 2007). Ultimately, this

study has shown the importance of pH adjustment, as it has a large effect on the particle size distribution, which is a factor to be considered with the coacervation technique.

Although complex coacervation is used to encapsulate various water-immiscible core materials such as plant oils and vitamins, there are some limiting constraints with this process to be considered. For example, this process is adversely affected by any agent that is surface active, alters the pH value in the bulk phase, or has limited water solubility. Furthermore, the shells resulting from complex coacervation processes are usually sensitive to atmospheric moisture content, and at 70 % humidity or higher, they become plasticised (Thies, 2003).

2.8.2. Interfacial Polymerization

Interfacial polymerization as a microencapsulation technique was first detailed in a study by Morgan *et al.* (1959), and the process was described to have high potential in reaching high polymer yields at ambient pressure and temperature conditions (Morgan and Kwolek, 1959; Perignon *et al.*, 2015). 60 years later, the initial articles composed by Morgan *et al.* (1959) are often seen to be the main reference source on subjects regarding interfacial polymerisation. (Morgan and Kwolek, 1959)

This technique concerns lipophilic and hydrophilic monomers polymerising on or at the interface of an oil-in-water (O/W) emulsion. A solution is prepared with the core material and a lipophilic monomer, which is then added into an aqueous solution that contains an emulsifier (Jamekhorshid, Sadrameli and Farid, 2014). This solution is then emulsified, and at this stage, a hydrophilic monomer is added into the solution. By adding the hydrophilic monomer, polymerisation is initiated, and a shell is formed. Subsequently, as the shell is formed, this becomes a diffusion barrier, thus limiting the interfacial polymerisation rate, which then

influences the uniformity and morphology of the microcapsule shell (Jamekhorshid, Sadrameli and Farid, 2014). Figure 2.7 conveys a typical process for the interfacial polymerization.

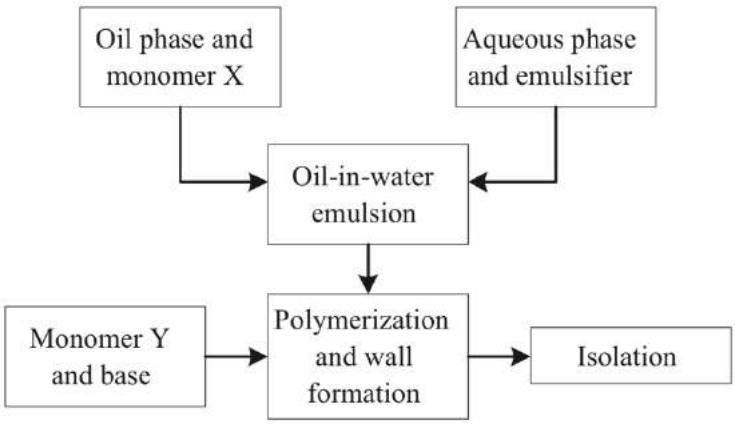

Figure 2.7 - Interfacial Polymerization Flow Diagram (Jamekhorshid, Sadrameli and Farid, 2014).

Early investigations of this microencapsulation process were carried out by Yadev, Suresh and Khilar (1990). The model was based on diffusion through the inner surface of HDMI (hexamethylene-1,6-diisocyanate), which is a hydrophobic monomer. It was shown that the permeability and the shell thickness can be changed by altering the crystallinity of the polymer.

A shell material of high interest for this process consists of urea-formaldehyde (UF) polymers. With the possibility of altering the crystallinity of the polymer, this builds upon the research conducted by Yadev, Suresh and Khilar (1990). With the preparation conditions, it is possible to control the crystallinity of the UF polymers. Tseng *et al.* (2005) investigated the encapsulation of three PCMs, namely n-pentadecane, n-eicosane, and a paraffin wax, using UF shell material. The microcapsules were formed for heat transfer and energy storage applications. The PCMs were emulsified as small droplets in a pre-polymer water-soluble UF solution, while utilising an acid-catalyst to polymerise the pre-polymer at the interface (Tseng et al., 2005). The shell and core of the microcapsules were characterized with SEM, FTIR and

DSC. It was described in the study that the larger capsules of ~ 242 μm had a much smoother profile than that of ~ 44 μm, shown in Figure 2.8 and Figure 2.9 (Tseng et al., 2005).

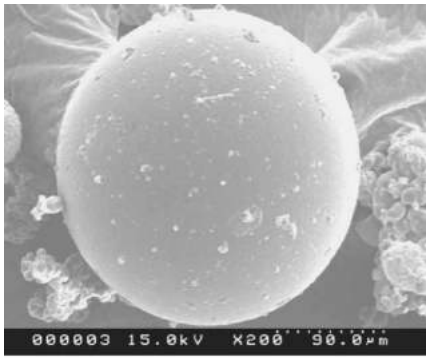

Figure 2.8 - SEM of encapsulated n-pentadecane with a mean diameter of 242μm (Tseng et al., 2005).

Figure 2.9 - SEM of encapsulated n-pentadecane with a mean diameter of 44μm (Tseng et al., 2005).

Hong and Park (1999) synthesized polyurethane microcapsules via interfacial polymerization, in an aqueous poly(ethylene) dispersion, and ethylene diamine was the chain extender of toluene diisocyanate, with poly(vinyl alcohol) (polyol) utilised as the stabilising agent. Various experimental procedures were carried out to investigate the effect that the polyol stabilising agent constituent has on the morphologies, average particle distribution and size, and loading content (Hong and Park, 1999). The purpose of the study was to design microcapsules for a sustained release of perfume oil. It was observed that higher molecular weights of the polyol gave a more porous and permeable micro-membranes due to the increase in the hydrophobic hard segments, thus conveying the effect that the molecular weight of the stabilising agent has on the capsule properties (Hong and Park, 1999).

Pasci, Garcia Valls and Giamberini (2006) prepared microcapsules of an O/W emulsion, which consisted of multifunctional carboxylic acids and epoxy resins. Using optical microscopy (OM) and SEM, the microcapsules were then characterized (Pascu, Garcia-Valls and Giamberini, 2008). It was observed that the experiments that had high stirring rates resulted in microcapsules in the range of 10 - 50 μm, whereas the lower stirring rate experiments resulted in microcapsules in the size range of 100 - 400 μm.

Although interfacial polymerization can generate high yield of microcapsules, there are still some limiting factors to consider with this process. For example, the final thickness of a shell produced by this method is limited by the diffusion of monomers through the film at the interface, and as the rate of diffusion gradually decreases with an increase in film thickness. The process is termed as 'self-limiting'. Therefore, controlling the shell thickness is dependent on the diffusion kinetics. Furthermore, the prediction of the reaction rate is made very difficult as factors such as the concentration of the monomers, reactivity of the monomers in the film, and the solubility of the polymers and oligomers in the solvent all affect the rate of reaction (Yadav, Suresh and Khilar, 1990).

2.8.3. IN SITU POLYMERIZATION

Unlike the interfacial polymerization, in the in situ polymerization process, no reactants are added to the core materials. In this process, the monomeric or oligomeric wall material is added onto the core material exclusively on the continuous side of the interface, and the core phase is dispersed to the desired size (Lee *et al.*, 2002). The polymerization of reagents located at this interface produces pre-polymers with a relatively low molecular weight, and as this pre-polymer grows in size, there is a deposition on the core oil phase, which then encapsulates the core phase (Lee *et al.*, 2002). The deposition of the pre-polymer onto the core phase can be

controlled by utilising precipitants, changing the temperature, changing the pH, or modifying the solvent quality (Nguon *et al.*, 2017).

A scheme has been identified for the preparation of a formaldehyde and urea/melamine polymeric network, as shown in Figure 2.10. In the first stage, the condensation reactions between the formaldehyde or methylene glycol (hydrated formaldehyde) and the amino-containing compound yield hydroxymethylated products, in a process termed 'methylolation', resulting in 'methylol urea' species. Substitution reactions can take place at up to three of the amide protons due to the multi-functionality of urea. Complete methylolation has not yet been reported (Nguon *et al.*, 2017). In the second stage, there is further reaction between the methylene glycols/formaldehyde and the methylol ureas, forming oligomeric hemiformals. This stage is analogous to the reaction of poly(methylene glycol) in aqueous formaldehyde solutions and is similarly hindered in the presence of alcohols (Nguon *et al.*, 2017). In the third stage, the condensation reaction between the intermediate species is promoted via the lowering of the pH, yielding ether-bridged and methylene bridged compounds. In the fourth stage, a thermoset network is assembled.

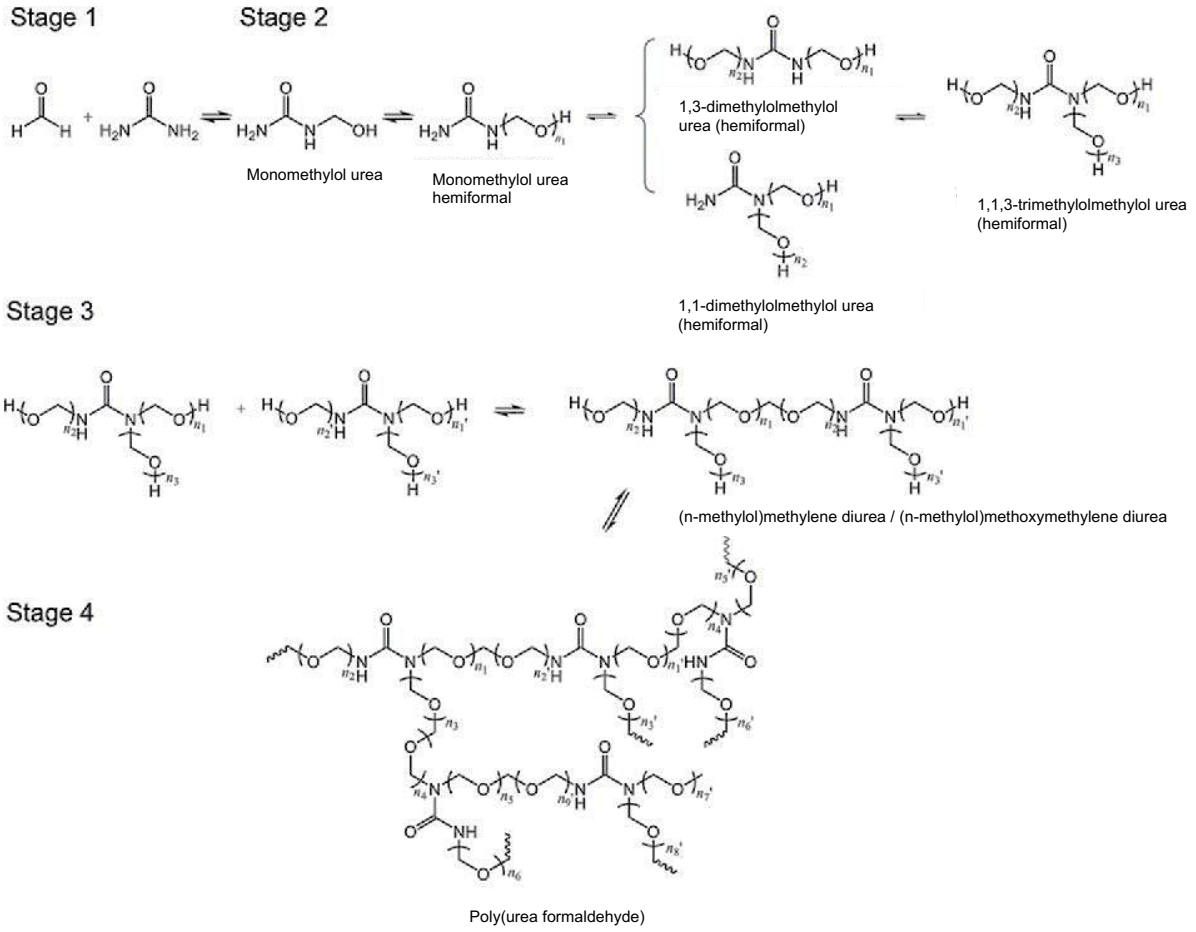

Figure 2.10 - The reaction mechanism of urea and formaldehyde to form a thermoset polymer network (Nguon et al., 2017)

The rates of the reactions taking place are dependent on the concentration of the acid or base, and by adjusting the pH during the process, one can control the advancement of each particular stage (Nguon *et al.*, 2017). The condensation of methylol urea is predominantly catalysed by acids, while the addition of urea and formaldehyde is catalysed by both acids and bases (Glutz and Zollinger, 1969). While there have been studies investigating the species formed during the polymerization process, there has not been as much work carried out that investigates the various reaction mechanisms of formation of the polymeric network.

It was demonstrated by Glutz and Zollinger (1969) that the kinetics of the reaction between urea and formaldehyde followed an acid/base catalysed mechanism. They conveyed that the rate constant exhibited minimum values at pH values between 5 and 8. Li *et al.* (2012) investigated the mechanism of the acid-catalysed reaction between urea and formaldehyde. It was observed that there were slower reactions between the urea and formaldehyde under neutral conditions, while under acidic conditions, the protonation of methylene glycol or formaldehyde catalysed the reaction, resulting in the formation of N-protonated methylol urea according to an SN2 mechanism. Nair and Francis (1983) experimentally confirmed the effect of pH on the reaction rate and reported that there is the predominant formation of methylene bridged compounds under acidic conditions, while under neutral or high pH, methylol ureas were more predominantly formed.

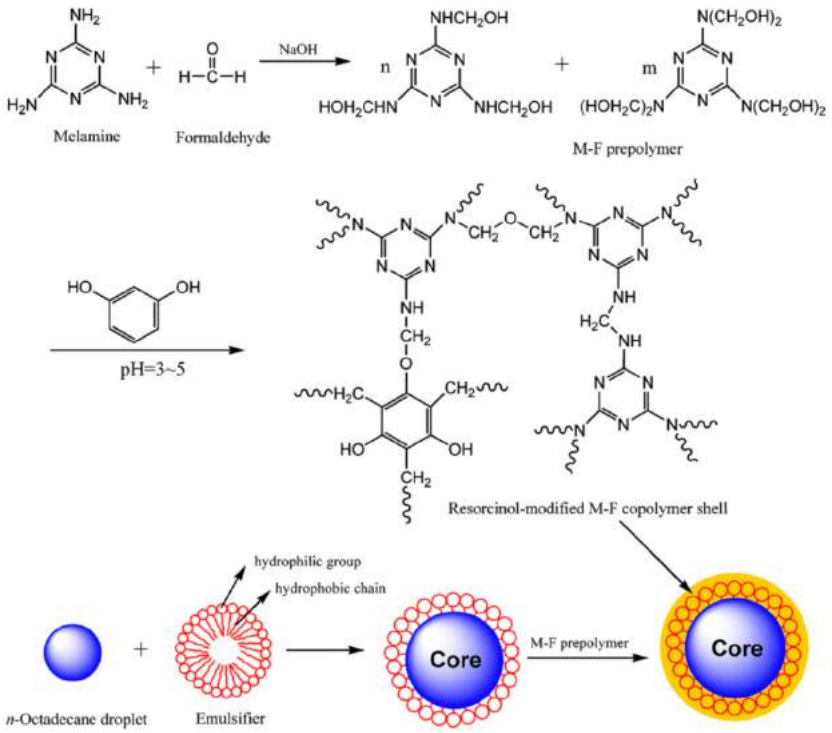

Figure 2.11 - Preparation of n-Octadecane Microcapsules via the in situ Polymerization Method (Zhang and Wang, 2009)

Zhang and Wang (2009) fabricated n-octadecane microcapsules via in situ polymerization, as shown by schematic diagram (Figure 2.11). The n-octadecane droplets are formed in an aqueous solution through emulsification, in which the hydrophilic groups of the emulsifier are arranged systematically via its hydrophobic chains, which associate with water molecules, and cover the n-octadecane surface with the hydrophobic chains orientated onto the oil droplet, and the hydrophilic chains oriented into the aqueous phase (Zhang and Wang, 2009). As the hydrolysis of the hydrophilic emulsifier groups occurs, the positively charged melamine-formaldehyde (MF) pre-polymers are attracted to the anionic carboxyl groups. The MF shell is then deposited onto the surface of the n-octadecane oil droplet via *in situ* polymerization, which was initiated under acidic experimental conditions. The resorcinol modifier was added into the solution, as the MF co-polymer is known to be brittle, to combat this and reinforce the strength of the shell material (Zhang and Wang, 2009).

Microcapsules with amino resin shells have been predominately prepared by the reaction of urea/melamine with formaldehyde. Often, the capsule synthesis is a two-step process, which primarily proceeds by the preparation of an amino pre-condensate solution in an acidic environment. Further condensation of the amino resins then leads to the formation of the polymeric network. This process is termed as ‘two-step in situ polymerization’. However, there is also a ‘one-step’ method in which the requirement of a pre-condensate is diminished, and the monomers polymerize directly in the aqueous phase. However, this process is very dependent on the surfactant used in the process, but it is very time efficient compared with the two-step method. In the literature, researchers have predominately utilised the two-step method more than the one-step method, likely owing to the sensitivity of the process with emulsifiers, leading to less ease of control (Zhang *et al.*, 2019).

2.8.3.1. TWO-STEP IN SITU POLYMERIZATION

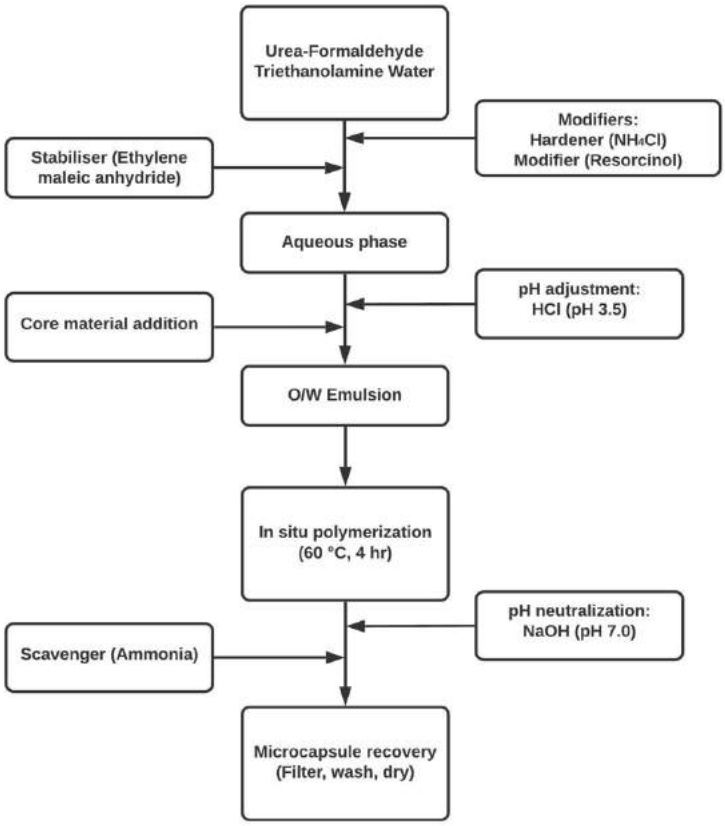

Figure 2.12 - General Flow Diagram for two-step in situ Polymerization of Microcapsules, Adapted from (Nguon et al., 2017).

Figure 2.12 conveys the common process for the microcapsule preparation via the two-step in situ polymerization procedure. The process initiates from a pre-polymer (pre-condensate) aqueous solution, which in this case consists of urea and formaldehyde. Triethanolamine is used to modify the pH to ~ 8-9. Subsequently, modifiers are added, which are species used to modify the polymeric shell properties. In this case, ammonium chloride is added as a hardener, and resorcinol has the property of making the shell water resistant, and promotes branching (Nguon *et al.*, 2017). Prior to the addition of the core material, the pH is then modified to an acidic range (~3.5) with the addition of hydrochloric acid. With the use of mechanical stirring, emulsification is achieved.

Nguon *et al.* (2017) states that the encapsulation process can also be initiated after the dissolution of the urea monomer species, with formaldehyde being added into the solution after emulsification had initiated. By changing the temperature and/or altering the pH of the solution, encapsulation is initiated. As there may be unreacted formaldehyde (less than 0.1% typically), scavengers are added to remove this. The microcapsules are then finally recovered via filtration, washing and drying (Nguon *et al.*, 2017).

There has been an array of researchers formulating microcapsules via the two-step synthesis route. For example, Guo, Zhao and Wang (2005) formulated UF microcapsules with a tetrachloroethylene and phthalocyanine green (PPG) core material, for electric field responses. The influences of various emulsifiers were investigated, and it was found that the lipophilicity of the PPG particles was improved due to their surface modification with octadecylamine (Guo, Zhao and Wang, 2005). Furthermore, the interfacial tension between the tetrachloroethylene and water with the UF pre-polymer reduced from 43 to 35 $mN.m^{-1}$, indicating surface activity properties for the polymer. Microcapsules were formulated with agitation rates of 1000 and 600 rpm, with mean diameters of 11 and 155 μm respectively.

Fang *et al.* (2009) utilised the two-step in situ polymerization process to formulate nanocapsules with an n-tetradecane PCM core. Sodium dodecyl sulphate was employed as the emulsifier, with resorcinol as the modifier. The SEM images amalgamated conveyed that the nanocapsules had a mean size of approximately 100 nm, and that the core was well encapsulated. Further DSC analysis proved that the mass content of the microcapsules was 60 %, and a latent heat of fusion of 134.15 $kJ.kg^{-1}$. TGA measurements insinuated that the thermal stability of the nanocapsules can be further improved by the addition of NaCl.

An array of MF microcapsules containing n-hexadecane cores were formulated via two-step in situ polymerization by Salaün *et al.* (2009). Partially etherified MF resin was used as the pre-condensate, and various reaction parameters were studied, such as pH, stirring rate, surfactant type/ratio, reaction time and core/shell ratio. It was indicated from the results that the most optimum parameters were a binary emulsifier mixture of Tween-20 and Brij-35 and pH 4. A stirring rate of 9500 rpm produced microcapsules with an average size of 7 μm.

2.8.3.2. ONE-STEP IN SITU POLYMERIZATION

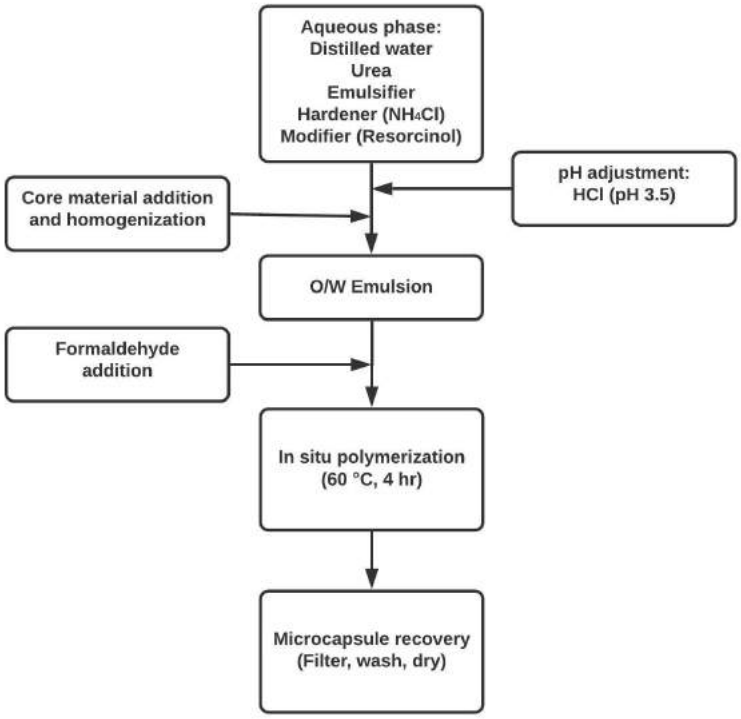

Figure 2.13 - General Flow Diagram for one-step in situ Polymerization of Microcapsules.

Figure 2.13 conveys the common process for the microcapsule preparation via the one-step synthesis route. Unlike the two-step route, a pre-condensate is not required. In this case, the modifiers and the urea/melamine shell material are added into the aqueous phase until dissolved, and pH adjustment to an acidic environment proceeds. Following this, the core material is added and homogenised, stabilized by the surfactant and creating an oil-in-water

(O/W) emulsion. Formaldehyde is then incorporated into this mixture, and the process is heated up to initiate the polymerization procedures. This is a much more time- and cost-efficient process than the two-step process, which is a great consideration for industrial and large-scale application. However, this process is much more sensitive to emulsifiers, as there is no pre-condensate produced. The sensitivity of emulsifiers can often make this process difficult, especially when encapsulating volatile core materials with very high vapour pressures as the emulsifier must stabilise the core content sufficiently and enable the polycondensation process to occur robustly.

Early work carried out via the one-step method was pioneered by Brown *et al.* (2003), in which dicyclopentadiene was encapsulated with a UF shell. Ethylene-maleic-anhydride (EMA) was utilised as the emulsifier, with agitation rates varying from 200 – 2000 rpm, and a pH of 3.5. The reaction was carried out for 4 hours at 55 °C. Microcapsules with an average diameter of 10 – 1000 μm were achieved with the variation of the agitation rates. The morphology of the microcapsules was observed to have a rough exterior, and a smooth inner membrane. This was seen to be a common feature for the amino resin microcapsules, as indicated by Han *et al.* (2001). As the agitation rate increased, the average diameter of the microcapsules decreased. The microcapsules had high yields of 80 – 90 %, and a fill content of 82 – 93 %. Furthermore, Brown *et al.* (2003) monitored the MC formation by optical microscopy and the evolution of temperature and pH during the reaction. It was observed that the polymerization initiated with an increase in temperature, and a lowering of the pH of the aqueous phase. As the reaction proceeded, the oligomeric water soluble species was formed and deposited onto the core. Brown *et al.* (2003) then stated that the interfacial tension between the aqueous continuous phase and the hydrophobic core acted as a driving force for the deposition of the polymer. As the colloidal particles grew, they became less water soluble and the rate decreased, until the reaction

completed, and the core material was encompassed. This gave a phenomenological description of the wall; however, the actual reaction mechanism remains a subject of interest and further discussion.

2.9. Effect of Emulsifiers on Microencapsulation Process

Colloidal dispersions of at least two immiscible liquids are termed as an 'emulsion'. In the case of this work carried out, the mechanism is an oil-in-water (O/W) emulsion. Naturally, O/W emulsions are thermodynamically unstable due to the high interfacial area of the dispersed phase. Emulsifiers, which include natural polymers such as proteins/polysaccharides, and chemical surfactants, are commonly utilised in microencapsulation processes to reduce the interfacial tension between the two immiscible phases (Sharipova *et al.*, 2017).

Emulsifiers can have a negatively charged polar head group (anionic) or a positively charged head group (cationic), or uncharged (non-ionic). When the charged emulsifiers surround the oil core material droplets in the aqueous phase, the negative or positive charges outside of the oil droplet electrostatically repels the aqueous phase binding to the oppositely charged head group. Non-ionic emulsifiers tend to have bulky head groups that point away from the oil droplets, which then tangle with the other head groups in the water phase, in a process termed as 'steric hindrance' (Sharipova *et al.*, 2017). Generally, depending on the application, anionic emulsifiers are often used in alkaline solutions, while cationic emulsifiers are typically employed in low/neutral pH conditions (Costa *et al.*, 2019). Non-ionic emulsifiers can also be synergistically employed with charged emulsifiers to enhance solution stability.

An expedient parameter to deliberate while optimizing the stability of O/W emulsions known as the hydrophile-lipophile balance (HLB). This parameter was first introduced by Griffin (Mohamed *et al.*, 2017). In a molecule, the HLB balance is calculated from the weight percentage of the hydrophilic groups to the hydrophobic groups (Nguon *et al.*, 2017). The most stable O/W emulsions in which surfactants are used are best formulated when the emulsifier or a combination of emulsifiers have HLB values close to that of the oil phase (Mohamed *et al.*, 2017). Typically, the HLB is affected by both the oil content and the amount/type of emulsifier used, as the lipophilic portion would be affected. Conventionally, surfactants with HLB values of 3 to 6 are used for O/W emulsions, and surfactants with HLB values of 7 to 20 are used for O/W emulsions (Schmidts *et al.*, 2010). However, this parameter does not consider the ionization as a function of pH, the temperature influences, and the concentration of the emulsifier.

As mentioned previously in section 2.8.3.2, a widely used emulsifier for the encapsulation of PCMs is PEMA, pioneered by Brown *et al.* (2003). Alternative compounds to PEMA were investigated by Yoshizawa *et al.* (2007). It was claimed by these researchers that it is imperative for the surfactant to have carboxyl groups, or maleic anhydride groups that hydrolyse to form carboxyl groups, for the formation of a crosslinked PUF microcapsule to be successful. They also stated that another important property of the surfactant was that it should have a high molecular weight, to aid the core material stabilization. However, this PhD project repudiates these claims, and the work carried out will convey that it is not necessary for there to be carboxyl/maleic anhydride groups for the successful production of PUF microcapsules with a more volatile core.

Further proof that anhydride or carboxyl groups are not necessary or pivotal was provided by Zhang *et al.* (2019). A series of emulsifiers, including hydrocolloids and synthetic polymers were utilised to synthesise volatile n-heptane cryoPCM microcapsules. Microcapsules with exceptionally large payloads were produced with emulsifiers lacking the anhydride/carboxyl groups, such as methyl cellulose and gelatin. Furthermore, when poly(ethylene-alt-maleic-anhydride) (PEMA) was utilised for the n-heptane core, there was very poor retention, and a porous shell was produced with poor barrier and mechanical properties. In the literature, many authors have used PEMA to synthesise microcapsules, however usually for less volatile core materials (Boh, Knez and Staresinic, 2005; Yoshizawa *et al.*, 2007; Wang *et al.*, 2013; Yin *et al.*, 2015; Fayyad, Almaadeed and Jones, 2016). Moreover, the findings in this work provide the fundamental discernments onto the role that emulsifiers have on this one-step process and increases the range of selective criteria.

Fan, Tang and Zhou (2013) studied the effect of poly(ethylene-alt-maleic-anhydride) (PEMA), sodium dodecylbenzene sulfuric (SDBS) and Gum Arabic (GA) emulsifiers on the one-step in situ polymerization of tetrachloroethylene. They observed that the SDBS and GA yielded microcapsules with much smaller size distributions than PEMA. Furthermore, the microcapsules produced with PEMA produced very rough microcapsules, with thicker shells, which is completely undesirable for the heat transfer processes in TES, due to the increased heat transfer barrier and reduced shell flexibility for the thermal cycling processes. Fan, Tang and Zhou (2013) stated that the carboxyl groups on the PEMA emulsifiers are likely to catalyse the polymerization process, and create large-chained polymers, resulting in the thicker and rougher shell.

Wu, Xu and Zhang (2018) studied the effect of emulsifiers on the encapsulation of n-dodecanol PMCs with an MUF shell. OP-10 and Tween-20 were used as non-ionic emulsifiers, while styrene maleic anhydride (SMA) was used as the anionic emulsifier. It was observed that increasing the amount of SMA led to smoother surface morphology and led to a narrower size distribution. Furthermore, it was observed that OP-10 and Tween-20 had little effect on the size distribution. Wu, Xu and Zhang (2018) claimed that the ionic groups on the SMA attracts the MUF shell material, as the MUF pre-polymer exhibits positive charges due to the reaction between the hydrogen ions and hydroxymethyl ions, yielding smoother MPCMs.

2.10. SUPERCOOLING PHENOMENA

Supercooling is a shift of the onset temperature required to freeze the PCM, which results in a significant reduction in the overall thermal efficiency of the thermal management system, as well as a longer thermal discharge period (Peng *et al.*, 2020). Many materials undergo the supercooling phenomenon, and the degree to which they supercool is related to their nucleation and solidification mechanisms. The degree of supercooling is influenced by the sample homogeneity, the sample size, the cooling rate, and the purity (Farid *et al.*, 2004b).

It is fundamental to understand the crystallization process in order to comprehend the supercooling phenomena. In terms of MPCM crystallization, there are various stages of crystallization; induction phase, crystal growth phase, and crystal regrowth stage (Al-Shannaq *et al.*, 2015). During the induction phase, nucleation centres are formed, in which nuclei are formed until they grow to a stable and sufficient size. During the crystal growth phase, the crystalline PCM then diffuses towards the nucleus, and there is PCM adsorption onto the surface of the nuclei, leading to an increase in the size of the nucleus. The material adsorbed onto the surface then migrates along the surface, until it is incorporated into a crystal form (Al-

Shannaq *et al.*, 2015). As time passes, the small crystals then grow and eventually become numerously sufficient and large enough to sustain rapid crystal growth. As the freezing process nears completion, the rate of crystallization reduces. During the crystal regrowth phase, even after the material is totally frozen, there is a redistribution process in which the nuclei continue to modify the particle shape and the size distribution (Al-Shannaq *et al.*, 2015).

The crystal growth of the PCM is governed and regulated by the size of the liquid droplets after nucleation (Zahir *et al.*, 2019). The effect of capsule sizes on the crystallization temperature of MF microcapsules was investigated by El Rhafiki *et al.* (2011). The microcapsules were produced with a diameter range of 5 – 1000 μm. The degree of supercooling for the samples were the same for the capsules in the range of 100 to 1000 μm, however the supercooling increased for the samples in the range of 5 – 100 μm. Therefore, as the microcapsule size decreased, the supercooling degree increased, which is in agreement with other bodies of work carried out (El Rhafiki *et al.*, 2011; Al-Shannaq *et al.*, 2015; Zahir *et al.*, 2019).

Organic PCMs in their pure form do not exhibit significant supercooling, whereas inorganic PCMs, such as salt hydrates, experience significant supercooling (Farid *et al.*, 2004b). Organic PCMs often exhibit congruent melting and homogenous nucleation, meaning that they can melt and freeze with little or no supercooling, without the degradation of the latent heat of fusion (Kenisarin *et al.*, 2020). During homogenous nucleation, a new phase is spontaneously formed as soon as the nuclei grow to a sufficient size.

Eutectic PCMs often exhibit phase separation during the supercooling process (Huang *et al.*, 2019). The terms phase separation and incongruent melting (incongruent phase transition) are typically referred to interchangeably and have been studied by a number of researchers (Lane and Shamsundar, 1983; Mohamed *et al.*, 2017; Huang *et al.*, 2019; Zahir *et al.*, 2019).

Incongruent melting is defined as when a new liquid and solid phase of a different composition may precipitate from the original composition with each melting/solidification cycle, with increasing precipitation as the cycles increase (Tan *et al.*, 2020). The new compositions, in severe cases, may exhibit different melting points from the original mixture. Therefore, there is resultant degradation in the storage capacity, unless the temperature is attuned, and the initial composition is restored again (Tan *et al.*, 2020). To achieve this, typically the material is bought to a completely liquid state, and then mixed. However, phase separation can be alleviated by ensuring the initial composition is adjusted to circumvent the region of incongruent melting, in which phase diagrams are very useful in this case (Tan *et al.*, 2020).

As discussed, pure paraffin without encapsulation exhibits very little supercooling. The amalgamation of a shell material over the paraffin PCM, which is essentially geometric confinement, gives rise to the supercooling phenomena (Peng *et al.*, 2020). Furthermore, the control of the size of the MPCMs to be large enough to minimize the effects of supercooling can also be a solution, however some MPCMs with large diameters may not function optimally in various processes due to the risk of low mechanical integrity and risk of rupture (Al-Shannaq *et al.*, 2015). Consequently, MPCMs with a suitable diameter and a low degree of supercooling has been receiving increasing attention (Al-Shannaq *et al.*, 2015). To overcome this issue, usually nucleating agents or additives are incorporated into the PCM prior to the microencapsulation process.

There have been efforts made by researchers to reduce the supercooling phenomena for the microencapsulated PCMs. For example, Chen *et al.* (2019) reduced the supercooling degree of MUF microcapsules with an n-octadecane core by incorporating alkylated graphene into the

core. This then promoted heterogeneous nucleation, and advanced the onset crystallization of the core, reducing the supercooling degree.

An investigation was conducted to supress supercooling on n-tetradecane MPCMs with the use of tetradecanol and silica fume (Alvarado *et al.*, 2006b). The MPCMs were formulated via two-step in situ polymerization, with an MF shell. It was indicated from the results that 1 – 4 wt. % tetradecanol greatly reduced the supercooling phenomena, whilst 0.2 wt. % of silica fume was ineffective.

Additionally, the degree of supercooling for MPCMs with an MF shell and n-dodecane core was reduced significantly when 2 wt. % of 1-tetradecanol was added as a nucleating agent (Yamagishi *et al.*, 1996a). Following this, the effect of other nucleating agents was observed in another study. It was observed that supercooling was significantly reduced with the addition of 9 wt. % 1-octadecanol into the core material, and the addition of 2 wt. % sodium chloride in the emulsion (Zhang *et al.*, 2005a). However, it was observed that the surface roughness of the microcapsules greatly increased, and there was poor aqueous dispersion.

Plentiful studies have also exhibited that nanoparticles dispersed in PCMs as nucleating agents can also significantly subdue supercooling (Yu *et al.*, 2014). Mo *et al.* (2013) studied the effect of several nanomaterials (SiB_6, BC_4, SiO_2, ZrB2, Si_3N_4 and AlN) as nucleating agents for sodium trihydrate. The results indicated that the addition of 10 wt. % ZrB2, 4 wt. % Si_3N_4 and 5 wt. % AlN completely eliminated the supercooling. Furthermore, it was shown that 2 wt. % of SiO_2 ultrasonically dispersed and melted in the PCM also eliminated the supercooling. Following this, Wu *et al.* (2009) investigated three different types of SiO_2 nanoparticles to study the surface effects of the interaction between the nanoparticle and hydrate salts during the phase change process. The most effective and stable nucleator was seen to be aerosol SiO_2. Overall,

the supercooling of hydrate salts was seen to be easily supressed via the nano-additives, due to the strong polar hydroxyl bonds on the surface and high specific surface area.

2.11. MPCM HEAT TRANSFER FLUIDS

The dispersion of an MPCM into a carrier fluid creates a suspension known as a 'microencapsulated phase change slurry' (MPCM slurry). The latent heat of the carrier fluid is enhanced when MPCMs are dispersed in the suspension (Zhang, Ma and Wang, 2010). The most used latent heat transfer fluid (LHF) is water, due to its sheer abundance, relative inertness, low cost, and chemical safety (Chandrasekaran et al., 2014). This is particularly interesting area in the thermal storage sector, as it yields many benefits. Such advantages of latent heat transfer fluids (LHF) include (1) higher heat transfer rates due to the phase change process, (2) heat exchange processes occurring at nearly constant temperatures, (3) lower required pumping power as a consequence of decrease in mass flow, (4) the high surface/volume of the MPCMs resulting in high heat transfer rates, and (5) a reduction in heat loss reducing the need for extra heat exchangers and process equipment (Delgado, Lázaro, Mazo, Marín, *et al.*, 2012).

Huang *et al.* (2011) deliberated the recommended properties that a MPCM slurry should have, stating that the phase transformation temperature range should match the designed operating temperature range, there should be little or no supercooling, small pressure drops in pump systems, high heat transfer rates and high heat transfer areas. Furthermore, the slurry should have long term storage stability, and present reversible melting/freezing cycles under thermal loads.

Although the use of MPCM slurries presents abundant advantages, there is arguably a lack of technical experience (Delgado, Lázaro, Mazo, Marín, *et al.*, 2012). The main issues currently

in this area involve the supercooling issues and thermal instability. Regarding the current level of literature, the main numerical studies agree that the most influential parameter is the Stefan number, but it is considered that other factors such as PCM concentration and the phase change temperature ranges also need more investigation (Delgado, Lázaro, Mazo, Marín, *et al.*, 2012). Rao *et al.* (2007) determined that in low mass flow rates, PCM slurries provided better cooling performance, and when the PCM concentration was increased, there was an increase in the convective heat transfer coefficient, similar to that of water. However, with the higher mass flow, deteriorated cooling performances ensued. Wang *et al.* (2007) carried out an experimental study that conveyed the increase of the heat transfer coefficient under both turbulent and laminar conditions, while Alvarado *et al.* (2007) attained lower heat transfer coefficients for the same velocities under turbulent conditions.

Other work carried out in similar conditions include the work carried out by Heinz and Streicher (2006) and Diaconu, Varga and Oliveira (2010). In the work carried out by Heinz and Streicher (2006), natural convection was compared to water in a tank with a spiral-type heat exchanger unit, with MPCM slurries with 20, 30 and 40 % PCM compositions, and a melting point of approximately 60 °C. In the work carried out by Diaconu, Varga and Oliveira (2010), natural convection was compared to water in a tank with helically coiled tube heat exchanger with an MPCM slurry with 45 % MPCM concentration, and a melting point of approximately 6 °C. In the first case, the natural convection was unilaterally worse for all the PCM concentrations, and in the second case the coefficient vastly improved during the phase change process when compared to water. Initial analysis from the literature suggests that currently, the effects that influence the heat transfer phenomenon are not completely clear yet. For example, the PCM concentration in the slurries seem to have opposite effects. On one hand, an increase in the

PCM concentration increases the viscosity and reduces thermal conductivity, deteriorating the heat transfer coefficient, while on the other hand an increase can cause enhanced heat capacity.

Viscosity measurements and rheological measurements must be considered as these factors play a significant role in determining the characteristics of the fluid flow. The Grashof and Reynolds numbers are chief parameters while deliberating fluid flow characteristics for the slurries. The Grashof number describes the ratio of buoyant forces to viscous forces, while the Reynolds numbers depicts the inertial forces to viscous forces (Dutkowski and Kruzel, 2019). Higher viscosity leads to a higher pressure drop, which leads to a higher requirement of pumping power. An increase in viscosity also leads to reduced turbulence of the slurry, which in turn reduces the heat transfer coefficient. Various numerical studies have been carried out to assess the corelation between the MPCM slurry viscosity in relation to the temperature, the size of the microcapsules and the concentration of microcapsules (Zhang and Zhao, 2011; Dutkowski and Fiuk, 2019; Dutkowski and Kruzel, 2019). As currently in the literature there is no commonly used and generalized equation equations to calculate the viscosity of the MPCM slurry, experimental data and numerical modelling of thermal flow has been useful to describe various correlations (Dutkowski and Kruzel, 2019).

In terms of pump power requirements, the ratio between the heat transported (Q) and the pumping power (W) are principal factors. For a laminar regime, the Q/W power is larger than in a turbulent regime (Inaba, Kim and Horibe, 2004). According to the literature survey, the majority of the published suggest that that when the volume fraction of the MPCM dispersed in the slurry is less than 25 %, Newtonian behaviour is observed (Zhang, Ma and Wang, 2010). Above approximately 30 %, shear thickening behaviour is generally observed (Zhang, Ma and Wang, 2010).

Other parameters of interest to reflect the heat transfer characteristics of MPCM slurries include the Nusselt number, heat transfer coefficient and wall temperature. The thermal properties of MPCM slurries were investigated by Zhang and Niu (2016). The MPCM slurries were utilized in a stratified water storage tank and a slurry storage device. It was shown that the PCM microcapsules had a high thermal storage capacity. Furthermore, Xu and Yang (2019) formulated MPCMs with carbon nanotubes as the shell material for the use in solar collectors. It was indicated that the slurry had excellent photothermal conversion performance, and very high heat storage capacity.

There are also other studies to propose that the phase change process for the MPCM slurries can also significantly change the viscosity characteristics of the suspensions (Dutkowski and Kruzel, 2019).The effect of concentration and temperature of an emulsion containing a paraffin was experimentally investigated by Wang, Fang and Zhang (2018), in which he noted that exceeding the melting point of the paraffin resulted in an increase of the viscosity of the suspension. After the melting point was exceeded further, there seemed to be a reversal in the viscosity profile, which took place regardless of the mass fraction of the emulsion ingredients. Similar results were observed by Huang, Doetsch and Pollerberg (2010) in which the viscosity curve as a function of temperature was deliberated. The viscosity and the paraffin phase change emulsion seemed to correspond to the freezing point peak, as evidenced by differential scanning calorimetry (DSC) analysis. Huang and Petermann (2015) also conducted a study on 15 – 20 wt. % RT10 emulsion viscosities during the phase transition period at constant shear rates and temperature ramp tests, in which the viscosity of the emulsion was observed to increase at the onset freezing temperature.

2.12. CHAPTER SUMMARY

In this chapter, a literature review was carried out and reviewed the classifications of PCMs, and each category's main advantages and disadvantages, and their unique roles of contributing to the TES field. Various methods of microencapsulation methods were also assessed and analysed, each with various applications.

It was gathered that although the one-step in situ polymerization process is a time-efficient process, various reaction mechanisms have not yet been explored deeply in the literature, which is a potential area of focus. The role of emulsifiers and modifiers and how these may affect the microcapsule morphology and core material retention was also deliberated. The challenges with the one-step in situ polymerization process herein lie in the difficulty to encapsulate volatile core materials, such as paraffins.

Furthermore, it was observed that supercooling poses as a challenge and barrier for the practical employment of MPCMs in this field and is an area that is also of great interest. In the literature, it was observed that there have been efforts made to reduce the supercooling phenomena of MPCMs, in the form of nanomaterials and nucleating agents, however this is still an area that can be improved upon to increase the potential scope of application. The rheological implications for MPCM slurries were also evaluated, as this is an area of consideration in terms of practical applications, i.e., required pumping requirements and tube sizing.

Overall, this chapter provides the reference sources and fundamental research areas for the subsequent chapters of this thesis. Theis chapter also provides a benchmark in the current level of research in this field, analysing potential gaps in literature and work that can be further built upon.

CHAPTER 3: EXPERIMENTAL METHODS

3.1. OVERVIEW

This chapter provides a detailed overview of the methods and techniques employed to carry out this study. The one step in situ polymerization method is deliberated, as well as the experimental set up, and the procedures executed. Furthermore, the quantitative identification of the payload, encapsulation efficiency and the yield of the microcapsules is exhibited. This chapter also details the analytical characterization methods performed to evaluate the microcapsule properties, as well as the mechanistic study between the reactants in the one step in situ polymerization process. Finally, the methods employed to characterize the phase change material slurry, and the rheological properties are conferred.

3.2. PCM MICROCAPSULE FORMULATION AND ANALYSIS METHODS

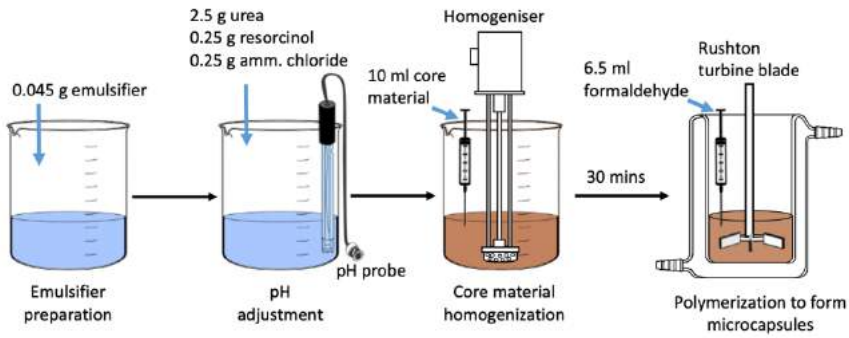

Figure 3.1. The one-step in situ polymerization process for the formulation of PCM microcapsules.

All the capsules synthesized in this study were formulated via the one-step in situ polymerization, and unless otherwise stated or specified, all the materials used in this process were used without further modification or purification. The emulsifier solutions were prepared prior to the experiment, by weighing the required amount of emulsifier and dissolving it into 150 g of distilled water, which was then dispersed into a 200 ml beaker.

A Sartorius Secura 124-IS Analytical Balance, with an acceptance of (+/−) 0.0005 g, was used to measure 2.5000 g urea, 0.2500 g ammonium chloride, and 0.2500 g resorcinol, which were then were assimilated into the previously prepared solution. Using an IKA RCT magnetic stirrer, the solution was stirred until it was completely clear. Subsequently, the pH was needed to be adjusted to the required value using a Mettler Toledo FiveEasy pH meter. Using a RS PRO 5 ml Pipette, HCl was added dropwise into the solution to adjust the pH to 3.5 ± 0.1. However, if the pH went below the required value, NaOH was required to elevate the pH level (addition of NaOH was avoided unless necessary, to avoid increasing solution ionic strength). The pH was left to stabilize for 5 minutes.

During the stabilization period, the core material was prepared. Nile red was dissolved in 10 mL heptane via ultra-sonification for 5 minutes. Nile red was dispersed into the core as a non-destructive core material retention indicator, based on the method proposed by Zhang et al. (2018). After the 5 minutes of pH stabilization, the 150 ml beaker was then placed under a Silverson L5M homogenizer under fume hood conditions. The homogenization was initiated, and the core material was injected into the 150 ml solution via a 10 ml syringe. This was left for 20 minutes to fully disperse the core material into the solution.

Successively, 6.5 ml of formaldehyde was measured into a 10 ml syringe. After the 20 minutes proceeded, the homogenised solution was transferred into a 250 ml jacketed beaker, which included a stainless steel 4 finned baffle to stimulate mixing. This was connected to a Julabo ME-F25 water bath. A Rushton turbine agitator blade (IKA R3004 30 mm diameter) connected to an IKA MINISTAR 20 Control Mixer was used to keep the emulsion stabilized, with a stirring speed of 600 rpm. The formaldehyde was injected into the jacketed beaker, and the program was set on the water bath to initiate the reaction. The program consisted of the temperature being maintained at 20 ºC for 30 mins, and then at a rate of 1 ºC.min^{-1}, the temperature was raised to the required reaction temperature. The temperature was held at the set temperature for the duration of the reaction time, and then cooled down to 20 ºC at a rate of 1 ºC.min^{-1}.

After the reaction concluded, the products were centrifuged 4 times at 5000 RPM with a Labnet Z-306 Hermle Universal Centrifuge, for 5 minutes each time. A vacuum filter was then used to wash the samples, with 5 l of warm water. Once the capsules were formulated successfully, they were re-dispersed in distilled water and kept in centrifuge tubes, which could then be dried and used for further characterization when needed.

3.3. Microstructure and Chemical Characterization

3.3.1. Optical and Fluorescence Microscopy (OM and FM)

The optimal images of the microcapsules were obtained from a Leica DMRBE microscope, attached to a Motic Pro 252 microscope camera. Figure 3.2 conveys the illustrative and schematic representation of the microscope configuration and components. As nile red was dispersed into the core material, the emission spectra of the nile red were gathered with a

CoolLED pE-300 SB LEDs illumination system, which was fitted onto the microscope, with an excitation maxima of 460 nm. In this case, nile red can be used as a core material indicator, employing the principle of solvatochromism (Zhang *et al.*, 2019). Solvatochromism is a phenomenon on which the fluorescence and/or absorbance spectrum of a molecule is directly dependant on the surrounding solvent environment. Nile red is a particularly effective solvatochromic dye, which contains an exocyclic diethylamine group, and a rigid aromatic group, with intense solvent dependent properties, alluding to it being a highly fluorescent laser dye. By emitting a blue light to the non-solvated form of nile red, it appears with a distinct red colour. However, in its solvated form (e.g. dispersed in heptane), this appears a distinctive green colour. Subsequently, a distinctive green colour under the current FM conditions would allude to there being core material present in the capsules, which can be used as a non-destructive indicator for capsule core material retention properties (Zhang, *et al.*, 2019).

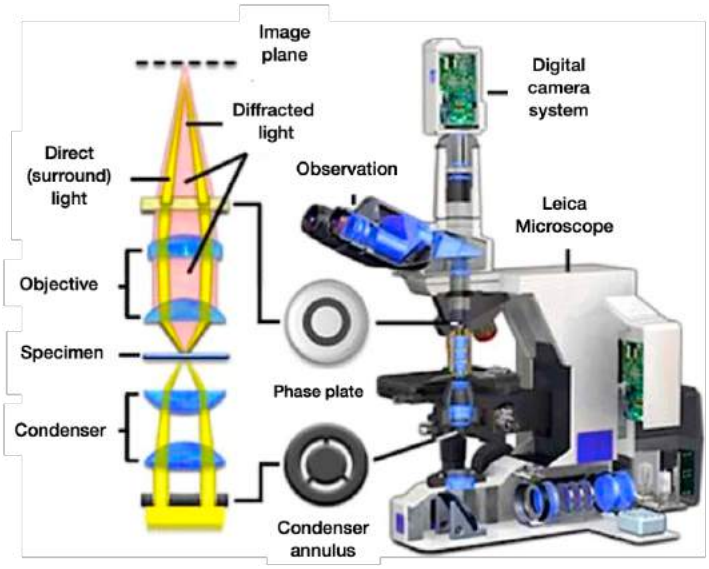

Figure 3.2. Optical microscope configuration diagram. Adapted from (Di Gianfrancesco, 2017).

3.3.2. SCANNING ELECTRON MICROSCOPE (SEM)

The morphology and shell thickness of the microcapsules were characterized with a Hitachi TM3030Plus Tabletop SEM, with a highly sensitive 4-subdivision backscattered electron detector. Before the SEM investigation, the capsules were coated with 5 nm of gold using a Quorum Q150R ES gold sputter, utilising argon as the inert gas, with a pressure of 0.5 bar. The operating voltage was 15 kV, with various magnifications from 100x to 5000x. Image J was used to process the images where the shell roughness was examined, in which the contrast enhancement was utilised to convey the surface particles as purely white, and the smoother shell as black, in which the ratio between the white and black area conveyed the percentage of surface particles.

The acquisition of signals produced by the electron beams interacting with the specimen is what determines the image formation in the SEM (Zhou *et al.*, 2007). The interaction of the electron beam and the sample are divided into two categories: elastic and inelastic scattering. Back scattered electrons (BSE) consist of very high-energy electrons from the electron beam that collide with the sample and are either back scattered or reflected from the specimen, leading to elastic scattering (Goldstein *et al.*, 2017). As light elements (with lower atomic numbers) backscatter the electrons weaker than heavier elements (with higher atomic number), these samples appear lighter in the SEM image (Goldstein *et al.*, 2017). Therefore, BSE electrons are very useful for the detection of chemical compositions shown by the vast contrast variations in the image. In contract, inelastic interactions between the electron beam and the sample surface have lower energies than the backscattered electrons (Zhou *et al.*, 2007). Secondary electrons are useful for topographic analysis of the sample surface. Figure 3.3 conveys the electron interaction with the samples, as well as the schematic representation of an SEM microscope.

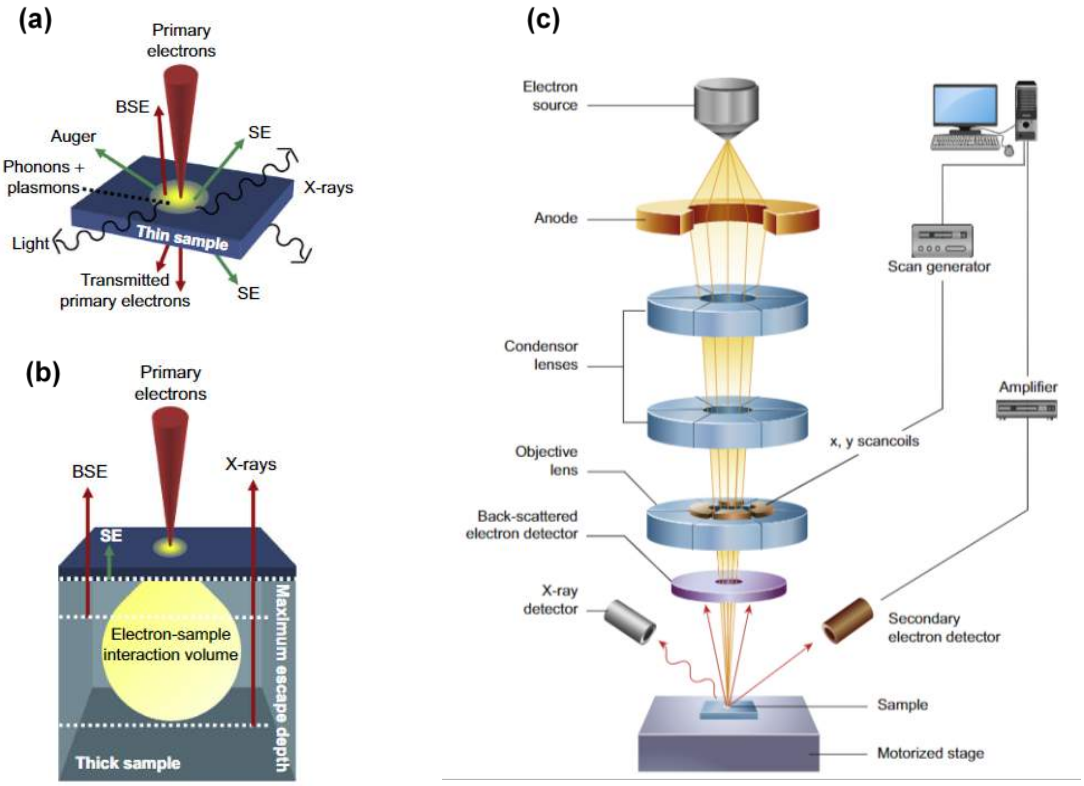

Figure 3.3. The primary electrons interacting with the sample, and the types of electrons transmitted (a); the absorption of primary electrons for thick samples, showing the profile difference for the SE and BSE (b); the schematic representation of an SEM microscope.

3.3.3. Fourier-Transform Infra-red Spectroscopy (FTIR)

To study the chemical structural components of the samples, Fourier transform infrared spectroscopy was used (Bruker FT-IR Microscope LUMOS 11) at a wavelength range of 400 to 4000 cm^{-1} in transmission mode. The samples were compressed in a punch die using a Lloyd X materials Testing Machine, with a force of 80 kN at 10 $mm.min^{-1}$ for 120 s. The tabletted sample was then placed directly into the sample holder, onto the path of the IR beam.

When the IR radiation passes through the sample, some radiation passes through the sample (is transmitted), and some is absorbed by the sample. As the photons transfer onto a molecule and get excited to a higher energy state, these excited states result in the vibrations of various

molecular bonds, e.g., twisting, bending and stretching occurring at various wavenumbers. The intrinsic physiochemical properties of the corresponding molecules are the determining factors of the transmitted peaks at specific wavelengths (Chen *et al.*, 2015).

3.3.4. INTERFACIAL TENSION

Interfacial tension is demarcated as the change in the Gibbs free energy per unit change in interfacial areas for two immiscible phases, such as gas-liquid or liquid-liquid interfaces (Shahid *et al.*, 2017). In this case, the interfacial tension of liquid-liquid interfaces is of particular importance, as O/W emulsion stability correlates to the interfacial tension between the bulk aqueous layer and the hydrophobic oil droplets. A droplet profile tensiometer is usually used to measure the interfacial tension, in which interfacial tension is correlated to the profile for a droplet at the needle and can be expressed by:

$$\gamma = \frac{\Delta\delta \; g \; R_0}{\beta} \tag{3.4}$$

where γ is the interfacial tension, $\Delta\delta$ is the difference in density between the two fluids, g is the gravity constant, R_0 is the droplet radius, β is the Young-Laplace droplet shape (correlated with the radii of the droplet curvature). A KRÜSS Drop Shape Analyser (DSA30) was used to study the interfacial tension between the core material and the various aqueous phase solutions. The core material was placed in a stainless-steel J-shaped needle via a 1 mL syringe, to form an upward drop due to the density difference between the core and bulk phase. The emulsifier solution bulk phase was inserted into a KRÜSS SC02you optical glass cuvette. The measurements were programmed to be collected in minute-long intervals, and the data acquisition was set to run for a total of 6 hours at ~25 °C.

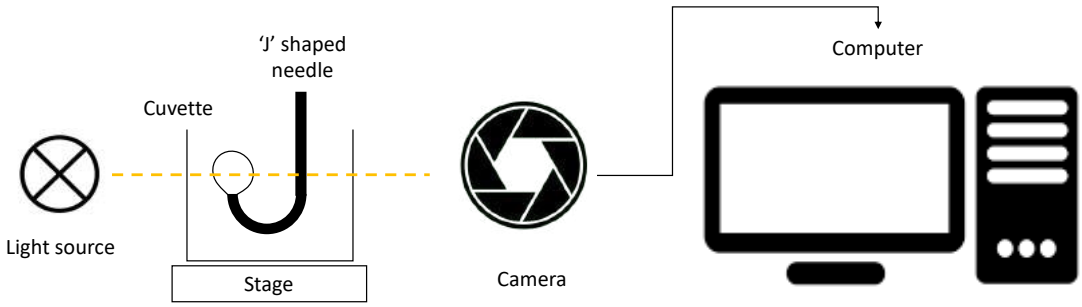

Figure 3.4. Illustrative diagram of interfacial droplet tensiometer.

3.3.5. BULK RHEOLOGY

Rheology is the study of flow of matter and deformation. The rheological characterization of materials provides information regarding the viscoelastic behaviour of samples. The physical stability of emulsions can be characterized by rheological measurements. The factors that can affect the rheological properties of emulsions are (1) the concentration of surfactants in the aqueous phase, (2) the size distribution of droplets, (3) the continuous phase rheology, (4) deformability of droplets, (4) temperature effects, (5) solubility of the core in the bulk phase, and (6) the drop phase volume.

For the O/W emulsions, it was important to compare the viscosity of the emulsifiers in the aqueous phase to study any potential correlations to the quality of the microcapsules. The dynamic viscosity (shear viscosity) of the bulk aqueous phase was measured using a HR-1 Discover Hybrid Rheometer (TA Instrument, UK). 7 ml of the solution was loaded into a TA Peltier concentric cylinder, with a double gap rotor and cup configuration. Within a shear rate range of 100 – 1000 s^{-1}, triplicate measurements were taken while maintaining the temperature at 25 °C. This shear rate range was used as below 100 s^{-1}, the measurements were very unstable due to lack of measurement sensitivity of the equipment.

The MPCM slurry rheology was measured to observe temperature and PCM concentration effects. The dynamic viscosity of the MPCM slurry was measured using an Anton Parr MCR 702 Rheometer. 5.5 mL of the slurry was injected into an Anton Parr Concentric Cylinder (CC) with a double gap rotor and cup configuration. The rheometer was attached to a 25 l liquid nitrogen Dewar for the temperature ramp studies. A shear rate of 100 – 1000 s^{-1} was employed, and the experiments were carried out in triplicate. A program was set to maintain the temperatures for measurements at 20 °C, 0 °C, –20 °C, –40 °C and –60 °C with a tolerance of $\pm$ 1.0 °C. For the temperature ramp measurements, a shear rate of 500 s^{-1} was maintained, with the temperature ramped from –40 °C to –60 °C.

3.3.6. Interfacial Dilatational Rheology

Dilatational rheology is a formidable tool to characterize and investigate the dynamic and equilibrium properties of complex interfacial layers containing surfactants, polymers, micro/nano-sized particles and proteins (Nenningsland, Simon and Sjöblom, 2014). A particularly effective experimental technique to measure the dilatational interfacial rheology is based on the acquisition of drop profiles via profile analysis tensiometers (PAT). This utilizes dilatational measurements, i.e., the changes in interfacial area of the droplet without alteration of the interfacial shape, to investigate the rheological properties of the O/W interface (Nenningsland, Simon and Sjöblom, 2014). At any given time, the area difference is:

$$\Delta A = A - A_0 = A_a sin(\omega t) \tag{3.5}$$

where A_0 is the equilibrium value, A_a is the amplitude area, and ω is the angular velocity. Furthermore, the resulting complex interfacial dilatational modulus is termed as $|E|$, which is defined as the change in the interfacial tension, γ^*, relative to the change in area, A^*.

$$|E| = \frac{d\gamma^*}{d\ ln\ A^*} \tag{3.6}$$

The Interfacial dilatational viscosity between the core material-water interface in the presence of various emulsifiers and surfactants was measured with a Sinterface Profile Analysis Tensiometer PAT1M. The core material was maintained at a constant volume of 25 µL with an inverted capillary (ϕ 3 mm), while the aqueous phase was inserted into an OG Hellma Optical Glass Cuvette (50 ± 0.5 mm) (Hellma Analytics, Germany), with the temperature maintained at 25 °C. When the interfacial tension became constant, the measurement was initiated. The period for the harmonic oscillation procedure was set to be 100 s with a frequency of 0.01 Hz, and an amplitude of 10 %.

3.3.7. Liquid chromatography-Electrospray Ionization Mass Spectroscopy (LC-MS)

Liquid chromatography – Mass spectroscopy (LC-MS) is a highly sensitive detection method based on the chromatographic separation from MS, usually used for trace component detection. LC is a physical separation method in which the components of liquid mixtures are distributed between two immiscible phases, namely mobile and stationary. Most commonly, the mobile phase consists of water and a mixture of another solvent, i.e., acetic acid or methanol. The stationary phase is often prepared via the attachment of long-chain alkyl groups to the surface of silica particles. As the sample is injected into the high-performance LC (HPLC), a high-

pressured pump drives the sample into the mobile phase stream, which passes through the stationary phase. The components of the mixture are thus separated depending on their chemical affinity with the stationary and mobile phases, in which the retention time can be attained.

The samples are then directed to the MS after elution from the LC. MS is an analytical method that measures the mass-to-charge ratio of ionized particles. Conventionally, the samples interleaved into the MS via an ion source, in which the samples are ionized by an electron gun in a vacuum environment. An ionization source therefore nebulizes, dissolves, and ionizes the sample, creating charged particles. The mass analyser then applies magnetic and electric fields onto the sample to characterize their masses.

A Thermo Finnigan Surveyor HPLC was used to analyse the water-soluble residue of the oligomer material in the supernatant. The sample was injected into the column, and the solvents transported the sample through the column. Solvent A was water and 0.05 % acetic acid, while solvent B was acetonitrile and 0.05 % acetic acid. The scouting gradient (used to determine the approximate solvent concentration required for compound elution) was set at 100 % A to 100 % B, over a period of 20 minutes.

The MS analysis was conducted on a Thermo Scientific LCQ Fleet Ion Trap LC/MS. The samples were passed through an ion transfer capillary, which was set at 10 V, and a temperature of 250 °C. The electrospray ionization ion (ESI) needle was set with a voltage of 5 kV, angled at 60 degrees to the capillary. The needle was set at 60° to keep it clean. The acquisition method was used to scan the sample from 50 – 2000 (m/z).

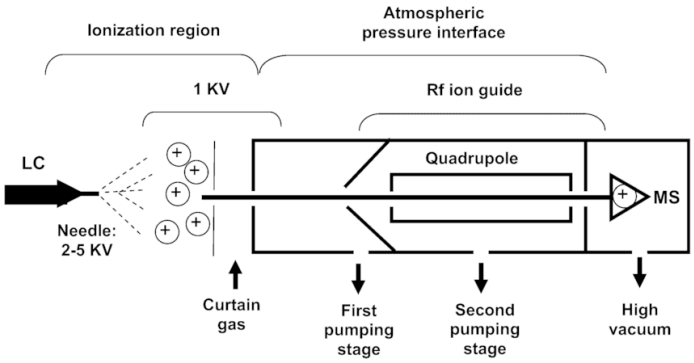

Figure 3.5. Schematic representation of LC-MS (Brima, Jenkins and Haris, 2006).

3.4. PHYSICAL PROPERTY CHARACTERIZATION

3.4.1. PAYLOAD

To characterize the payload of the microcapsules with heptane cores, the dried samples were weighed and then compressed with a Lloyd X Materials Testing Machine. A maximum force of 80 kN at 10 mm.min^{-1} for 120 s was used to compress the microcapsules to breakage, to release the heptane. Successively, the capsules were left to dry in a fume hood for a duration of 4 hours for further evaporation of the heptane. The dry capsule shells were then weighed. The payload of the formulated microcapsules (PL) which is the mass ratio of the core materials to the microcapsules was calculated by:

$$PL = 1 - \frac{w_{dc}}{w_d} \tag{3.1}$$

where w_{dc} is the weight of the compressed capsule shells, and w_d is the weight of the uncompressed dried microcapsules. The yield of the formulation process which is the mass ratio of the product to raw materials was then calculated by:

$$Yield = \frac{w_t}{w_{Rtot}} \tag{3.2}$$

where w_t is the total mass of the formulated dry microcapsules, and w_{Rtot} is the weight of all the materials used for synthesizing the shell and core, excluding the water. The encapsulation efficiency (EE) which is the percentage of encapsulated core materials was then calculated by:

$$EE = \frac{W_T \times PL}{Hep_{in}} \tag{3.3}$$

where Hep_{in} is the total amount of heptane supplied for the homogenization process.

For the microcapsules with the decane cores, a Netzsch 449-F1 Simultaneous Thermal Analyser (STA) was used to characterize the payload. The boiling point of decane is around 174 °C, and therefore the samples had to be heated above this value to ensure evaporation of the core. The samples were heated from 25 °C to 230 ºC, at a rate of 10 ºC.min^{-1}, and was held at this temperature for 2 hours. The thermo-gravimetric (TG) signal indicated the mass loss of the microcapsules, in which the mass difference conveyed the payload.

3.4.2. MASTERSIZER

The size distributions of the microcapsules and polymer size kinetic studies were examined using a Malvern Mastersizer 2000 Particle Size Analyzer with a wet dispersion unit (Hydro 2000S). Distilled water was used as the dispersant. The refractive index of the UF material was set at 1.55. The Mastersizer uses the principles of the Mie theory, and static light scattering (SLS) to calculate particle sizes in a sample.

The Mie theory utilises the refractive index difference between the dispersion medium and the particle to predict the intensity of the resulting scattered light. As shown by Figure 3.6, the scattering angle of the incident light is related to the size of the particles. It is observed that smaller particles/microcapsules would result in a larger scattering angle, which would result in a lower light intensity to the detector. Larger particles/microcapsules produce a narrower scattering angle, with a higher light intensity.

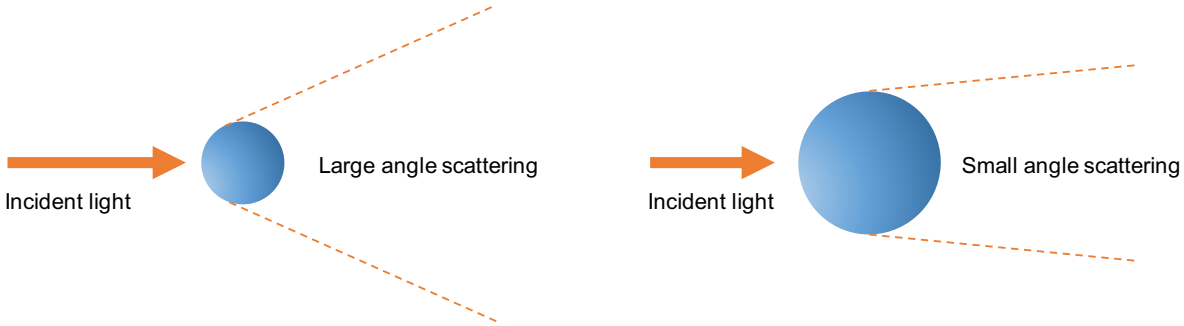

Figure 3.6. Schematic diagram of the incident light source interacting with particles of various sizes.

3.4.3. X-RAY DIFFRACTION (XRD)

To gather information about the crystalline properties of the samples in a non-destructive manner, X-ray diffraction was carried out. This analytical method determines the crystallographic structure of materials based on the irradiation of monochromatic incident X-rays onto a sample and measuring the scattering angles and intensities leaving the sample. The measured diffraction pattern can then be analysed to gather information on unit cell dimensions and phase identification.

The principle of this analytical method comprises of the emissions of incident X-rays from a cathode ray tube, with a monochromatic radiation filter in a parallel focus, directed towards the sample (Park and Jeong, 2011). The interaction of the X-rays and the sample can be described

by Bragg's Law ($n\lambda = 2d\ sin\theta$), as seen in Figure 3.7. In this equation, n is an integer (order of diffraction), λ is the radiation wavelength, d is the inter-planar spacing and θ is the angle between the incident X-ray and the crystal planes. This relates the wavelength of the electromagnetic radiation to the lattice spacing in a sample, and the angle of diffraction. Furthermore, due to the random orientation of various samples, the diffraction directions are generated through the range of 2θ. These diffraction peaks generated are then converted into a set of intrinsic 'd-spacings', unique to each material.

Under ambient conditions, Bruker D8 Advance X-Ray Diffractometer with a Cu Tube (1.5418 Å) and a LYNXEYE detector was utilised to characterise the crystallographic structure of the microcapsules. The powder samples were loaded into a silicon ingot, and the XRD was operated at 40 kV and 40 mA, with an angular increment of 0.01º and a scanning rate of 0.8 s per step. The scans were collected in a range of 2θ = 10º – 70º.

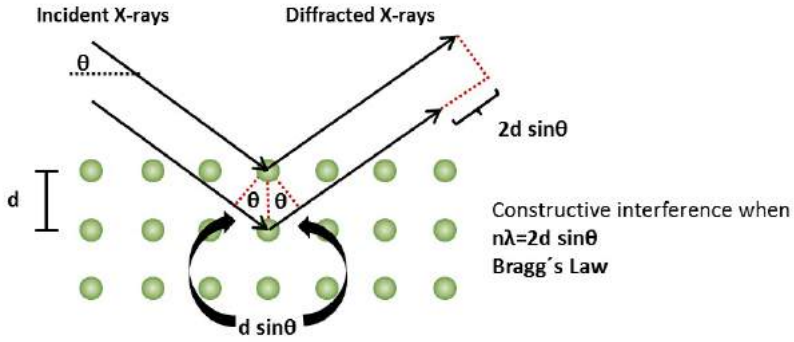

Figure 3.7. Schematic representation of the Bragg equation (Anton Paar, 2020)

3.4.4. THERMAL CYCLING

A pivotal property that the MPCMs should have is long term mechanical strength and thermal cycling stability. As the PCM must undergo several cycles and phase changes, any leakage of the microcapsules can pose as a safety issue, and the effectiveness of the MPCM system is

severely depleted. Thermal cycling for the microcapsules was carried out using a TA Instruments DIL 806 Dilatometer, incorporated with a liquid nitrogen Dewar and a PolyScience water bath. Ultrathin double-sided tape (Tesa 68,557 ultrathin PET tape) was placed on a glass slide, and the microcapsules were placed on top. The microcapsules were observed under FM before and the cycling, with a precise marked location. 10 cycles were then performed with 25 L of liquid nitrogen from 25 °C to – 140 °C, at a heating/cooling rate of 7.5 ºC.min^{-1}. The samples were then observed in the same location after cycling under FM, for comparison of the integrity and core material retention.

3.4.5. MICROMANIPULATION

It is essential to characterize the mechanical properties of the microcapsules, to analyse potential rupture issues in the processing, handling, storage and usage of the microcapsules, and to ensure that the end-use performance is significantly optimized. To characterize the mechanical properties, various experimental methods can be used, such as optical tweezers, atomic-force microscopy (AFM) and micropipette aspiration. However, the diametrical compression of individual microcapsules can also be used to characterize the mechanical properties in a method known as ‘micromanipulation’.

This method is founded on the compression of single microcapsules placed between a glass slide and a compression probe. With this method, various valuable mechanical properties can be ascertained, such as the rupture force, the deformation at the rupture point, the microcapsule size, the elastic-plastic behaviour, and the viscoelastic behaviour. The force versus displacement data can be mathematically modelled to determine the intrinsic properties of the microcapsules, such as shell thickness, stress/strain at the rupture point, yield stress and the Young’s modulus.

Figure 3.8 conveys a schematic representation of the apparatus. The key feature of the setup is that high-speed compressions can be carried out with a compression probe, using a Piezoelectric stack. The microcapsules are typically compressed against the force transducer probe, and the displacement is measured and collated by the computer. For result analysis, the Hertz model can be utilized. This model demonstrates the mechanics of a spherical particle which is compressed between two flat surfaces, i.e., the probe and the glass slide:

$$F = \frac{4E\sqrt{R}}{3(1-v^2)}\delta^{1.5} \tag{3.7}$$

where F is the compressive force, E is the Young's modulus of the microcapsule, R is the radius of the microcapsule, v is the Poisson's ratio and δ is half of the sum of the axial compression displacement, applying to < 10 % strain (Yan *et al.*, 2009).

The micromanipulation measurements were performed on a lab-built system (Hu, Chen and Zhang, 2009), with a self-mounted Nikon M Plan APO ELWD 20x/0.42 camera system mounted onto a Newport M-340-RC stage. A force transducer GS0-10 (Transducer Techniques, serial no. 345657) with a diameter of approximately 150 μm was glued onto a polished glass needle. The acquisition time was 0.01872 seconds, and compression velocity of 2 $\mu m.s^{-1}$. The samples were dispersed onto pre-cut glass and placed onto the stage. To compensate for displacement and acquire accurate results, compliance tests were carried out 3 times prior to the measurement initiation, in which the average was acquired. 30 completely random capsules were selected for each measurement.

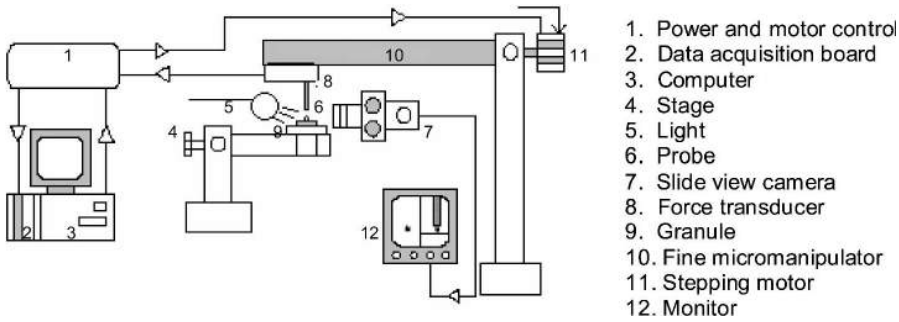

Figure 3.8. Micromanipulation rig schematic diagram (Bouwman *et al.*, 2005).

3.4.6. DIFFERENTIAL SCANNING CALORIMETRY (DSC)

Differential scanning calorimetry (DSC) is a widely used characterization method for PCMs, in which the difference in the heat requirement to increase the temperature of a reference and sample is measured as a function of temperature. A sample of a known mass is cooled or heated, and the changes in its heat flow and heat capacity are tracked with the temperature profile. This characterization technique is extremely useful, especially when studying phase transition temperatures. Moreover, glass transitions, curing, heat of fusion, reaction energy and oxidation induction times can be measured.

A Mettler Toledo DSC 3 was used to observe the phase transition of the MPCMs, with liquid nitrogen employed as the coolant. The N_2 gas flow was set at 20 $ml.min^{-1}$, and the cooling/heating rates were 5 °C/min. The microcapsules were sealed inside 40 µL aluminium crucibles. The temperature profile was set to cool down from –60 °C to –140 °C, then isothermally maintaining this temperature for 5 minutes, and then heating back up to 60 °C, all at a rate of 5 $°C.min^{-1}$.

3.4.7. THERMAL CONDUCTIVITY – LASER FLASH ANALYSIS (LFA)

The thermal conductivity of PCMs is a very important factor to characterize, as enhanced thermal conductivity results in accelerated heat transfer rates, thus shortening the time required for the PCM to undergo charging and discharging processes. For this process, laser flash analysis (LFA) can be carried out to achieve this. LFA is a method in which an energy pulse is used to heat one side of a sample, and then the resultant time dependant rises in temperature of the sample is due to the heat input is detected and measured.

The three-layer model is implemented in LFA measurements. The three layers consist of (1) the sample with unknown diffusivity, (2) the crucible lid with known diffusivity and (3) the sample holder with known diffusivity. This method is widely used in the literature and is known to be accurate (Nomura *et al.*, 2015). The density and specific heat values of the sample are required, and thus the diffusivity (k) can be calculated:

$$k = \rho \times c_p \times a \tag{3.8}$$

where k is the thermal conductivity, ρ is the sample density, c_p is the specific heat capacity and a is the thermal diffusivity.

For the MPCM samples in this work, Laser Flash Analysis (LFA Netzsch 427, Selb) was used to measure the thermal diffusivity of the samples. For the LFA measurements, the sample was placed inside a Netzcsh 427 Pt/Rh sample holder (12.7 mm diameter). For accurate and reliable signals to be obtained. A graphite layer (CRC Black Graphite Aerosol Conductive Lacquer, RS) was coated on the bottom of the sample holder and the top of the lid, to enhance the noise/signal ratio and increase the absorption and emissivity.

CHAPTER 4: A SYSTEMATIC STUDY OF THE REACTION MECHANISMS FOR THE ONE-STEP IN SITU POLYMERIZATION PROCESS

4.1. CHAPTER OVERVIEW

This chapter presents the various proposed reaction mechanisms contributing to the formulation of PUF microcapsules. Microcapsules with a volatile heptane core were initially formulated with a commonly used emulsifier, namely poly-ethylene-alt-maleic-anhydride (PEMA), followed by the characterization and comparison with results reported in literature. Following this, several alternative emulsifiers were compared in terms of functional groups, charges, and current use in the literature. The selected emulsifiers were then further characterized via optical and fluorescence microscopy, microcapsule morphology, size distribution, payload, yield, encapsulation efficiency, FTIR analysis, XRD analysis and thermal cycling. Following this, the proposed mechanisms are investigated. Initially, the effect that the emulsifiers have on the interfacial tension was investigated. Following this, both the bulk rheology and interfacial dilatational rheology was investigated, and how the various emulsifiers contribute to these factors. Subsequently, the additional chemical reactions as a result of the incorporation of the emulsifiers are systematically investigated. PUF microcapsules are usually produced with

various additives to augment capsule properties, such as shell material density enhancement and improved mechanical strength (Nguon *et al.*, 2017). Ammonium chloride is commonly used as a hardener and is said to reduce the pH values during the synthesis. In situ pH monitoring was carried out for ammonium chloride, and other salt alternatives, such as ammonium nitrate and ammonium carbonate. Resorcinol is commonly used during the formulation process to enhance the UF network formation and to increase capsule water resistance. It is proposed that the reaction between resorcinol and the emulsifier is a significant factor contributing to the reaction mechanism, and thus alternatives to resorcinol are implemented to the formulation process to examine the effects this has on the microcapsule properties. Liquid chromatography-electrospray ionization mass spectroscopy was utilised to study the supernatant area of the synthesis products, post centrifugation, to observe the various molecular weight retention times for the various species. Finally, the in situ reaction rate monitoring of the microencapsulation process was studied using a Mastersizer, to observe the rate and size profile of the shell material over a 4-hour period.

4.2. INITIAL RESULT OBSERVATIONS

In this section, a range of preliminary experiments were carried out to observe the effect of emulsifiers on the encapsulation process, and how the various emulsifiers affect the microcapsule properties, such as payload, encapsulation efficiency, yield, morphology, shell thickness, shell roughness and the chemical and physical microstructures of the products. The results would hereby indicate any potential trends associated with the emulsifier properties, such as chemical functional groups, and how such groups may contribute to the disparities in microcapsule quality observed.

4.2.1. PEMA: AN EARLY REACTIVE FOOTHOLD

Poly(ethylene-alt-maleic-anhydride) (PEMA) has long been used as a reactive foothold for the PUF polycondensation reaction (Yoshizawa *et al.*, 2007). Early use of this polymeric emulsifier can be traced back to Brown *et al.* (2003) who encapsulated dicyclopentadiene with a urea-formaldehyde wall, via one-step in situ polymerization, resulting in capsule yields of 79 – 92 %.

PEMA was then decided to be used as a model surfactant for this study. Figure 4.1 conveys the wet (recovered microcapsules with no drying) and the microcapsules after being dried for 24-hours at ambient temperatures. As shown by the OM and FM images, the microcapsules had a coarse appearance, and after drying, there was leakage of the core, as indicated by the elimination of the fluorescent green colour under the FM. The SEM micrographs in Figure 4.2 also convey a very rough and porous exterior structure. This suggests there was not sufficient cross-linking density exhibited for the shell, alluding to a porous structure.

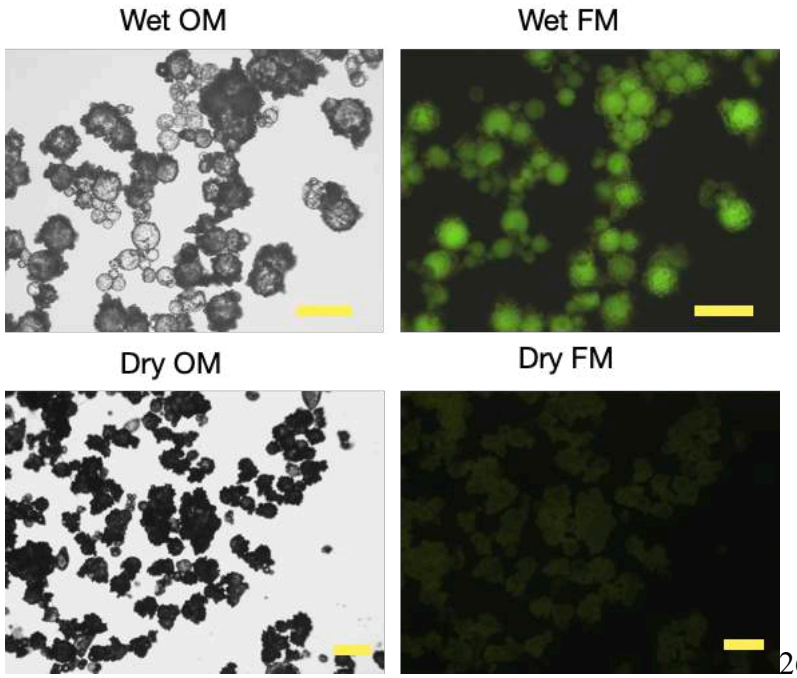

[264]

Figure 4.1. PEMA microcapsules in wet (left in the distilled water phase) and 24-hour dried OM and FM conditions. All scale bars are 100 µm.

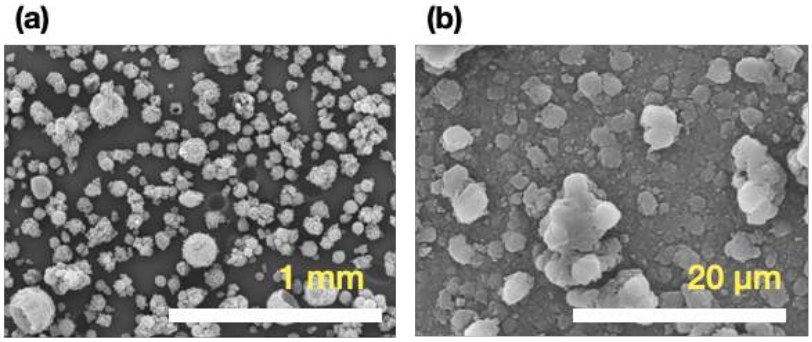

Figure 4.2. SEM micrographs of (a) the overall morphology of the PEMA microcapsules and (b) the surface roughness of the PEMA microcapsules.

The payload of the PEMA microcapsules was observed to be 14.13 %, a much lower value than that obtained by Brown *et al.* (2003). One factor that may be attributed to the accelerated leakage of the heptane microcapsules is the difference in vapour pressure, compared to those made by various other researchers. At 20 °C, the vapour pressure of heptane is around 5.33 kPa, whereas dicyclopentadiene is 0.18 kPa, which renders heptane much more difficult to contain as a core material in the microcapsule over the extended periods of time. Overall, it seems that PEMA may be acceptable for less volatile core materials. But for volatile organic compounds, such as heptane, it produces porous microcapsules with poor barrier properties.

4.2.2. Hydrocolloids and Synthetic Polymers as Emulsifiers

To further explore the effect that emulsifiers have on the barrier and mechanical properties of the microcapsules, an array of hydrocolloid and synthetic polymer candidates were considered as substitutes. Gelatin (GEL), chitosan (CHI), xanthan gum (XG), gellan gum (GG), alginic acid (AA) and methyl cellulose (MC) were chosen as natural polymers, as shown in Table 4.1, as well as their functional groups and net charges. PEMA, polyethylene glycol (PEG), polyacrylamide (PAM), poly(ethylenimine) (PEI) and polymethylvinylether (PMVE) were chosen as the synthetic polymers, also shown in Table 4.1. The chemical structures of these candidates can be seen in Figure 4.3.

Table 4.1. Hydrocolloid and synthetic polymers - functional groups and net charges. *PEMA COOH groups hydrolyse in water to form anhydride moieties.

Hydrocolloid	Functional Groups			Charge
	−OH	−NH2	−COOH	
Gelatin (GEL)	Yes	Yes	Yes	Positive
Chitosan (CHI)	Yes	Yes	No	Positive
Xanthan Gum (XG)	Yes	No	Yes	Negative
Gellan Gum (GG)	Yes	No	Yes	Negative
Alginic Acid (AA)	Yes	No	Yes	Neutral
Methyl Cellulose (MC)	Yes	No	No	Neutral

Synthetic Polymer	Functional Groups			Charge
	−OH	−NH2	−COOH	
PEMA	No	No	Yes*	Positive
Polyethylene glycol (PEG)	Yes	No	No	Neutral
Polyacrylamide (PAM)	No	Yes	No	Neutral
Poly(ethylenimine) (PEI)	No	Yes	No	Negative
Polymethylvinylether (PMVE)	No	No	No	Positive

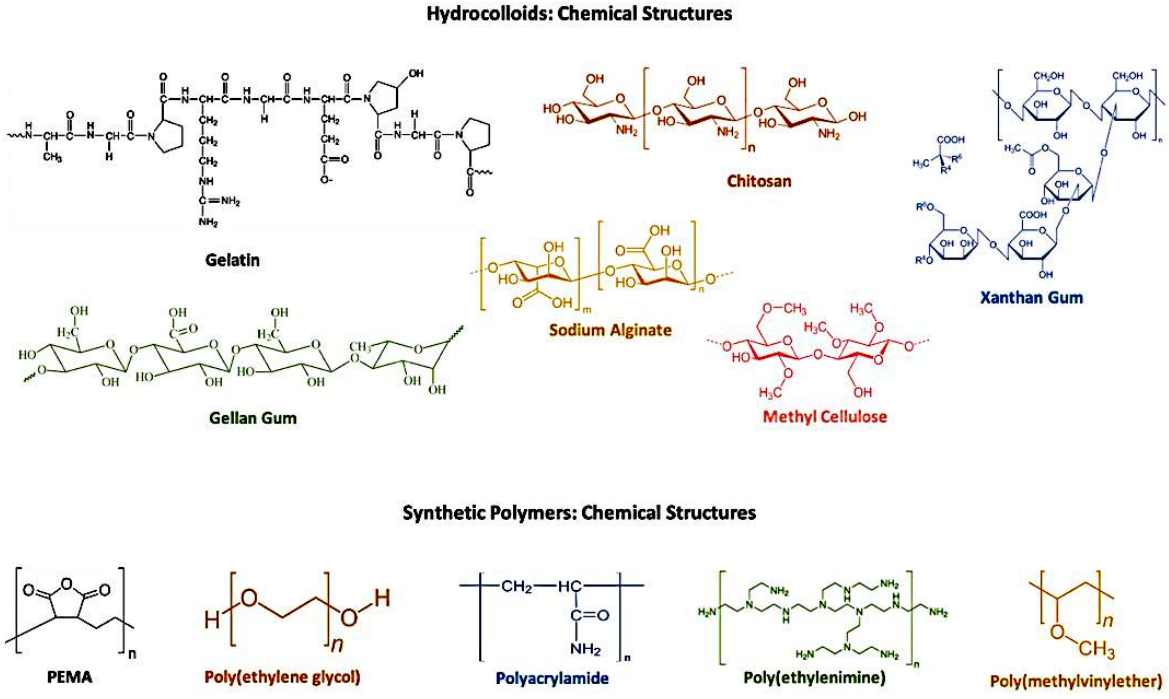

Figure 4.3. Chemical structures of hydrocolloids and synthetic polymers used for the microcapsule synthesis.

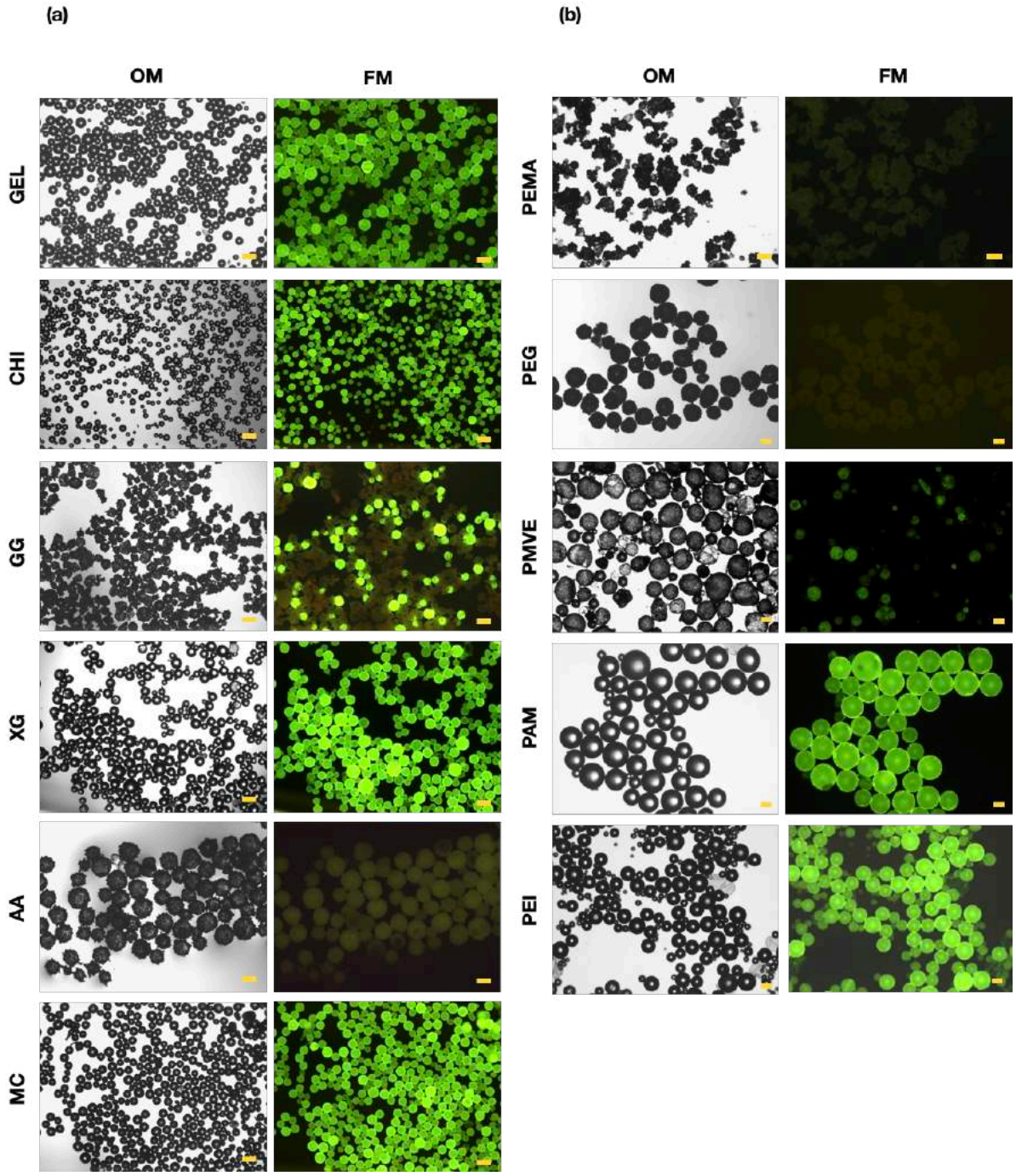

Figure 4.4. OM and FM images of microcapsules formulated with (a) hydrocolloids and (b) synthetic polymers. All samples were dried for a period of 24 hours. All scale bars are 100 μm.

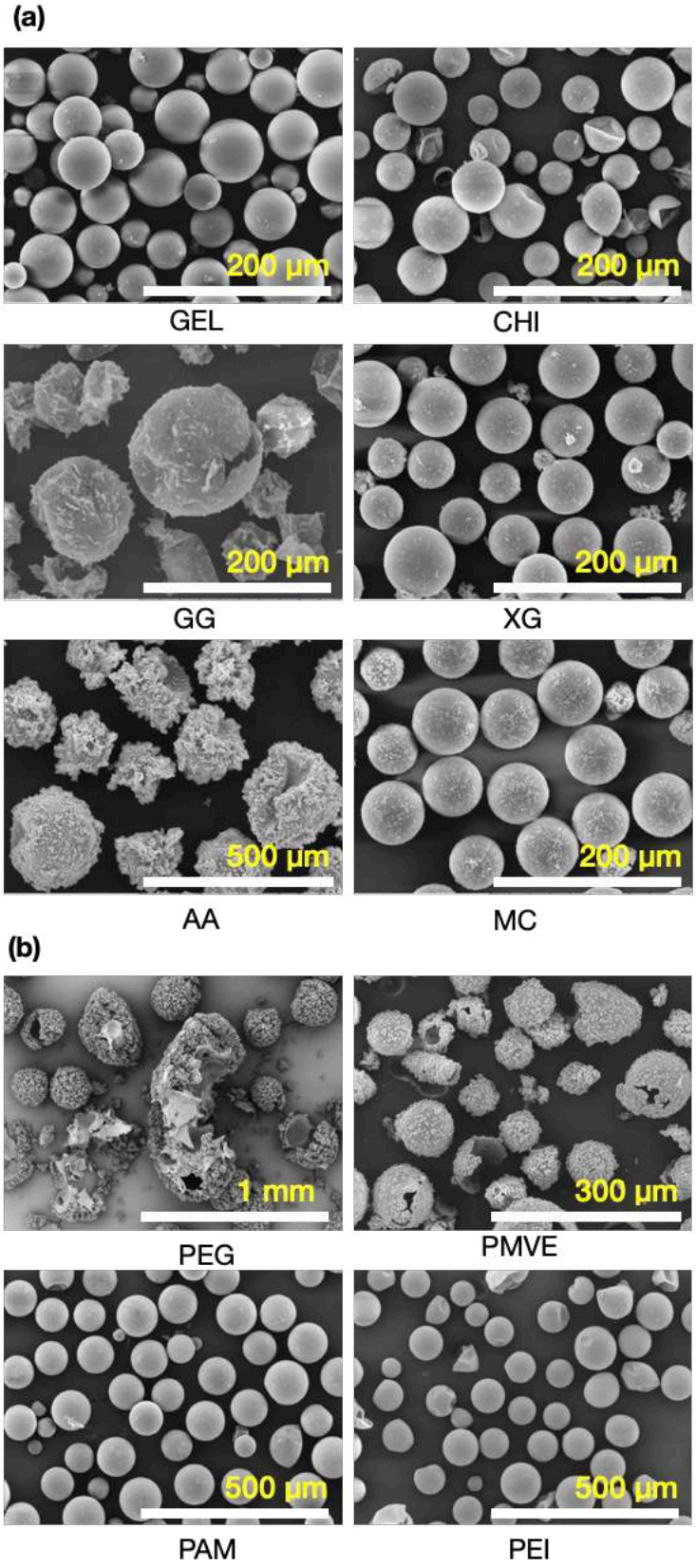

Figure 4.5. SEM micrographs of microcapsules formulated with (a) hydrocolloids and (b) synthetic polymers.

Table 4.2. Payload, yield, encapsulation efficiency and shell thickness values of MPCM samples made with hydrocolloid and synthetic polymer emulsifiers.

Hydrocolloids	Payload (%)	Yield (%)	Encapsulation efficiency (%)	Shell thickness (μm)
GEL	95.6 ± 0.6	30.3 ± 0.2	71.2 ± 0.7	$0.26 \pm 17 \times 10^{-3}$
CHI	94.8 ± 0.7	29.8 ± 0.9	65.7 ± 1.2	$0.26 \pm 23 \times 10^{-3}$
XG	88.8 ± 1.8	20.6 ± 1.1	31.3 ± 1.6	$0.54 \pm 50 \times 10^{-3}$
GG	24.4 ± 0.8	6.4 ± 1.2	9.4 ± 0.9	$0.45 \pm 42 \times 10^{-3}$
AA	18.1 ± 0.8	8.1 ± 0.9	10.1 ± 1.4	$6.99 \pm 62 \times 10^{-2}$
MC	85.6 ± 1.4	35.6 ± 1.0	58.9 ± 1.0	$0.21 \pm 11 \times 10^{-3}$
Synthetic polymers	Payload (%)	Yield (%)	EE (%)	Shell thickness (μm)
PEMA	12.1 ± 1.2	5.6 ± 1.6	7.4 ± 0.9	$0.82 \pm 79 \times 10^{-3}$
PEG	10.6 ± 0.9	5.3 ± 0.7	5.7 ± 1.2	$0.68 \pm 70 \times 10^{-3}$
PAM	90.4 ± 0.5	28.8 ± 1.1	47.8 ± 0.8	$0.66 \pm 16 \times 10^{-3}$
PEI	86.7 ± 0.9	28.4 ± 0.8	44.4 ± 0.9	$0.64 \pm 16 \times 10^{-3}$
PMVE	13.5 ± 0.5	6.1 ± 0.2	8.9 ± 0.8	$0.91 \pm 12 \times 10^{-2}$

All the formulated microcapsule samples using different emulsifiers were left to dry for a period of 24 hours, and then OM and FM images were taken, as seen in Figure 4.4. From primary observation, the emulsifiers that produced the microcapsules with good payloads are GEL, CHI. XG, MC, PEI and PAM. All the mentioned samples had payloads of above 80 %, with gelatine having the highest value of 95.6 %, as seen in Table 4.2. Payload, yield, encapsulation efficiency and shell thickness values of MPCM samples made with hydrocolloid and synthetic polymer emulsifiers. The benefits of the high payload capsules stem from their usefulness in them potentially qualifying as efficient carriers for volatile core materials to be used as cargos for various applications.

As seen by the SEM images in Figure 4.5, the microcapsules had varying morphology and surface roughness depending on the emulsifier utilised in the formulation process. In terms of the synthetic polymers, GEL had the smoothest outer shell when compared to the other hydrocolloids. CHI, MC and XG also resulted in microcapsules with relatively good barrier

properties in terms of retaining the core material. However, GG and AA had very poor results in terms of mechanical and barrier properties, with evident pores and cracked shells. It is worth noting that these two emulsifiers have distinct carboxyl groups, which is a feature in common with PEMA as discussed earlier. In terms of the synthetic polymers, PEI and PAM yielded the best results in terms of shell roughness and barrier properties. However, PEG and PMVE yielded very poor results, mirroring the poor payload values for these microcapsules.

The size distribution of the microcapsules is displayed in Figure 4.6. The two microcapsules with the largest average sizes are AA and GG, both of which also contain primarily carboxyl groups, with average D[3,2] values of 177 and 114 µm, respectively. GEL produced the smallest average sized capsules, with an average size of 49 µm, as well as the narrowest size distribution with a span of 0.68, while AA produced the widest distribution with a span of 1.02. In terms of the synthetic polymers, the two groups with the largest sizes were PEMA, and PEG, with average sizes of 199 and 210 µm, respectively. While PAM produced the smallest sized capsules on average, with a value of 44 µm, PEI produced the microcapsules with the narrowest size distribution, with a span of 0.70, compared to PAM's span of 0.72.

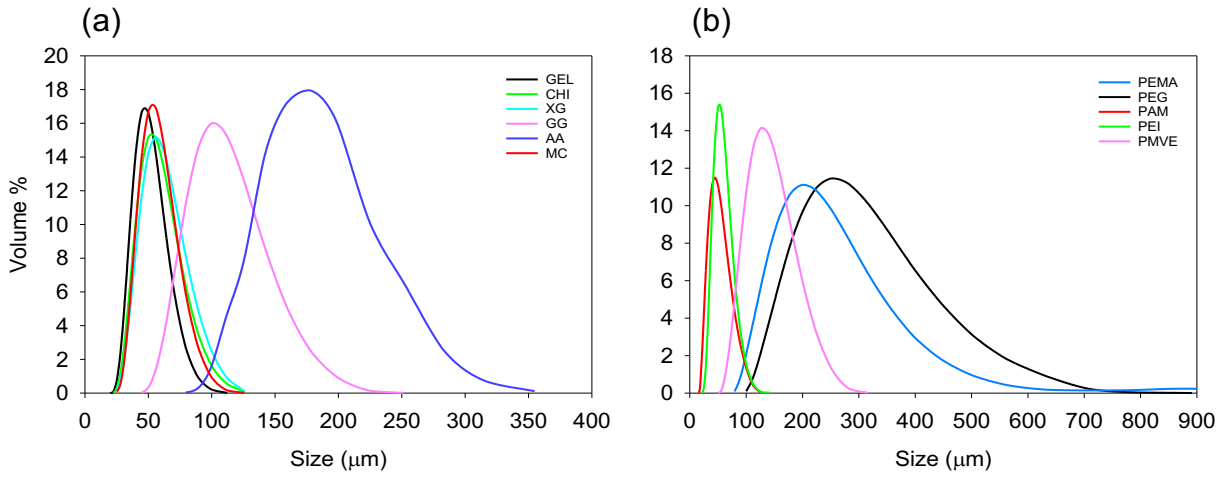

Figure 4.6. Size distributions for (a) MPCMs produced with hydrocolloid emulsifiers, and (b) MPCMs produced with synthetic polymers.

As seen in Table 4.2 and Figure 4.7, there is large discrepancy in shell thickness values depending on the type of emulsifier used. Initial observations convey that AA engendered extremely thick and rough shells, which is not desirable for MPCMs. With an average shell thickness of 6.99 µm, this was significantly thicker than all the other samples. PMVE and PEMA also yielded thick shells, with values of 0.91 and 0.82 µm, respectively. AA and PMVE both contain carboxyl groups, which is an early indication that perhaps the functional groups play a vital role in the barrier properties and the mechanism of shell formation onto the core material. The MPCMs with the thinner shells include MC, CHI and GEL, with values of 0.21, 0.26 and 0.26 µm, respectively. MC has hydroxyl groups, CHI contains both hydroxyl and amino groups, while GEL contains hydroxyl, amino and carboxyl groups. This conveys the significant roles that the emulsifiers play, as such a small concentration can drastically alter the shell roughness and thickness.

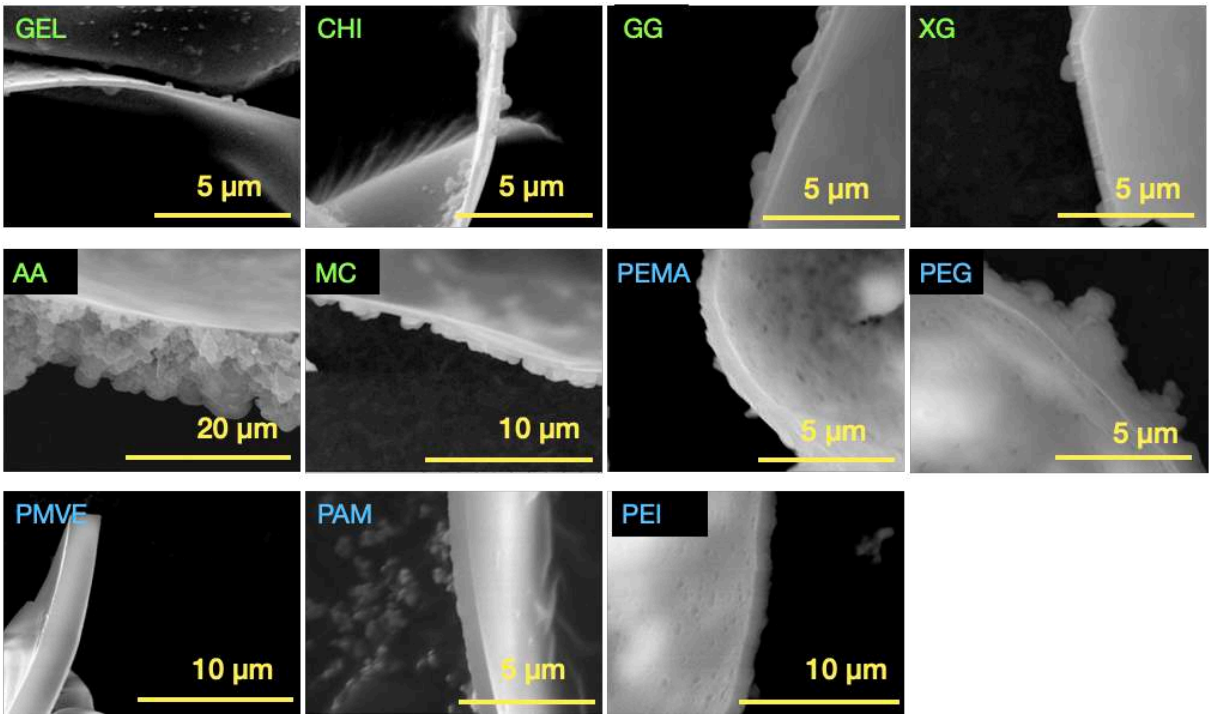

Figure 4.7. SEM micrographs used to determine the shell thickness of microcapsules produced with the hydrocolloids (green labels) and the synthetic polymer emulsifiers (blue label).

As shown by the previous results, and contrary to previous work carried out in the literature (Yoshizawa *et al.*, 2007), carboxyl or anhydride groups are not a pre-requisite in ensuring the successful encapsulation process. IR microscopy was carried out for the cured UF resins produced by hydrocolloid and synthetic polymer samples for the comparison of the chemical composition, shown in Figure 4.8. The broad band at 3300–3350 cm^{-1} was assigned to the N–H stretching of secondary amides. Urea contains primary amines, which indicates that the urea might be fully reacted during the resin preparation and curing process. However, the PMVE and PEG samples have not displayed this broad peak, possibly alluding to incomplete reaction of the urea. Furthermore, peaks at 1632 cm^{-1} and 1550 cm^{-1} were attributed to the stretching of carbonyl group (CO) and C–N stretching of secondary amines, respectively.

The peak at 1378 cm^{-1} was assigned to $–CH_2OH$, which illustrates the typical reaction between urea and formaldehyde (Liu *et al.*, 2017). The peak of 1238 cm^{-1} was attributed to the stretching of C–N and N–H of tertiary amines. The other observed peaks of 1130 cm^{-1} and 1035 cm^{-1} were assigned to C–O aliphatic ether and methylene bridge ($–NCH_2N–$), respectively. The occurrences of the bands confirmed the polymerization of UF resins during a curing process. The obtained results were similar to the other FTIR spectra of cured UF resins with the addition of hardeners (Cosco *et al.*, 2007; Fayyad, Almaadeed and Jones, 2016; Shahabudin, Yahya and Gan, 2016).

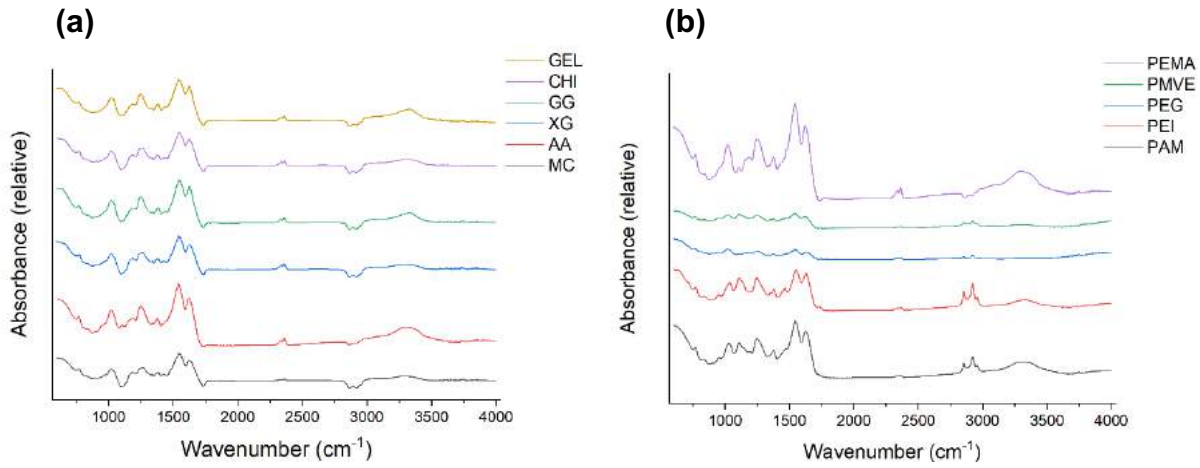

Figure 4.8. FTIR scans for (a) MPCMs produced with hydrocolloid surfactants and (b) synthetic polymer surfactants.

The X-ray diffraction patterns for the samples mostly conveyed similar characteristics, with a large prominent peak around 19.4º, and a diminutive peak at 42.1º, conveyed in Figure 4.9. Similar peaks were observed when a melamine-urea-formaldehyde (MUF) resin was produced by Liu *et al.* (2017). However, GG, AA, PEMA, PEG and PMVE all conveyed a much lower CPS profile than the other samples. An interesting pattern here is that these samples all have predominately carboxyl groups as their functional groups.

Interestingly, the low crystallinity assumed by these sets of microcapsules agree with the OM, FM, SEM and payload measurements carried out earlier, as they produced very porous MPCMs with poor barrier properties. Two factors that may be important by way of explanation is the species formed during the polymerization process, and the rate at which these species are formed. The proportion of methylol urea to the more branched polymers is especially important, as it was shown by Park and Jeong (2011) that when they isolated dimethylol urea and observed the XRD diffractogram compared to PUF resin, there was little overlap between the crystalline regions of the cured UF resin, and the dimethylol urea peaks. This showed that the crystal structure of the monomethylol urea did not contribute as much as that of the cured UF resin to the overall crystalline nature of the system. It is possible that the carboxyl groups favour the

production of methylol urea species. Furthermore, the carboxyl groups may accelerate the reaction faster than the surfactants with amino or hydroxy groups, leading to incomplete shells and non-compact shells.

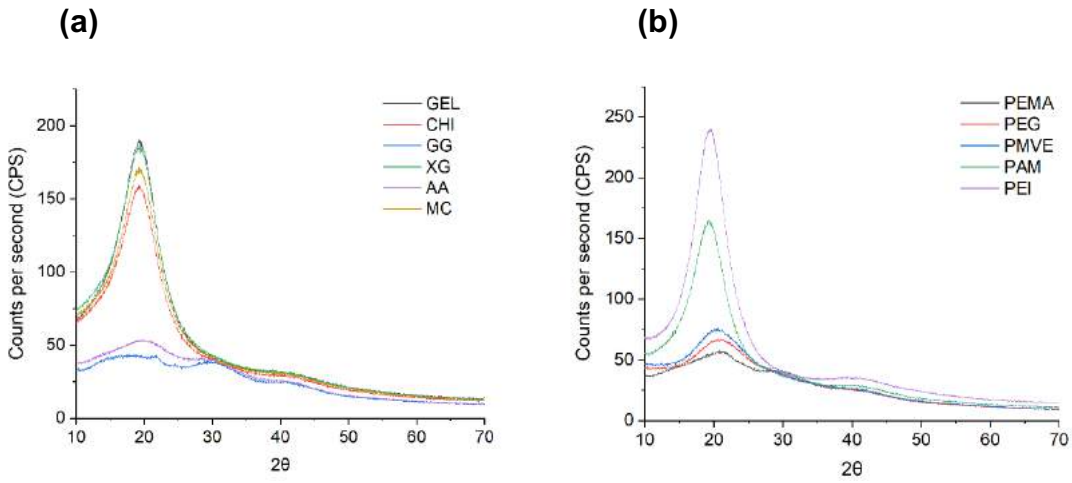

Figure 4.9. XRD scans for (a) MPCMs produced with hydrocolloid surfactants and (b) synthetic polymer surfactants.

4.3. MECHANISTIC STUDY OF THE ENCAPSULATION PROCESS

In this section, a more detailed study on how the various reaction mechanisms play a role in the encapsulation process is deliberated, and how emulsifiers also contribute to the drastic differences in microcapsule properties. As emulsion stability is a pre-requisite in the microencapsulation process, the interfacial tension, as well as the bulk and interfacial rheology were also observed. Furthermore, the role that the reactive additives play, such as ammonium chloride and resorcinol are observed, and also how they interact with the various emulsifiers. Finally, the rate of which the PUF particles are formed depending on the emulsifier properties and functional groups were deliberated via the measurement of the shell particle sized over a period of time, to observe both the initial rate and maximum polymer size.

4.3.1. Reaction Mechanism

The proposed potential reaction mechanism pathway is shown in Figure 4.10. In the first stage (1), the hydrocolloids and the urea, resorcinol and ammonium chloride are surrounding the oil core, at the O/W interface. As the time proceeds, the ammonium chloride reacts with water to produce the hydrogen chloride, which then disrupts the stability of the UF nanoparticles in the solution, to then enrich the O/W interface in the second stage (2) (Fan, Tang and Zhou, 2013). With the addition of formaldehyde in part (3), this reacts with the urea to the O/W bound region, leading to the growth of the initial seeding layer of the shell material (scheme 4).

Depending on the emulsifier, it is proposed that the reaction can take part at different rates, with slow, intermediate, and fast reactions. With the slow reactions, the UF oligomers have poor coverage of the seeding layer, and this leads to porous and incomplete regions of the shell. With the fast reactions, the rapid reaction to form the UF oligomers and PUF polymers leads to thick non-compact and rough shells with voids and incomplete regions. However, the intermediate reaction section is assumed to produce compact shells with excellent barrier properties, with no voids or pores, to contain the core material superbly. This theory is then explored in the following sections.

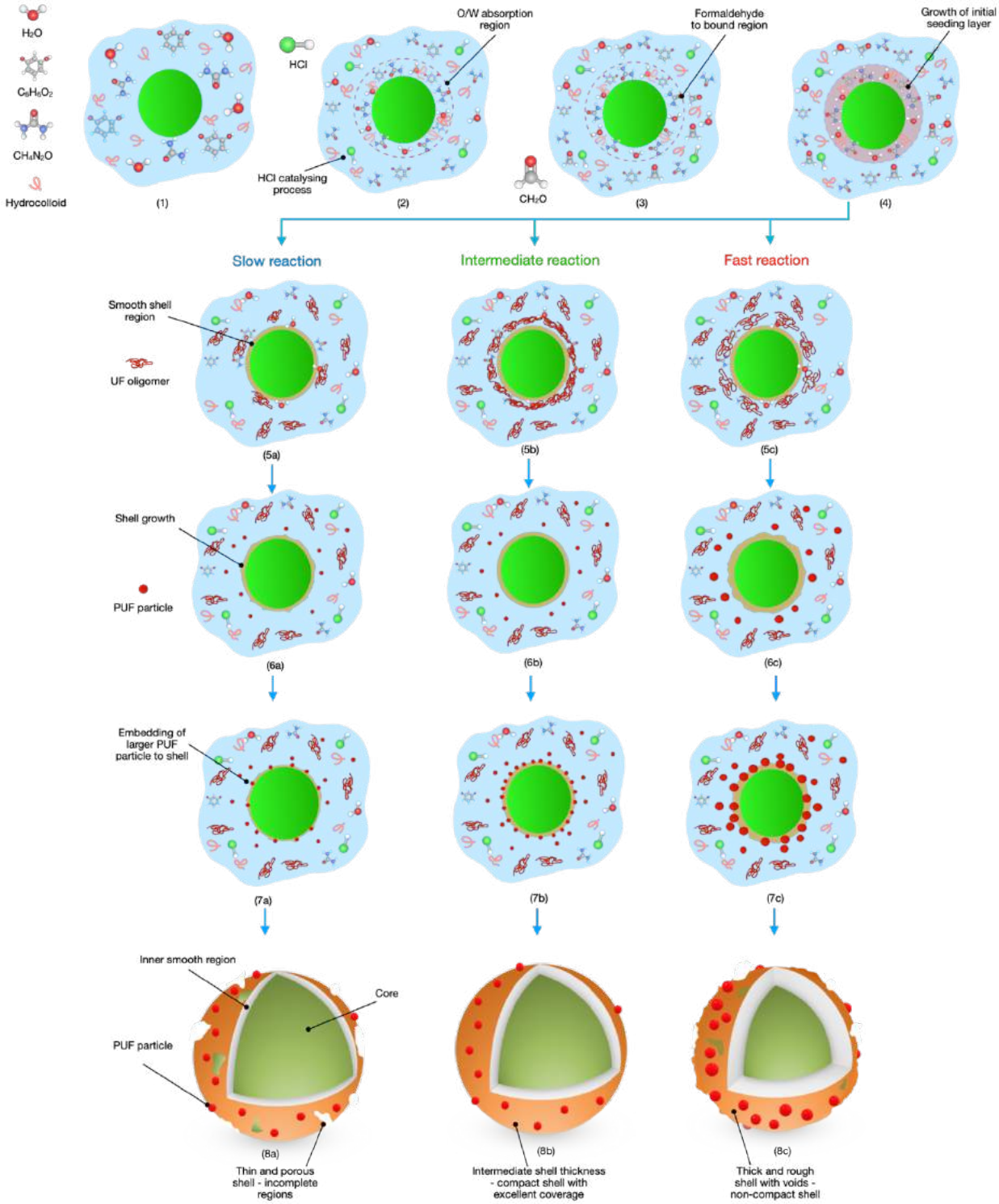

Figure 4.10. Schematic representation of the one-step in situ polymerization process with the natural emulsifiers: (1) the O/W interface representation prior to the addition of formaldehyde; (2) the adsorption of the hydrocolloids and the enrichment of the other solutes to the O/W interface, with the ammonium chloride producing additional HCl species; (3) the additional of formaldehyde; (4) the heating and pH drop of the reaction initiating the seeding of the initial shell with the shell materials; (5a-c) the slow, intermediate and fast reactions PUF shell growth on top of the initial smooth layer progress; (6a-c) the continued shell growth; (7a-c) the PUF large molecular weight particles embedding on the outer layer of the shell; (7a-c) the final MPCM with various shell properties after the process.

4.3.2. THE ROLE OF: INTERFACIAL TENSION AND EMULSION STABILITY

The hydrophobic oil droplet stability and size in an aqueous environment can be determined by understanding the disruptive forces (associated with turbulent disturbances) and cohesive forces (such as interfacial tension and viscosity) (Güell *et al.*, 2017). Due to the electrostatic interaction with oppositely charged surfactants, complexes can be formed by polyelectrolytes to modify the interfacial properties and result in emulsion stability. Owing to the various chemical properties of the chosen emulsifiers, the interfacial tension of each emulsifier in the O/W emulsion was studied, as well as pure water only for a period of 6 hours (at 25 °C) until stability was ensured. The results can be seen in Table 4.3.

The heptane-distilled water (DW) interfacial tension was measured via the pendant drop method and was evaluated to be 49.8 ± 0.4, in agreement with previous work in literature (Zhang *et al.*, 2014). Immediate observations from Table 4.3 is that XG and PAM have relatively high IFT values of 35.5 and 34.4 $mN.m^{-1}$ respectively, however both produced fairly good microcapsules. Furthermore, MC and PMVE have the lowest values of 18.7 and 18.5 $mN.m^{-1}$ respectively, and MC produces superb microcapsules while PMVE is unsuccessful in producing microcapsules with adequate barrier properties. Even though it is a pre-requisite to have core material stability during the microencapsulation process, this may not be the most predominant driving force that determines the surfactants' contribution to the microcapsule properties. However, with this being said, emulsion stability is still extremely important in microencapsulation processes, but may come in form of other cohesive forces such as stearic hindrance via viscosity modifications or electrostatic repulsion (Sharipova *et al.*, 2017).

Table 4.3. IFT values for hydrocolloids and synthetic polymer surfactants in the O/W emulsion.

Substance	IFT $mN.m^{-1}$
DW	49.8 ± 0.4
Hydrocolloids	**IFT $mN.m^{-1}$**
GEL	21.3 ± 0.3
CHI	21.7 ± 0.9
XG	35.5 ± 0.5
GG	28.7 ± 0.5
AA	23.9 ± 1.0
MC	18.7 ± 1.1
Synthetic polymers	**IFT $mN.m^{-1}$**
PEMA	15.9 ± 1.2
PEG	29.6 ± 0.1
PAM	34.4 ± 0.4
PEI	24.6 ± 1.4
PMVE	18.5 ± 0.5

Alongside the interfacial tension measurements, the heptane was injected and homogenized at 1200 rpm for 20 minutes into the aqueous solution with 0.03 wt.% emulsifier, and observed under the OM in 0 hour, 3 hour, 6 hour and 24 hour increments. As the reaction takes place for approximately 6 hours overall, it is important that the oil droplets are stable for this duration especially. The OM images for the natural emulsifiers are observed in Figure 4.11, while the synthetic emulsifiers can be observed in Figure 4.12. In terms of the emulsion stability for the natural emulsifiers, GEL, CHI, GG, XG and MC all had oil droplets with definitive shape retention after even the 24-hour period. However, the AA sample had a noticeable reduction in the stable oil droplets after this period, but at 6 hours, there were still stable oil droplets present, although there was a reduction in sizes and also some apparent coalescence in some instances.

Moreover, in terms of the synthetic emulsifiers, PEMA, PAM and PEI all had stable oil droplets at the 24-hour time period, while the PEG and PMVE both had similar results in terms of oil stability. At 6 hours, there were cases of coalescence and collapse of the oil droplets, and at 24 hours there were very few surviving oil droplets present.

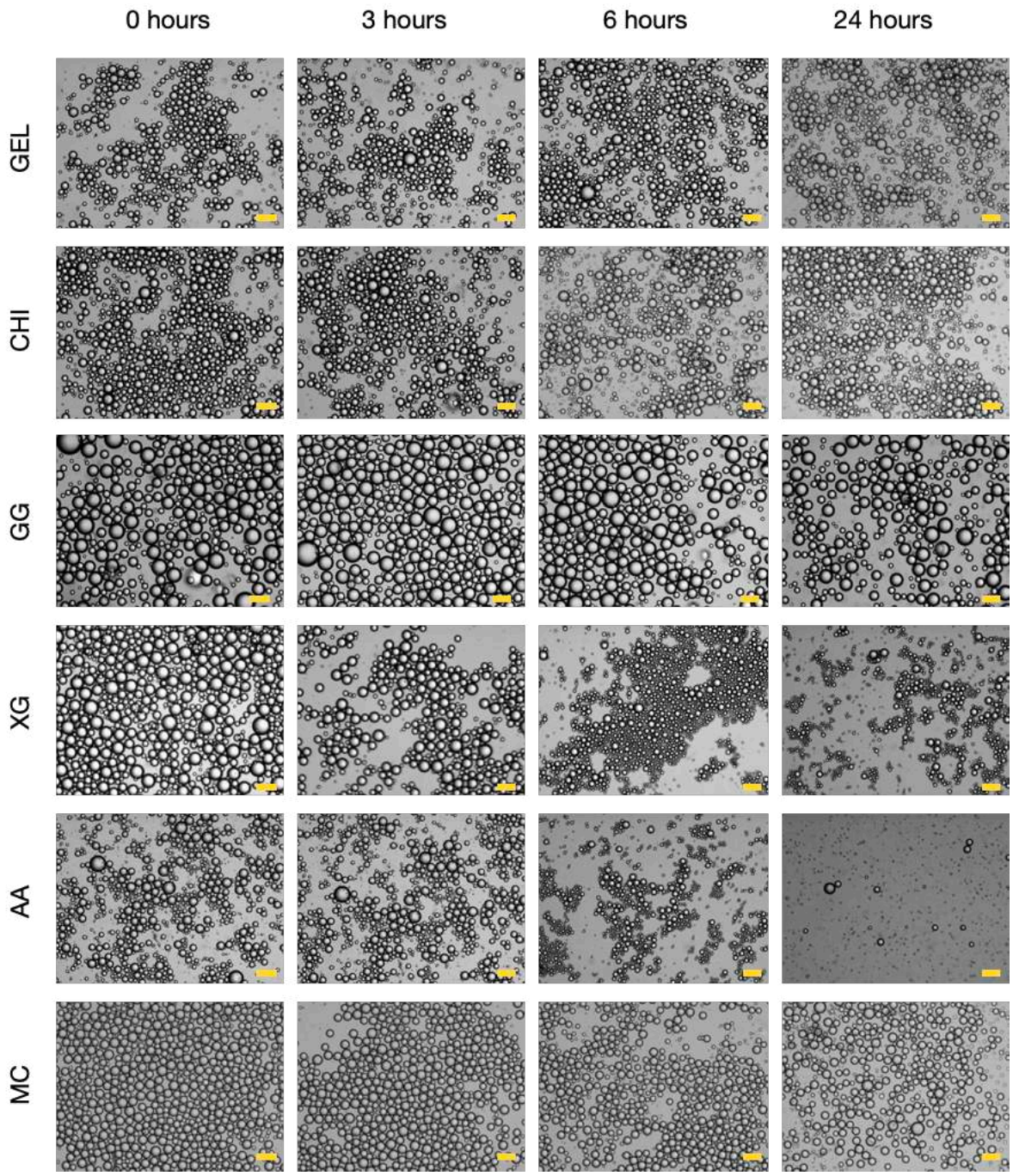

Figure 4.11. OM images of the heptane oil droplets in the aqueous solution and the natural emulsifiers, observed at 0 hours, 3 hours, 6 hours and 24 hours. All scale bars are 100 μm.

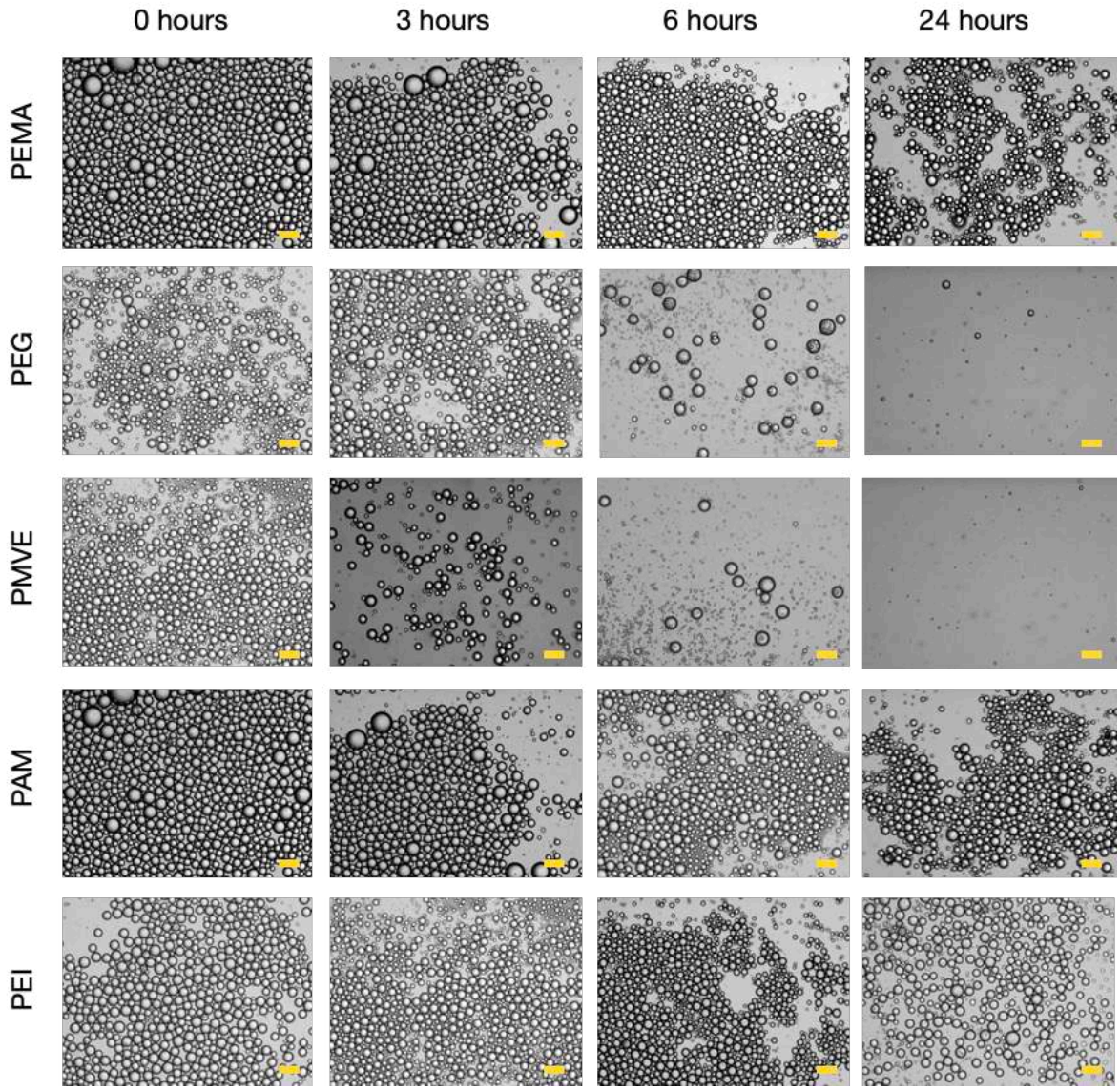

Figure 4.12. OM images of the heptane oil droplets in the aqueous solution and the synthetic emulsifiers, observed at 0 hours, 3 hours, 6 hours and 24 hours. All scale bars are 100 μm.

4.3.3. The Role of: Rheology (Bulk and Interfacial)

Emulsifiers can enhance the stability of a hydrophobic core in an aqueous solution via an increase in viscosity in the bulk phase (Fink, 2020). The well-known Stokes-Einstein equation takes into account the diffusion coefficient of a particle undergoing Brownian motion in a quiescent fluid (Fink, 2020). The micelle formation and arrangement are believed to impart the

increase in viscosity in aqueous fluids (Fink, 2020). Spherical micelles are not known to increase viscosity by a great amount, however when the micelles have an elongated formation, e.g., worm or rod-shaped, they become entangled with one another, and the viscosity of the fluid is increased. With an increase in viscosity, the polycondensation process can be inhibited from proceeding too quickly, as the collision probability and diffusion rates have been reduced (Lovell and Schork, 2020).

A study carried out by Zhang *et al.* (2019) conveyed that increases in viscosities resulted in thinner shells for MPCM capsules. As shown in Figure 4.13 (a), XG drastically increased the viscosity of the aqueous phase, while GEL had the lowest effect on the overall bulk viscosity. Although AA and GG also have carboxyl groups and similar viscosity, they yielded poor microcapsules compared to XG, which had the highest viscosity. This may suggest that the carboxyl moieties may accelerate the polycondensation reactions, but this may be offset by the higher viscosity. All of the synthetic polymers interestingly exhibited similar profiles in terms of viscosity profile, suggesting that in that case the viscosity may not be the most prominent factor in determining the oil retention in microcapsule.

However, it can be argued that the interfacial viscosity may be a more relevant suggestion. Figure 4.13 (c) and (d) convey the interfacial dilatational rheology for the various surfactants surrounding the heptane droplet in water. From primary observations, GEL and PMVE have similar dilatational viscosity values, but GEL produces pristine capsules while PEMA produces poor quality and incomplete capsules. Initially there does not seem to be a correlation and the interfacial dilatational viscosity may not be the principal cause for enhanced retention, however this surely still may play a part in the reaction kinetics occurring at the O/W interface.

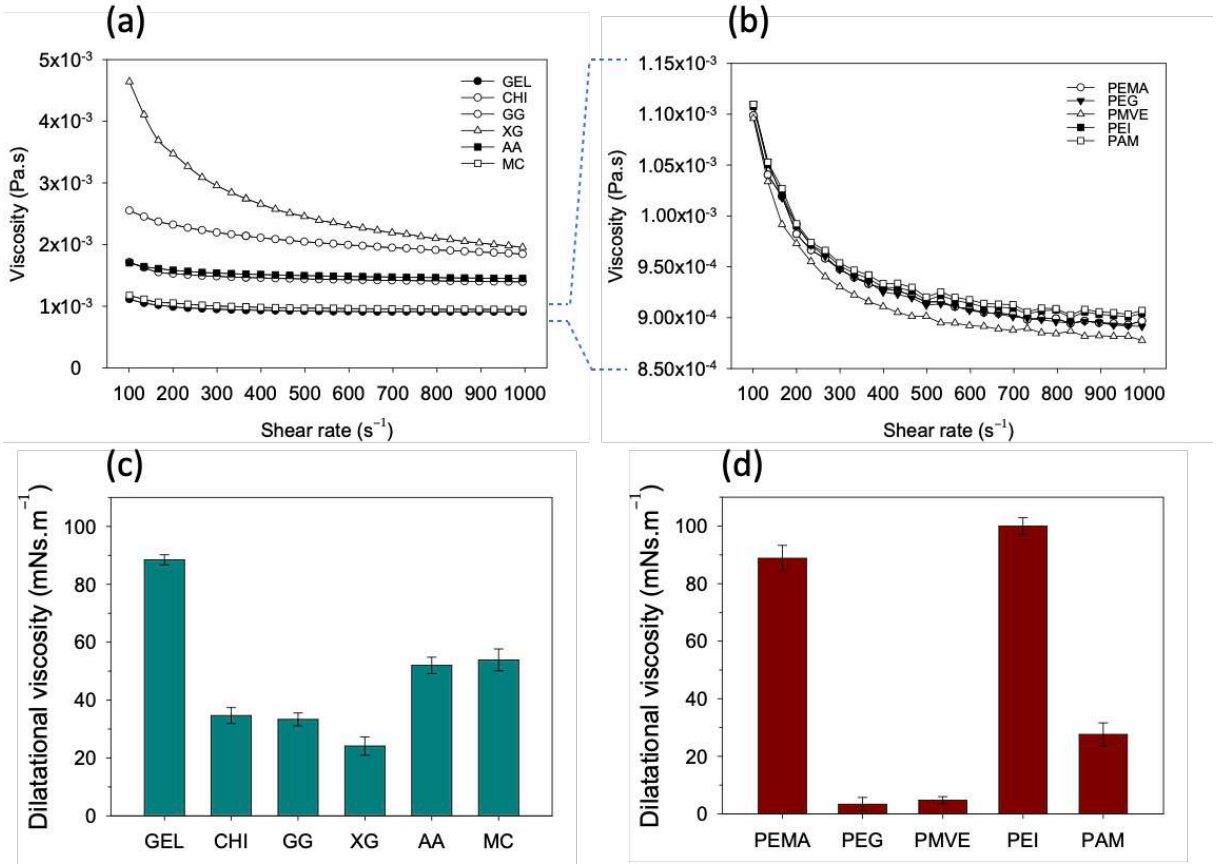

Figure 4.13. The bulk viscosity of (a) hydrocolloid emulsifiers in water and (b) the synthetic polymers in water. Blue dotted line indicates the scale difference from (a) to (b). Also, the interfacial dilatational viscosity of (c) hydrocolloid samples in the O/W emulsion and the (d) synthetic polymers in the O/W emulsion (at 25 °C).

4.3.4. Reaction study (1): The Role of Resorcinol

Having demonstrated that the interfacial tension and the bulk and interfacial rheology contributions may not be the most focal factors in regard to the drastic variances in the microcapsule properties, it is important to investigate the contributions of resorcinol to the in situ polymerization process. As resorcinol is a branching agent, it is expected that this would play a large role in the shell material formation. To investigate this, two resorcinol alternatives were initially tested with the GEL emulsifier. The resorcinol crosslinker was replaced with isomers, namely the ortho-(catechol) and para(hydroquinone) configurations of

dihydroxybenzenes. This study was carried out to examine how a slight change in the position of the hydroxy group on the benzene influences the MPCM properties.

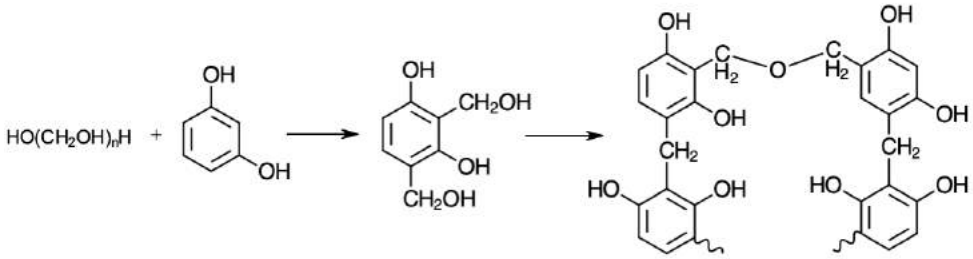

Figure 4.14. Reaction mechanism between resorcinol and formaldehyde to yield hydroxymethylated resorcinol and high molecular weight compounds.

The synthesis of resorcinol-formaldehyde generally is believed to follow the reaction mechanism conveyed in Figure 4.14. It is believed that the first step is catalysed by bases, such as hydroxides or sodium/potassium carbonates (Gaca, Parkinson and Sefcik, 2017), while the second step is promoted by elevated temperatures and acidic temperatures. As in the in situ polymerization process, the temperature increases and pH of the solution decreases over time, this may then promote the formation of the resorcinol-formaldehyde resins.

The reactivity of resorcinol is principally determined by the electron density in the benzene ring. Simple phenolic structures typically exhibit strong activating effects on the benzene ring due to the higher electron density in the ring, which is supplied by the hydroxy group, and therefore various phenolic substitution reactions can occur without the need for catalysts (Šebenik, Osredkar and Vizovišek, 1981). Due to the lone pair of electrons on the hydroxy group, this acts as an electron source, therefore creating various resonance structures (Šebenik, Osredkar and Vizovišek, 1981). The stability of these resonance structures therefore depends on the position and number of hydroxy groups on the benzene rings. Resorcinol has relatively

stable resonance structures, which therefore react with formaldehyde to form hydroxymethylated resorcinol, and condensates to form high molecular weight compounds with methylene and ether bridges (Lewicki, Fox and Worsley, 2015). However, in this case, the resonance structures catechol and hydroquinone are not as stable as resorcinol, and therefore under these conditions, fewer compounds would be formed, leading to incomplete microcapsules.

The inductive effect is also another pivotal factor in regards of the reaction mechanism. Through inductive effects, electron withdrawing compounds can make the phenolic structures more acidic via the delocalization of the negative charge (Ouellette and Rawn, 2015). Due to the position of the hydroxy group in resorcinol, this leads to an intermediate inductive effect, while hydroquinone has a weak inductive effect. Catechol has a very strong inductive effect, but there is also a counter-effective mesomeric effect in which the pi electron moves away from the OH group to the rest of the phenolic structure. This conveys that resorcinol has the required properties to react successfully with formaldehyde to yield high molecular weight compounds to form the shell material. This theory is in agreement with the work carried out by Kirkwood and Jackson (Kirkwood and Jackson, 2020), in which the reactivity of resorcinol, catechol and hydroquinone were investigated. It was suggested in the study that the order of reactivity was meta > ortho > para (resorcinol > catechol > hydroquinone). Furthermore, kinetic analysis revealed that activation enthalpies of 30 $kJ.mol^{-1}$ were observed for catechol and hydroquinone, while resorcinol had an activation enthalpy of 41 $kJ.mol^{-1}$ (Kirkwood and Jackson, 2020).

When the ortho and para configurations of the dihydroxybenzenes species are introduced, drastically inferior results are observed in terms of microcapsule morphology and core material retention. As shown in Figure 4.15, when compared to resorcinol, incomplete microcapsules are formed when catechol and hydroquinone were used as crosslinkers. Broken pieces of shell material were formed with absolutely no retention of the core material. Therefore, the polymerization process was greatly hindered by the introduction of these alternate crosslinkers.

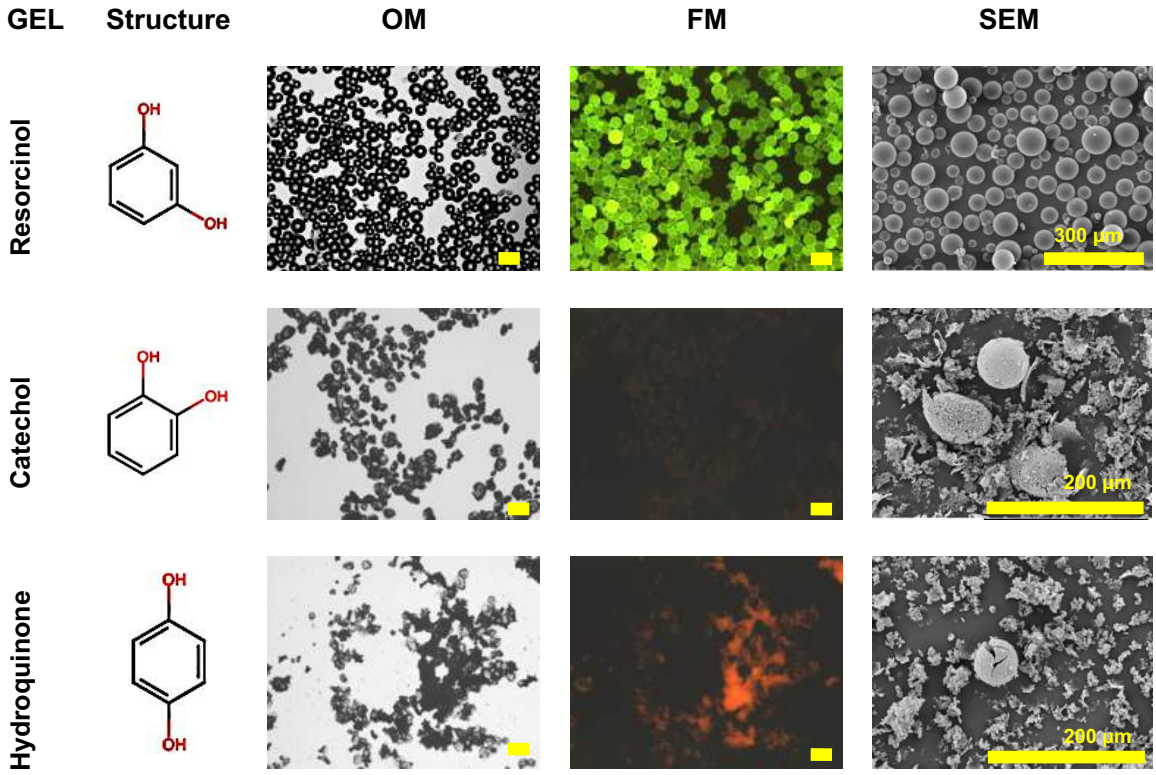

Figure 4.15. OM, FM and SEM images of the GEL MPCMs and resorcinol, catechol, and hydroquinone as the cross-linking agent. OM and FM scale bars are all 100 µm.

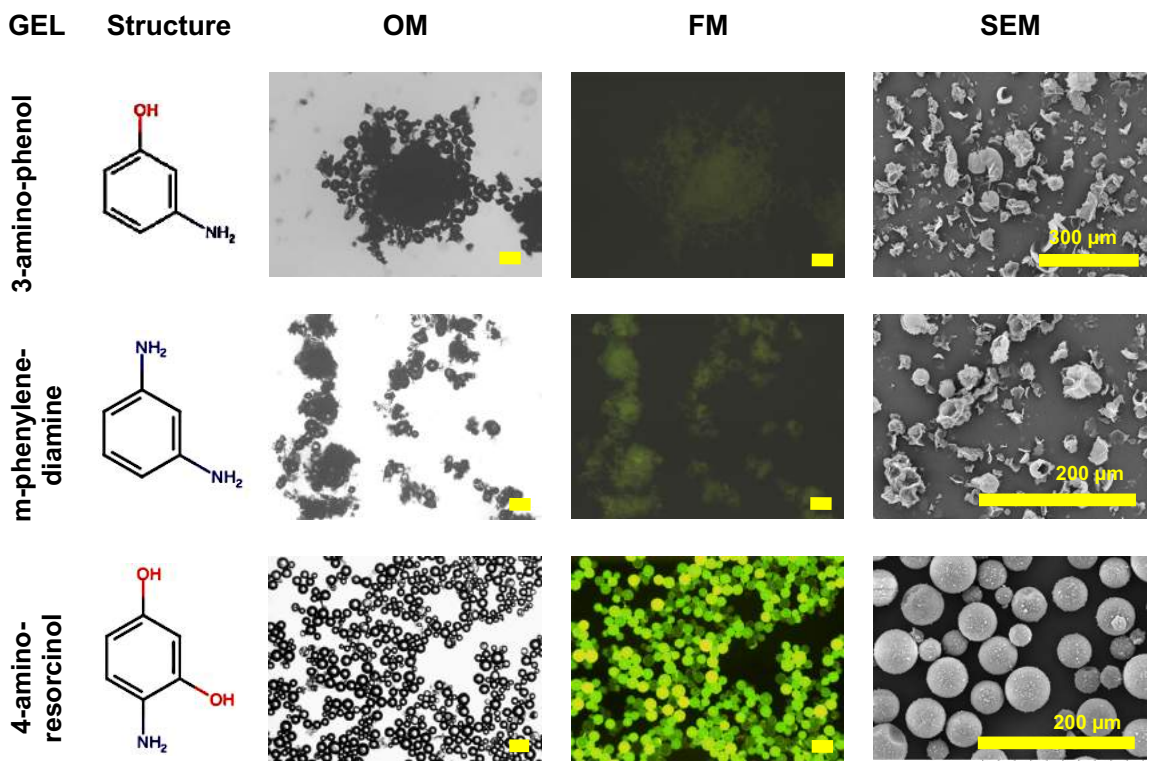

Figure 4.16. OM, FM and SEM images of the GEL MPCMs and 3-amino-phenol, m-phenylene-diamine, and 3-amino-phenol as the cross-linking agents. OM and FM scale bars are all 100 µm.

To further investigate alternative phenolic compounds, two meta compounds (3-amino-phenol and m-phenylene-diamine) were also compared with resorcinol, as well as 4-amino resorcinol. As mentioned previously, the meta configuration had the most stable resonance structures, and the hydroxy groups were replaced with amino groups, as well as another additional amino group on the 4-amino-resorcinol. It is observed in Figure 4.16 that both the 3-aminophenol and m-phenylene-diamine did not successfully yield microcapsules, even though the functional groups are in the meta position. In terms of nucleophilicity, NH_2 groups are stronger nucleophiles than OH groups, however, there seems to be a detrimental effect on the shell material formation. Compared to resorcinol, m-phenylenediamine provides more of a resonance effect to the benzene ring (delocalises electrons to the benzene ring), rendering it more reactive. However, this reaction may therefore proceed too quickly compared to resorcinol, and the branching is not completed in a controlled manner to form a continuous and high molecular weight polymer.

For the 3-aminophenol, there is a non-cooperative effect between the hydroxy group and amino group, reducing the reactivity of the benzene ring (Palusiak *et al.*, 2014). When the 4-aminoresorcinol was trialled, it seemed to produce microcapsules with excellent oil retention and a slightly rougher shell. It is possible that the resorcinol structure undergoes the main reaction, while the amine group slightly hinders the formaldehyde attaching onto the para position. Nonetheless, the products are relatively successful when compared to the other branching agent alternatives.

Due to the effect of emulsifiers in this system, XG was also tested with the catechol and hydroquinone alternatives. However, it is clearly seen in Figure 4.17 that the results for this are much better than those formulated with the GEL emulsifier. One significant difference between the emulsifiers is the viscosity, as XG is a natural thickener with much higher viscosity in the bulk phase. Therefore, it is suggested that the viscosity may introduce stearic stability into the system during the mechanical stirring in the formulation process, to allow the formaldehyde and catechol/hydroquinone to react in a more stable manner. As shown by the FM images in Figure 4.17, the catechol and hydroquinone samples mostly collapsed, but after 24 hours there were a few surviving capsules, compared with the GEL capsules which completely collapsed. The SEM images in Figure 4.18 more clearly convey the capsules made with catechol with the GEL and XG emulsifiers, conveying the significant improvement in capsule morphology. As mentioned previously, it was suggested that the carboxyl groups greatly accelerate the rate of reaction between the emulsifiers and reactive substituents for the shell material, and out of all the emulsifiers with mostly COOH groups, XG yielded the best results. It is therefore proposed that the viscosity effect of the XG does indeed play a part in the encapsulation process, due to the stability enhancement of the bulk phase.

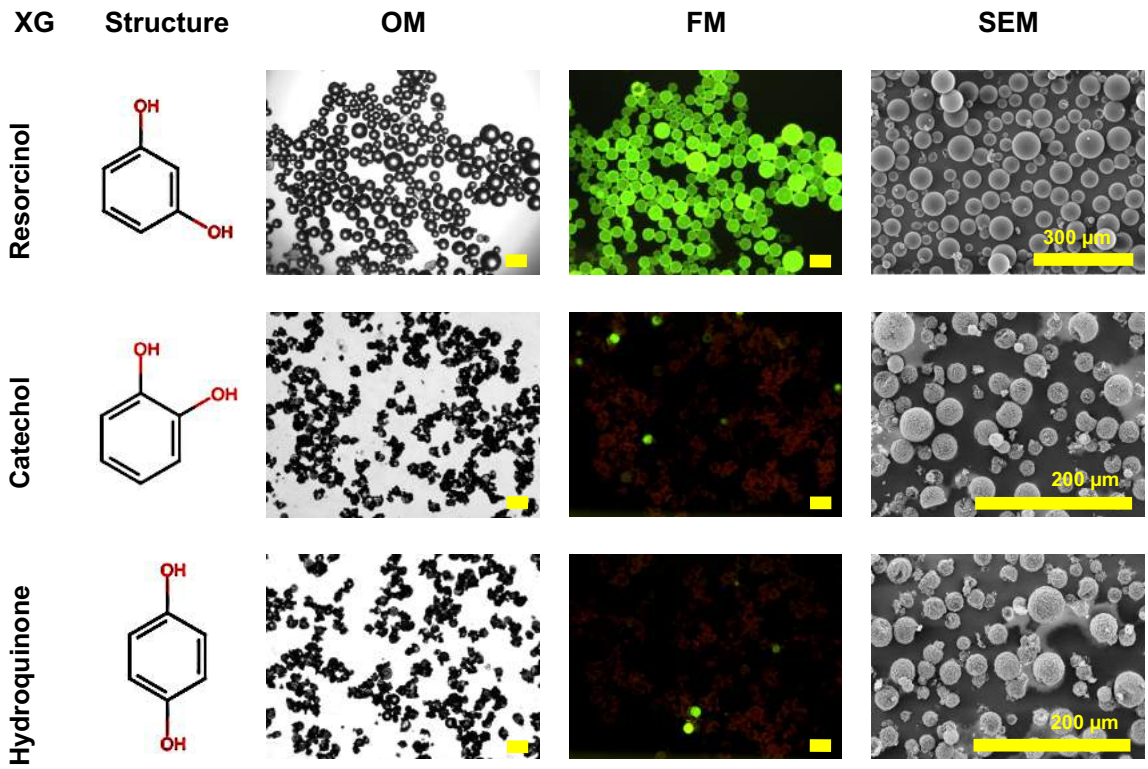

Figure 4.17. OM, FM and SEM images of the XG MPCMs and resorcinol, catechol and hydroquinone as the cross-linking. agent. OM and FM scale bars are all 100 µm.

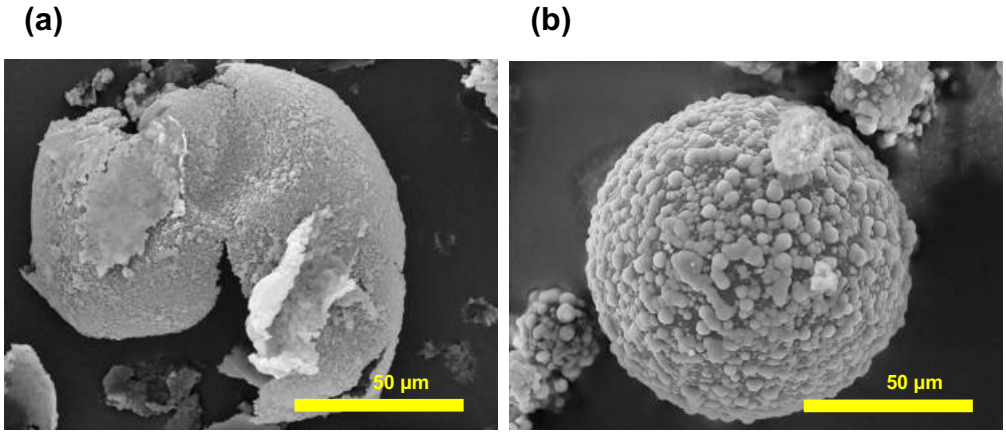

Figure 4.18. SEM micrographs for individual (a) GEL-catechol MPCMs and (b) XG-catechol MPCMs.

The electrospray ionization mass spectrometry (ESI-MS) analysis was then performed for the supernatants of the products after centrifugation, as shown in Figure 4.19. For the GEL samples, it was seen that when using resorcinol, the majority of the species appeared to have longer retention times, around 8 ~ 10 minutes, which corresponds to much larger molecular weight compounds (Zhang, *et al.*, 2019). Meanwhile, the catechol and hydroquinone samples resulted in product species with lower retention times, approximately 3 minutes, alluding to lower molecular weight samples. This is further evidenced by the centrifuge images in Figure 4.20, in which the supernatants were cloudy prior to centrifugation when produced with resorcinol, and clear when produced with both hydroquinone and resorcinol. This again suggests that resorcinol more readily reacts with formaldehyde to form higher molecular weight compounds when compared with catechol and hydroquinone. However, with the XG samples, catechol had the lowest amount of both low and high molecular compounds in regard to the retention time, while the resorcinol samples conveyed larger amounts of low and high molecular compounds.

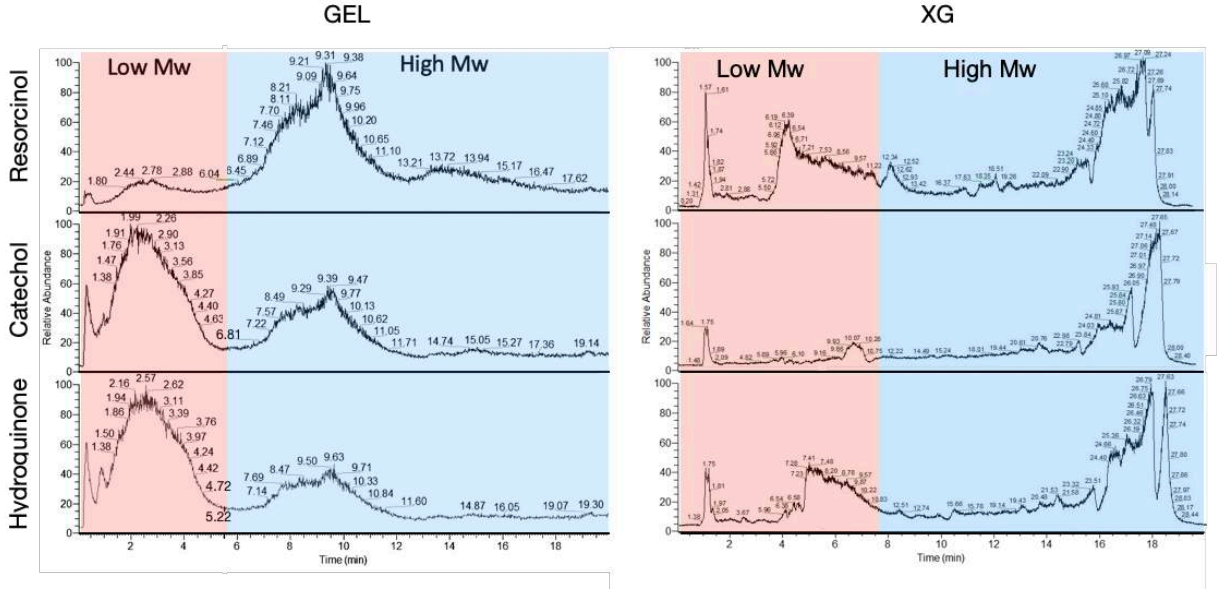

Figure 4.19. The ESI-MS for the supernatant products from the GEL and XG samples containing resorcinol, catechol and hydroquinone crosslinkers.

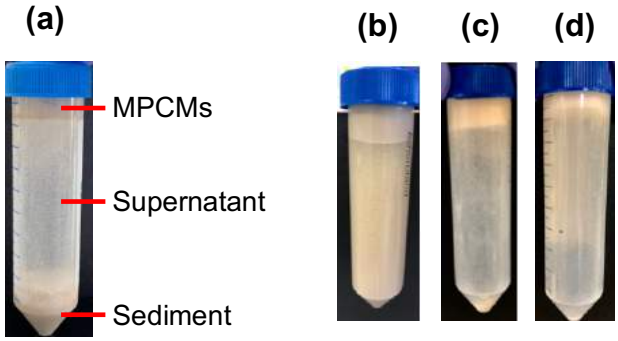

Figure 4.20. (a) The GEL-resorcinol centrifuge tube after centrifugation to separate the microcapsules, the supernatant and the sediment, (b) the GEL-resorcinol sample before sedimentation, (c) the GEL-catechol sample before sedimentation (d) the GEL-hydroquinone sample before sedimentation.

4.3.5. Reaction study (2): The Role of Ammonium Chloride

The addition of ammonium chloride (NH_4Cl) is pivotal in the microencapsulation process, as the addition of this modifier improves the sealing performance, heat resistance and mechanical strength of the microcapsules (Nguon *et al.*, 2017). The change of the pH in the aqueous phase with and without the addition of ammonium chloride has been a topic of interest to a few researchers (Brown *et al.*, 2003b; Fan, Tang and Zhou, 2013). Previous work expressed that the implementation of ammonium chloride results in a reduction in the pH during the reaction. It is typically believed that the reaction that causes the reduction in pH during the reaction is as follows (Fan, Tang and Zhou, 2013):

$$4NH_4Cl + 6CH_2O \rightleftharpoons (CH_2)_6N_4 + 6H_2O + 4HCl$$

$$NH_4^+ + H_2O + NH_3 \rightleftharpoons H_2O + H^+$$

The production of HCl therefore results in a reduction of the pH as the reaction proceeds. It is believed that the introduction of ammonium chloride disrupts the stability of the UF nanoparticles in the solution, therefore resulting in a rougher but less porous outer layer on the

microcapsule shell (Fan, Tang and Zhou, 2013). To investigate the effect of ammonium chloride and alternative salts, as well as the effect of initial pH on the encapsulation process, 5 sets of reactions were completed. Microcapsules with the GEL emulsifier were prepared with no ammonium chloride at both initial pH 2.5 and 3.5, and ammonium chloride, ammonium nitrate (NH_4NO_3) and ammonium carbonate ($(NH_4)_2CO_3$) were all prepared at an initial pH of 3.5. It is believed that the reaction between formaldehyde and NH_4NO_3 is as follows, to yield nitric acid:

$$4NH_4NO_3 + 6CH_2O \rightleftharpoons (CH_2)_6N_4 + 4HNO_3 + 6H_2O$$

While the reaction between formaldehyde and $(NH_4)_2CO_3$ is as follows, to yield carbonic acid:

$$2(NH_4)_2CO_3 + 6CH_2O \rightleftharpoons (CH_2)_6N_4 + 6H_2CO_3 + 6H_2O$$

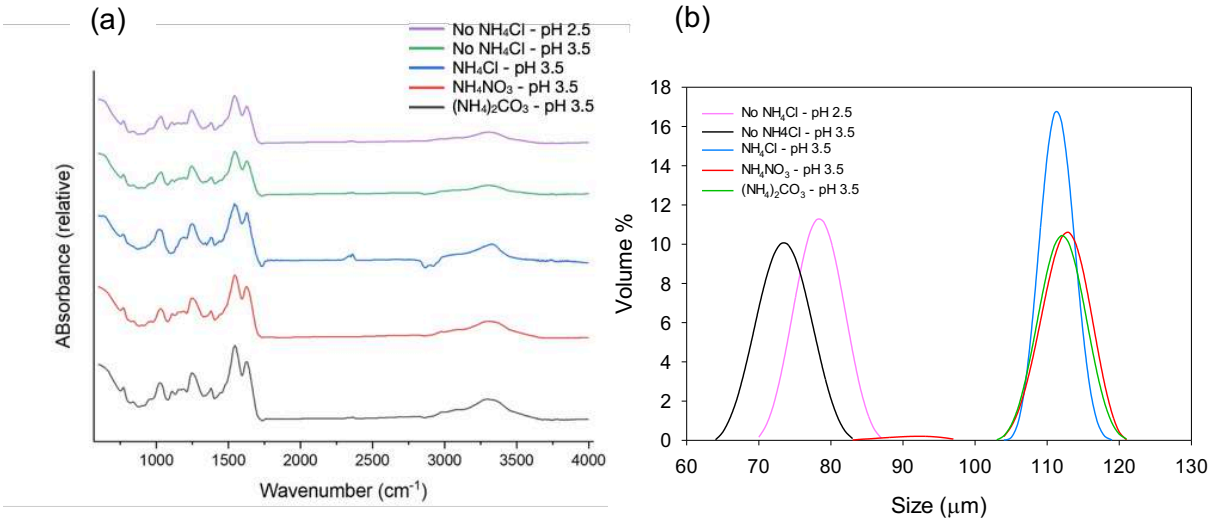

Figure 4.21. (a) FTIR analysis for the samples with and without salts and (b) the size distribution for the samples with and without salts.

FTIR analysis was then carried out for all the samples, as seen in Figure 4.21 (a). It can be observed that generally all the samples displayed very similar spectra. The size distribution for the microcapsule samples is conveyed in Figure 4.21 (b). As shown here, the samples without ammonium chloride have a smaller average size than those with incorporated salts. The sample with NH_4Cl exhibited the narrowest size distribution.

Subsequently, OM, FM and SEM images were curated, as shown in Figure 4.22. One immediate factor that was noticed is that the samples without NH_4Cl at pH 3.5 did not have any surviving microcapsules after the curing and ambient drying. The SEM images also convey very porous and incomplete shells, because of the incomplete shell formation. However, interestingly, the samples without NH_4Cl but with an initial pH of 2.5 exhibited improved results, with more surviving microcapsules. Fan *et al.* (Fan, Tang and Zhou, 2013) states that usually the pH of the reaction with the addition of NH_4Cl drops from the initial pH 3.5 to pH 2.5 as the reaction proceeds, so a manual reduction of the initial pH would suggest that the pH may be the driving force in the disruption of the stability of the UF nanoparticles, which proceeds to enrich the core. The two alternative salts conveyed excellent results, very similar to that of NH_4Cl, with the majority of the microcapsules surviving after 24 hours. Furthermore, the SEM of the samples with incorporated salts all conveyed a smooth and continuous shell.

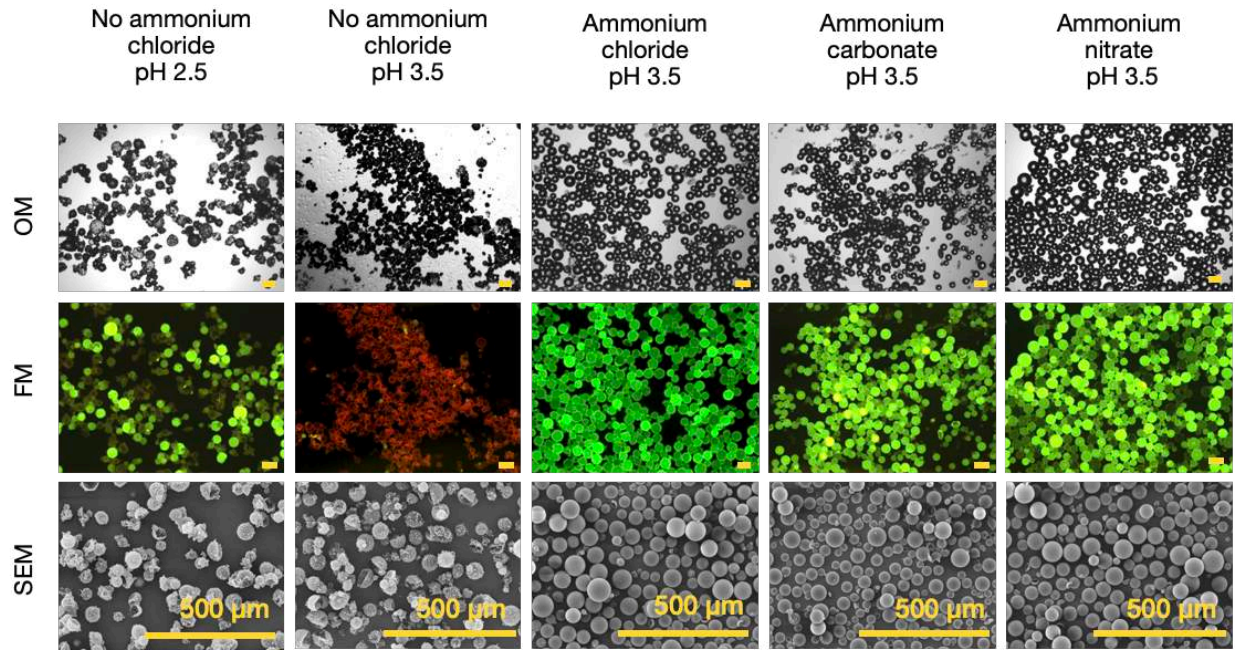

Figure 4.22. OM, FM and SEM images of microcapsule samples created with and without the addition of salts - dried after a period of 24 hours. OM and FM scale bars are 100 µm.

Various experiments were carried out to investigate the pH values during the reaction. As discussed previously, PEMA gave undesirable results when used as an emulsifier, producing porous and incomplete microcapsules, while GEL produced excellent microcapsules with superb oil retention. A comparative study was carried out in which the reaction conditions were identical for the two emulsifiers, and the initial pH was 3.5, and NH_4Cl was included. As shown in Figure 4.23 (a), the pH profile was very similar for both emulsifiers, with a correlation to the reaction temperature. As the reaction temperature rose from 20 °C to 55 °C, there was a rapid drop in pH from 3.5 to ~2.0. As the profiles were almost identical for both profiles, this suggests that in this case the emulsifier doesn't have a significant effect on the interaction of NH_4Cl with the reaction system. As shown in Figure 4.23 (b), the samples without NH_4Cl at initial pH 2.5 and 3.5 both conveyed a relatively constant pH value with no drop during the reaction duration. The addition of the alternative salts into the reactions conveyed similar pH profiles, with NH_4Cl and NH_4CO_3 dropping to pH 2.0, and $(NH_4)_2CO_3$ dropping to 2.15. These similar results to

when ammonium chloride was added conveyed that these salts can also reduce the pH to the required value during the polycondensation process and are suitable to be used as alternative salts.

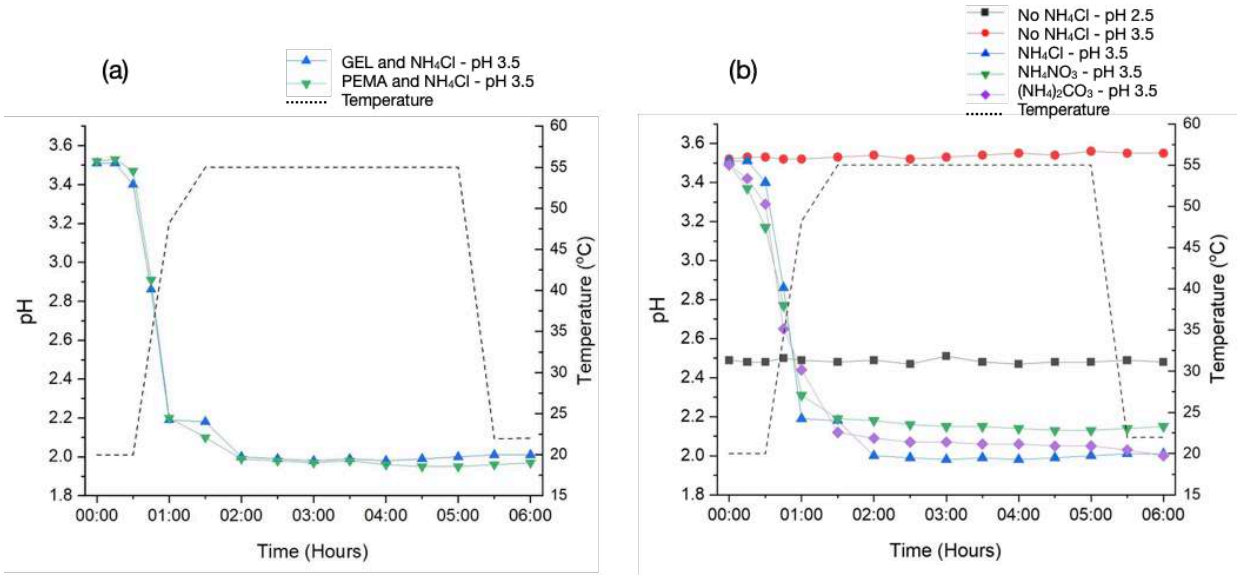

Figure 4.23. (a) The reaction pH study with GEL and PEMA; (b) the reaction pH profile study for the GEL samples with and without the addition of salts.

4.3.6. Reaction Study (3): Emulsifiers Influencing the Rate of Reactions

As shown by the previous results, the emulsifiers are seen to play a significant role in the formulation process, and greatly affects the microcapsule morphology, barrier, and mechanical properties. Interestingly, it seems that the emulsifiers with various functional groups, such as carboxyl, amine, amide and hydroxyl, seem to greatly affect the rate of reaction, from initial observation. An experimental study was then carried out to examine this, in which the aqueous emulsifier solution and the UF shell material was produced without any core material, to observe the rate of reaction over the duration of the reaction, in which monomodal particles were generated. For this, Mastersizer measurements were carried out at a temperature of 55 °C for the reaction products, for a duration of 4 hours.

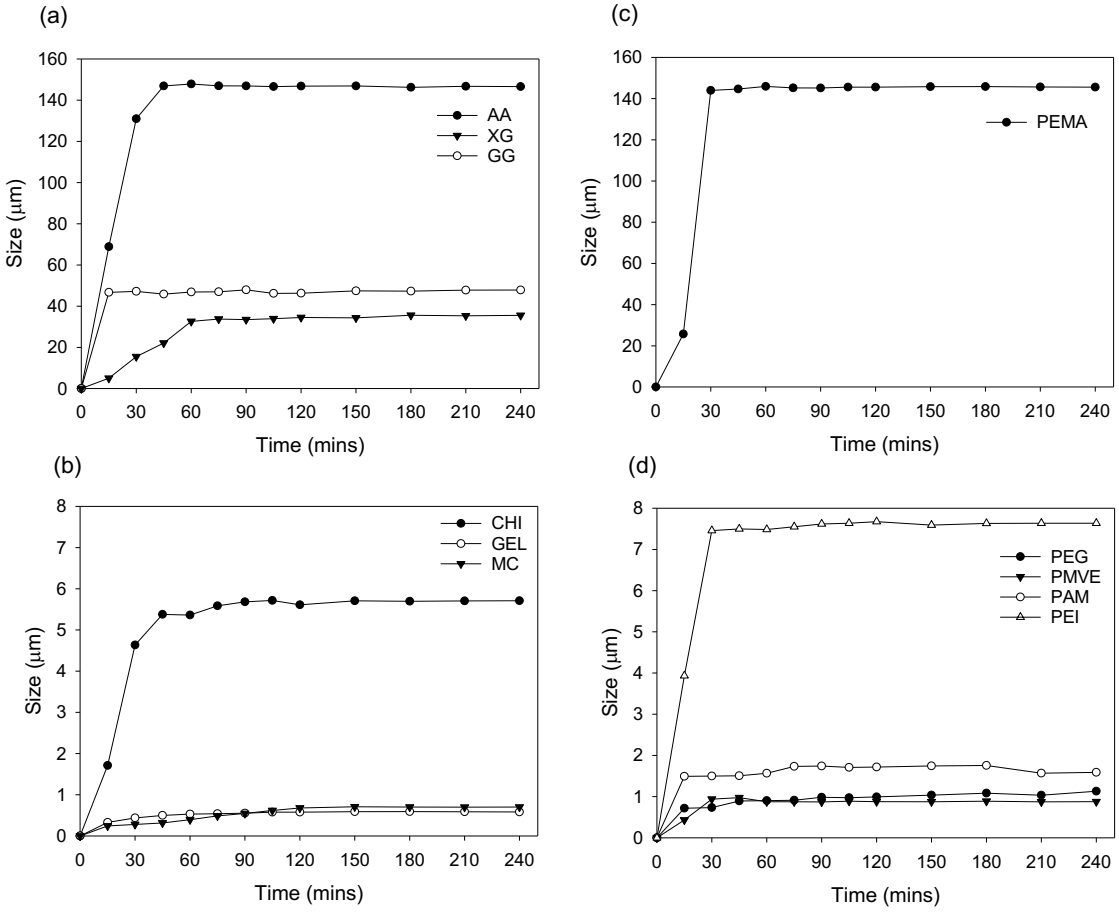

Figure 4.24. Mastersizer measurements for the UF polymer formation for (a) fast hydrocolloid reactions, (b) intermediate and slow hydrocolloid reactions, (c) fast synthetic polymer reactions, (d) intermediate and slow synthetic polymer reactions. The average D[3,2] values are shown.

Table 4.4. Initial reaction rates for the samples created with hydrocolloid and synthetic polymer emulsifiers.

Hydrocolloid	Functional Groups			Initial rate
	−OH	−NH2	−COOH	(µm.min^{-1})
GEL	Yes	Yes	Yes	0.02
CHI	Yes	Yes	No	0.11
XG	Yes	No	Yes	0.34
GG	Yes	No	Yes	3.11
AA	Yes	No	Yes	4.60
MC	Yes	No	No	0.02

Synthetic Polymer	Functional Groups			Initial rate
	−OH	−NH2	−COOH	(µm.min^{-1})
PEMA	No	No	Yes	1.72
PEG	Yes	No	No	0.05
PAM	No	Yes	No	0.10
PEI	No	Yes	No	0.26
PMVE	No	No	No	0.03

The reaction rate studies are conveyed in Figure 4.24, calculated using the tangent method in Sigma Plot (V.14.5) From primary observation, there is a significant disparity between the rates of reaction and also the polymer size with the various emulsifiers. AA and PEMA create extremely large UF particles compared to the other emulsifiers, with a maximum value of ~ 146 and 145 μm respectively. Interestingly, both emulsifiers have predominantly carboxyl (COOH) groups, suggesting that this group may greatly increase the rate of polymerization. Both emulsifiers also have the fastest initial rate, as shown in Table 4.4, with values of 4.60 and 1.72 $\mu m.min^{-1}$ respectively. As shown in Figure 4.24 (a), the hydrocolloids that also created large UF particles in a rapid manner were GG and XG, with the initial rate values of 3.11 and 0.34 $\mu m.min^{-1}$ respectively. Correspondingly, these two emulsifiers also have COOH groups, contributing again to the hypothesis suggesting that the polymerization process is accelerated by the COOH groups. As shown in the previous results, out of all the emulsifiers with the COOH groups, XG yields the most desirable microcapsules with excellent retention, while the other emulsifiers with COOH groups were not successful. This coupled with the slower rate, and the interaction with resorcinol, suggests that the viscosity factor of XG plays a part in the reaction process stability.

In Figure 4.24(b), the hydrocolloid emulsifier that had intermediate reaction rates was CHI, which has both OH and NH_2 groups, while the lowest reaction rate was conveyed by GEL and MC. GEL has COOH, NH_2 and OH groups, while CHI only has OH groups. In terms of the hydrocolloid emulsifiers, GEL produced superb microcapsules with excellent payloads, and it is interesting that all three of the main functional groups are present. The synthetic polymers that have intermediate reaction rates are PEI and PAM, with a reaction rate of 0.26 and 0.10 $\mu m.min^{-1}$. PEG and PMVE conveyed the lowest initial rate for the synthetic polymers, and these two emulsifiers do not have distinctive functional groups contributing to the process.

The crosslinking of GEL in the presence of formaldehyde and resorcinol was studied by (Gringras and Sjöstedt, 1975), in which UV-spectra suggested that the reactions occurring are (1) a Mannich type reaction and (2) a resol type reaction in which there is a dimetylene ether bridge. Furthermore, PEI and PAM are suggested to also react in a similar manner (Gringras and Sjöstedt, 1975). The Mannich reaction consists of amino-alkylation of acidic protons, placed alongside carbonyl functional groups by formaldehyde and a primary or secondary amine. A final β-amino-carbonyl compound is formed, which is termed as a 'Mannich base'. Since urea also has amino groups, the emulsifiers with these groups may also react in a similar manner. This scheme is conveyed in Figure 4.25.

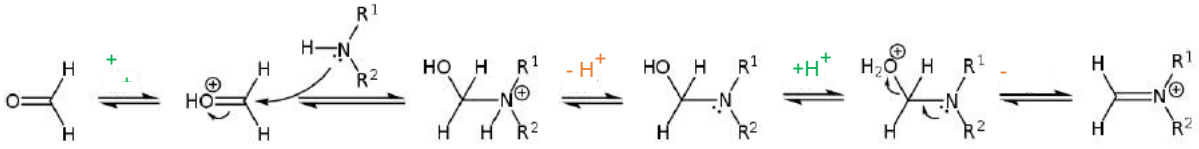

Figure 4.25. Mannich Base reaction mechanism

In the case of the one step in situ polymerization process, and collating all the evidence in this research paper, we therefore suggest that the reaction rate ranking in terms of functional groups are as follows:

Carboxyl > Amine/amide > hydroxide

The carboxyl acids on the emulsifiers greatly accelerate the formation of the UF particles, in a manner that is too fast to produce compact, dense, and structurally sound shells, with the exception of XG. The emulsifiers with amine/amide groups such as GEL, MC, PAM and PEI all produced superb microcapsules with excellent retention. The emulsifiers with OH groups conveyed the slowest initial rate, and PEG produced samples with extremely porous shells,

exhibiting core material leakage. With these factors conveyed, this may then provide an input on the selection criteria for the one step in situ polymerization processes and the emulsifiers of choice, dependant on the microcapsule target applications.

4.4. CONCLUSIONS

In this chapter, a range of emulsifiers and their role in the formulation of volatile core microcapsules via the one-step in situ polymerization process were investigated. These emulsifiers contain an array of functional groups, with carboxyl, amine, amide and hydroxy groups. Previous researchers have claimed the importance of carboxylic acids/anhydrides as functional groups for emulsifiers; however, in the case of our more volatile PCM core, these emulsifiers produced very porous and rough MPCMs. A few emulsifiers were screened, and a volatile heptane core with very high payloads and excellent oil retention was encapsulated. Notable emulsifiers with successful results include GEL, MC, XG, CHI, PAM and PEI.

It was evidenced by this work that the interfacial tension and dilatational rheology influencing the emulsion stability, although it is a pre-requisite, was not the determining correlating factor in terms of the emulsifier contributions. However, the importance of resorcinol was clearly conveyed in this work, due to the more stable resonance structures compared to catechol and hydroquinone alternatives. Also demonstrated was the effect of alternative salts, and how the emulsifiers did not exhibit much interaction in this case. However, it was established that the reduction of the pH via the addition of salts is incredibly necessary. Without the reduction of the pH caused by the dissociation of the H+ ions, the microcapsules did not survive the ambient drying after the formulation and filtration process.

Moreover, to further prove the effect of emulsifiers in this process, the reaction rate studies confirmed that the emulsifier functional groups have the following reactivity: carboxyl > amine/amide > hydroxide, a key finding in this section. Therefore, this work has strongly proved the extent to which emulsifier selection is crucial to the one step in situ polymerization process, and how such emulsifiers affect the microcapsule properties, which is a fundamental consideration when considering the practical applications of the MPCMs.

CHAPTER 5: TAGUCHI AND ANOVA ANALYSIS: THE PROCESS OPTIMIZATION FOR THE MICROENCAPSULATION OF A VOLATILE PCM

The work presented in this chapter has been published in the following journal paper: **Abdullah Mustapha,** Yan Zhang, Zhibing Zhang, Yulong Ding, Qingchun Yuan, Yongliang Li. (2020) '*Taguchi and ANOVA analysis for the optimization of the microencapsulation of a volatile phase change material'*. **Journal of Materials Research and Technology.** DOI: 10.1016/j.jmrt.2021.01.025

5.1. CHAPTER OVERVIEW

The microencapsulation process relies on multiple controllable and uncontrollable formulation process parameters, which interrelate in a synergistic manner (Nguon *et al*., 2017). The optimal combination of key controllable parameters is pivotal for the overall process, in terms of increasing production output, process efficiency, reducing energy consumption, as well as decreasing the effects of uncontrollable parameters. Due to the capacious variables that are involved in the encapsulation process, it can be an arduous task to assign the individual outcome of specific parameters (Chuanjie, Juntao and Xiaodong, 2013). Conventionally, optimization studies involve the variation of one controllable parameter, while other controllable parameters

remain constant. However, this is a very strenuous technique that can be both time consuming and expensive (Pundir, Chary and Dastidar, 2018). In order to determine the optimal conditions for the formulation of the microcapsules to gain high payload and encapsulation efficiency, a time-efficient orthogonal factorial design method known as the 'Taguchi' method was utilised instead in this chapter as it offers the advantage of optimizing the process with fewer required experimental procedures (Sharma and Choudhary, 2017). The Taguchi method is a powerful tool to identify the optimal combination of process parameters to reduce the cost, improve the quality, and/or increase the efficiency.

In conjunction with the 'Taguchi' technique, the Analysis of Variance (ANOVA) method is an established method that is utilised to verify the percentage contribution of each process parameter on the desired outputs. In particular, the parametric studies have been carried out on PCM microcapsules with less volatile core materials, such as PMMA (Sharma and Choudhary, 2017), paraffin wax (Jamekhorshid, Sadrameli and Bahramian, 2014), hexadecane (Khakzad *et al*., 2014) and lauric acid (Sami, Sadrameli and Etesami, 2018). The recent advancement in the retention of volatile organic compounds for low temperature energy storage applications inflates the requirement of optimising process conditions for the successful and efficient core encapsulation (Zhang, *et al*., 2019).

In this chapter, experimental work on the microencapsulation of volatile PCMs was conducted firstly to find the optimal combination of formulation parameters (including reaction time, pH, homogenization speed and reaction temperature) using the Taguchi technique, and then to examine the contribution of these parameters using the ANOVA method. The overall goal was to identify the optimal controllable process parameter values and also which parameters were

needed to be precisely controlled while maintaining reasonably high payload, yield, and encapsulation efficiency for potential scale-up manufacturing.

5.2. PROCESS PARAMETER SELECTION

In this study, various process parameters can be selected to be optimized, in order to maximise the yield, payload and/or encapsulation efficiency. Nguon *et al*. (2017) discussed the various variables that can be manipulated to target various determining parameters. For example, to optimize yield, previous studies variables that were optimized included core/shell ratio, reaction time, homogenization speed, initial pH, and the heating rate (Nguon *et al*., 2017). For the payload, parameters such as reaction temperature, homogenization rate, reaction time and core/shell ratios were deliberated. In our process, the payload as well as the encapsulation efficiency are the key optimal targets while the yield is a secondary indictor, as the core/shell ratio optimization is the most used method to increase the yield (Nguon *et al*., 2017).

As a compact MPCM shell is required to retain the highly volatile core material, a constant and low core/shell ratio was selected based on our preceding experience (Zhang *et al*., 2018; Zhang *et al*., 2019a; Zhang *et al*., 2019b). As a result, reaction time, reaction temperature, pH value and homogenization speed were selected as the process controllable parameters. Furthermore, after selecting these process conditions, screening experiments were carried out to identify a suitable operating range of these parameters, and to have an initial identification on how they may contribute to the formulation process. Additionally, 0.03 % GEL was used as the emulsifier of choice throughout all of the formulation processes in this chapter due to the excellent core retention, payload, mechanical properties observed in Chapter 4.

5.2.1. The Effect of Reaction Time

To preliminarily explore the effect of time on the reaction progression, a batch was made at pH 3.5 and 55 ºC, consisting of the reactive substituents without the heptane core material, to examine the size growth of the shell polymer particles over time. The experimental conditions were based on the method carried out by Brown *et al*. (2003). As shown by Figure 5.1, it seems that a rapid increase in the polymer size occurs from time 15 min to ~ 90 min and stabilises at ~ 120 minutes onwards. Therefore, a 3-hour reaction time was proposed as the minimum, followed by 4 hours, and 8 hours. A 2-hour batch (containing the heptane core) was initially formulated but there was immediate leakage of the heptane, as observed under the fluorescence microscope (FM), whereas a 3-hour batch survived the 24 hours of ambient drying, as shown in Figure 5.1 (b) and (c).

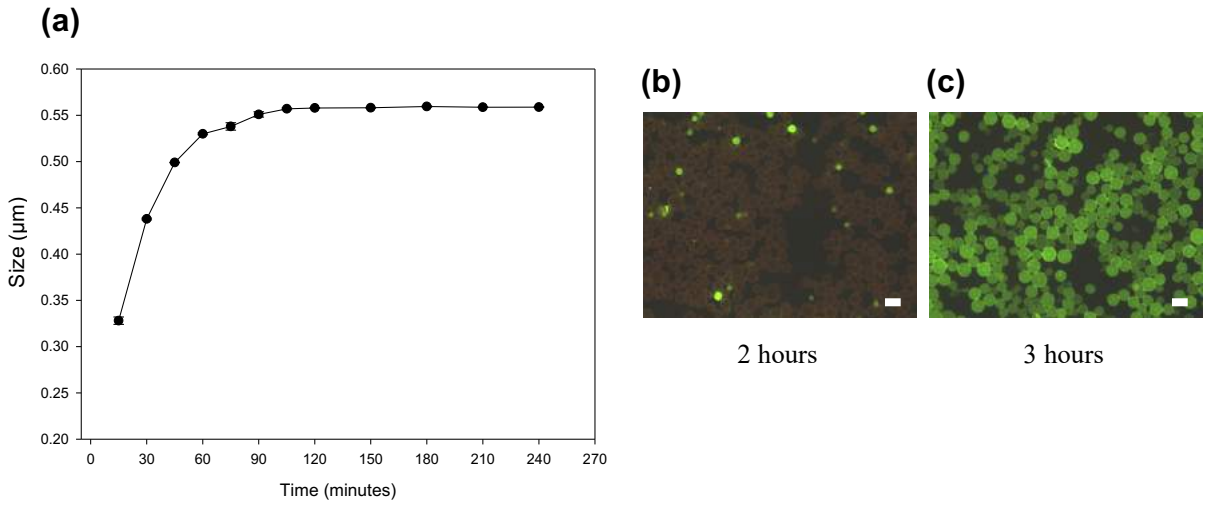

Figure 5.1. (a) Size growth profile of the shell particles over a duration of 4 hours; (b) 24-hour dried FM image of the microcapsules formulated over 2 hours; (c) 24-hour dried FM image of the microcapsules formulated over 3 hours. Scale bars are 100 µm, and average D[3,2] values are shown.

5.2.2. The Effect of Reaction pH

As the in situ polymerization reaction is dependent on the initial pH of the reaction, this was an essential factor to study. Since methylol-ureas are low molecular weight pre-polymers that are formed in the initial stages of the encapsulation process, higher pH values would result in higher amounts of methylol-ureas, leading to smoother samples. Lower pH values result in methylene and ether bridged compounds, resulting in rougher and potentially more porous shells (Nair and Francis, 1983), which may affect the payload and the long term retention of the core. However, it is important to note that the one-step in situ polymerization process can only occur in acidic pH, and there must be a limitation on how low the pH is set to bequeath smooth microcapsules. Rochmadi, Prasetya and Hasokowati (2010) stated that in acidic conditions, the rate of condensation is higher, and provided a proposed reaction rate equation:

$$R_{uf} = k_r\left(C_{uf}\right)^2 + k_c a\left(C_{uf} + C_{uf,s}\right) \quad (5.1)$$

where R_{uf} is the overall condensation reaction rate for the formation of urea-formaldehyde (UF) particles, k_r is rate constant, $k_c a$ is the mass transfer coefficient, C_{uf} is the aqueous phase UF pre-polymer concentration, $C_{uf,s}$ is the UF pre-polymer concentration on the microcapsule surface, $k_r(C_{uf})^2$ is the rate of formation of the UF polymer micro/nanoparticles, and $k_c a\left(C_{uf} + C_{uf,s}\right)$ is the rate of formation of the microcapsule shell.

Rochmadi, Prasetya and Hasokowati (2010) also stated that the reaction rate constant, k_r, is proportional to the H+ concentration in the solution. Therefore, a very high H+ concentration in the solution (a low pH), results in a higher k_r, consequently promoting the rate of formation of branched UF particles at an accelerated manner. This is in agreement with the work carried

out by Katoueizadeh, Zebarjad and Janghorban (2019), who stated that at high pH values (above 7), the condensation reactions did not occur.

Yuan, Gu and Liang (2008) investigated the effect of pH for the formulation of liquid poly sulphide with a UF shell, with a pH range of 2 to 4.5. It was observed that at pH 4.5, there was a deceleration of the polymerisation rate, while at pH 2, accelerated polymerization was observed, with increased surface roughness of the microcapsules due to participate formation.

To investigate the effect of pH, 3 batches were made, all with 3 hours reaction time, 55 ºC and a homogenization speed of 1200 rpm. The initial pH values were altered, all with values of 2.5, 3.5 and 4.5. It can be seen from the SEM micrographs on Figure 5.2 (a) that the pH 2.5 samples had a much rougher shell surface, with a larger proportion of UF microparticles. The sample with pH 4.5 yielded a much smoother profile, with smaller UF satellite nanoparticles present. Central areas of the image were selected and using ImageJ (an image processing programme) and MATLAB, the proportion of the smooth profile to the lighter satellite particles (surface particles) in terms of total area on the SEM micrographs were quantified, as seen on Figure 5.2 (b). With 5 images taken, the average proportion of satellite particles (SP) to the smoother membrane (M) was postulated. It was calculated that the pH 2.5 had a SP composition of 13.3 %, while pH 3.5 had 6.3 %, and pH 4.5 with 3.3 %. Therefore, the pH range was selected to be 2.5 – 4.5 for the process optimization parameter experiments.

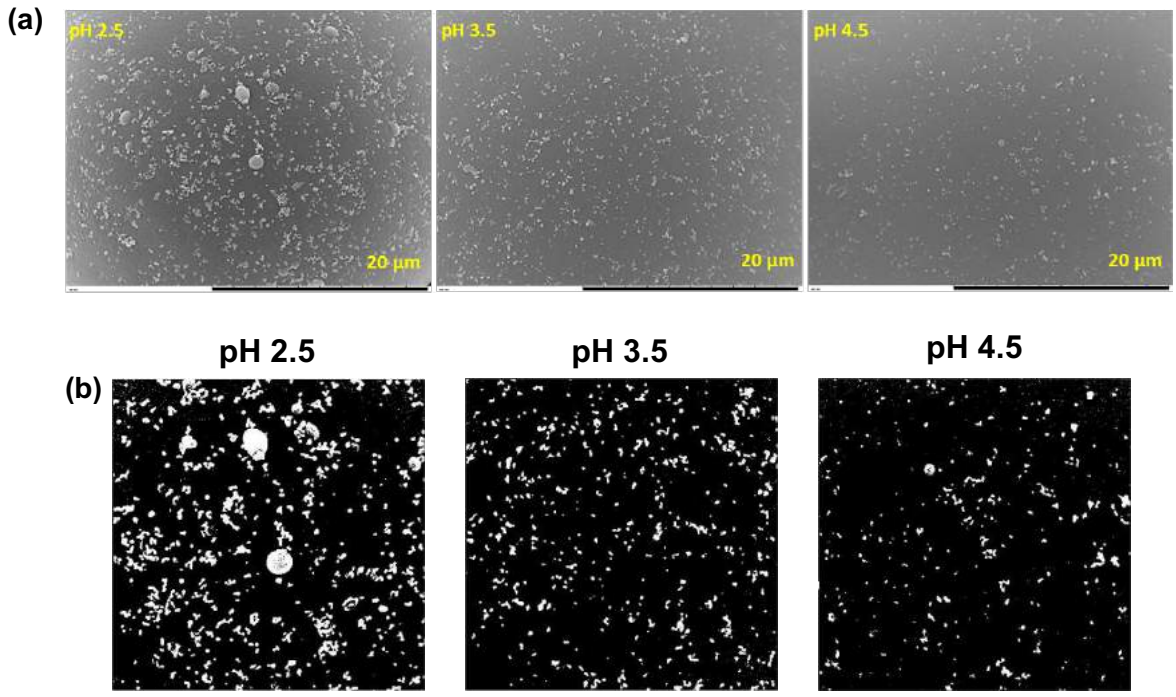

Figure 5.2. (a) SEM micrographs of the surface of individual microcapsules with various pH values made with the following reaction conditions: 3 h reaction time, 55 °C reaction temperature, 1200 rpm homogenization speed; (b) binary images of the SEM images for the increasing pH samples (binary images are all 650 pixels by 650 pixels).

5.2.3. The Effect of Reaction Temperature

The reaction temperature in the one step in situ polymerization process is also another important factor to study. The rate of UF polymer formation and microcapsule shell thickness is proposed to be determined by the pH and reaction temperature (Nguon *et al*., 2017). Fan and Zhou (2010) propositioned that the porosity of the outer shell layer is dependent on the rate of UF nanoparticle formation. Nguon *et al*. (2017) suggested that the rate of nanoparticle formation is dependent on the rate of polycondensation, which is also affected by the reaction temperature. For example, during the encapsulation of palm oil with a UF shell, an increase of the reaction temperature from 50 °C to 70 °C resulted in the increase of nanoparticle formation and resulted in a reduction of encapsulation efficiency by 80 % (Rochmadi, Prasetya and Hasokowati, 2010).

Furthermore, the encapsulation of liquid polysulphide with a UF shell at 80 ºC resulted in very irregular microcapsules with poor core material retention and large precipitates (Yuan, Gu and Liang, 2008). Increasing the rate of polymer formation (by increasing the temperature), results in greater formations of nanoprecipitates, shortening the deposition on the core surface (Nguon *et al*., 2017). However, a temperature that is too low is not enough to break the energy barrier required for the reaction. Cosco *et al*. (2007) disclosed that during the encapsulation of epoxy with a UF shell at 60 °C and 40 °C, low reaction temperatures affected the encapsulation efficiency. To explore the effects that reaction temperatures have on the encapsulation efficiency and payload, a range of 45 °C, 55 °C and 65 °C was used for the orthogonal array.

5.2.4. The Effect of Homogenization Speed

For the core material dispersion into the aqueous phase, a minimum shear rate is required for the mixing between the two immiscible phases. If this minimum shear rate is achieved, there is an inverse relationship between the size of the droplets, and the homogenization rate (Nguon *et al*., 2017). Depending on the shear rate, the morphology and size distribution of the microcapsules will vary. During the encapsulation of n-octadecane, Zhang *et al*. (2004) observed an increase in diameter with a decrease in homogenization speed, as well as a smoother shell, leading to a higher payload. Dong *et al*. (2007) also observed that an increase in the homogenization speed while encapsulating peppermint oil, led to multinuclear microcapsules with a lower oil content. There have been many studies in which the homogenization speed has been varied to study the effects on the microcapsules, many of which ranging from 400 rpm to 2000 rpm (Brown *et al*., 2003a; Dong *et al*., 2007; Salaün *et al*., 2009; Fan and Zhou, 2010; Sami, Sadrameli and Etesami, 2018). For this study, a range of 600 rpm, 1200 rpm and 1800 rpm were used.

5.2. TAGUCHI ORTHOGONAL ARRAY

The Taguchi orthogonal array was utilized to identify the optimal process parameter combination. In this chapter, the controlled variables were altered in order to manipulate the noise factors (uncontrollable factors). These noise factors are external stimuli that are difficult to control, affecting the formulation process. Examples of these include ambient temperature, process equipment vibrations and environmental humidity. The identification and consequent exploitation of the optimal control factor settings is therefore the aim to enhance the formulation process.

From the results, the signal to noise ratio (S/N) can calculated, in which the key control variables can be identified to reduce the noise factors (Kivak, Samtaş and Çiçek, 2012; Sharma and Choudhary, 2017; Pundir, Chary and Dastidar, 2018). In this study, the S/N ratios for each of the control factors were calculated, to maximise the payload, yield, and encapsulation efficiency of the microencapsulation process. Depending on the goal of the experimental targets, there are three main cases of S/N ratios, as shown in Table 5.1.

Table 5.1. S/N ratio experimental goals and equations.

S/N Ratio	Experimental Goal	Ratio
Nominal is the best	Positive, zero or negative	$\left(\frac{S}{N}\right) = -10\log\left(\frac{1}{n}\sum_{i=1}^{n}(y_i^2 - y_0^2\right)$
Larger is better	Maximise the response	$\left(\frac{S}{N}\right) = -10\log\left(\frac{1}{n}\sum_{i=1}^{n}\frac{1}{y_i^2}\right)$
Smaller is better	Minimising the response	$\left(\frac{S}{N}\right) = -10\log\left(\frac{1}{n}\sum_{i=1}^{n}y_i^2\right)$

These three cases are termed as 'nominal is best', 'larger is better' and 'smaller is better' S/N values. Since this study is aimed to maximise the yield, payload and encapsulation efficiency, the S/N ratio targets to achieve that 'the larger is better' were used. The S/N values are calculated from experimental outputs, in which S is the signal value, N is the noise value, n is the number of experimental repetitions, y_i is the measured response value (payload, yield, or encapsulation efficiency). The S/N ratio values were used to quantitively measure a response (e.g., the microcapsule payload) as a result of altering a parameter in the formulation process.

As discussed in section 5.2, the four factors to be investigated include reaction time, pH, temperature and homogenization speed. Table 5.2 conveys the synthesis conditions utilized to prepare the microcapsules, all of which have 3 levels. Minitab, a statistical design software package, was utilised to design the Taguchi orthogonal array, as shown in Table 5.3.

Table 5.2. Selected reaction control factors and respective levels.

Level	Factor			
	Reaction time (h)	**pH**	**Temp (°C)**	**Homog. Speed (rpm)**
1	3	2.5	45	600
2	4	3.5	55	1200
3	8	4.5	65	1800

Table 5.3. Orthogonal array of process variables for optimization.

Run	Reaction time (h)	pH	Temp (°C)	Homog. speed (rpm)
1	3	2.5	45	600
2	3	3.5	55	1200
3	3	4.5	65	1800
4	4	2.5	55	1800
5	4	3.5	65	600
6	4	4.5	45	1200
7	8	2.5	65	1200
8	8	3.5	45	1800
9	8	4.5	55	600

Table 5.4. Taguchi orthogonal experimental results for the payload, yield, and encapsulation efficiency, as well as the respective calculated S/N values.

Run	Factors				Results					
	Time	pH	Temp	Homog. Speed (rpm)	PL (%)	S/N PL	Yield (%)	S/N Yield	EE (%)	S/N EE
1	3	2.5	45	600	30.5	34.5	11.8	26.2	5.9	20.2
2	3	3.5	55	1200	95.2	44.3	30.5	34.5	71.1	41.8
3	3	4.5	65	1800	87.3	43.6	28.6	33.9	61.7	40.6
4	4	2.5	55	1800	85.5	43.4	28.7	33.9	61.9	40.6
5	4	3.5	65	600	96.1	44.4	28.9	33.9	68.7	41.5
6	4	4.5	45	1200	15.2	28.4	13.8	27.6	5.3	19.3
7	8	2.5	65	1200	41.1	37.0	16.1	28.9	33.9	35.4
8	8	3.5	45	1800	24.2	32.4	12.3	26.6	7.4	22.2
9	8	4.5	55	600	95.3	44.4	28.7	33.9	67.4	41.3

The effects of the reaction factors on the payload, yield and encapsulation efficiency were collated and quantified, as displayed in Table 5.4. The experimental results were evaluated, and the corresponding S/N values were calculated. From primary observation, it is apparent that the lowest payloads were obtained for the samples produced at 45 ºC, with 30.5% (S/N 34.5), 15.2 % (S/N 28.4) and 24.2 % (S/N 32.4) for reaction-set 1, 6 and 8 respectively. A similar trend is also observed for yield and encapsulation efficiency. To further explore this, OM and FM were utilised to observe the microcapsules.

Over a 24-hour period, the core material retention was studied, by utilising FM to study the Nile red preservation in the capsule. It is conveyed in Figure 5.3, Figure 5.4, and Figure 5.5 that all of the capsules produced at 45 ºC (set 1,6 and 8) had very poor retention, with the majority of the capsules collapsing over a 24-hour period. Furthermore, another batch that was produced at 65 ºC, and the capsules also collapsed after 24 hours, as seen on image 7(C) on Figure 5.5.

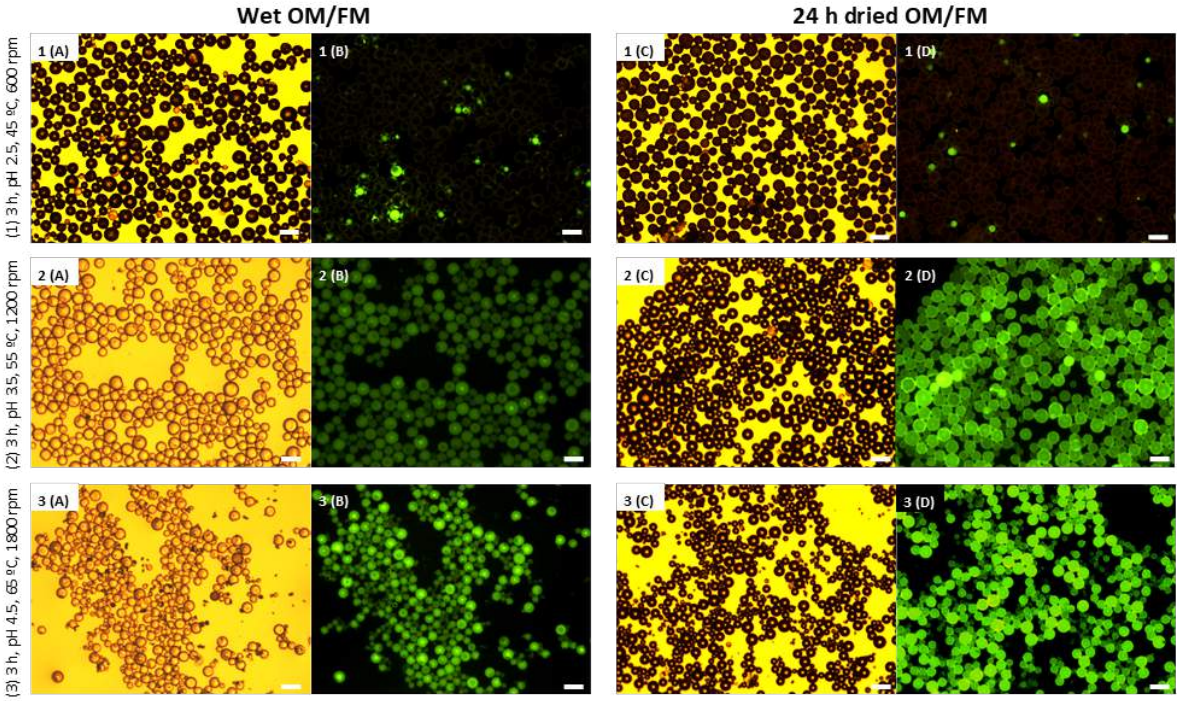

Figure 5.3. OM and FM images of set 1-3 microcapsules, dispersed in water and after a 24 h drying period. All scale bars are 100 µm.

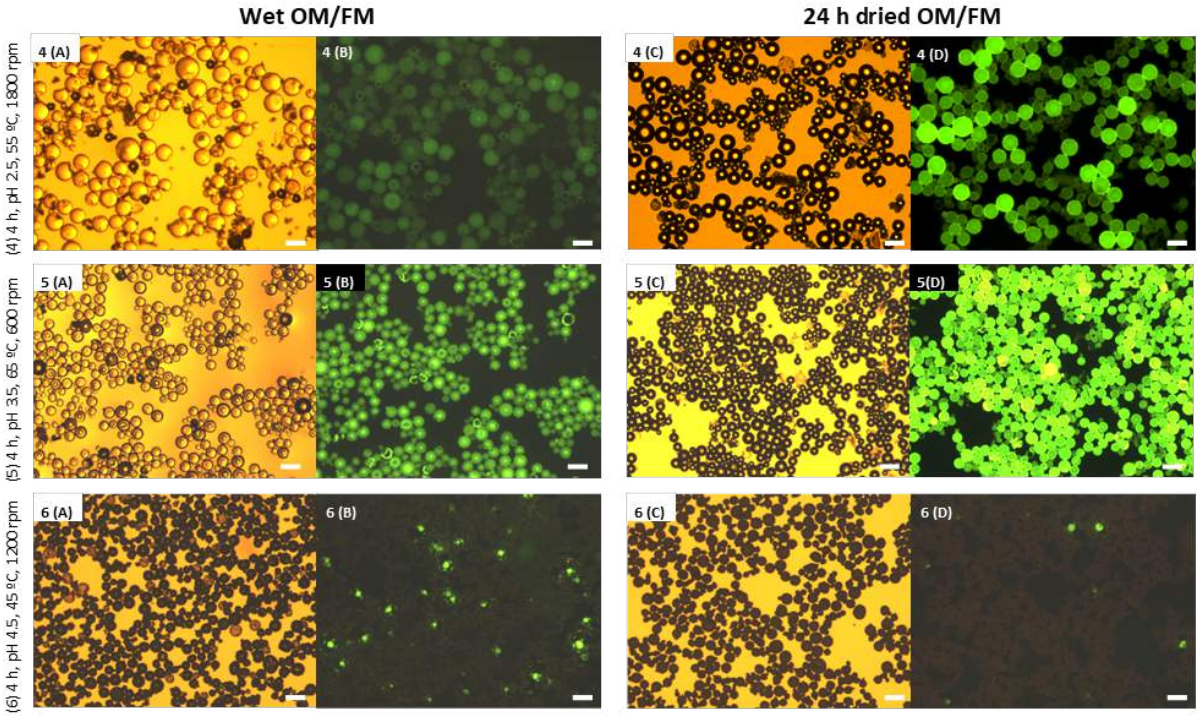

Figure 5.4. OM and FM images of set 4-6 microcapsules, dispersed in water and after a 24 h drying period. All scale bars are 100 µm.

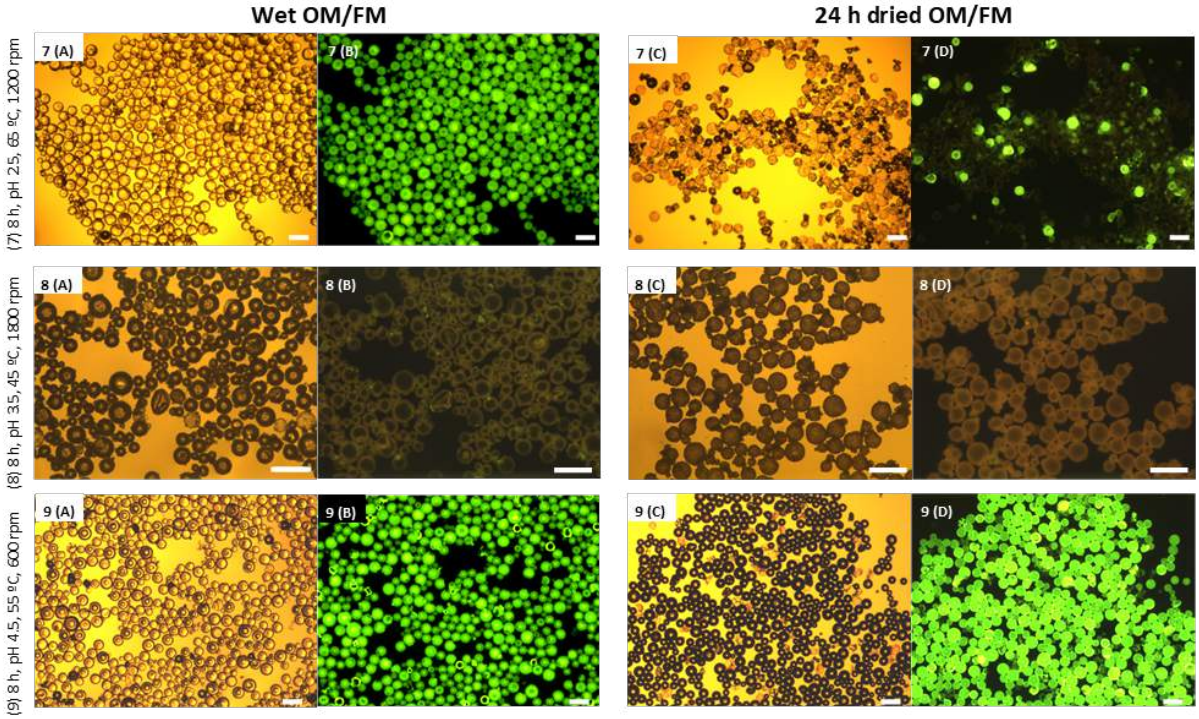

Figure 5.5. OM and FM images of set 7-9 microcapsules, dispersed in water and after a 24 h drying period. All scale bars are 100 µm.

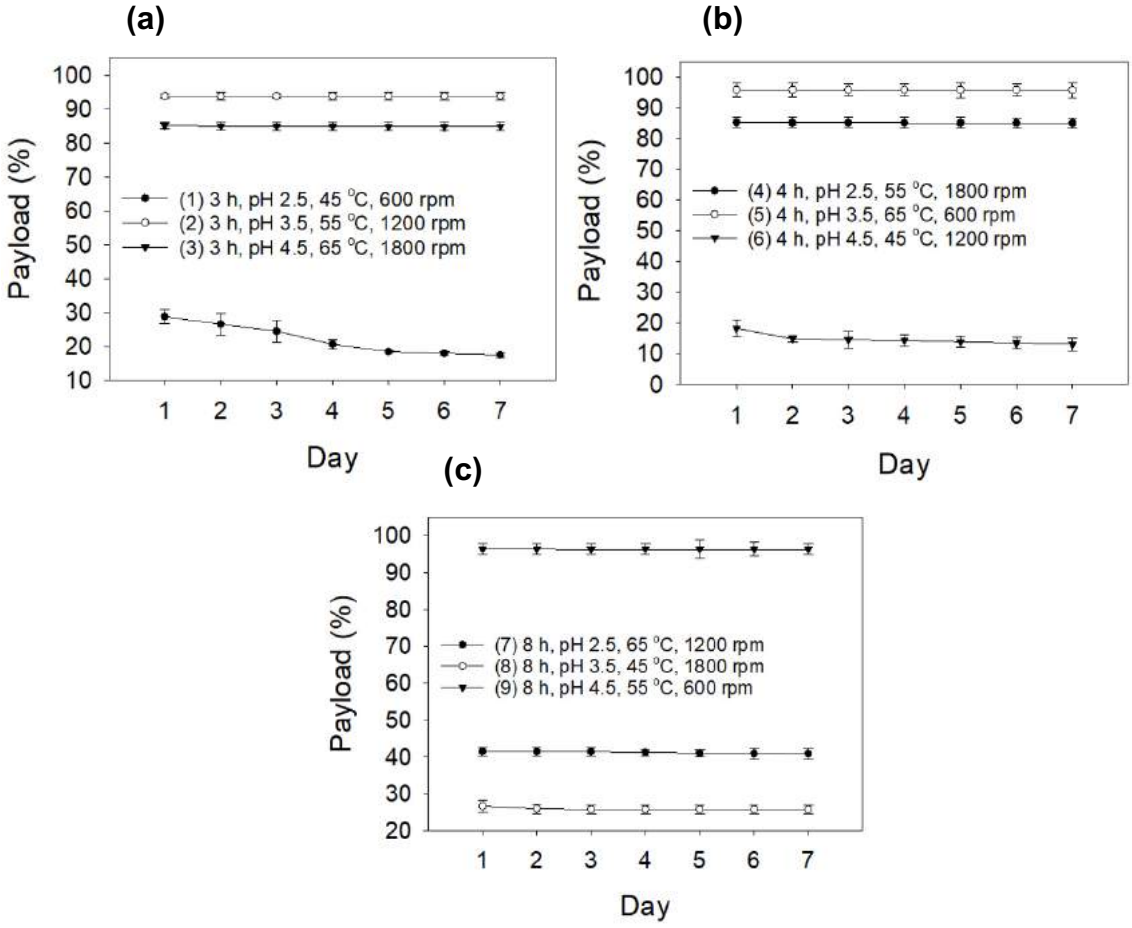

Figure 5.6. Payload measurements over a 7-day period for the 9 sets of formulated batches, with (a) 3 hour reaction, (b) 4 hour reaction and (c) 8 hour reaction.

As well as the OM and FM images to analyse core material retention, a 7-day payload analysis was carried out by observing the weight change over time, as shown in Figure 5.6. The results are in agreement with the OM and FM images, and all of the capsules prepared at 45 ºC had very low retention, with set (1) having 17 % on the 7th day, set (6) having 13 %, and set (8) having 25 %. Furthermore, set (7) also had a low payload of 41 %, in agreement with the FM image 7(D) in Figure 5.5. There were 3 batches that had exceptionally high payloads above 90 %, which included set (2) obtaining 94 %, set (5) obtaining 96 % and set (9) obtaining 95 % after the 7-day ambient drying period. However, reaction-set 2 was produced with the lowest reaction time of 3 hours, while reaction-set 5 and 9 were 4 and 8 hours respectively. In terms

of time and cost saving, a 3- or 4-hour reaction time with excellent payload would be beneficial, while an 8-hour reaction would not provide any additional benefits in terms of payload in this case.

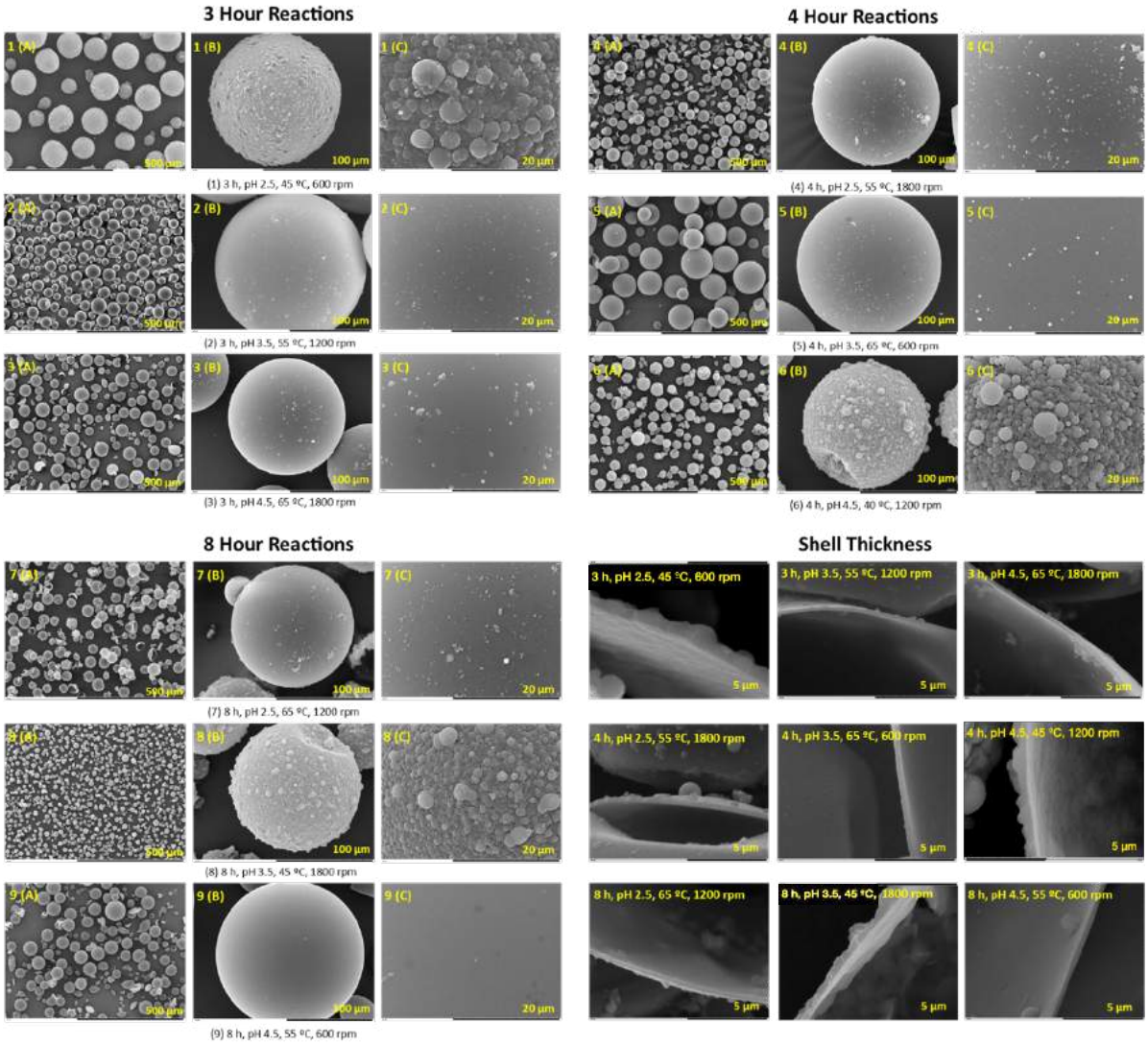

Figure 5.7. SEM micrographs of reaction sets 1-9 for the 3-hour, 4-hour and 8-hour reaction. For each set, the overall morphology, individual capsule, and surface roughness is shown. Shell thickness micrographs for sets 1-9 also displayed.

Discerned in Figure 5.7 are the microcapsule SEM micrographs and shell thickness. All of the in situ polymerisation processes at 45 °C (sets 1, 6 and 8) produced much rougher microcapsules, as well as thicker shells. For example, reaction set (1) had a shell thickness of 984 ± 86 nm, while reaction set (2) and (3) had shell thicknesses of 255 ± 19 nm and 217 ± 14 nm respectively. The UF particles formed at 45 ºC engendered thick and rough shells, with poor coverage and high resultant porosity, which may contribute to the poor payload and high leakage of the microcapsules. It is also evident that the higher the temperature for the microcapsules, the thinner the shells are observed to be. However, as deliberated, the prerogative over the kinetics of the reaction is also affected by the pH of the reaction, which can also affect the surface roughness. It is onerous to discern whether reaction time had much of an effect on the shell thickness, due to the synergistic properties of the multi-component factorial experimental conditions.

S/N ratio plots were then plotted for each process parameter studied; (a) the reaction time, (b) the pH, (c) the reaction temperature and (d) the homogenization speed, as conveyed in Figure 5.8. As the aim of this work was to maximise the response, the higher the S/N ratio, the more significant that parameter was at reducing the noise factors. Considering the 9 orthogonal arrays, 3 hours reaction time had the highest S/N ratio. A pH of 3.5 was calculated to have the highest S/N ratio, followed by a stirring speed of 1200 rpm, as well as a temperature of 55 ºC. Therefore, the most efficient combination of process parameters is 3 h, pH 3.5, 55 ºC and 1200 rpm. Customarily, a confirmation experiment is required for these specific parameters to evaluate the individual S/N ratios for the payload, yield, and encapsulation efficiency, however, it is expedient that reaction-set 2 has these exact parameters, as shown in Table 5.3. With these results, it is evident that 3 hours reaction time is sufficient to create capsules with excellent core material content and retention.

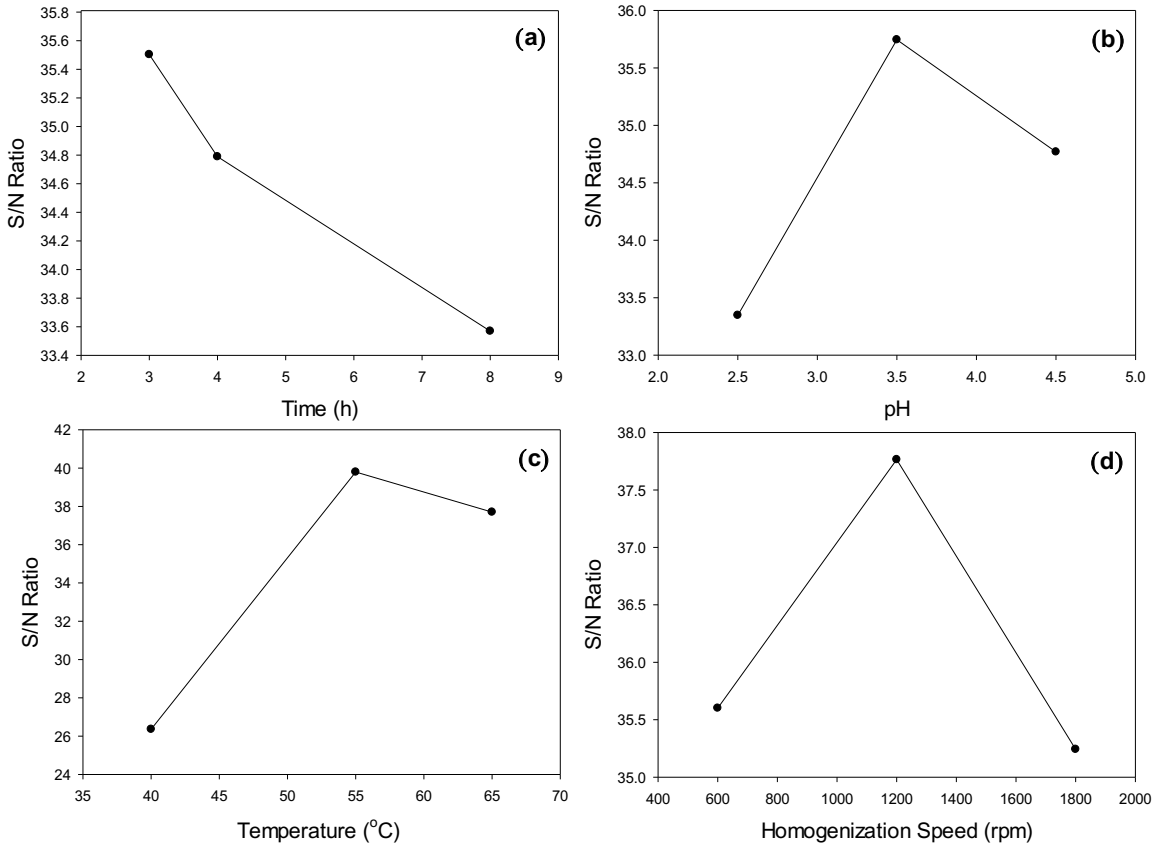

Figure 5.8. S/N ratio plots for the effects of process parameters on (a) the reaction time, (b) the pH, (c) the reaction temperature and (d) the homogenisation speed.

The study carried out by Brown *et al*. (2003) for the formulation of dicyclopentadiene microcapsules had process parameters of 4 h, pH 3.5, 55 ºC, and various stirring speeds from 200 – 2000 RPM. Other examples of the formulation processes being maintained for 4 hours include Ullah *et al*. (2016), Bolimowski, Kozera and Boczkowska (2018) and Zhang, Zhou and Ye (2019). However, this study has shown that conceivably 3 hours would have been sufficient for the reaction time, for a more volatile core material, which would result in saving of time and cost.

5.3. MICROMANIPULATION OF CURED MICROCAPSULES

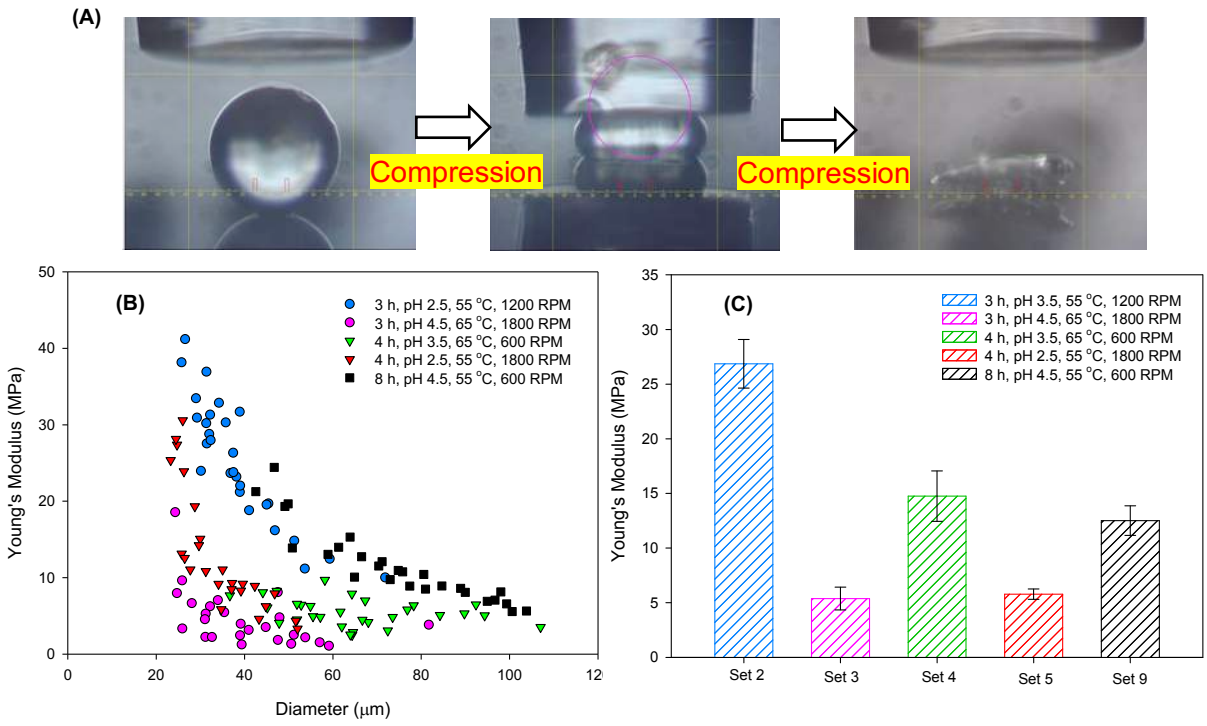

Figure 5.9. (A) Illustrating the compression of a singular microcapsule by the micromanipulation probe; (B) Young's modulus against the diameter of the 5 batches of microcapsules; (C) the mean Young's modulus of the formulated microcapsules.

As shown by the Taguchi analysis, the most efficient parameter combination were the batches produced with the 3 h, pH 3.5, 55 ºC and 1200 rpm process conditions. It would also be useful to analyse the mechanical strength of the microcapsules of various batches, to further convey the robustness of this analysis. For this study, 5 batches with adequate payload and core retention were tested in the micromanipulation rig.

Figure 5.9 (A) illustrates the isolation and compression of single microcapsules made with the reaction-set 2 parameters. The Hertz model was utilized to analyse the data, representing the relationship between the force and displacement of microcapsules, assuming to denote nominal deformation of ≥ 10 %. As shown in is seen with Figure 5.9 (B) the relationship between the Young's modulus and the diameter of the microcapsules is conveyed. In general, it can be observed that the Young's modulus decreases with an increase of the microcapsule diameter. This trend has been reported by various (Zhang, Saunders and Thomas, 1999; Zhang, et al., 2019). The average Young's modulus was then plotted, as shown on Figure 5.9 (C) Reaction-set 2, shown by the Taguchi experiments to have the most efficient process parameter conditions, produced the highest average Young's modulus.

This demonstrates yet again the beneficial properties of these reaction conditions. It can also be observed that the two batches that had the lowest Young's modulus both of had reaction temperatures of 65 ºC. As higher temperatures induce higher levels of UF nanoparticle formation than lower temperatures, this can be said to be a contributing factor to the thinner shells observed, which were not as robust as the shells produced at 55 °C.

5.4. THERMOSTABILITY OF MPCMS

The thermostability of MPCS is a pivotal factor to ensure the successful utilization in latent heat energy storage systems. Subsequently, by measuring the thermo-physical properties of the PCMs, thermal stability of PCMs can be established. Thermal cycling of the PCMs was then carried out with the microcapsules produced with the most efficient parameters (3 h, pH 3.5, 55 ºC and 1200 rpm) and the results are seen in Figure 5.10 (a) and (b). It is observed that the FM images before and after cycling showed very little differences after 10 cycles, as the bright green-fluorescent colour and shape integrity of the microcapsules were maintained.

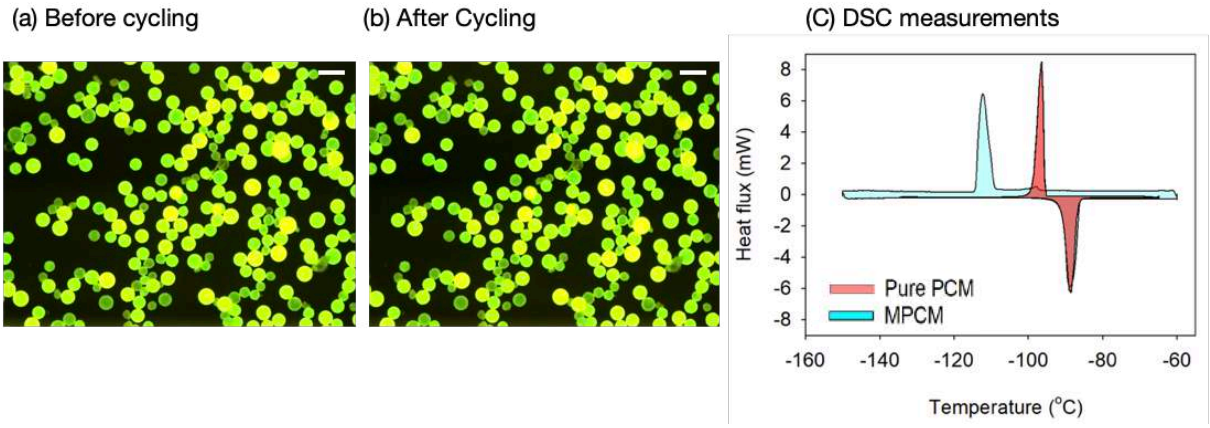

Figure 5.10. (a) FM images of microcapsules before and (b) after thermal cycling (10 cycles) (Scale bars are 100 µm). (c) DSC measurements of pure heptane PCM and the microencapsulated PCM with the reaction conditions of 3 h, pH 3.5, 55 °C and 1200 rpm.

As seen in Figure 5.10 (C), the freezing point of the MPCM was –113 °C, and the melting point was –89 °C, compared to the pure heptane sample with a freezing and melting point of –93 °C and –89 °C respectively. The latent heat for the MPCM sample was calculated to 99.8 $J.g^{-1}$ via the integration of the DSC data. This is comparable to other studies in which PUF-paraffin microcapsules formulated via in situ polymerization had latent heat values of 74.2 $J.g^{-1}$ (Xin *et al.*, 2014), 47.7 $J.g^{-1}$ (Li, Chen and Wu, 2014) and poly(melamine-formaldehyde) (PMF)-paraffin microcapsules with values of 102.9 $J.g^{-1}$ and 90.8 $J.g^{-1}$ (J. Liu *et al.*, 2017).

5.5. ANOVA ANALYSIS

Analysis of Variance (ANOVA) is a statistical model that is utilised to evaluate the mean response magnitude (% contribution) for each parameter in the orthogonal experiments (Athreya and Venkatesh, 2012). The influence of each experimental factor with respect to the payload, yield, and the encapsulation efficiency was determined by one-way ANOVA analysis. In this analysis, the sum of the squares (total variation) is equal to the sum of the squares of deviation for all the experimental parameters and the error components (e.g., adding the variation for each experimental factor). The following equations were used:

$$SS_T = SS_P + SS_Y + SS_{EE} \tag{5.2}$$

$$SS_T = \sum_1^n y_i^2 - \frac{G^2}{n} \tag{5.3}$$

$$SS_k = \sum_{i=1}^{t} \left(\frac{Sy_i^2}{t}\right) - \frac{G^2}{n} \tag{5.4}$$

where SS_T is the total sum of squares, SS_P is the sum of squares of the payload, SS_Y is the sum of squares of the yield, SS_{EE} is the sum of squares of the encapsulation efficiency, n is the number of repeats, Sy_i^2 is the sum of all the trials involving parameter k at level i, and G is the resultant data for all the trial runs.

One-way ANOVA analysis was carried out for the payload, encapsulation efficiency and the yield, as conveyed in Table 5.5, Table 5.6, and Table 5.7. For the payload, it is observed that temperature had the highest contribution, followed by homogenization speed, pH, and time. It was expected that temperature would have a large effect on this factor, as observed in section 5.2. capsules produced at 45 °C did not survive ambient drying conditions. As the homogenization speed also affects the morphology and core content of the microcapsules, this is perhaps why it is the second most significant factor. For the yield, as seen in Table 5.6, temperature again is the most significant factor, followed by pH, reaction time and homogenization speed. Again, temperature is observed to be the most significant parameter in this case. For the encapsulation efficiency, as conveyed in Table 5.7 temperature again is the most imperative parameter, followed by pH, reaction time and homogenization speed.

Figure 5.11 illustratively conveys the percentage contributions on the radar graphs for the payload (a), yield (b) and encapsulation efficiency (c), as well as the combined overall contribution for the payload, yield, and encapsulation efficiency. The combined bar chart has very consistent overall results, exhibiting that temperature is the main determinant, with a value of about 83.1 % contribution, followed by pH at 6.8 %, proceeded by reaction time at 5.2 %, and finally a homogenization speed contribution of 4.9 %.

Overall, it is very clear that temperature is the main governing factor in these reactions, which is in agreement with the results observed in Table 5.4. This has ultimately shown the key considerations when designing experimental conditions for in situ polymerization processes.

Table 5.5. ANOVA for the microcapsule payloads

Payload - Analysis of variance				
Source	Degree of Freedom	Sum of Squares	Variance	Percentage Contribution
Time	2	479.8	239.9	5.0
pH	2	597.8	298.9	6.2
Temp	2	7670.1	3835.0	79.9
H. Speed	2	849.6	424.8	8.9
Error	0	0	0	0
Total	8	9597.3	4798.6	100.0

Table 5.6. ANOVA for the microcapsule yield

Yield - Analysis of variance				
Source	Degree of Freedom	Sum of Squares	Variance	Percentage Contribution
Time	2	43.9	22.0	7.9
pH	2	48.7	24.4	8.8
Temp	2	442.1	221.1	79.9
H. Speed	2	18.4	9.2	3.4
Error	0	0	0	0
Total	8	553.2	276.7	100.0

Table 5.7. ANOVA for the microcapsule encapsulation efficiency

Encapsulation Efficiency - Analysis of variance				
Source	Degree of Freedom	Sum of Squares	Variance	Percentage Contribution
Time	2	144.6	91.5	2.7
pH	2	291.2	183.5	5.3
Temp	2	5866	3087.9	89.5
H. Speed	2	259.2	86.4	2.5
Error	0	0	0	0
Total	8	6561	3449.4	100.0

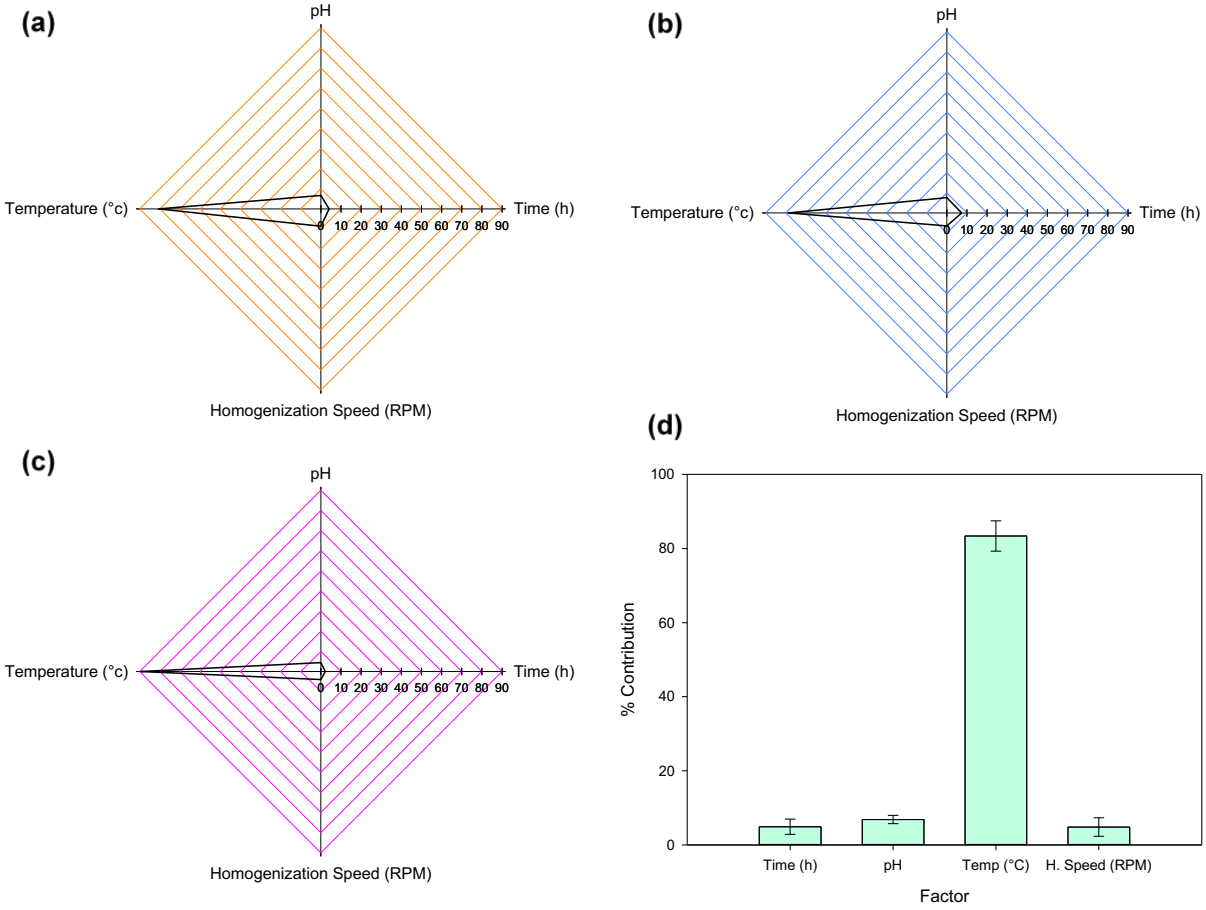

Figure 5.11. Radar graphs conveying the percentage contributions of the process conditions on (a) the payload, (b) the yield (c) the encapsulation efficiency; (d) the combination of all the contributions.

5.6. CONCLUSIONS

In this chapter, the Taguchi orthogonal experimental design was used to study the process optimisation of PUF microcapsules containing a core of volatile heptane paraffin as PCM. The influences of experimental parameters of reaction time, pH, temperature, and homogenization speed were all examined. The S/N ratio plots for the four parameters conveyed the most efficient combination: 3 h, pH 3.5, 55 ºC and 1200 rpm. Systematically, it was observed that capsules with exceptional payload (95.2 %) long-term core material retention and thermal stability were produced. Such findings convey the significance of this work, with many researchers utilising 4 h and longer reaction times for less volatile core materials, as well as higher temperatures for the formulation process, which is superfluously more timely and costly. The ANOVA analysis presented an insightful observation into the parameters that had the most governing effects of the process. It was observed that temperature had the highest effect, and microcapsules were not formed under 45 ºC.

CHAPTER 6: THERMAL AND RHEOLOGICAL STUDIES OF MPCMS AND MPCM SUSPENSIONS

6.1. CHAPTER OVERVIEW

PCM microcapsules that exhibit supercooling significantly limits the potential for widespread applications for their use in LHES systems (Farid *et al.*, 2004b; Wang *et al.*, 2013). When a liquid or solid is cooled below its stipulated freezing point and there is a delay in the freezing process, and this is defined as supercooling (Farid *et al.*, 2004b). Therefore, in applications utilizing phase change process, it is necessary for the temperature to be reduced below the phase transition temperature to initiate the crystallization process thereby usually associating with more energy input. For example, in TES applications, as supercooling results in reduced crystallization temperatures, this means that the latent heat of PCM will be released at a lower temperature, resulting in a wider phase change related temperature range. As a result, a larger temperature difference between the charging and discharging cycles of the PCM and more energy input are subsequently required to fully employ the PCM latent heat for TES, which is disadvantageous. The geometric confinement of PCM via a shell or the lack of a nucleating agent commonly leads to the supercooling phenomena. As the thermal performance of the MPCM is therefore affected negatively, due to the more required discharge energy and time, as a result of a shift on the onset phase change transition temperature. Therefore, understanding

the factors that cause supercooling and diminishing the adverse effects of this phenomenon on PCM phase change process are fundamental to increase the effectiveness, efficiency, and practicability of MPCMs, especially in TES applications.

Additionally, MPCMs suspended in a base fluid have prodigious potential for TES and fluid heat transfer applications (Huang *et al.*, 2019). For example, the specific heat capacity of such suspensions is higher than the base fluids. The rheological properties of such MPCM suspensions are also unique and important when being used as the working fluid in thermal energy storage and exchange applications, as well as the mechanical stability of the microcapsules under high shear forces. Water is the most widely utilised base fluid in this case, due to the sheer abundance, cheap cost, and large specific heat capacity. However, as the target application is for lower temperatures, di(propylene glycol) methyl ether was selected as the carrier fluid of MPCMs considering its low melting point (approximately – 80 °C).

Efforts were carried out to tackle the supercooling phenomena of decane-MPCMs via various methods. Such methods include a study on how the microcapsule size affects the onset freezing point of MPCM. Nucleating agents including dodecane, hexadecane and octadecanol were implemented into the core material to observe the extent of supercooling reduction. Copper chloride ($CuCl_2$) particles were also embedded into the non-PCM shell for MPCMs with various cores. To explore the mechanical integrity of MPCMs in suspension, two carrier fluids were studied, namely water and di(propylene glycol) methyl ether. The investigations of mechanical stability and long-term energy storage capability of the suspended MPCMs were conducted by circulating the MPCM suspension through a TES system over a one-month period, meanwhile the rheological properties of the MPCMs were characterized by the viscosity of the suspension measured under various temperature ranges.

6.2. Result Section 1: Supercooling Reduction of MPCMS

6.2.1. Decane paraffin PCM: Pure and MPCM studies

Prior to the encapsulation of the PCM, pure decane was used as a baseline study to observe supercooling without the encapsulation process. The advantages of organic paraffin PCMs such as decane is that in their pure form, they exhibit very little or no supercooling, as well as high latent heat capacities compared to their inorganic counterparts. DSC measurements were carried out for the pure decane, as shown in Figure 6.1 (a). Decane has a theoretical melting point of approximately –29.7 °C. The two peaks attained via the measurements exhibited a melting and freezing peak at –27.5 °C and –34.5 °C respectively, conveying a temperature difference of 7.0 °C, with the sample freezing 2.2 °C below the theoretical value. Decane was then encapsulated with the PUF shell and 0.03 % GEL emulsifier solution. SEM and OM images of these MPCMs are displayed in Figure 6.2, exhibiting a smooth morphology, with excellent retention and a payload of ~ 95 %. The DSC measurements were also conducted for the pure and microencapsulated decane, in which a drastic increase in the peak temperature difference and supercooling degree for the samples were found. As conveyed in Figure 6.1 (b), melting and freezing peaks of –24.1 °C and –61.7 °C were observed respectively, with a temperature difference of 37.6 °C and the sample freezing 32 °C below the stipulated theoretical value. The results reveal that the encapsulated decane freezes at a much lower temperature than pure decane, which means a higher power input is required to initiate the crystallization process for the MPCM samples and therefore a compromise in overall TES system efficiency.

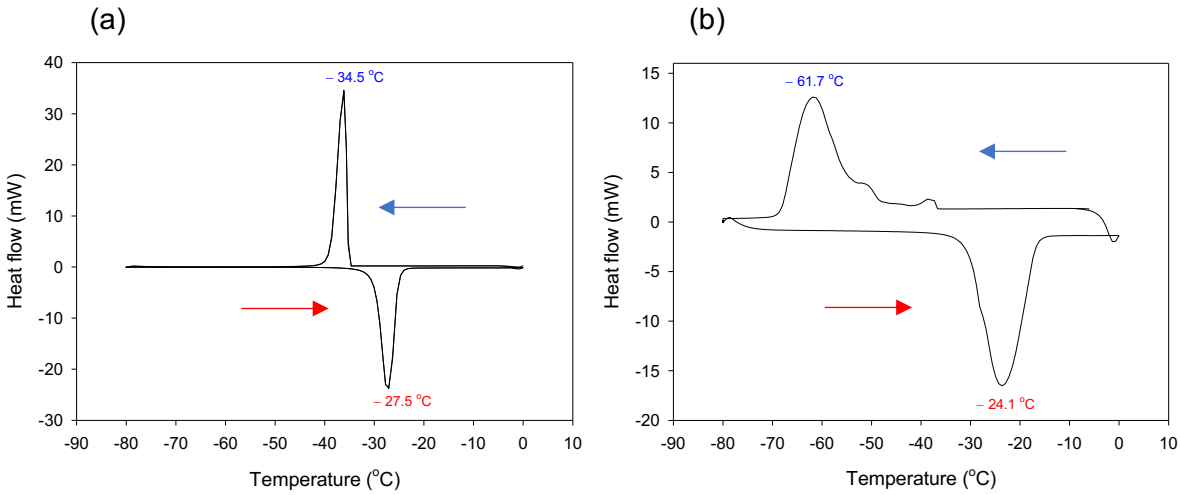

Figure 6.1. DSC measurements for (a) the pure decane sample and (b) the 1200 rpm MPCM decane sample

Table 6.1. Heating and cooling sample temperature measurements for the pure and MPCM samples.

Sample	Heating Process (°C)			Cooling process (°C)			ΔT_{peak} (°C)
	T_{onset}	T_{peak}	T_{endset}	T_{onset}	T_{peak}	T_{endset}	(Heating-cooling)
Pure PCM	–34.1	–27.5	–23.6	–34.7	–34.5	–41.3	7.0
MPCM	–33.5	–24.1	–15.7	–47.3	–61.7	–69.0	37.6

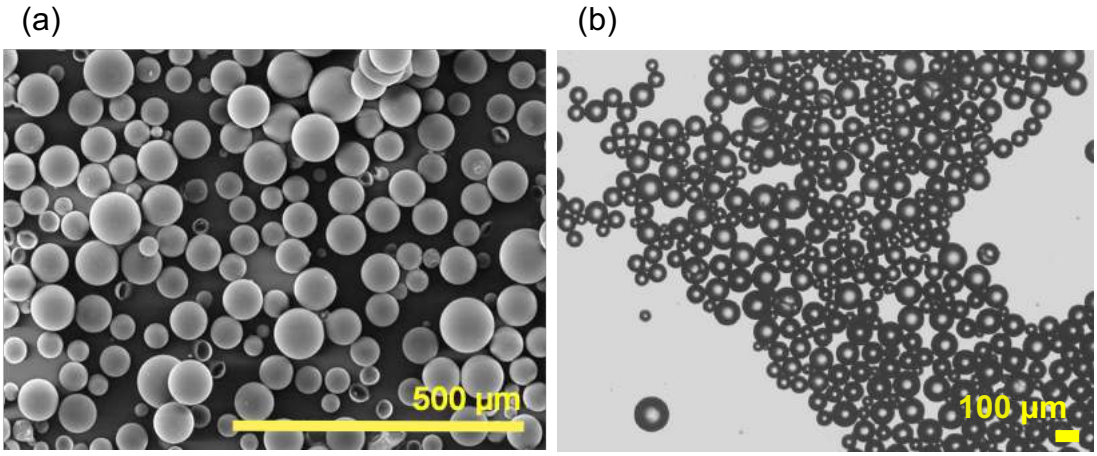

Figure 6.2. (a) SEM micrographs for the MPCM samples, (b) OM image after 24 hours drying for the MPCM sample.

6.2.2. EFFECT OF MPCM SIZE ON SUPERCOOLING

To further investigate the suppression of the MPCM supercooling phenomena, the size effects of the microcapsules were explored. The effect of MF/n-dodecane MPCM sizes correlating with the crystallization temperatures were investigated by (Yamagishi *et al.*, 1996b). The samples prepared had a diameter range of 5 – 1000 μm. It was observed that the degree of supercooling didn't convey notable differences for the samples in the 100 – 1000 μm size range, however for the 5 – 100 μm size range, the degree of supercooling increased as the diameter reduced. This is in agreement with (Zhang *et al.*, 2005b). To continue the investigation, MPCMs with different sizes were obtained using 800 and 1200 rpm homogenization speeds, respectively. Particle size distribution measurements were then carried out for these samples, displayed in Figure 6.3. The 800 rpm MPCMs had a D[3,2] value of 76 μm, while the 1200 rpm MPCMs had a D[3,2] value of 43 μm. Furthermore, both samples had a small population of microcapsules between 500 μm to 1000 μm, which may be due to agglomeration in the suspension.

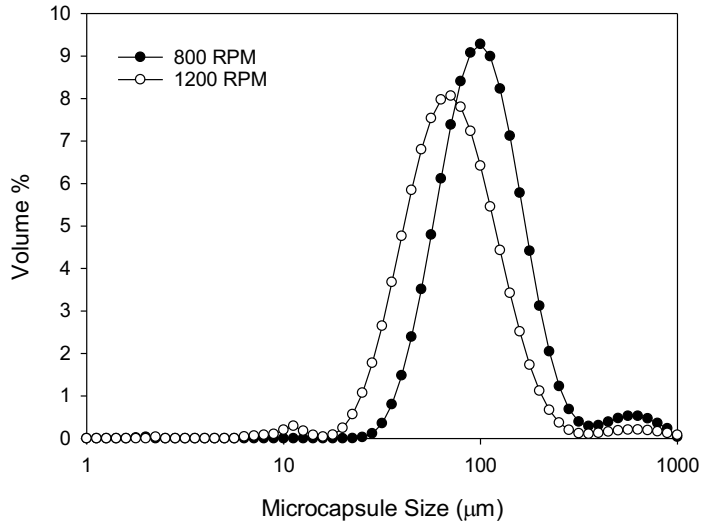

Figure 6.3. Size distribution for the 800 and 1200 rpm MPCM samples.

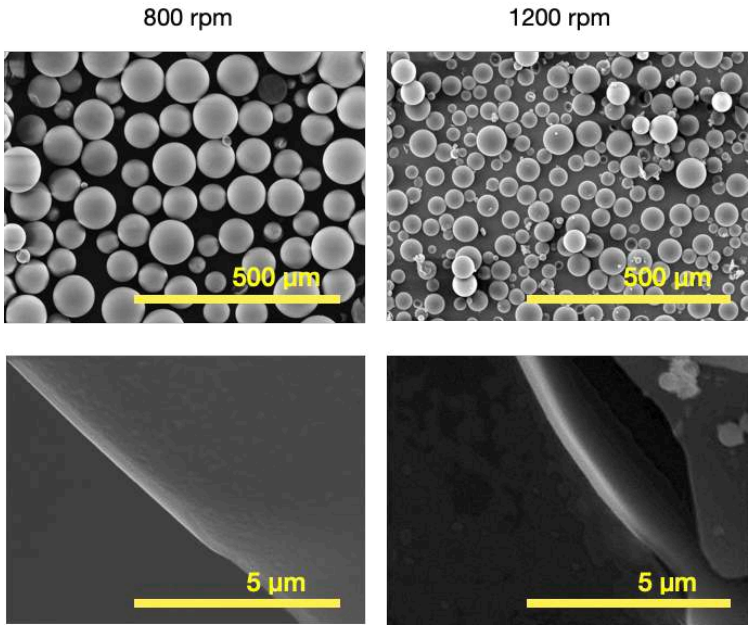

Figure 6.4. SEM micrographs for the 800 and 1200 rpm samples.

SEM micrographs for the samples are displayed in Figure 6.4, further demonstrating the particle size distribution difference between the 800 and 1200 rpm samples. Moreover, the shell thickness values increased with an increase in the rpm, with the 800 rpm samples resulting in an average shell thickness of 238 $\pm$ 12 nm, and the 1200 rpm samples with an average size of 255 $\pm$ 17 nm, which are very similar values. It is therefore imperative to also evaluate the mechanical properties of the MPCM samples, as desirable MPCMs should not only have reduced supercooling, but they must also have excellent core retention and mechanical strength. To investigate these factors, a 4-week payload test was carried out for the two samples, as well as micromanipulation measurements for the same period. The payload testing is conveyed on Figure 6.5 (a), in which both samples had excellent results over the 4-week period. The 800 rpm samples had an initial payload of 96.1 %, and after 4 weeks this value slightly dropped to 96.0 %. The 1200 rpm samples had an initial value of 95.9 %, with a very slight reduction to 95.8 %. In this case, both samples exhibited excellent core material retention.

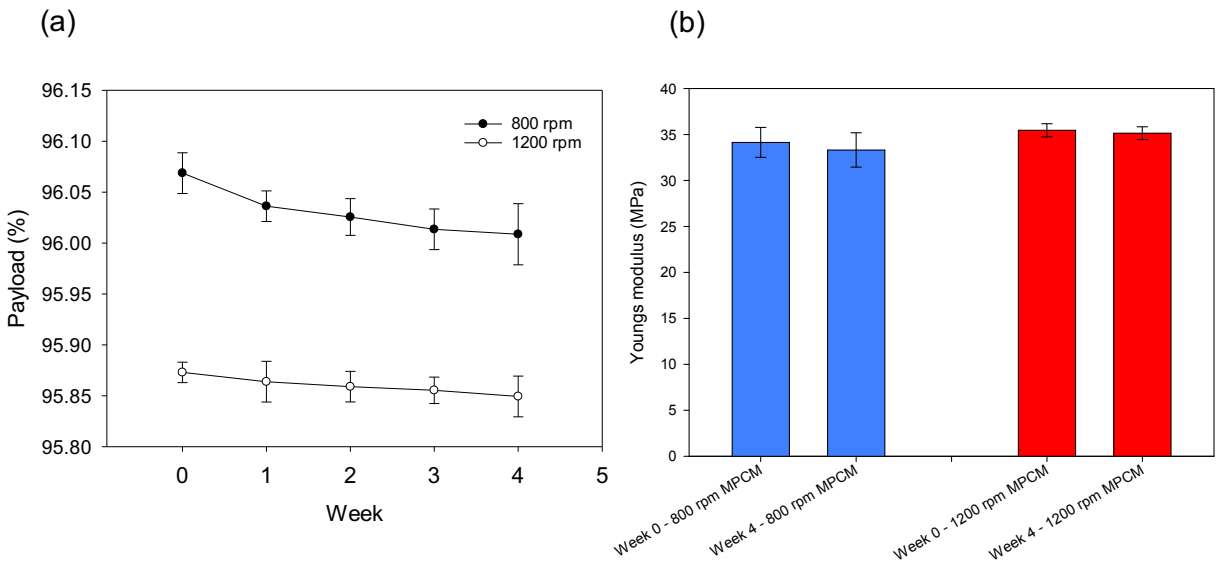

Figure 6.5. (a) Payload measurements for the 800 and 1200 rpm samples over a 4-week period; (b) the Young's modulus micromanipulation characterization for the 800 and 1200 rpm samples for a 4-week period.

The micromanipulation measurements of the MPCM samples were conducted and the resulted Young's modulus values are illustrated in Figure 6.5 (b). It can be noticed from the figure that both the 800 and 1200 rpm samples did not exhibit a significant reduction in mechanical stability over a 4-week period. Overall, the 1200 rpm samples conveyed the highest Young's modulus values, with a week-0 value of 35.6 MPa and a week-4 value of 35.2 MPa, while the 800 rpm samples exhibited values of 34.2 MPa and 33.4 MPa for the week-0 and week-4 measurements respectively, which are not significantly different. As shown by these results, although the 1200 rpm samples conveyed higher Young's modulus values, the 800 rpm samples had a higher payload, even after the 4-week measurements.

After these initial characterization methods, DSC measurements were then carried out for the two samples to evaluate the effects MPCM size on the degree of supercooling. As shown by Figure 6.6 (a), the 800 rpm samples resulted in a reduction of the onset crystallization temperature. The 800 rpm samples had a melting and freezing point of –25.1 °C and –53.5 °C respectively, resulting in a peak temperature difference of 28.4 °C, which is an improvement of 9.2 °C compared to the temperature difference of 37.6 °C exhibited by the 1200 rpm samples.

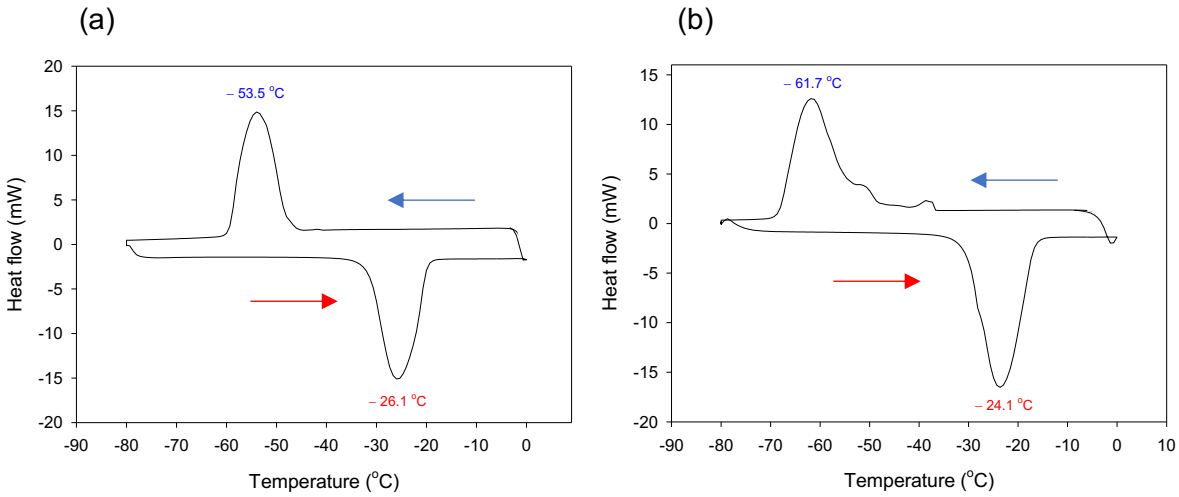

Figure 6.6. DSC measurements for (a) the 800 rpm sample and (b) the 1200 rpm sample.

Table 6.2. Heating and cooling sample temperature measurements for the 800 and 1200 rpm samples.

Sample	Heating Process (ºC)			Cooling process (ºC)			ΔT_{peak}
	T_{onset}	T_{peak}	T_{endset}	T_{onset}	T_{peak}	T_{endset}	(Heating-cooling)
800 rpm	–35.2	–26.1	–19.1	–45.2	–53.5	–40.3	27.4
1200 rpm	–33.5	–24.1	–15.7	–47.3	–61.7	–69.0	37.6

The effect of microcapsule size on the supercooling process can be explained by the crystallization process, which happens in a series of various phases. These phases include the induction phase, the crystal growth phase, and the crystal regrowth phase. In the induction phase, the crystallization forms inside droplets from the generation of miniscule crystalline nuclei, until they become abundant in number and of a sufficient size, creating nucleation centres. In this specific case, there are two processes in which nucleation centres are formed, known as homogenous and heterogenous nucleation. Homogeneous nucleation is the process in which nucleation centres are formed inside a liquid, whereas heterogenous nucleation occurs on the surface of solid substances. In the second stage, the crystal growth phase occurs, in which the crystallization PCM diffuses towards the nucleus, which then gets absorbed on the surface of the nucleus to increase the nucleus size.

The crystalline PCM material adsorbed onto the nucleus migrates along the surface, and in assimilated into a crystalline structure. These small crystal structures subsequently continue to grow in number and size until they are numerous and large enough for there to be sustained and crystal growth. In the last stage, there is a redistribution process in which after the material is totally frozen, the size distribution and particle shape continues to alter due to the crystalline material rearranging from within the PCM. Therefore, by increasing the size of the MPCMs, there is more physical space for the nuclei to form, in which more rapid induction phases occur, leading to faster and more stable crystal growth phases (Al-Shannaq *et al.*, 2015).

6.2.3. Effect on Nucleating Agents on Supercooling

Controlling the size of MCPMs seems like an attractive option to reduce the supercooling phenomena and promote the use of MPCMs in various applications, however MPCMs with large diameters may not function as well as smaller diameter MPCMs as they are prone to shell rupture during mixing processes (Al-Shannaq *et al.*, 2015). The goal of obtaining MPCMs with combined features of smaller diameters and a lower degree of supercooling has received increasing attention by various researchers. To achieve the desired MPCMs, nucleating agents are often introduced to the PCM core prior to the encapsulation process aiming to facilitate the nucleation process.

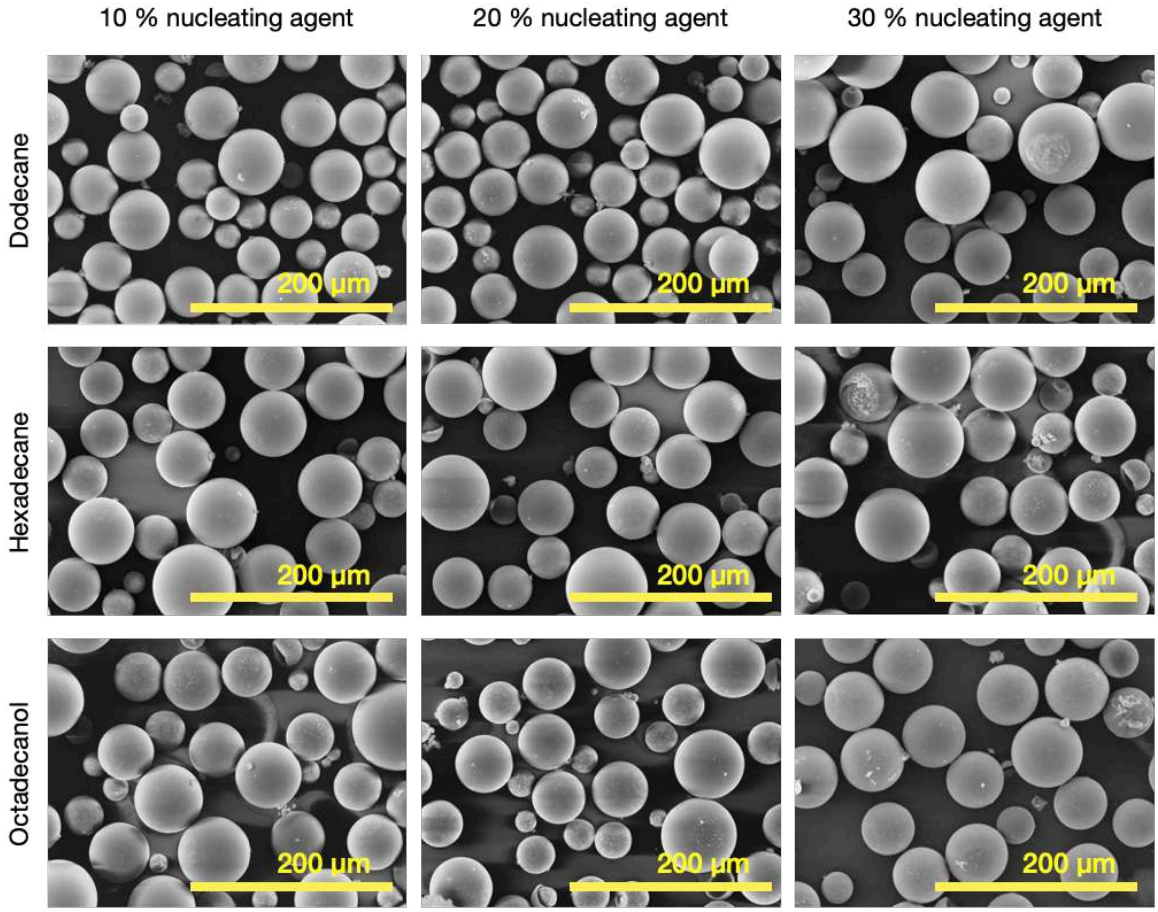

Figure 6.7. SEM micrographs for MPCMs containing 10 %, 20 % and 30 % dodecane, hexadecane and octadecanol nucleating agents.

Usually, preferable nucleating agents are those with similar crystal structures to that as the solid PCM core, in order to allow the solid PCM phase to rapidly grow on their surfaces in a homogeneous manner (Al-Shannaq *et al.*, 2015). In this case, the original core is decane, with a melting point of approximately –30 ºC. The three nucleating agents of choice include dodecane, hexadecane and octadecanol, with melting points of approximately –10 ºC, 18 ºC and 58 ºC respectively.

Figure 6.7 conveys the SEM micrographs for the MPCM samples produced with 10 – 30 % nucleating agent contents. It is observed that for all the samples, there are no discernible differences in terms of surface roughness or shell porosity. As the SEM images may not fully demonstrate the microcapsule morphology e.g., micropores in the shell structure, a payload mass loss analysis was carried out for the 9 samples with various nucleating agent compositions, as shown in Figure 6.8. Generally, all the samples had payloads above 95 % over the 4-week period, which displays superb PCM core retention overall. Specifically, the uses of dodecane and hexadecane as MPCM nucleating agents did not considerably affect the payload of the MPCM samples over the 4-week period, however the highest payload reduction was examined when 30 % octadecanol was employed in which there was a 0.16 % reduction in payload. Again, this is not a significant drop, conveying excellent core retention over the elongated time period. Al-Shannaq *et al.* (2015) also utilised octadecanol as a nucleating agent, and it was also observed that the mass loss was also accelerated with the incorporation of octadecanol, however the supercooling was greatly reduced. Nonetheless, in this case, the mass loss is not as significant, with excellent retention for the 4-week period.

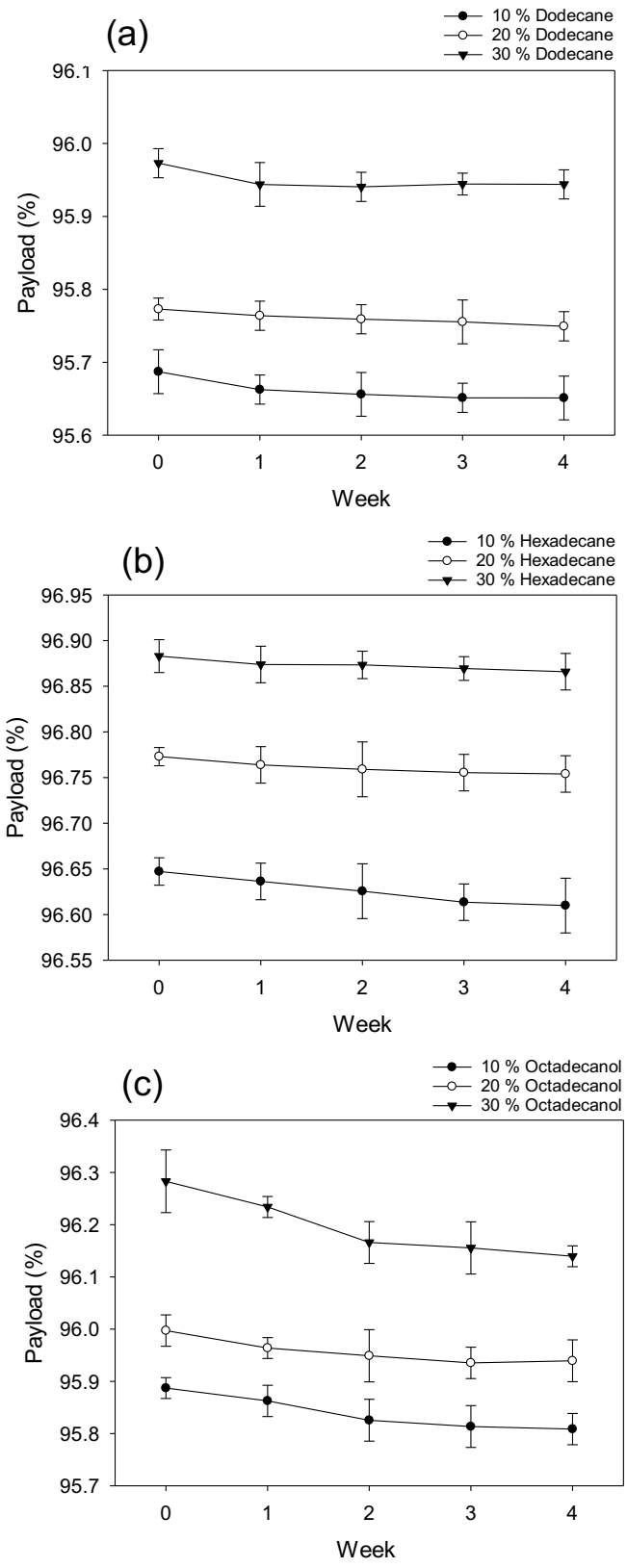

Figure 6.8. Payload measurements for a 4-week period for (a) samples with dodecane nucleating agents, (b) hexadecane nucleating agents, (c) octadecanol nucleating agents.

Furthermore, in a similar experiment carried out by Fan *et al.* (2004), in which 9.1 % octadecanol was used as a nucleating agent, an accelerated mass loss test revealed that there were significant mass loss of MPCMs, as well as with extremely rough outer shells, shell buckling and poor dispersibility in water. They stated that the reactions between the hydroxy groups (–OH) in the octanol and the functional groups in the MF resin including hydroxyl groups (–OH) and amino groups ($–NH_2$) led to the increase in surface roughness. However, in the procedure carried out in our case, the UF shell did not exhibit a drastic increase in roughness with the incorporation of 10 – 30 % octadecanol as nucleation agent.

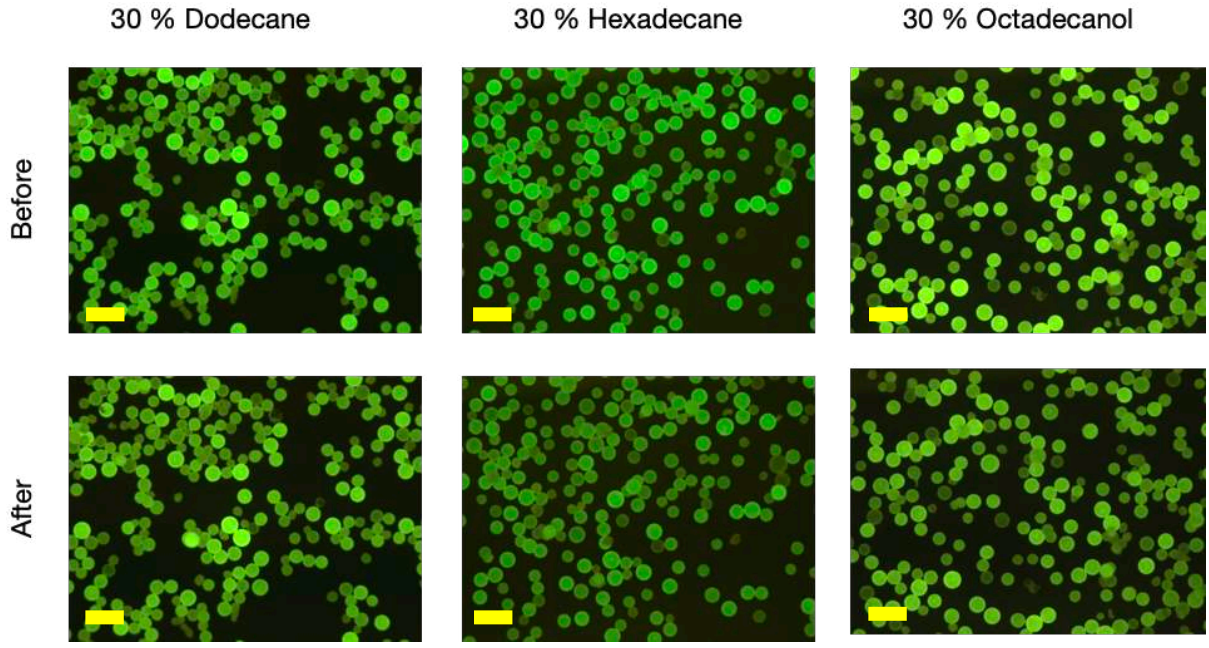

Figure 6.9. FM images after 12 thermal cycles for the 30 % dodecane, hexadecane and octadecanol samples. All scale bars are 100 µm.

Thermal cycling was then carried out to further explore the practical applicability of the PCM microcapsules and the retention of PCM core after the cycling process. The results are shown in Figure 6.9, in which 12 cycles were carried out from 0 °C to –80 °C. It is noticed that all of the samples had excellent retention after the cycling processes, and there was no significant leakage of the core material for the 30 % nucleating agent samples. Based on the thermal cycling results, it is established that the PCM microcapsule properties in terms of core material retention morphology before and after cycling were not substantially altered with the incorporation of nucleating agents.

DSC measurements were then performed for all of the MPCM samples formed with the incorporation of the nucleating agents, and these results are plotted in Figure 6.10, Figure 6.11 and Figure 6.12 for the dodecane, hexadecane and octadecanol respectively. Generally, it is observed that an increase in the nucleating agent contents in the microcapsule core correlated with a reduction in the supercooling phenomena. The pure decane MPCM samples exhibited supercooling of 37.6 °C, and when compared to the pure MPCM decane samples, the 10 % dodecane sample exhibited reduced supercooling with a value of 31.5 °C, while the 10 % hexadecane was 27.5 °C and 10 % octadecanol was 27.7 °C. For 20 % nucleating agent loadings, the dodecane sample exhibited supercooling degree of 27.5 °C, while hexadecane and octadecanol resulted with values of 26.4 °C and 20.8 °C respectively. However, the highest supercooling reduction improvements were associated with the 30 % nucleating agent loading samples, in which dodecane exhibited a supercooling degree of 21.6 °C, while hexadecane was 20.8 °C, and octadecanol was 14.7 °C. Overall, the 30 % octadecanol loading as the nucleating agent for MPCMs reduced the supercooling degree by the largest amount, which is expected because it had the highest melting point value out of the three nucleating agents (Zhang *et al.*, 2005b).

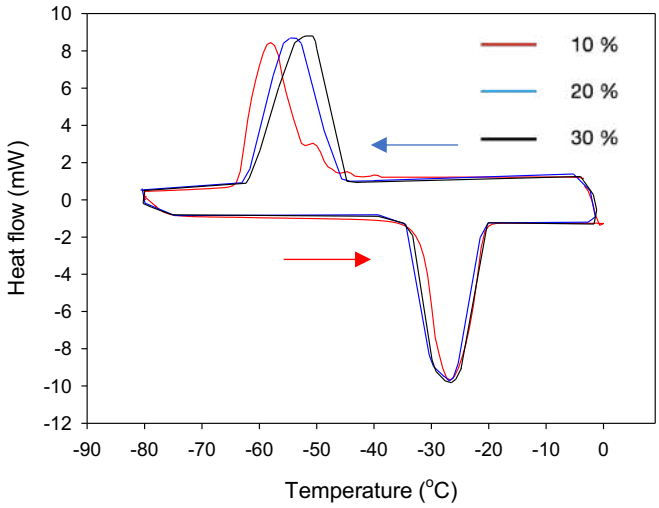

Figure 6.10. DSC measurements for the 10 % dodecane, 20 % dodecane and 30 % dodecane nucleating agent samples.

Table 6.3. Heating and cooling sample temperature measurements for the 10 % dodecane, 20 % dodecane and 30 % dodecane nucleating agent samples

Sample	Heating Process (ºC)			Cooling process (ºC)			ΔT_{peak} (ºC)
	T_{onset}	T_{peak}	T_{endset}	T_{onset}	T_{peak}	T_{endset}	(Heating-cooling)
10 % hexadecane	–31.6	–27.2	–20.0	–42.9	–58.7	–62.9	31.5
20 % hexadecane	–31.8	–27.4	–20.1	–44.1	–55.1	–62.0	27.7
30 % hexadecane	–31.9	–27.5	–20.1	–44.1	–49.1	–61.8	21.6

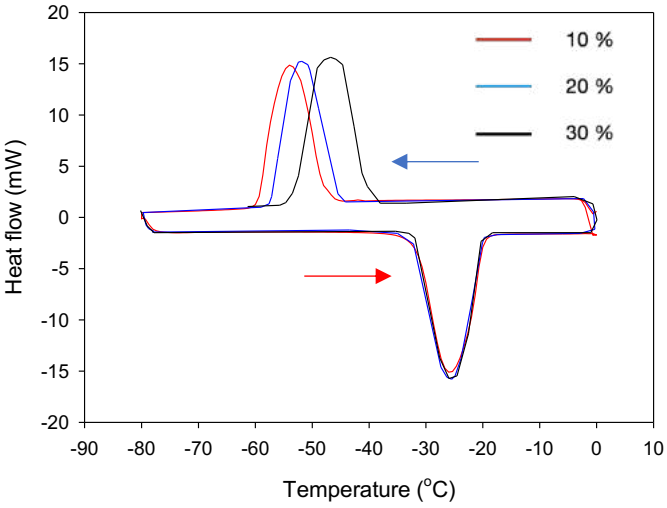

Figure 6.11. DSC measurements for the 10 % hexadecane, 20 % hexadecane and 30 % hexadecane nucleating agent samples.

Table 6.4. Heating and cooling sample temperature measurements for the 10 % hexadecane, 20 % hexadecane and 30 % hexadecane nucleating agent samples.

Sample	Heating Process (ºC)			Cooling process (ºC)			ΔT_{peak} (ºC)
	T_{onset}	T_{peak}	T_{endset}	T_{onset}	T_{peak}	T_{endset}	(Heating-cooling)
10 % octadecanol	–33.5	–25.8	–19.6	–45.9	–53.7	–61.1	27.9
20 % octadecanol	–34.6	–25.7	–19.9	–44.3	–52.1	–57.9	26.4
30 % octadecanol	–36.3	–25.8	–19.8	–37.9	–46.6	–55.0	20.8

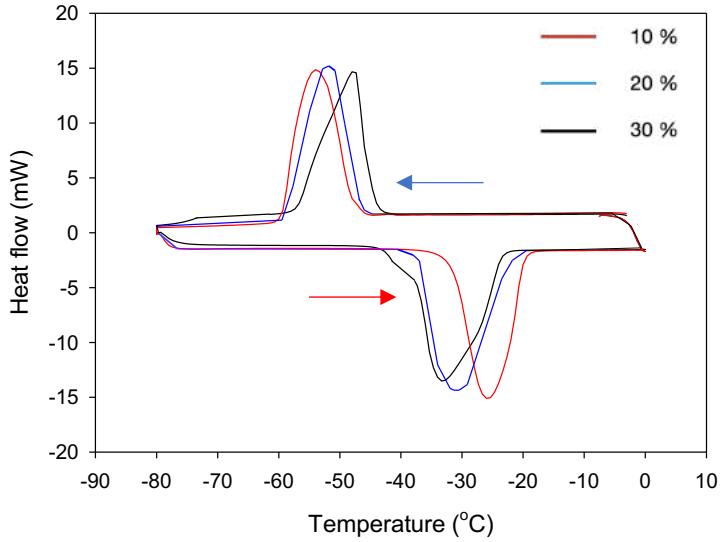

Figure 6.12. DSC measurements for the 10 % octadecanol, 20 % octadecanol and 30 % octadecanol nucleating agent samples.

Table 6.5. Heating and cooling sample temperature measurements for the 10 % octadecanol, 20 % octadecanol and 30 % octadecanol nucleating agent samples.

Sample	Heating Process (ºC)			Cooling process (ºC)			ΔT_{peak} (ºC)
	T_{onset}	T_{peak}	T_{endset}	T_{onset}	T_{peak}	T_{endset}	(Heating-cooling)
10 % octadecanol	–34.0	–25.9	–18.1	–46.2	–53.6	–61.0	27.7
20 % octadecanol	–39.9	–31.1	–19.6	–45.0	–51.9	–59.5	20.8
30 % octadecanol	–43.7	–33.2	–22.9	–42.2	–47.9	–57.8	14.7

Thermal conductivity is an essential factor to also consider with the MPCMs, as this affects the heat exchange rate and the overall efficiency of TES system. The thermal conductivity of the pure PCM and the MPCMs with the various nucleating agents were measured the LFA at 25 °C to study the effects of adding nucleating agents on the overall MPCMs thermal conductivity values. The results are summarized in Table 6.6 and Table 6.7, respectively. The thermal conductivity of the pure decane samples and the MPCM decane samples were observed to be 0.140 $W.m^{-1}.K^{-1}$ and 0.138 $W.m^{-1}.K^{-1}$ respectively. The results indicated a reduction in the thermal conductivity when the pure decane was encapsulated, which is as expected that the lower thermal conductivity of the UF resin, coupled with the thermal resistance at the core-shell interface would consequently result in a decline in MPCM overall thermal conductivity, and thereby delay the thermal response of the MPCM for heat release or storage.

Considering the potential negative effects of nucleating agents may have in the thermal conductivities of MPCM samples, all the samples were tested with the 10 – 30 % nucleating agent compositions. It is found that when dodecane is used as the nucleating agent, 10 % loading resulted in the MPCM thermal conductivity value of 0.125 $W.m^{-1}.K^{-1}$. When compared to the pure decane MPCM sample, an increase of the thermal conductivity is observed with the 20 % and 30 % loading samples, with values of 0.131 and 0.134 $W.m^{-1}.K^{-1}$ respectively. For the samples with the hexadecane nucleating agent, the 10 %, 20 % and 30 % loading samples exhibited thermal conductivity values of 0.137, 0.139 and 0.141 $W.m^{-1}.K^{-1}$ respectively. The addition of octadecanol also increases the thermal conductivity of the samples, with values of 0.126, 0.134 and 0.136 $W.m^{-1}.K^{-1}$ for the 10 %, 20 % and 30 % loading samples respectively. Overall, the addition of 30 % hexadecane as nucleating agent leads to the largest increase in MPCM thermal conductivity, which is also found effective in the reduction of MPCM supercooling.

Table 6.6. Thermal conductivity of the pure non-encapsulated PCM samples.

Sample	Thermal conductivity ($W.m^{-1}.K^{-1}$)
Pure decane	0.140
Pure dodecane	0.147
Pure hexadecane	0.196
Pure octadecanol	0.180

Table 6.7. Thermal conductivity of the pure MPCM sample and with 10 - 30 % nucleating agents.

Sample	Thermal conductivity ($W.m^{-1}.K^{-1}$)
Pure decane MPCM	0.138
10 % dodecane	0.125
20 % dodecane	0.131
30 % dodecane	0.134
10 % hexadecane	0.137
20 % hexadecane	0.139
30 % hexadecane	0.141
10 % octadecanol	0.126
20 % octadecanol	0.134
30 % octadecanol	0.136

6.2.4. $CuCl_2$ Imbedding Into the Shell of MPCMs

Metallic coating / embedding of MPCM has recently been an area of interest in this field, especially regarding the increased thermal conductivity of the samples (Al-Shannaq *et al.*, 2016). Examples of MPCM shell modifications include MF MPCMs coated with a silver layer and dispersed into polyalphaolefins (PAO) in order to produce high thermal conductivity fluid (Cao *et al.*, 2015). Furthermore, a silver coating of MPCMs were performed in an aqueous ammonia solution, in which a rough silver layer on the shell was obtained (Xu *et al.*, 2014). During this work, there was an increase in the thermal conductivity of the MPCMs from 0.152 $W.m^{-1}.K^{-1}$ to 0.251 $W.m^{-1}.K^{-1}$

In this section, copper (II) sulphate ($CuSO_4$) was reduced to copper (II) chloride, creating Cu nanoparticles which were then imbedded into the shell of MPCM samples. In recent years, the preparation of Cu nanoparticles has become a popular area of research interest, because of the superb physical and chemical properties of Cu nanoparticles such as high chemical activity and thermal and electrical conductivity (Nomura *et al.*, 2015). There are various methods to prepare Cu nanoparticles, including thermal reduction, laser ablation, vacuum vapor deposition and aqueous reduction (Nomura *et al.*, 2015). Amongst these methods, the aqueous reduction method is attractive due to its simplicity and effectiveness, as well as high yield, low cost, and ease of control. Considering its effective reducing ability, sodium borohydride ($NaBH_4$) was used as the reducing agent for this process, in which the Cu nanoparticles were produced to be imbedded into the shells of MPCMs.

The reaction between the Cu^{2+} ions and the $BaBH_4$ in the aqueous solution immediately yields a brown-black solution, as well as immediate gas evolution. Due to the positive redox potential of copper, solid metallic Cu particles are formed in its reaction with $NaBH_4$, as shown by the reaction scheme:

$$2Cu^{2+}\,(aq) + 4BH4^{-}\,(aq) + 12H_2O \rightleftharpoons 2Cu(s) + 14H_2 + 4B(OH)_3$$

Dropwise $NaBH_4$ is added to the aqueous solution containing distilled water and 0.36 g of $Cu_2SO_4.H_2O$, until the distinct black colour appears, creating solid Cu nanoparticles. The clear colour difference of the solution is shown in Figure 6.13.

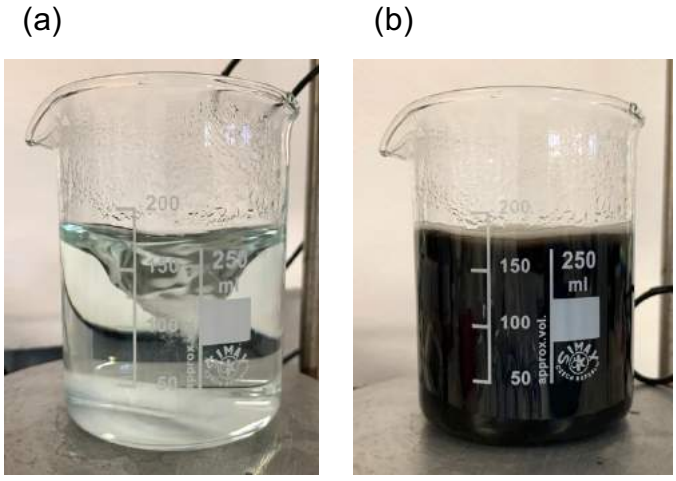

Figure 6.13. (a) Aqueous solution before the addition of $NaBH_4$, (b) aqueous solution after the addition of $NaBH_4$.

Figure 6.14 includes OM and SEM images for the MPCM capsules with the Cu nanoparticles imbedded onto their shells. As shown by the OM images on Figure 6.14 (b), this produced darker microcapsules than previously seen without the incorporation of Cu nanoparticles. The SEM images in Figure 6.14 (c and d) clearly show a much rougher shell surface morphology, with Cu nanoparticles imbedded on the shell.

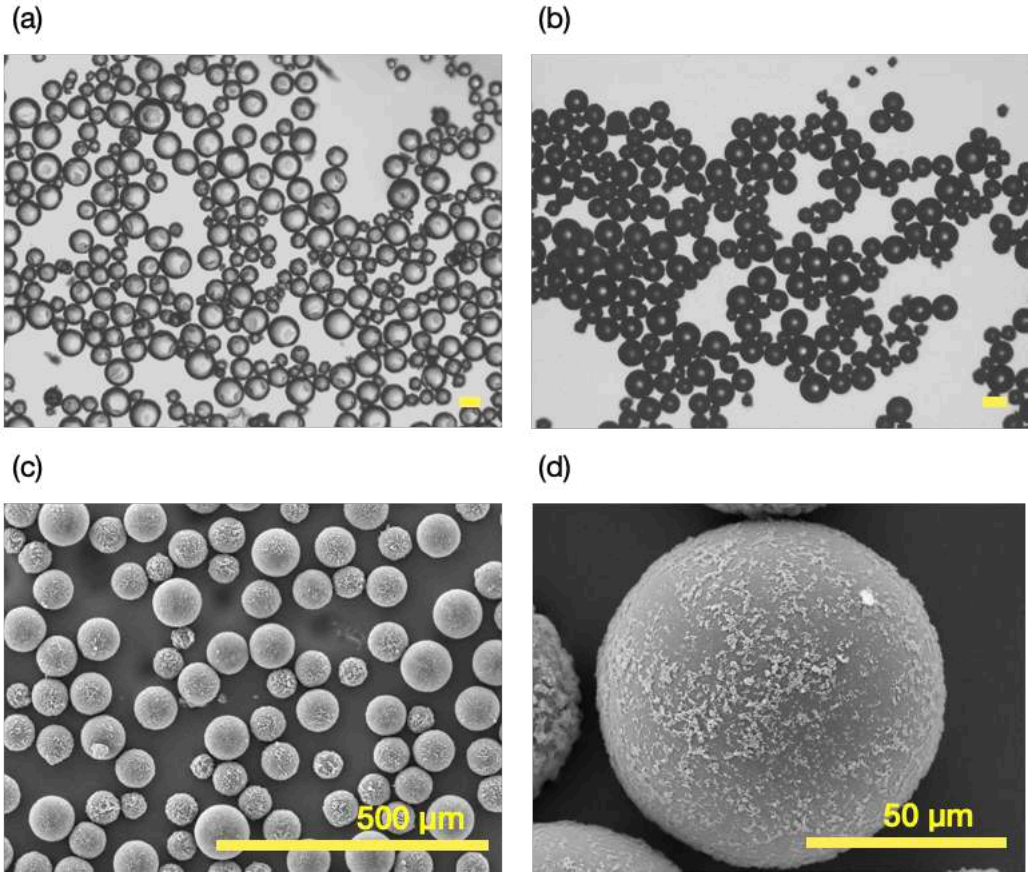

Figure 6.14. (a) OM images of wet $CuCl_2$ imbedded MPCM, (b) OM of 24-hour dried $CuCl_2$ imbedded MPCM, (c) SEM of $CuCl_2$ imbedded MPCM, (d) SEM of individual $CuCl_2$ imbedded MPCM.

However, OM and SEM images are not sufficient to confirm that indeed Cu nanoparticles are the species imbedded onto the shell. EDX analysis was then carried out to confirm the presence of the metallic Cu on the MPCM shell. As illustrated by the EDX elemental mapping analysis, Figure 6.15 (b) and (d) indeed confirm the presence of Cu nanoparticles on the MPCM shell, establishing that the reduction process of the Cu_2SO_4 was indeed successful, and the nanoparticles were imbedded into the shell.

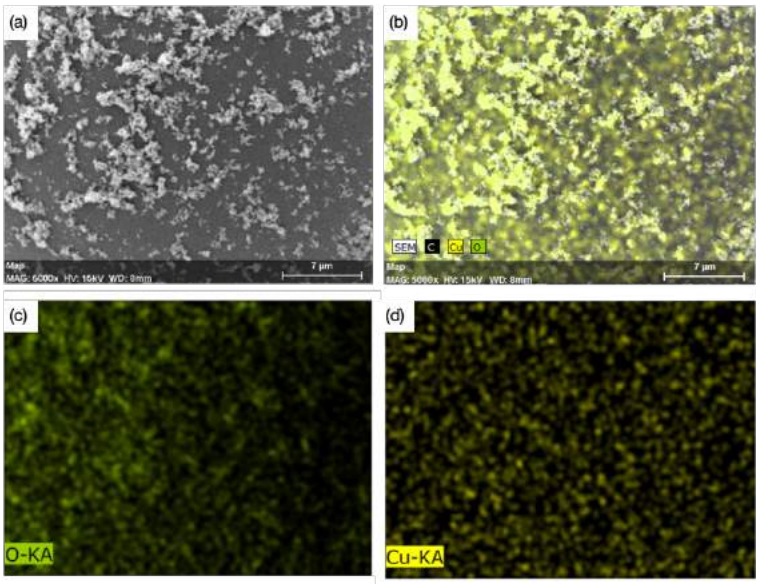

Figure 6.15. SEM EDX elemental mapping (a) unmapped surface image; (b) carbon, copper and oxygen mapped image; (c) oxygen mapped image; (d) copper mapped image.

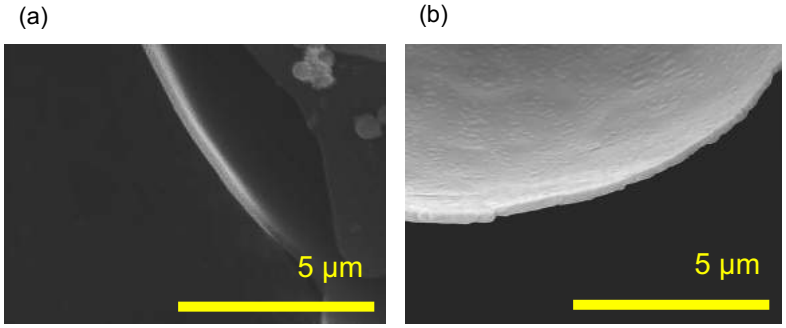

Figure 6.16. SEM micrograph for (a) MPCM without Cu shell thickness; (b) MPCM with the addition of Cu nanoparticles shell thickness.

The shell thickness with and without the Cu nanoparticles were then investigated. Figure 6.16 shows the SEM micrographs of the samples with and without the incorporation of the nanoparticles. The average shell thickness for the MPCPMs without the addition of Cu nanoparticles is 255 $\pm$ 17 nm, while the shell thickness of the samples with the Cu nanoparticles exhibits a shell thickness of 268 $\pm$ 28 nm, which is not a significant increase. Overall, the shell thickness of the samples did not increase by a substantial amount due to the coating of Cu nanoparticles on the shell.

Since the shell surface roughness gets increased by the imbedded nanoparticles, the performance of MPCMs with Cu nanoparticle coatings must be tested sustaining continuous thermal cycling processes, as the propagation of cracks on the shell may occur in the cycling process due to the flexing of the shell. As the shell flexes with the temperature changes, there may be 'concentration zones' in which there are Cu nanoparticles in crucial areas perpendicular to the flexing motion, and with continuous flexing, this may lead to the rupture of the shell. Therefore, three samples were prepared with the Cu nanoparticle incorporation, with three different core materials, including decane, dodecane and hexadecane. Corresponding FM images before and after 12 thermal cycles are displayed in Figure 6.17. As the FM images indicate, there were no samples with substantial collapse or rupture after the 12 thermal cycles, with the core material still well encapsulated.

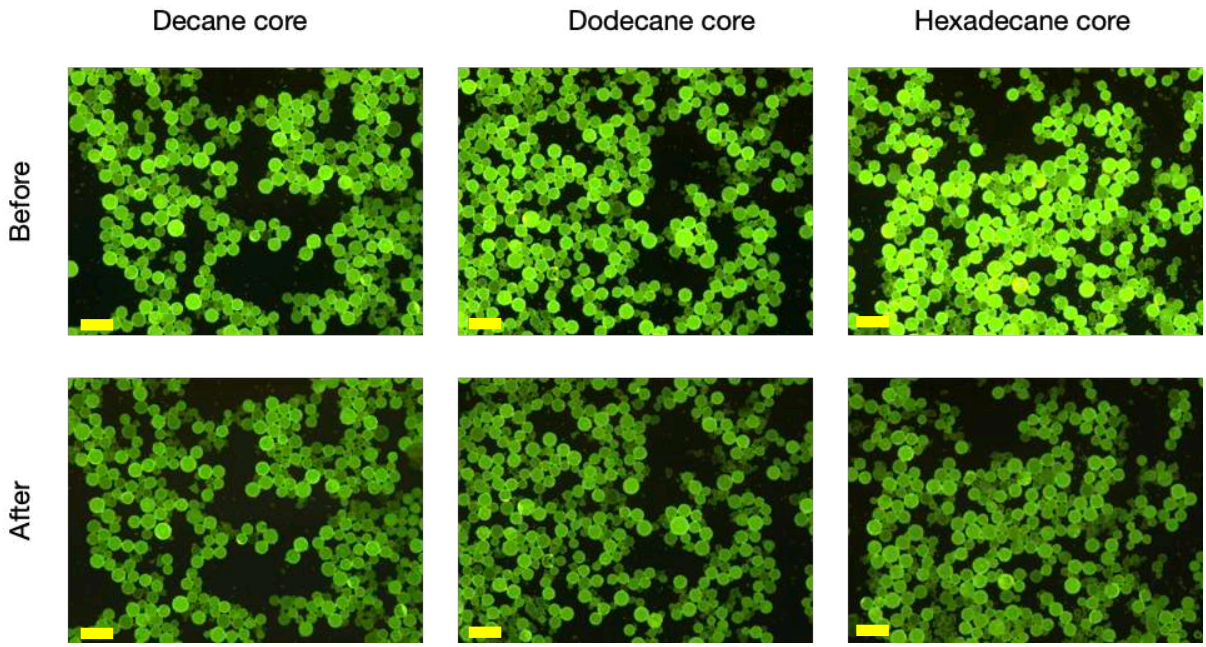

Figure 6.17. FM images after 12 thermal cycles for the Cu imbedded decane, decane and hexadecanol samples. All scale bars are 100 μm.

Imbedding metallic nanoparticles/layer to MPCM shell may affect the overall thermal conductivity as well as subcooling degree of the MPCM. Wang (2008) observed silver coated MPCM particles and the reduction in supercooling, in which the results demonstrated that the coated samples slightly reduced the supercooling degree by approximately 3 °C when compared to the pure samples.

To observe any changes in the melting and freezing points of the samples, DSC measurements were performed for the three samples with the decane, dodecane and hexadecane core. For the measurements, the pure PCM, the encapsulated PCM, and the encapsulated PCM with imbedded nanoparticles were carried out. These results are displayed in Figure 6.18, Figure 6.19 and Figure 6.20 respectively. For the decane samples, the pure sample had a supercooling degree of 7.0 °C, while the encapsulated decane sample had a supercooling degree of 37.6 °C, and the Cu nanoparticle incorporated sample exhibited a supercooling degree of 33.0 °C. Meanwhile, for the dodecane sample, a similar trend was established. For the pure dodecane PCM, there was a supercooling degree of 9.5 °C, while the encapsulated sample had a value of 28.1 °C, and the nanoparticle incorporated sample had a value of 26.5 °C. Finally, the hexadecane sample conveyed little change in the supercooling degree, with the pure PCM sample exhibiting a supercooling value of 13.4 °C, the encapsulated hexadecane established a value of 22.2 °C, and the nanoparticle incorporated sample resulted in a value of 20.6 °C. In this case, the decane samples with the Cu nanoparticles achieved the highest reduction in supercooling, with a 4.6 °C reduction.

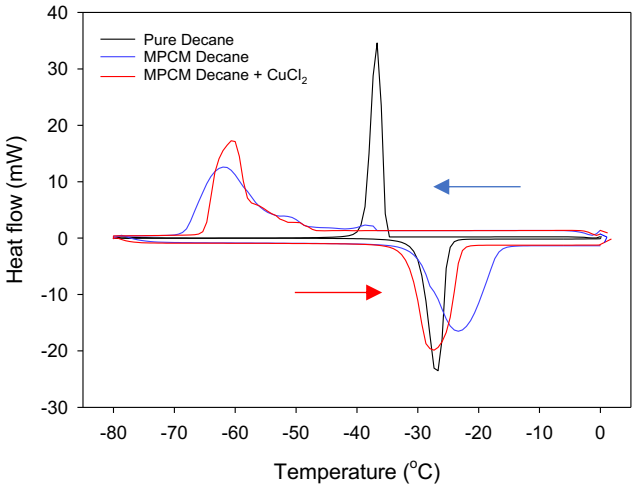

Figure 6.18. DSC measurements for the pure decane, MPCM decane and MPCM decane and Cu nanoparticle samples.

Table 6.8. Heating and cooling sample temperature measurements for the pure decane, MPCM decane and MPCM decane and Cu nanoparticle samples.

Sample	Heating Process (°C)			Cooling process (°C)			ΔT_{peak} (°C)
	T_{onset}	T_{peak}	T_{endset}	T_{onset}	T_{peak}	T_{endset}	(Heating-cooling)
Pure decane	–34.1	–27.5	–23.6	–34.7	–34.5	–41.3	7.0
MPCM decane	–33.5	–24.1	–15.7	–47.3	–61.7	–69.0	37.6
MPCM decane + Cu	–34.1	–27.4	–21.8	–47.7	–60.4	–65.4	33.0

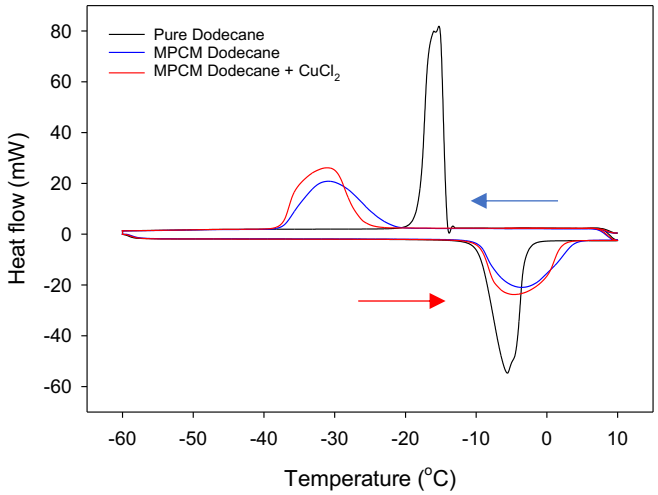

Figure 6.19. DSC measurements for the pure dodecane, MPCM dodecane and MPCM dodecane and Cu nanoparticle samples.

Table 6.9. Heating and cooling sample temperature measurements for the pure dodecane, MPCM dodecane and MPCM dodecane and Cu nanoparticle samples

Sample	Heating Process (ºC)			Cooling process (ºC)			ΔT_{peak} (ºC)
	T_{onset}	T_{peak}	T_{endset}	T_{onset}	T_{peak}	T_{endset}	(Heating-cooling)
Pure dodecane	–11.4	–5.8	–1.6	–13.4	–15.3	–20.2	9.5
MPCM dodecane	–10.4	–3.2	3.7	–21.5	–31.3	–37.4	28.1
MPCM dodecane + Cu	–10.8	–4.7	2.5	–24.6	–31.2	–37.6	26.5

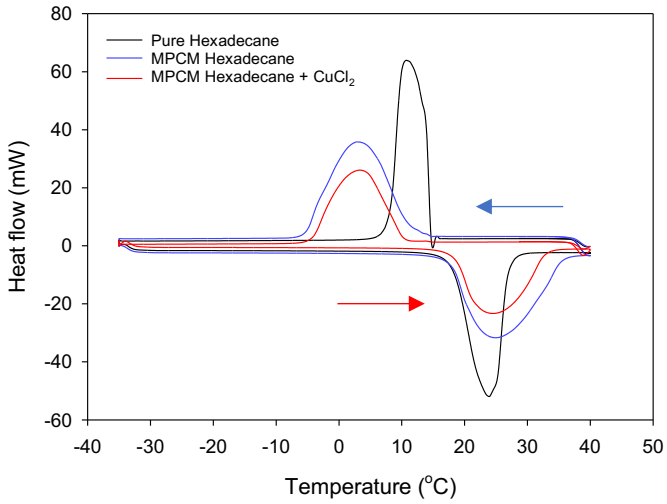

Figure 6.20. DSC measurements for the pure hexadecane, MPCM hexadecane and MPCM hexadecane and Cu nanoparticle samples.

Table 6.10. Heating and cooling sample temperature measurements for the pure hexadecane, MPCM hexadecane and MPCM hexadecane and Cu nanoparticle samples.

Sample	Heating Process (ºC)			Cooling process (ºC)			ΔT_{peak} (ºC)
	T_{onset}	T_{peak}	T_{endset}	T_{onset}	T_{peak}	T_{endset}	(Heating-cooling)
Pure hexadecane	15.1	23.9	28.6	15.8	10.5	6.0	13.4
MPCM hexadecane	17.0	25.2	37.2	14.8	3.0	–6.3	22.2
MPCM hexadecane + Cu	16.9	24.0	34.0	10.5	3.4	–5.3	20.6

Considering the high thermal conductivity of Cu nanoparticles which is much higher than both MPCM shell and core materials, it is expected that the thermal conductivity of the samples should be enhanced with the introduction of the metallic nanoparticles. The three groups of samples were then tested for thermal conductivity, and these results are conveyed in Table 6.11, Figure 6.12, and Table 6.13. In terms of the decane samples, the pure decane had a value of 0.140 $W.m^{-1}.K^{-1}$ while the MPCM sample had a value of 0.138 $W.m^{-1}.K^{-1}$, and the Cu nanoparticle incorporated samples had a value of 0.140 $W.m^{-1}.K^{-1}$. This conveyed an improvement in the thermal conductivity of the encapsulated sample due to the addition of Cu nanoparticles. Furthermore, for the samples with dodecane, the pure dodecane sample resulted in a thermal conductivity value of 0.147 $W.m^{-1}.K^{-1}$, and the MPCM sample had a value of 0.144 $W.m^{-1}.K^{-1}$, while the Cu incorporated sample increased this to 0.146 $W.m^{-1}.K^{-1}$. Lastly, the pure hexadecane samples had a thermal conductivity value of 0.196 $W.m^{-1}.K^{-1}$, while the MPCM sample resulted in 0.173 $W.m^{-1}.K^{-1}$, and again the Cu incorporated value resulted in an increase in the MPCM thermal conductivity to 0.182 $W.m^{-1}.K^{-1}$.

Table 6.11. Thermal conductivity the pure decane, MPCM decane and MPCM decane and Cu nanoparticle samples.

Sample	Thermal conductivity ($W.m^{-1}.K^{-1}$)
Pure decane	0.140
MPCM decane	0.138
MPCM decane and Cu	0.140

Table 6.12. Thermal conductivity the pure dodecane, MPCM dodecane and MPCM dodecane and Cu nanoparticle samples.

Sample	Thermal conductivity ($W.m^{-1}.K^{-1}$)
Pure dodecane	0.147
MPCM dodecane	0.144
MPCM dodecane and Cu	0.146

Table 6.13. Thermal conductivity the pure hexadecane, MPCM hexadecane and MPCM hexadecane and Cu nanoparticle samples.

Sample	Thermal conductivity ($W.m^{-1}.K^{-1}$)
Pure hexadecane	0.196
MPCM hexadecane	0.173
MPCM hexadecane and Cu	0.182

6.3. RESULT SECTION 2: RHEOLOGICAL STUDY OF MPCMS

For MPCMs to be eventually used in practical applications, the rheological properties of MPCMs suspended in carrier fluids especially the viscosity of the suspension/slurry are a pivotal aspect to be considered. Also, the slurry may seem homogeneous at the macroscopic level, but the presence of additional solid particles may significantly modify the rheological behaviour of the slurry (Delgado, Lázaro, Mazo and Zalba, 2012). Consequently, the nature of the fluid can change from initially a Newtonian fluid to non-Newtonian fluids, exhibiting shear thinning/thickening characteristics. The main physical properties that may influence the rheological properties of the MPCM slurry include the size of the MPCM, the MPCM core content, the phase volume of the MPCM in the slurry, and the slurry temperature.

6.3.1. MICROMANIPULATION FOR MPCM AND MPCS

Prior to the rheological measurements of the MPCS, it is pivotal to test the long-term mechanical stability of MPCMs in the slurry. Long term energy storage capability of MPCMs in the slurry is an essential indicator to examine the long-term durability and structural integrity of the MCPM samples. In this case, MPCMs with a decane core were produced at both 800 rpm and 1200 rpm, and three sets of samples were prepared with each rpm value. These three sets include pure dried MPCMs, MPCMs dispersed in distilled water, and MPCMs dispersed in di(propylene glycol) methyl ether (as the HTF). These samples were characterized after stationary sitting in the lab for over a 4-week period, to monitor any long-term effects on the slurry.

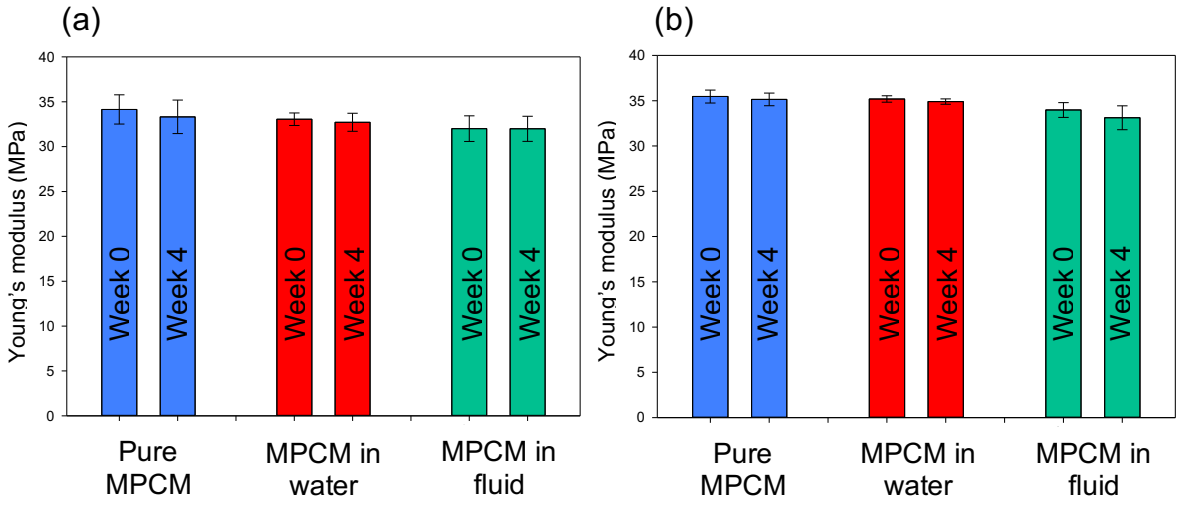

Figure 6.21. (a) the 800 rpm MPCM and MPCS micromanipulation measurements over a 4-week period for pure samples, samples dispersed in water and samples dispersed in the heat transfer fluid (b) the 800 rpm MPCM and MPCS micromanipulation measurements over a 4-week period for pure samples, samples dispersed in water and samples dispersed in the HTF.

Figure 6.21 shows the micromanipulation results of MPCMs and MPCM slurry over the 4-week time period. For the pure MPCM samples obtained under 800 rpm and 1200 rpm, Young's modulus values slightly reduced for both samples over the 4-week period. For the 800 rpm sample, the week-0 Young's modulus value was 34.2 MPa, which dropped to 33.4 MPa after 4 weeks, while the values of 1200 rpm sample changed from 35.5 to 35.2 MPa over the 4-week period. Overall, the 1200 rpm sample had a less significant reduction in the mechanical strength over time.

When the samples were dispersed in water, there was a slight reduction in Young's modulus for both samples when compared to the non-dispersed samples. The 800 rpm samples dispersed in water exhibited a week-0 Young's modulus value of 33.2 MPa, with a slight drop to 33.0 MPa after 4 weeks, while the 1200 rpm samples exhibited a week-0 Young's modulus value of 35.7 MPa, with an even more slight drop to 35.6 MPa after 4 weeks. For the 800 rpm samples in the HTF, the Young's modulus was 32.7 MPa for week-0 with a negligible drop to 32.6 over the 4 weeks. Similarly, the 1200 rpm sample established a Young's modulus of 34.1 MPa for week-0, with a reduction to 33.7 MPa over the 4-week period.

One factor to consider when evaluating the storage of MPCMs in water or fluids is the hydrolysis process of the cured UF resin shell material. The ageing process of the UF resins usually involves the liberation of the formaldehyde, and therefore resulting in the gradual deterioration of their mechanical integrity (Dutkiewicz, 1983). In general, it has been pointed out that UF resins are less stable in both humid conditions and at higher temperatures (Dutkiewicz, 1983). Reaction scheme 6.1 conveys the hydrolytic decomposition of formaldehyde in an aqueous solution, which occurs in both acid or alkaline conditions:

$$–CH_2NHCONHCH_2– + –H_2O \rightleftharpoons –CH_2NHCOOH + H_2NCH_2 \rightleftharpoons –CH_2NH_2 + CO_2 + H_2NCH2–$$

The mechanism of the hydrolytic disturbance of the UF resin usually involves the scission of the C–N amide bonds, which therefore leads to the decrease in the functional carbonyl content in the resin composition (Dutkiewicz, 1983). Furthermore, the evolution of formaldehyde occurs accompanying the dissociation of N-methylol groups with the breakdown of the UF polymeric network.

6.3.2. MPCS Dispersion and Rheological Measurements

The 1200 rpm MPCMs with the decane core were dispersed in di(propylene glycol) methyl ether to form MPCM slurry. The MPCMs were left in the fluid for a one-week period, before the MPCM slurry with various MPCM concentrations were examined for their stability, as shown in Figure 6.22. The slurries with 10 – 40 % microcapsule mass concentrations survived over the one-week period without major particle agglomerations and precipitations, as shown by the bright green fluorescence indicators in Figure 6.22.

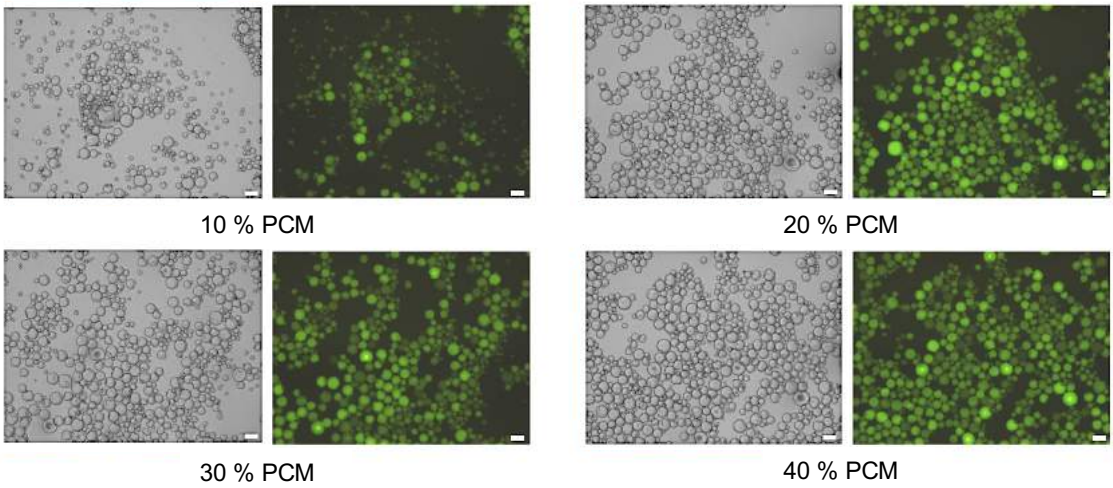

Figure 6.22. OM and FM images of 10 - 30 % MPCMs dispersed in di(propylene glycol) methyl ether after one week. All scale bars are 100 μm.

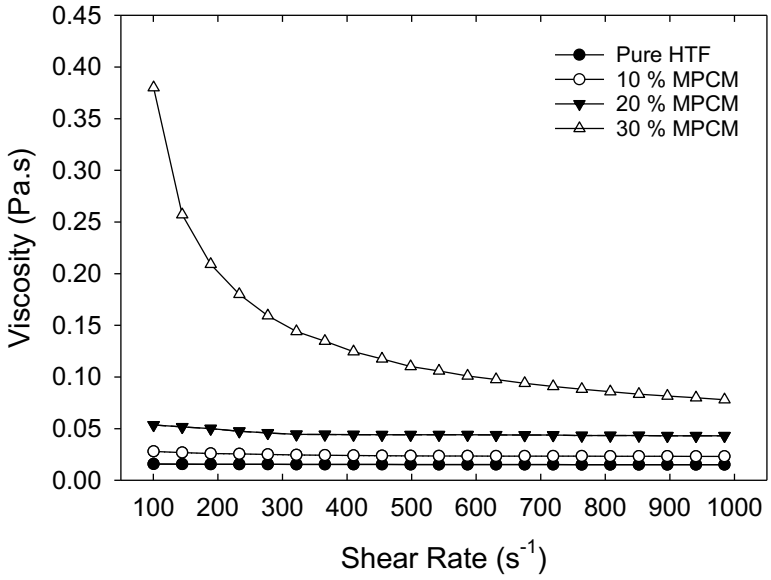

Figure 6.23. Rheological measurements for the pure HTF, 10 wt. % MPCM, 20 wt. % MPCM and 30 wt. % MPCM in HTF (at 25 °C).

Table 6.14. Weight % of the 10 %, 20 % and 30 % MPCM slurries and their corresponding volume fractions (%) in the HTF.

Weight % of MPCM	Phase volume (%)	
	HTF	MPCM
10 wt. %	86	14
20 wt. %	73	27
30 wt. %	61	39

The viscosity profiles of slurries with 10 wt. % , 20 wt. % and 30 wt. % (phase volumes of 14 %, 27 % and 39 % respectively) MPCM contents were determined at 25 °C by a rheometer, as shown in Figure 6.23. Their corresponding phase volume percentages are conveyed in Table 6.14, with the 10 % occupying 14 % of the volume, the 20 wt. % MPCM occupying 27 % of the volume, and the 30 wt. % occupying 39 % of the volume. It is elucidated that the pure HTF exhibits Newtonian flow behaviour, with no increase or decrease in viscosity with increasing shear rates. The 10 wt. % MPCM slurry also performs like a Newtonian fluid, with no shear thinning/thickening characteristics, while the 20 wt. % MPCM slurry exhibited minor shear thinning up to ~250 s^{-1}. However, the 30 wt. % MPCM slurry showed obvious shear thinning behaviour. There was a reduction in viscosity with increasing shear rate (up to ~350 s^{-1}), until the rate of change of viscosity reduced. This can be explicated by the spacial arrangement of the MPCMs in the slurry. When the slurry is at rest and stable, there is random dispersion of the microcapsules. There is no cooperative motion between the microcapsules at this low shear rate, and therefore there is no general bulk flow direction. Moreover, as the shear rate increases, the MPCMs begin to move in a parallel motion to the bulk flow (moving in a more organized manner), thus leading to a more linear and organized flow of the capsules within the slurry, with more alignment. This therefore leads to a reduction in viscosity, which can be perceived with the shear thinning behaviour exhibited with the 30 % MPCM slurry.

Yamagishi *et al.* (1999) reported that octadecane 30 wt. % MCs dispersed in water exhibited Newtonian behaviour. It is to be noted that the microcapsules used in their study were however in the range of 2 – 10 μm, which are much smaller than the capsules used in this study, and generally other MPCM slurry measurements by other researchers (Yamagishi *et al.*, 1999; Tumuluri *et al.*, 2011; Zhang and Zhao, 2011). However, in other reports, 20 – 25 % mass concentration MPCM in slurry was seen to be the highest concentration for the slurry to remain

Newtonian. This is in agreement with (Charunyakorn, Sengupta and Roy (1991) whom also proposed that 25 wt. % should be the typical mass concentration limit for MPCM slurry to be Newtonian.

6.3.3. The Effects of Temperature on MPCM slurry Rheological Measurements

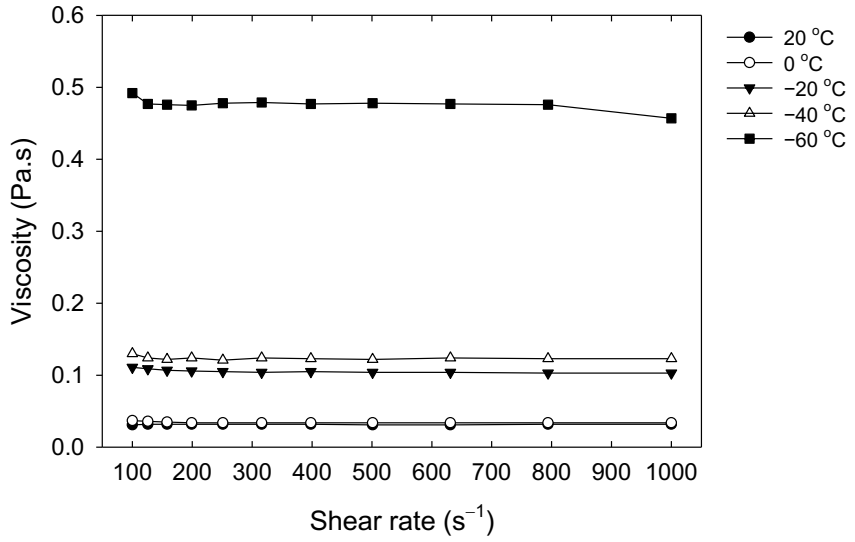

Figure 6.24. Rheological measurements for the pure MPCS at 20 °C, 0 °C, –20 °C, –40 °C and –60 °C.

Newtonian MPCM slurry with as high as possible PCM contents are usually favourable in TES applications because of its low required pumping power and high phase change energy, thus the MPCS with 20 wt. % (27 % phase volume) MPCM mass concentration was selected for further investigation of the slurry viscosity profile under various temperatures. A total of 5 temperatures were considered, from –60 °C to 20 °C. The results in Figure 6.24 indicates that the viscosity profiles of MPCM slurry for 20 °C and 0 °C are very similar, with Newtonian flow behaviour with viscosity values around ~0.03 Pa.s for both samples. However, as the temperature reduces to –20 °C, there was an increase in the viscosity of the slurry to ~0.1 Pa.s,

with a slight increase at –40 °C to ~0.13 Pa.s. However, the most drastic increase in viscosity was when the temperature reduced to –60 °C, in which the viscosity drastically increased to ~0.48 Pa.s. It is noticeable that as the temperature of the suspension decreases, the overall viscosity increases. This is related to the overall increase in the viscosity of the base HTF. The melting point of the HTF is approximately ~ –80 °C, and it is expected that the viscosity of the HTF increases as this temperature is approached. Moreover, another mechanism of the viscosity increase may be attributed to the shape and volume change of the microcapsule.

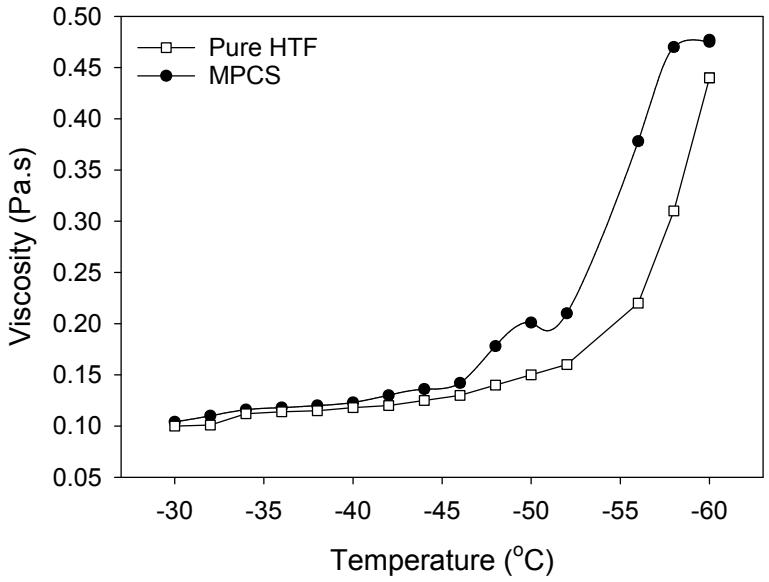

Figure 6.25. Pure HTF and MPCS rheology profile at a shear rate of 500 s^{-1}, between the temperatures of –40 °C and –60 °C.

To further investigate the viscosity change of MPCM slurry at low temperatures, the viscosities of the HTF and MPCS were measured under temperatures from –30 °C to –60 °C. A constant shear rate of 500 s^{-1} was employed during the viscosity measurements. As the results in Figure 6.25 show, as the temperature of the samples reduce, the viscosity of both the MPCS and the pure HTF increase. It is worth noting that during the temperature reduction for the MPCS, at approximately –45 °C to –50 °C, there is a sharp increase in viscosity, deviating from the trend.

After the –50 °C point, the trend of viscosity vs. temperature changes again to follow the trend of the pure HTF sample. This may imply that the phase change process (occurs at approximately after 45 °C) may in fact cause the volume change of the PCM, in which result in the bulk viscosity change of the fluid. Similar results were observed when Dutkowski and Fiuk (2019) carried out an experiment with DS 5039 Slurry, in which there was also a sudden increase in the viscosity around the MPCMs phase transition temperature.

As the temperature of the MPCS reduces, the PCM nuclei are activated. The nuclei are small molecules or atoms that initiate the crystallization procedure, in which crystals start to form around them, creating clusters (Dutkowski and Fiuk, 2019). As previously mentioned, the melting point of the pure 800 rpm MPCM sample is around –53.5 °C and approaching this temperature would trigger the crystallization process. However, until there is complete nucleation of the MPCMs within the suspension, there would be liquid PCMs, liquid/solid PCMs and solid PCMs (Dutkowski and Fiuk, 2019). The rotation of a liquid-filled particle during the shear is different to that of a solid-filled particle. In the solid samples, the entire PCM rotates relative to the centre of rotation, located at the core. However, solid/liquid PCMs may have a solid region surrounded by liquid coatings, in which the coating first undergoes rotation due to the inertial forces, which then eventually dissipates onto the core of the microcapsule (Dutkowski and Fiuk, 2019). Therefore, the rotational speed for the solid MPCMs is higher than that of mostly liquid or liquid/solid MPCMs. Therefore, when the temperature reduces, there is more of a disparity between the rotational speeds of the MPCMs, in which there is less homogeneous flow of movement for the bulk MPCMs. This is also observed in Figure 6.24, in which the lower temperature sample at –60 °C exhibited slight sheer thinning, which may be attributed to the lower levels of homogenous flow of the MPCMs in the MPCS, as well as the sharp increase in local viscosity as observed in Figure 6.25 at approximately –50 °C.

6.4. CONCLUSIONS

In this chapter, efforts were made to reduce the supercooling phenomena in decane MPCMs. The influence of the MPCM size on the nucleation process was evaluated, and the results revealed that the 1200 rpm MPCM sample had a ΔT_{peak} (ºC) of 37.6 °C, while the 800 rpm sample established a reduced ΔT_{peak} (ºC) of 27.4 °C. Furthermore, the effects of nucleating agents on MPCM subcooling were investigated, in which dodecane, hexadecane and octadecanol were employed as the nucleating agents. Overall, octadecanol reduced the supercooling by the highest amount, resulting in a ΔT_{peak} (ºC) of 14.7 °C. The effects of Cu nanoparticles embedded into the MPCM shell were also explored. In this case, the decane MPCM samples with the Cu nanoparticles achieved the highest reduction in supercooling, with a 4.6 °C reduction in the offset melting point when compared to the pristine MPCM samples. The introduction of the Cu nanoparticles also increased the thermal conductivity for all the tested samples when compared to the pure MPCMs.

The rheological properties of the MPCM suspensions with di(propylene glycol) methyl ether as the HTF were also studied. It was observed that the 10 – 20 % MPCM mass concentration (14 – 27 % phase volume) samples did not exhibit shear thinning behaviour (Newtonian-like), while the 30 % (39 % phase volume) sample displayed substantial shear thinning characteristics (non-Newtonian like). Furthermore, during the process of reducing MPCM slurry temperature, there was a sharp increase in slurry viscosity at the temperatures around PCM crystallization temperature, which may be attributed to the non-cooperative motion and the volume changes of the MPCM capsules in the slurry due to phase change.

CHAPTER 7: CONCLUSIONS AND FURTHER RECOMMENDATIONS

7.1. CONCLUSIONS

The motivation for this work stemmed from the need to reduce the environmental impacts for energy usage, and to further investigate TES methods and to optimize the fabrication process for the containment of cryo-PCM cargos to be employed for CES applications. There has been limited work in the low temperature applications, especially with the volatile core materials encapsulated in amino resin shells. A solid understanding on the reaction mechanisms can shed light into how to further utilise and fabricate such MPCMs with ever increasing advantageous properties. Furthermore, additional insight into these properties and reaction mechanisms can provide further guidance into the feasibility of employing such amino resins as shell materials for the low temperature applications, as well as highlight any key challenges or issues that may be exhibited by using such material for such demanding conditions. The work carried out therefore shed new insights on the reaction mechanisms taking place during the polymerization process, and how the various reactive substituents can vastly affect the microcapsule properties, which can be fine-tuned for the desired applications. Furthermore, work was carried out to optimize the formulation process to maximise the microcapsule barrier and mechanical properties, and to increase the efficiency by reducing required time and costs. Lastly, the rheological behaviour of MPS was deliberated, in which it was observed that the phase change process of MPCMs can influence the viscosity of heat transfer fluids.

7.1.1. Microcapsule Formulation Reaction Study

A range of emulsifiers were employed to encapsulate the cryo-PCM, with the one step in situ polymerization method employed. A range of natural and synthetic emulsifiers were employed to supplement the encapsulation process, with an array of functional groups, including carboxyl, amine, amide, and hydroxyl groups. There has been work carried out previously by a range of researchers that have claimed the sheer importance of the carboxyl/anhydride groups for the emulsifiers, however with our much more volatile core material, emulsifiers with these functional groups garnered microcapsules with extremely rough shells. Furthermore, we demonstrated that a wider range of emulsifiers can be employed to generate MPCMs with excellent payload and core material retention. Notable emulsifiers that generated excellent microcapsules include GEL, MC, XG, CHI, PAM and PEI.

Factors that influence the emulsion stability during this process includes the interfacial and dilatational rheology. Although these are a pre-requisite in ensuring emulsion stability, this was not the most dominant factor in terms of affecting the chemical reactions during the polymerization processes. However, the resorcinol additive was proven to exert a significant contribution to the reaction process, and it was observed that when alternative dihydroxybenzenes were utilised (hydroquinone and catechol), there was not successful formation of the MPCMs. This conveyed the importance of the resonance and inductive effects of resorcinol, and its overall stability compared to the alternatives. Alternative salts were employed to compare with the ammonium chloride, including ammonium nitrate and ammonium carbonate. These salts gave very similar results, and reduced the pH of the reaction system in a analogous fashion.

Moreover, to further investigate the emulsifier effects in this process, reaction rate studies were carried out to examine the influence that the functional groups enact on the polymerization process. It was confirmed that the emulsifier functional groups rank in the following order reactivity: amine/amide > hydroxide. Therefore, the work carried out in this section strongly substantiates the importance of emulsifier selection in this process, and how such emulsifiers affect the microcapsule properties depending on the functional groups.

7.1.2. Process Optimization of Microencapsulation Process

The process optimization of the MPCM microcapsules was also carried out in this work. Various process parameters and their influences were investigated, including reaction time, pH, temperature and homogenization speed. The methods employed to investigate the process optimization include the Taguchi orthogonal array, and the ANOVA analysis method. The S/N ratio results demonstrated that the most efficient combination of parameters are as follows: 3 h, pH 3.5, 55 ºC and 1200 rpm. Furthermore, microcapsules produced with these reaction parameters demonstrated excellent payload values of 95.2 %, as well as excellent thermal stability and long-term core material retention. The importance of this work is not only the excellent MPCM properties, but also the reduction in reaction time. Many researchers are utilising 4 hours to encapsulate less volatile core materials, and at higher temperatures, which is not only more time consuming, but also costly. By reducing the time and cost of this process, this is extremely advantageous for industrial applications. The ANOVA analysis then provided an insight into the parameters that had the most dominant effects in the process. It was stipulated that temperature had the highest effect with a contribution percentage of 83.1 %. Microcapsules could not be formed at temperatures lower than 45 ºC. This was followed by pH (6.8 %), and reaction time (5.2 %) and homogenization speed (4.9 %).

7.1.3. SUPERCOOLING REDUCTION OF MPCMS

The supercooling phenomena for the MPCMs were also investigated. It was proven that the organic PCMs without encapsulation exhibit very little to no supercooling, while the MPCMs exhibit significant supercooling. Various efforts were made in this work to reduce the supercooling phenomena, including the influence of the MPCM sizes. The results in this work conveyed that the sample produced at 1200 rpm had a ΔT_{peak} (ºC) of 37.6 °C, while the 800 rpm sample established a reduced ΔT_{peak} (ºC) of 27.4 °C. Additionally, the effects of nucleating agents were also deliberated, including dodecane, hexadecane and octadecanol. Overall, it was stipulated that the nucleating agent that reduced the supercooling by the highest amount was octadecanol, resulting in a ΔT_{peak} (ºC) of 14.7 °C. Copper nanoparticles were also imbedded into the shell of microcapsules with decane, dodecane and hexadecane cores. The results showed that decane MPCMs with the Cu nanoparticles exhibited the highest reduction in supercooling, with a with a 4.6 °C reduction in the offset melting point when compared to the pristine MPCM samples without the Cu addition. Furthermore, the addition of the Cu nanoparticles increased the thermal conductivity for all the samples when compared to the pure MPCMs.

7.1.4. RHEOLOGICAL PROPERTIES OF MPCS

The MPCM samples were then suspended in di(propylene glycol) methyl ether as the HTF. In this work, it was established that the suspensions with 10 – 20 wt. % (14 – 27 % phase volume) MPCM content did not exhibit sheer thinning behaviour, while the suspensions with 30 wt. % (39 % phase volume) MPCM content demonstrated significant sheer thinning characteristics. Additionally, it was evident that during the temperature reduction for the MPCS, there is a sharp increase in local viscosity at approximately –45 °C to –50 °C, deviating from the trend. This

was associated with the volume changes in the MPCM samples, as well as the non-cooperative motion of the samples within the slurry. There was trend reversal after the –50 °C point, in which the temperature reduction resulted in a decrease to more closely follow the trend of the pure di(propylene glycol) methyl ether sample. This trend consequently indicated that the phase change process at this temperature may in fact result in the volume change of the PCM, in which the bulk viscosity of the fluid is affected.

7.2. FUTURE RECOMMENDATIONS

Due to time and equipment constraints, there is potential to further increase the scope of this work, and recommendations for further work are as follows:

- Investigate the potential of creating MPCMs without formaldehyde, if there are potential alternatives that are non-carcinogenic and toxic. This would be excellent for health considerations.

- Explore the incorporation of metallic nanomaterials in the core material to promote crystallization, and to reduce supercooling and to increase thermal conductivity.

- Incorporate both nucleating agents and nanoparticles to the MPCM shell and/or core, to further reduce the microcapsule phenomena and to increase thermal conductivity.

- Preparation of MPCMs with metal coating via the electroless plating method, a wide range of metals and comparison on how this may enhance the PCM thermal properties.

- To investigate thermal cycling for more than 12 cycles with the dilatometer – 100 + cycles would provide an excellent impact on the survivability under more cycles.

- Process optimization with an alternative method to the Taguchi and ANOVA analysis, such as the Response Surface Methodology.

- Perform size exclusion chromatography for resorcinol, catechol, and hydroquinone dihydroxybenzenes samples to gain a more quantitative result for supernatant reaction products after the polymerization process.

- Encapsulate a wider range of core materials in terms of melting points to gain a wider overall picture on the microcapsule properties depending on the volatility of the core.

- Produce nanocapsules with the same cryo-PCM core material and compare such properties with the microcapsules, including yield, payload, encapsulation efficiency, thermal conductivity, mechanical properties, and long-term core retention.

- Investigate the water binding ability of the microcapsules – perhaps through the Karl Fischer titration method.

REFERENCES

Abhat, A. *et al.* (1981) 'Development of a modular heat exchanger with an integrated latent heat storage', *Report no. BMFT FBT*, pp. 50–81.

Agyenim, F. *et al.* (2010) 'A review of materials, heat transfer and phase change problem formulation for latent heat thermal energy storage systems (LHTESS)', *Renewable and Sustainable Energy Reviews*. doi: 10.1016/j.rser.2009.10.015.

Akeiber, H. *et al.* (2016) 'A review on phase change material (PCM) for sustainable passive cooling in building envelopes', *Renewable and Sustainable Energy Reviews*, pp. 1470–1497. doi: 10.1016/j.rser.2016.03.036.

Al-Shannaq, R. *et al.* (2015) 'Supercooling elimination of phase change materials (PCMs) microcapsules', *Energy*. doi: 10.1016/j.energy.2015.05.033.

Al-Shannaq, R. *et al.* (2016) 'Innovative method of metal coating of microcapsules containing phase change materials', *Solar Energy*, 129, pp. 54–64. doi: 10.1016/j.solener.2016.01.043.

Alexiadis, A. (2007) 'Global warming and human activity: A model for studying the potential instability of the carbon dioxide/temperature feedback mechanism', *Ecological Modelling*. doi: 10.1016/j.ecolmodel.2006.11.020.

Alkan, C., Aksoy, S. A. and Anayurt, R. A. (2015) 'Synthesis of poly(methyl methacrylate-co-acrylic acid)/n-eicosane microcapsules for thermal comfort in textiles', *Textile Research Journal*. doi: 10.1177/0040517514548751.

Alkan, C. and Sari, A. (2008) 'Fatty acid/poly(methyl methacrylate) (PMMA) blends as form-stable phase change materials for latent heat thermal energy storage', *Solar Energy*. doi: 10.1016/j.solener.2007.07.001.

Alva, G. *et al.* (2017) 'Synthesis and characterization of microencapsulated myristic acid–palmitic acid eutectic mixture as phase change material for thermal energy storage', *Applied Energy*, 203, pp. 677–685. doi: 10.1016/j.apenergy.2017.06.082.

Alvarado, J. L. *et al.* (2006) 'Characterization of supercooling suppression of microencapsulated phase change material by using DSC', *Journal of Thermal Analysis and Calorimetry*. doi: 10.1007/s10973-005-7430-0.

Alvarado, J. L. *et al.* (2007) 'Thermal performance of microencapsulated phase change material slurry in turbulent flow under constant heat flux', *International Journal of Heat and Mass Transfer*, 50(9–10), pp. 1938–1952. doi: 10.1016/j.ijheatmasstransfer.2006.09.026.

Anisur, M. R. *et al.* (2013) 'Curbing global warming with phase change materials for energy storage', *Renewable and Sustainable Energy Reviews*. doi: 10.1016/j.rser.2012.10.014.

Athreya, S. and Venkatesh, Y. D. (2012) 'Application Of Taguchi Method For Optimization Of Process Parameters In Improving The Surface Roughness Of Lathe Facing Operation', *International Refereed Journal of Engineering and Science*. doi: 2319-1821.

Atinafu, D. G. *et al.* (2018) 'Introduction of organic-organic eutectic PCM in mesoporous N-doped carbons for enhanced thermal conductivity and energy storage capacity', *Applied Energy*, 211, pp. 1203–1215. doi: 10.1016/j.apenergy.2017.12.025.

Aydin, D., Casey, S. P. and Riffat, S. (2015) 'The latest advancements on thermochemical heat storage systems', *Renewable and Sustainable Energy Reviews*, 41, pp. 356–367. doi: 10.1016/j.rser.2014.08.054.

Azizi-Lalabadi, M. *et al.* (2019) 'Antimicrobial activity of Titanium dioxide and Zinc oxide nanoparticles supported in 4A zeolite and evaluation the morphological characteristic', *Scientific Reports*. doi: 10.1038/s41598-019-54025-0.

Bayés-García, L. *et al.* (2010) 'Phase Change Materials (PCM) microcapsules with different shell compositions: Preparation, characterization and thermal stability', *Solar Energy Materials and Solar Cells*, 94(7), pp. 1235–1240. doi: 10.1016/j.solmat.2010.03.014.

Biswas, D. R. (1977) 'Thermal energy storage using sodium sulfate decahydrate and water', *Solar Energy*, 19(1), pp. 99–100. doi: 10.1016/0038-092X(77)90094-9.

Bland, A. *et al.* (2017) 'PCMs for Residential Building Applications: A Short Review Focused on Disadvantages and Proposals for Future Development', *Buildings 2017, Vol. 7, Page 78*, 7(3), p. 78. doi: 10.3390/BUILDINGS7030078.

Boh, B., Knez, E. and Staresinic, M. (2005) 'Microencapsulation of higher hydrocarbon phase change materials by in situ polymerization', *Journal of Microencapsulation*, 22(7), pp. 715–735. doi: 10.1080/02652040500162139.

Bolimowski, P. A., Bond, I. P. and Wass, D. F. (2016) 'Robust synthesis of epoxy resin-filled microcapsules for application to self-healing materials', *Philosophical Transactions of the Royal Society A: Mathematical, Physical and Engineering Sciences*. doi: 10.1098/rsta.2015.0083.

Bolimowski, P. A., Kozera, R. and Boczkowska, A. (2018) 'Poly(urea-formaldehyde) microcapsules – synthesis and influence of stirring speed on capsules size', *Polimery/Polymers*. doi: 10.14314/polimery.2018.5.2.

Bouwman, A. M. *et al.* (2005) 'The relation between granule size, granule stickiness, and torque in the high-shear granulation process', *Pharmaceutical Research*, 22(2), pp. 270–275. doi: 10.1007/s11095-004-1194-2.

Brima, E. I., Jenkins, R. O. and Haris, P. I. (2006) 'Understanding arsenic metabolism through spectroscopic determination of arsenic in human urine', *Spectroscopy*. IOS Press, pp. 125–151. doi: 10.1155/2006/759046.

Brown, E. N. *et al.* (2003a) 'In situ poly(urea-formaldehyde) microencapsulation of dicyclopentadiene', *Journal of Microencapsulation*, 20(6), pp. 719–730. doi: 10.1080/0265204031000154160.

Brown, E. N. *et al.* (2003b) 'In situ poly(urea-formaldehyde) microencapsulation of dicyclopentadiene', *Journal of Microencapsulation*. doi: 10.1080/0265204031000154160.

Butstraen, C. and Salaün, F. (2014) 'Preparation of microcapsules by complex coacervation of gum Arabic and chitosan', *Carbohydrate Polymers*, 99, pp. 608–616. doi: 10.1016/j.carbpol.2013.09.006.

Cai, Y. *et al.* (2012) 'Preparation, morphology and thermal properties of electrospun fatty acid eutectics/polyethylene terephthalate form-stable phase change ultrafine composite fibers for thermal energy storage', in *Energy Conversion and Management*, pp. 245–255. doi: 10.1016/j.enconman.2012.04.018.

Cao, F. *et al.* (2015) 'Synthesis and heat transfer performance of phase change microcapsule enhanced thermal fluids', *Journal of Heat Transfer*, 137(9). doi: 10.1115/1.4030234.

Charunyakorn, P., Sengupta, S. and Roy, S. K. (1991) 'Forced convection heat transfer in microencapsulated phase change material slurries: flow in circular ducts', *International Journal of Heat and Mass Transfer*. doi: 10.1016/0017-9310(91)90128-2.

Chen, C., Wang, L. and Huang, Y. (2011) 'Electrospun phase change fibers based on polyethylene glycol/cellulose acetate blends', *Applied Energy*, 88(9), pp. 3133–3139. doi: 10.1016/J.APENERGY.2011.02.026.

Chen, D. Z. *et al.* (2019) 'Fabrication, morphology and thermal properties of octadecylamine-grafted graphene oxide-modified phase-change microcapsules for thermal energy storage', *Composites Part B: Engineering*. doi: 10.1016/j.compositesb.2018.08.066.

Chen, Y. *et al.* (2015) 'Applications of micro-fourier transform infrared spectroscopy (FTIR) in the geological sciences—A Review', *International Journal of Molecular Sciences*. doi: 10.3390/ijms161226227.

Chuanjie, F., Juntao, T. and Xiaodong, Z. (2013) 'Effects of process parameters on the physical properties of poly (urea-formaldehyde) microcapsules prepared by a one-step method', *Iranian Polymer Journal (English Edition)*. doi: 10.1007/s13726-013-0165-z.

Cosco, S. *et al.* (2007) 'Properties of poly(urea-formaldheyde) microcapsules containing an epoxy resin', *Journal of Applied Polymer Science*. doi: 10.1002/app.26263.

Costa, C. *et al.* (2019) 'Emulsion formation and stabilization by biomolecules: The leading role of cellulose', *Polymers*. MDPI AG. doi: 10.3390/polym11101570.

Cui, J. and Hao, J. (2011) 'Nanoengineered polymer capsules from fabrication to applications.', in *Self-Assem. Struct.*, pp. 35–77. doi: 10.1201/b10479-3.

Cui, Y. *et al.* (2017) 'A review on phase change material application in building', *Advances in Mechanical Engineering*. doi: 10.1177/1687814017700828.

Darvin, J. R. *et al.* (2019) 'Concentrated Ag Nanoparticles in Dodecane as Phase Change Materials for Thermal Energy Storage', *ACS Applied Nano Materials*. doi: 10.1021/acsanm.9b01027.

Delgado, M., Lázaro, A., Mazo, J., Marín, J. M., *et al.* (2012) 'Experimental analysis of a microencapsulated PCM slurry as thermal storage system and as heat transfer fluid in laminar flow', *Applied Thermal Engineering*, 36(1), pp. 370–377. doi: 10.1016/j.applthermaleng.2011.10.050.

Delgado, M., Lázaro, A., Mazo, J. and Zalba, B. (2012) 'Review on phase change material emulsions and microencapsulated phase change material slurries: Materials, heat transfer studies and applications', *Renewable and Sustainable Energy Reviews*, pp. 253–273. doi: 10.1016/j.rser.2011.07.152.

Dhaidan, N. S. and Khodadadi, J. M. (2015) 'Melting and convection of phase change materials in different shape containers: A review', *Renewable and Sustainable Energy Reviews*, 43, pp. 449–477. doi: 10.1016/j.rser.2014.11.017.

Diaconu, B. M., Varga, S. and Oliveira, A. C. (2010) 'Experimental assessment of heat storage properties and heat transfer characteristics of a phase change material slurry for air conditioning applications', *Applied Energy*, 87(2), pp. 620–628. doi: 10.1016/j.apenergy.2009.05.002.

Dincer, I. and Rosen, M. (2011) *Thermal Energy Storage Systems and Applications*, *Fuel Cells, Batt Energy Storage- ...*.

Ding, Y. *et al.* (2016) 'Liquid Air Energy Storage', in *Storing Energy: With Special Reference to Renewable Energy Sources*. doi: 10.1016/B978-0-12-803440-8.00009-9.

Dong, Z. J. *et al.* (2007) 'Effect of processing parameters on the formation of spherical multinuclear microcapsules encapsulating peppermint oil by coacervation', *Journal of Microencapsulation*. doi: 10.1080/02652040701500632.

Dubey, R., Shami, T. C. and Bhasker Rao, K. U. (2009) 'Microencapsulation technology and applications', *Defence Science Journal*, 59(1), pp. 82–95. doi: 10.14429/dsj.59.1489.

Dutkiewicz, J. (1983) 'Hydrolytic degradation of cured urea–formaldehyde resin', *Journal of Applied Polymer Science*, 28(11), pp. 3313–3320. doi: 10.1002/app.1983.070281101.

Dutkowski, K. and Fiuk, J. J. (2019) ‘Experimental research of viscosity of microencapsulated PCM slurry at the phase change temperature’, *International Journal of Heat and Mass Transfer*, 134, pp. 1209–1217. doi: 10.1016/j.ijheatmasstransfer.2019.02.036.

Dutkowski, K. and Kruzel, M. (2019) ‘Microencapsulated PCM slurries’ dynamic viscosity experimental investigation and temperature-dependent prediction model’, *International Journal of Heat and Mass Transfer*, 145, p. 118741. doi: 10.1016/j.ijheatmasstransfer.2019.118741.

El-Kotb, M. *et al.* (2006) ‘Thermal characteristics of paraffin wax for solar energy storage’, *Energy Sources, Part A: Recovery, Utilization and Environmental Effects*. doi: 10.1080/009083190932132.

Fan, C., Tang, J. and Zhou, X. (2013) ‘Role of ammonium chloride in preparing poly(urea-formaldehyde) microcapsules using one-step method’, *Journal of Applied Polymer Science*. doi: 10.1002/app.39008.

Fan, C. and Zhou, X. (2010) ‘Influence of operating conditions on the surface morphology of microcapsules prepared by in situ polymerization’, *Colloids and Surfaces A: Physicochemical and Engineering Aspects*. doi: 10.1016/j.colsurfa.2010.04.012.

Fan, C. and Zhou, X. (2011) ‘Effect of emulsifier on poly(urea-formaldehyde) microencapsulation of tetrachloroethylene’, *Polymer Bulletin*. doi: 10.1007/s00289-010-0355-1.

Fan, L. and Khodadadi, J. M. (2011) ‘Thermal conductivity enhancement of phase change materials for thermal energy storage: A review’, *Renewable and Sustainable Energy Reviews*, pp. 24–46. doi: 10.1016/j.rser.2010.08.007.

Fan, Y. F. *et al.* (2004) ‘Super-cooling prevention of microencapsulated phase change material’, *Thermochimica Acta*. doi: 10.1016/j.tca.2003.11.006.

Fang, G. *et al.* (2009) ‘Preparation and characterization of nano-encapsulated n-tetradecane as phase change material for thermal energy storage’, *Chemical Engineering Journal*. doi: 10.1016/j.cej.2009.06.019.

Fang, G., Chen, Z. and Li, H. (2010) ‘Synthesis and properties of microencapsulated paraffin composites with SiO2 shell as thermal energy storage materials’, *Chemical Engineering Journal*. doi: 10.1016/j.cej.2010.07.054.

Fang, G., Tang, F. and Cao, L. (2014) ‘Preparation, thermal properties and applications of shape-stabilized thermal energy storage materials’, *Renewable and Sustainable Energy Reviews*, 40, pp. 237–259. doi: 10.1016/j.rser.2014.07.179.

Fang, X. *et al.* (2014) ‘Thermal energy storage performance of paraffin-based composite phase change materials filled with hexagonal boron nitride nanosheets’, *Energy Conversion and Management*, 80, pp. 103–109. doi: 10.1016/j.enconman.2014.01.016.

Farid, M. M. *et al.* (2004a) 'A review on phase change energy storage: Materials and applications', *Energy Conversion and Management*. doi: 10.1016/j.enconman.2003.09.015.

Farid, M. M. *et al.* (2004b) 'A review on phase change energy storage: Materials and applications', *Energy Conversion and Management*. doi: 10.1016/j.enconman.2003.09.015.

Fayyad, E. M., Almaadeed, M. A. and Jones, A. (2016) 'Preparation and characterization of urea–formaldehyde microcapsules filled with paraffin oil', *Polymer Bulletin*. doi: 10.1007/s00289-015-1518-x.

Fink, J. (2020) 'Thickeners', in *Hydraulic Fracturing Chemicals and Fluids Technology*. Elsevier, pp. 55–79. doi: 10.1016/b978-0-12-822071-9.00010-4.

Gaca, K. Z., Parkinson, J. A. and Sefcik, J. (2017) 'Kinetics of early stages of resorcinol-formaldehyde polymerization investigated by solution-phase nuclear magnetic resonance spectroscopy', *Polymer*, 110, pp. 62–73. doi: 10.1016/j.polymer.2016.12.069.

Ge, Z. *et al.* (2014) 'Carbonate-salt-based composite materials for medium- and high-temperature thermal energy storage', *Particuology*, 15, pp. 77–81. doi: 10.1016/j.partic.2013.09.002.

Di Gianfrancesco, A. (2017) 'Technologies for chemical analyses, microstructural and inspection investigations', in *Materials for Ultra-Supercritical and Advanced Ultra-Supercritical Power Plants*. Elsevier Inc., pp. 197–245. doi: 10.1016/B978-0-08-100552-1.00008-7.

Glutz, B. R. and Zollinger, H. (1969) 'Allgemeine Säure-Basen-Katalyse der Monomethylol-Bildung aus Harnstoff und Formaldehyd in Wasser', *Helvetica Chimica Acta*. doi: 10.1002/hlca.19690520722.

Goldstein, J. I. *et al.* (2017) *Scanning electron microscopy and x-ray microanalysis*, *Scanning Electron Microscopy and X-ray Microanalysis*. doi: 10.1007/978-1-4939-6676-9.

Gringras, L. and Sjöstedt, G. (1975) 'Crosslinking of gelatin with formaldehyde in the presence of some poly-hydroxybenzenes', *Angewandte Makromolekulare Chemie*, 42(1), pp. 123–138. doi: 10.1002/apmc.1975.050420108.

Güell, C. *et al.* (2017) 'Apparent interfacial tension effects in protein stabilized emulsions prepared with microstructured systems', *Membranes*. doi: 10.3390/membranes7020019.

Guo, H., Zhao, X. and Wang, J. (2005) 'Synthesis of functional microcapsules containing suspensions responsive to electric fields', *Journal of Colloid and Interface Science*. doi: 10.1016/j.jcis.2004.10.056.

Han, L. *et al.* (2001) 'Preparation and Characterization of Microcapsules Containing Lemon Oil', *Journal of Colloid and Interface Science*. doi: 10.1007/s12155-013-9327-2.

Hawlader, M. N. A., Uddin, M. S. and Khin, M. M. (2003) 'Microencapsulated PCM thermal-energy storage system', *Applied Energy*. doi: 10.1016/S0306-2619(02)00146-0.

Heinz, A. and Streicher, W. (2006) 'Application of Phase Change Materials and PCM slurries for thermal energy storage'. . Available at: https://graz.pure.elsevier.com/en/publications/application-of-phase-change-materials-and-pcm-slurries-for-therma (Accessed: 8 February 2021).

Hong, K. and Park, S. (1999) 'Preparation of polyurethane microcapsules with different soft segments and their characteristics', *Reactive and Functional Polymers*, 42(3), pp. 193–200. doi: 10.1016/S1381-5148(98)00068-6.

Hong, Y. (2000) 'Preparation of polyethylene-paraffin compound as a form-stable solid-liquid phase change material', *Solar Energy Materials and Solar Cells*, 64(1), pp. 37–44. doi: 10.1016/S0927-0248(00)00041-6.

Hu, J., Chen, H. Q. and Zhang, Z. (2009) 'Mechanical properties of melamine formaldehyde microcapsules for self-healing materials', *Materials Chemistry and Physics*. doi: 10.1016/j.matchemphys.2009.07.004.

Huang, C. *et al.* (2020) 'A novel bifunctional microencapsulated phase change material loaded with ZnO for thermal energy storage and light-thermal energy conversion', *Sustainable Energy and Fuels*. doi: 10.1039/d0se00718h.

Huang, L., Doetsch, C. and Pollerberg, C. (2010) 'Low temperature paraffin phase change emulsions', *International Journal of Refrigeration*, 33(8), pp. 1583–1589. doi: 10.1016/j.ijrefrig.2010.05.016.

Huang, L. and Petermann, M. (2015) 'An experimental study on rheological behaviors of paraffin/water phase change emulsion', *International Journal of Heat and Mass Transfer*, 83, pp. 479–486. doi: 10.1016/j.ijheatmasstransfer.2014.12.037.

Huang, M. J. *et al.* (2011) 'Microencapsulated phase change slurries for thermal energy storage in a residential solar energy system', *Renewable Energy*. doi: 10.1016/j.renene.2011.04.004.

Huang, X. *et al.* (2019) 'Thermal properties and applications of microencapsulated PCM for thermal energy storage: A review', *Applied Thermal Engineering*. doi: 10.1016/j.applthermaleng.2018.11.007.

Huang, Y. I. *et al.* (2007) 'Microencapsulation of extract containing shikonin using gelatin-acacia coacervation method: A formaldehyde-free approach', *Colloids and Surfaces B: Biointerfaces*, 58(2), pp. 290–297. doi: 10.1016/j.colsurfb.2007.04.013.

Inaba, H., Kim, M. K. and Horibe, A. (2004) 'Melting heat transfer characteristics of microencapsulated phase change material slurries with plural microcapsules having different diameters', *Journal of Heat Transfer*, 126(4), pp. 558–565. doi: 10.1115/1.1773584.

International Energy Agency (2008) *World Energy Outlook 2008*, *International Energy Agency, Paris, France*. doi: 10.1049/ep.1977.0180.

International Energy Agency (IEA) (2015) 'Energy and climate change. World energy outlook special report', *World Energy Outlook Special Report*. doi: 10.1038/479267b.

Jamekhorshid, A., Sadrameli, S. M. and Bahramian, A. R. (2014) 'Process optimization and modeling of microencapsulated phase change material using response surface methodology', *Applied Thermal Engineering*. doi: 10.1016/j.applthermaleng.2014.05.011.

Jamekhorshid, A., Sadrameli, S. M. and Farid, M. (2014) 'A review of microencapsulation methods of phase change materials (PCMs) as a thermal energy storage (TES) medium', *Renewable and Sustainable Energy Reviews*. doi: 10.1016/j.rser.2013.12.033.

Katoueizadeh, E., Zebarjad, S. M. and Janghorban, K. (2019) 'Investigating the effect of synthesis conditions on the formation of urea-formaldehyde microcapsules', *Journal of Materials Research and Technology*. doi: 10.1016/j.jmrt.2018.04.013.

Kenisarin, M. M. (2010) 'High-temperature phase change materials for thermal energy storage', *Renewable and Sustainable Energy Reviews*, pp. 955–970. doi: 10.1016/j.rser.2009.11.011.

Kenisarin, M. M. *et al.* (2020) 'Melting and solidification of PCMs inside a spherical capsule: A critical review', *Journal of Energy Storage*. doi: 10.1016/j.est.2019.101082.

Khakzad, F. *et al.* (2014) 'Optimization of parameters in preparation of PCM microcapsules based on melamine formaldehyde through dispersion polymerization', *Colloid and Polymer Science*. doi: 10.1007/s00396-013-3076-9.

Khan, Zakir, Khan, Zulfiqar and Ghafoor, A. (2016) 'A review of performance enhancement of PCM based latent heat storage system within the context of materials, thermal stability and compatibility', *Energy Conversion and Management*, pp. 132–158. doi: 10.1016/j.enconman.2016.02.045.

Kirkwood, K. and Jackson, S. D. (2020) 'Hydrogenation and Hydrodeoxygenation of Oxygen-Substituted Aromatics over Rh/silica: Catechol, Resorcinol and Hydroquinone', *Catalysts*, 10(5), p. 584. doi: 10.3390/catal10050584.

Kivak, T., Samtaş, G. and Çiçek, A. (2012) 'Taguchi method based optimisation of drilling parameters in drilling of AISI 316 steel with PVD monolayer and multilayer coated HSS drills', *Measurement: Journal of the International Measurement Confederation*. doi: 10.1016/j.measurement.2012.02.022.

Klugmann-Radziemska, E. and Wcisło-Kucharek, P. (2017) 'Photovoltaic module temperature stabilization with the use of phase change materials', *Solar Energy*, 150, pp. 538–545. doi: 10.1016/J.SOLENER.2017.05.016.

Konuklu, Y., Unal, M. and Paksoy, H. O. (2014) 'Microencapsulation of caprylic acid with different wall materials as phase change material for thermal energy storage', *Solar Energy Materials and Solar Cells*, 120(PART B), pp. 536–542. doi: 10.1016/j.solmat.2013.09.035.

Kumar, N. and Banerjee, D. (2018) 'Phase change materials', in *Handbook of Thermal Science and Engineering*. doi: 10.1007/978-3-319-26695-4_53.

Lane, G. A. (1980) 'Low temperature heat storage with phase change materials', *International Journal of Ambient Energy*, 1(3), pp. 155–168. doi: 10.1080/01430750.1980.9675731.

Lane, G. A. and Shamsundar, N. (1983) 'Solar Heat Storage: Latent Heat Materials, Vol. I: Background and Scientific Principles', *Journal of Solar Energy Engineering*. doi: 10.1115/1.3266412.

Lee, H. Y. *et al.* (2002) 'Microencapsulation of fragrant oil via in situ polymerization: Effects of pH and melamine-formaldehyde molar ratio', *Journal of Microencapsulation*, 19(5), pp. 559–569. doi: 10.1080/02652040210140472.

Lewicki, J. P., Fox, C. A. and Worsley, M. A. (2015) 'On the synthesis and structure of resorcinol-formaldehyde polymeric networks - Precursors to 3D-carbon macroassemblies', *Polymer*, 69(1), pp. 45–51. doi: 10.1016/j.polymer.2015.05.016.

Li, M., Chen, M. and Wu, Z. (2014) 'Enhancement in thermal property and mechanical property of phase change microcapsule with modified carbon nanotube', *Applied Energy*. doi: 10.1016/j.apenergy.2014.04.029.

Li, T. H. *et al.* (2012) 'A computational exploration of the mechanisms for the acid-catalytic urea-formaldehyde reaction: New insight into the old topic', *Journal of Physical Organic Chemistry*. doi: 10.1002/poc.1880.

Liang, S. *et al.* (2015) 'Nanoencapsulation of n-octadecane phase change material with silica shell through interfacial hydrolysis and polycondensation in miniemulsion', *Energy*. doi: 10.1016/j.energy.2015.10.024.

Lin, Y. *et al.* (2018) 'Review on thermal conductivity enhancement, thermal properties and applications of phase change materials in thermal energy storage', *Renewable and Sustainable Energy Reviews*, pp. 2730–2742. doi: 10.1016/j.rser.2017.10.002.

Liu, C. *et al.* (2015) 'Review on nanoencapsulated phase change materials: Preparation, characterization and heat transfer enhancement', *Nano Energy*, pp. 814–826. doi: 10.1016/j.nanoen.2015.02.016.

Liu, H. *et al.* (2019) 'Fabrication and applications of dual-responsive microencapsulated phase change material with enhanced solar energy-storage and solar photocatalytic effectiveness', *Solar Energy Materials and Solar Cells*. doi: 10.1016/j.solmat.2019.01.012.

Liu, J. *et al.* (2017) 'Preparation of graphite nanoparticles-modified phase change microcapsules and their dispersed slurry for direct absorption solar collectors', *Solar Energy Materials and Solar Cells*. doi: 10.1016/j.solmat.2016.09.020.

Liu, M. *et al.* (2017) 'Characterization of the crystalline regions of cured urea formaldehyde resin', *RSC Advances*. doi: 10.1039/c7ra08082d.

Lopez, J. *et al.* (2010) 'Confined melting in deformable porous media: A first attempt to explain the graphite/salt composites behaviour', *International Journal of Heat and Mass Transfer*, 53(5–6), pp. 1195–1207. doi: 10.1016/j.ijheatmasstransfer.2009.10.025.

Lovell, P. A. and Schork, F. J. (2020) 'Fundamentals of Emulsion Polymerization', *Biomacromolecules*. American Chemical Society, pp. 4396–4441. doi: 10.1021/acs.biomac.0c00769.

Lu, P. *et al.* (2017) 'Embedding Lauric Acid into Polystyrene Nanofibers To Make High-Capacity Membranes for Efficient Thermal Energy Storage', *ACS Sustainable Chemistry and Engineering*, 5(8), pp. 7249–7259. doi: 10.1021/ACSSUSCHEMENG.7B01476.

Ma, G. *et al.* (2017) 'Binary eutectic mixtures of stearic acid-n-butyramide/n-octanamide as phase change materials for low temperature solar heat storage', *Applied Thermal Engineering*, 111, pp. 1052–1059. doi: 10.1016/j.applthermaleng.2016.10.004.

Ma, T. *et al.* (2015) 'Using phase change materials in photovoltaic systems for thermal regulation and electrical efficiency improvement: A review and outlook', *Renewable and Sustainable Energy Reviews*, pp. 1273–1284. doi: 10.1016/j.rser.2014.12.003.

Ma, Y. *et al.* (2012) 'Preparation and characterization of poly(methyl methacrylate-co-divinylbenzene) microcapsules containing phase change temperature adjustable binary core materials', *Solar Energy*. doi: 10.1016/j.solener.2012.04.008.

Marx, R., Bauer, D. and Drueck, H. (2014) 'Energy efficient integration of heat pumps into solar district heating systems with seasonal thermal energy storage', in *Energy Procedia*. doi: 10.1016/j.egypro.2014.10.302.

Memon, S. A. *et al.* (2015) 'Utilization of macro encapsulated phase change materials for the development of thermal energy storage and structural lightweight aggregate concrete', *Applied Energy*, 139, pp. 43–55. doi: 10.1016/J.APENERGY.2014.11.022.

Meng, Z. N. and Zhang, P. (2017) 'Experimental and numerical investigation of a tube-in-tank latent thermal energy storage unit using composite PCM', *Applied Energy*, 190, pp. 524–539. doi: 10.1016/j.apenergy.2016.12.163.

Mishra, M. (2015) 'Overview of Encapsulation and Controlled Release', in *Handbook of Encapsulation and Controlled Release*, pp. 3–19. doi: 10.1201/b19038.

Mo, S. *et al.* (2013) 'Reduction of supercooling of water by TiO2 nanoparticles as observed using differential scanning calorimeter', *Journal of Experimental Nanoscience*. doi: 10.1080/17458080.2011.572085.

Mohamed, A. I. A. *et al.* (2017) 'Influence of Surfactant Structure on the Stability of Water-in-Oil Emulsions under High-Temperature High-Salinity Conditions', *Journal of Chemistry*, 2017. doi: 10.1155/2017/5471376.

Mohamed, S. A. *et al.* (2017) 'A review on current status and challenges of inorganic phase change materials for thermal energy storage systems', *Renewable and Sustainable Energy Reviews*, pp. 1072–1089. doi: 10.1016/j.rser.2016.12.012.

Moreno, P. *et al.* (2014) 'PCM thermal energy storage tanks in heat pump system for space cooling', *Energy and Buildings*. doi: 10.1016/j.enbuild.2014.07.044.

Morgan, P. W. and Kwolek, S. L. (1959) 'Interfacial polycondensation. II. Fundamentals of polymer formation at liquid interfaces', *Journal of Polymer Science*, 40(137), pp. 299–327. doi: 10.1002/pol.1959.1204013702.

Mousavi Baygi, S. R. and Sadrameli, S. M. (2018) 'Thermal management of photovoltaic solar cells using polyethylene glycol 1000 (PEG1000) as a phase change material', *Thermal Science and Engineering Progress*, 5, pp. 405–411. doi: 10.1016/J.TSEP.2018.01.012.

Mustapha, A. N. *et al.* (2021) 'Latent heat thermal energy storage: A bibliometric analysis explicating the paradigm from 2000–2019', *Journal of Energy Storage*, 33, p. 102027. doi: 10.1016/J.EST.2020.102027.

Nair, B. R. and Francis, D. J. (1983) 'Kinetics and mechanism of urea-formaldehyde reaction', *Polymer*. doi: 10.1016/0032-3861(83)90118-0.

Nenningsland, A. L., Simon, S. and Sjöblom, J. (2014) 'Influence of Interfacial Rheological Properties on Stability of Asphaltene-Stabilized Emulsions', *Journal of Dispersion Science and Technology*, 35(2), pp. 231–243. doi: 10.1080/01932691.2013.784196.

Nguon, O. *et al.* (2017) 'Microencapsulation by in situ Polymerization of Amino Resins', *Polymer Reviews*, pp. 1–50. doi: 10.1080/15583724.2017.1364765.

Niu, X. W. *et al.* (2012) 'Synthesis of enhanced urea-formaldehyde resin microcapsules doped with nanotitania', *Journal of Applied Polymer Science*. doi: 10.1002/app.34099.

Nomura, T. *et al.* (2015) 'High thermal conductivity phase change composite with percolating carbon fiber network', *Applied Energy*. doi: 10.1016/j.apenergy.2015.05.042.

Nomura, T. *et al.* (no date) 'Microencapsulation of Metal-based Phase Change Material for High-temperature Thermal Energy Storage'. doi: 10.1038/srep09117.

Olivares, R. I. and Edwards, W. (2013) 'LiNO3-NaNO3-KNO3 salt for thermal energy storage: Thermal stability evaluation in different atmospheres', *Thermochimica Acta*, 560, pp. 34–42. doi: 10.1016/j.tca.2013.02.029.

Ouellette, R. J. and Rawn, J. D. (2015) 'Aromatic Compounds', in *Principles of Organic Chemistry*. Elsevier, pp. 133–162. doi: 10.1016/B978-0-12-802444-7.00005-7.

Palusiak, M. *et al.* (2014) 'The substituent effect on benzene dications', *Physical Chemistry Chemical Physics*, 16(10), pp. 4752–4763. doi: 10.1039/c3cp54089h.

Park, B. D. and Jeong, H. W. (2011) 'Hydrolytic stability and crystallinity of cured ureaformaldehyde resin adhesives with different formaldehyde/urea mole ratios', *International Journal of Adhesion and Adhesives*. doi: 10.1016/j.ijadhadh.2011.05.001.

Park, J. J., Butt, D. P. and Beard, C. A. (2000) 'Review of liquid metal corrosion issues for potential containment materials for liquid lead and lead-bismuth eutectic spallation targets as a neutron source', *Nuclear Engineering and Design*, 196(3), pp. 315–325. doi: 10.1016/S0029-5493(99)00303-9.

Pascu, O., Garcia-Valls, R. and Giamberini, M. (2008) 'Interfacial polymerization of an epoxy resin and carboxylic acids for the synthesis of microcapsules', *Polymer International*, 57(8), pp. 995–1006. doi: 10.1002/pi.2438.

Peng, G. *et al.* (2020) 'Phase change material (PCM) microcapsules for thermal energy storage', *Advances in Polymer Technology*. doi: 10.1155/2020/9490873.

Perignon, C. *et al.* (2015) 'Microencapsulation by interfacial polymerisation: Membrane formation and structure', *Journal of Microencapsulation*, 32(1), pp. 1–15. doi: 10.3109/02652048.2014.950711.

Pundir, R., Chary, G. H. V. C. and Dastidar, M. G. (2018) 'Application of Taguchi method for optimizing the process parameters for the removal of copper and nickel by growing Aspergillus sp.', *Water Resources and Industry*. doi: 10.1016/j.wri.2016.05.001.

Qin, Y., Dong, Y. and Li, J. (2019) 'Effect of modifiction with melamine-urea-formaldehyde resin on the properties of eucalyptus and poplar', *Journal of Wood Chemistry and Technology*. doi: 10.1080/02773813.2019.1636821.

Rao, Y. *et al.* (2007) 'Convective heat transfer characteristics of microencapsulated phase change material suspensions in minichannels', *Heat and Mass Transfer/Waerme- und Stoffuebertragung*, 44(2), pp. 175–186. doi: 10.1007/s00231-007-0232-0.

El Rhafiki, T. *et al.* (2011) 'Crystallization of PCMs inside an emulsion: Supercooling phenomenon', *Solar Energy Materials and Solar Cells*. doi: 10.1016/j.solmat.2011.03.027.

Rochmadi, Prasetya, A. and Hasokowati, W. (2010) 'Mechanism of microencapsulation with Urea-Formaldehyde polymer', *American Journal of Applied Sciences*. doi: 10.3844/ajassp.2010.739.745.

Rozanna, D. *et al.* (2005) 'Fatty Acids as Phase Change Materials (PCMs) for Thermal Energy Storage: A Review', *International Journal of Green Energy*, 1(4), pp. 495–513. doi: 10.1081/GE-200038722.

Safari, A. *et al.* (2017) 'A review on supercooling of Phase Change Materials in thermal energy storage systems', *Renewable and Sustainable Energy Reviews*. doi: 10.1016/j.rser.2016.11.272.

Salaön, F. (2013) ‘Microencapsulation by Interfacial Polymerization’, in *Encapsulation Nanotechnologies*, pp. 137–173. doi: 10.1002/9781118729175.ch5.

Salaün, F. *et al.* (2009) ‘Influence of process parameters on microcapsules loaded with n-hexadecane prepared by in situ polymerization’, *Chemical Engineering Journal*. doi: 10.1016/j.cej.2009.07.018.

Salaün, F. (2019) ‘Phase Change Materials for Textile Application’, in *Textile Industry and Environment*. doi: 10.5772/intechopen.85028.

Sami, S., Sadrameli, S. M. and Etesami, N. (2018) ‘Thermal properties optimization of microencapsulated a renewable and non-toxic phase change material with a polystyrene shell for thermal energy storage systems’, *Applied Thermal Engineering*. doi: 10.1016/j.applthermaleng.2017.11.119.

Sánchez-Silva, L. *et al.* (2018) ‘Poly(urea-formaldehyde) microcapsules containing commercial paraffin: in situ polymerization study’, *Colloid and Polymer Science*. doi: 10.1007/s00396-018-4365-0.

Sar, A. and Kaygusuz, K. (2003) ‘Some fatty acids used for latent heat storage: Thermal stability and corrosion of metals with respect to thermal cycling’, *Renewable Energy*, 28(6), pp. 939–948. doi: 10.1016/S0960-1481(02)00110-6.

Sari, A. (2003) ‘Thermal reliability test of some fatty acids as PCMs used for solar thermal latent heat storage applications’, *Energy Conversion and Management*, 44(14), pp. 2277–2287. doi: 10.1016/S0196-8904(02)00251-0.

Sari, A. and Kaygusuz, K. (2006) ‘Thermal energy storage characteristics of myristic and stearic acids eutectic mixture for low temperature heating applications’, *Chinese Journal of Chemical Engineering*, 14(2), pp. 270–275. doi: 10.1016/S1004-9541(06)60070-0.

Schmidts, T. *et al.* (2010) ‘Multiple W/O/W emulsions-Using the required HLB for emulsifier evaluation’, *Colloids and Surfaces A: Physicochemical and Engineering Aspects*, 372(1–3), pp. 48–54. doi: 10.1016/j.colsurfa.2010.09.025.

Sciacovelli, A., Vecchi, A. and Ding, Y. (2017) ‘Liquid air energy storage (LAES) with packed bed cold thermal storage – From component to system level performance through dynamic modelling’, *Applied Energy*, 190, pp. 84–98. doi: 10.1016/j.apenergy.2016.12.118.

Šebenik, A., Osredkar, U. and Vizovišek, I. (1981) ‘Polycondensation of higher phenols and unsaturated aldehydes’, *Polymer Bulletin*, 5(9–10), pp. 557–561. doi: 10.1007/BF00254364.

Shahabudin, N., Yahya, R. and Gan, S. N. (2016) ‘Microcapsules of Poly(urea-formaldehyde) (PUF) Containing alkyd from Palm Oil’, in *Materials Today: Proceedings*. doi: 10.1016/j.matpr.2016.01.012.

Shahid, M. Z. *et al.* (2017) 'Initial Interfacial Tension for Various Organic-Water Systems and Study of the Effect of Solute Concentration and Temperature', *Journal of Chemical and Engineering Data*, 62(4), pp. 1198–1203. doi: 10.1021/acs.jced.6b00703.

Shalaby, S. M., Bek, M. A. and El-Sebaii, A. A. (2014) 'Solar dryers with PCM as energy storage medium: A review', *Renewable and Sustainable Energy Reviews*, 33, pp. 110–116. doi: 10.1016/j.rser.2014.01.073.

Sharipova, A. *et al.* (2017) 'The Use of Polymer and Surfactants for the Microencapsulation and Emulsion Stabilization', *Colloids and Interfaces*, 1(1), p. 3. doi: 10.3390/colloids1010003.

Sharma, A. *et al.* (2009) 'Review on thermal energy storage with phase change materials and applications', *Renewable and Sustainable Energy Reviews*, pp. 318–345. doi: 10.1016/j.rser.2007.10.005.

Sharma, R. K. *et al.* (2015) 'Developments in organic solid-liquid phase change materials and their applications in thermal energy storage', *Energy Conversion and Management*. doi: 10.1016/j.enconman.2015.01.084.

Sharma, S. and Choudhary, V. (2017) 'Parametric study for epoxy loaded PMMA microcapsules using Taguchi and ANOVA methods', *Express Polymer Letters*. doi: 10.3144/expresspolymlett.2017.96.

Song, G. *et al.* (2010) 'Preparation and characterization of flame retardant form-stable phase change materials composed by EPDM, paraffin and nano magnesium hydroxide', *Energy*, 35(5), pp. 2179–2183. doi: 10.1016/j.energy.2010.02.002.

Song, Y. *et al.* (2019) 'Experimental and numerical investigation on dodecane/expanded graphite shape-stabilized phase change material for cold energy storage', *Energy*. doi: 10.1016/j.energy.2019.116175.

Swet, C. J. (1980) 'Phase change storage in passive solar architecture', *Proc. Annu. Meet. - Am. Sect. Int. Sol. Energy Soc.; (United States)*, 5.1.

Tan, P. *et al.* (2020) 'Effect of phase separation and supercooling on the storage capacity in a commercial latent heat thermal energy storage: Experimental cycling of a salt hydrate PCM', *Journal of Energy Storage*. doi: 10.1016/j.est.2020.101266.

Telkes, M. (1980) 'Thermal energy storage in salt hydrates', *Solar Energy Materials*, 2(4), pp. 381–393. doi: 10.1016/0165-1633(80)90033-7.

Thies, C. (2003) 'MICROCAPSULES', *Encyclopedia of Food Sciences and Nutrition*, pp. 3892–3903. doi: 10.1016/B0-12-227055-X/01369-9.

Tokuç, A., Başaran, T. and Yesügey, S. C. (2015) 'An experimental and numerical investigation on the use of phase change materials in building elements: The case of a flat roof in Istanbul', *Energy and Buildings*, 102, pp. 91–104. doi: 10.1016/J.ENBUILD.2015.04.039.

Tseng, Y. H. *et al.* (2005) 'Preparation of microencapsulated phase-change materials (MCPCMs) by means of interfacial polycondensation', *Journal of Microencapsulation*, 22(1), pp. 37–46. doi: 10.1080/02652040400026558.

Tumuluri, K. *et al.* (2011) 'Thermal performance of a novel heat transfer fluid containing multiwalled carbon nanotubes and microencapsulated phase change materials', *International Journal of Heat and Mass Transfer*. doi: 10.1016/j.ijheatmasstransfer.2011.07.031.

Ullah, H. *et al.* (2016) 'Synthesis and Characterization of Urea-formaldehyde Microcapsules Containing Functionalized Polydimethylsiloxanes', in *Procedia Engineering*. doi: 10.1016/j.proeng.2016.06.519.

Wang, F., Fang, X. and Zhang, Z. (2018) 'Preparation of phase change material emulsions with good stability and little supercooling by using a mixed polymeric emulsifier for thermal energy storage', *Solar Energy Materials and Solar Cells*, 176, pp. 381–390. doi: 10.1016/j.solmat.2017.10.025.

Wang, H. *et al.* (2013) 'Preparation and properties of microencapsulated phase change materials containing two-phase core materials', *Industrial and Engineering Chemistry Research*. doi: 10.1021/ie401055r.

Wang, H. *et al.* (2017) 'Facile and low energy consumption synthesis of microencapsulated phase change materials with hybrid shell for thermal energy storage', *Journal of Physics and Chemistry of Solids*. doi: 10.1016/j.jpcs.2017.08.002.

Wang, L. (2008) 'Supercooling of Silver Nano Composite PCM Microcapsules', *Journal of Fiber Bioengineering and Informatics*, 1(3), pp. 239–248. doi: 10.3993/JFBI12200810.

Wang, X., Li, C. and Zhao, T. (2018) 'Fabrication and characterization of poly(melamine-formaldehyde)/silicon carbide hybrid microencapsulated phase change materials with enhanced thermal conductivity and light-heat performance', *Solar Energy Materials and Solar Cells*. doi: 10.1016/j.solmat.2018.03.019.

Wang, Xichun *et al.* (2007) 'Flow and heat transfer behaviors of phase change material slurries in a horizontal circular tube', *International Journal of Heat and Mass Transfer*, 50(13–14), pp. 2480–2491. doi: 10.1016/j.ijheatmasstransfer.2006.12.024.

Wu, N., Xu, L. and Zhang, C. (2018) 'The influence of emulsifiers on preparation and properties of microencapsules of melamine-urea-formaldehyde resins with n-dodecanol as phase-change material', *Advances in Polymer Technology*, 37(8), pp. 3492–3498. doi: 10.1002/adv.22133.

Wu, X. *et al.* (2009) 'The anti-supercooling effect of surface-modified nano-scaled SiO 2 in hydrated salts phase transition system', in *Journal of Physics: Conference Series*. doi: 10.1088/1742-6596/188/1/012046.

X-Ray diffraction (XRD) :: Anton Paar Wiki (no date). Available at: https://wiki.anton-paar.com/en/x-ray-diffraction-xrd/ (Accessed: 9 February 2021).

Xiao, X., Zhang, P. and Li, M. (2013) ‘Preparation and thermal characterization of paraffin/metal foam composite phase change material’, *Applied Energy*. doi: 10.1016/j.apenergy.2013.04.050.

Xin, C. *et al.* (2014) ‘Effect of curing temperature on the performance of microencapsulated low melting point paraffin using urea-formaldehyde resin as a shell’, *Textile Research Journal*. doi: 10.1177/0040517513507367.

Xu, C. *et al.* (2014) ‘Silver-coated glass fibers prepared by a simple electroless plating technique’, *Journal of Materials Science: Materials in Electronics*, 25(10), pp. 4638–4642. doi: 10.1007/s10854-014-2216-4.

Xu, D. and Yang, R. (2019) ‘Efficient preparation and characterization of paraffin-based microcapsules by emulsion polymerization’, *Journal of Applied Polymer Science*. doi: 10.1002/app.47552.

Yadav, S. K., Suresh, A. K. and Khilar, K. C. (1990) ‘Microencapsulation in polyurea shell by interfacial polycondensation’, *AIChE Journal*, 36(3), pp. 431–438. doi: 10.1002/aic.690360312.

Yamagishi, Y. *et al.* (1996a) ‘Evaluation of microencapsulated PCM for use in cold energy transportation medium’, in *Proceedings of the Intersociety Energy Conversion Engineering Conference*. doi: 10.1109/iecec.1996.553442.

Yamagishi, Y. *et al.* (1996b) ‘Evaluation of microencapsulated PCM for use in cold energy transportation medium’, in *Proceedings of the Intersociety Energy Conversion Engineering Conference*. IEEE, pp. 2077–2083. doi: 10.1109/iecec.1996.553442.

Yamagishi, Y. *et al.* (1999) ‘Characteristics of microencapsulated PCM slurry as a heat-transfer fluid’, *AIChE Journal*. doi: 10.1002/aic.690450405.

Yan, Y. *et al.* (2009) ‘Mechanical characterization of agarose micro-particles with a narrow size distribution’, *Powder Technology*. doi: 10.1016/j.powtec.2008.12.006.

Yin, D. *et al.* (2015) ‘Microencapsulation of n-hexadecanol by in situ polymerization of melamine-formaldehyde resin in emulsion stabilized by styrene-maleic anhydride copolymer’, *International Journal of Energy Research*. doi: 10.1002/er.3276.

Yoshizawa, H. *et al.* (2007) ‘Investigation of alternative compounds to poly(E-MA) as a polymeric surfactant for preparation of microcapsules by phase separation method’, *Journal of Microencapsulation*. doi: 10.1080/02652040601162699.

Yu, J. *et al.* (2014) ‘Influence of nanoparticles and graphite foam on the supercooling of acetamide’, *Journal of Nanomaterials*. doi: 10.1155/2014/313674.

Yu, Q. *et al.* (2018) ‘Thermo-mechanical analysis of microcapsules containing phase change materials for cold storage’, *Applied Energy*, 211, pp. 1190–1202. doi: 10.1016/j.apenergy.2017.12.021.

Yu, S., Wang, X. and Wu, D. (2014) 'Microencapsulation of n-octadecane phase change material with calcium carbonate shell for enhancement of thermal conductivity and serving durability: Synthesis, microstructure, and performance evaluation', *Applied Energy*. doi: 10.1016/j.apenergy.2013.10.029.

Yuan, L. *et al.* (2006) 'Preparation and characterization of poly(urea-formaldehyde) microcapsules filled with epoxy resins', *Polymer*, 47(15), pp. 5338–5349. doi: 10.1016/j.polymer.2006.05.051.

Yuan, L. *et al.* (2007) 'The permeability and stability of microencapsulated epoxy resins', *Journal of Materials Science*, 42(12), pp. 4390–4397. doi: 10.1007/s10853-006-0606-6.

Yuan, L., Gu, A. and Liang, G. (2008) 'Preparation and properties of poly(urea-formaldehyde) microcapsules filled with epoxy resins', *Materials Chemistry and Physics*. doi: 10.1016/j.matchemphys.2008.02.035.

Zahir, M. H. *et al.* (2019) 'Supercooling of phase-change materials and the techniques used to mitigate the phenomenon', *Applied Energy*. doi: 10.1016/j.apenergy.2019.02.045.

Zhang, G. *et al.* (2014) 'Encapsulation of copper-based phase change materials for high temperature thermal energy storage', *Solar Energy Materials and Solar Cells*, 128, pp. 131–137. doi: 10.1016/j.solmat.2014.05.012.

Zhang, G. H. and Zhao, C. Y. (2011) 'Thermal and rheological properties of microencapsulated phase change materials', *Renewable Energy*. doi: 10.1016/j.renene.2011.04.002.

Zhang, H. *et al.* (2016) 'Thermal energy storage: Recent developments and practical aspects', *Progress in Energy and Combustion Science*, pp. 1–40. doi: 10.1016/j.pecs.2015.10.003.

Zhang, H. and Wang, X. (2009) 'Fabrication and performances of microencapsulated phase change materials based on n-octadecane core and resorcinol-modified melamine-formaldehyde shell', *Colloids and Surfaces A: Physicochemical and Engineering Aspects*, 332(2–3), pp. 129–138. doi: 10.1016/j.colsurfa.2008.09.013.

Zhang, K., Zhou, Q. and Ye, H. M. (2019) 'Optimizing the preparation of semi-crystalline paraffin/poly(urea-formaldehyde) microcapsules for thermal energy storage', *Applied Sciences (Switzerland)*. doi: 10.3390/app9030599.

Zhang, P., Ma, Z. W. and Wang, R. Z. (2010) 'An overview of phase change material slurries: MPCS and CHS', *Renewable and Sustainable Energy Reviews*. doi: 10.1016/j.rser.2009.08.015.

Zhang, S. *et al.* (2014) 'Interfacial tensions for system of n -heptane + Water with quaternary ammonium surfactants and additives of NaCl or C2-C4 alcohols', *Journal of Chemical and Engineering Data*, 59(3), pp. 860–868. doi: 10.1021/je400963d.

Zhang, S. and Niu, J. (2016) 'Two performance indices of TES apparatus: Comparison of MPCM slurry vs. stratified water storage tank', *Energy and Buildings*. doi: 10.1016/j.enbuild.2016.05.085.

Zhang, X. X. *et al.* (2004) 'Fabrication and properties of microcapsules and nanocapsules containing n-octadecane', *Materials Chemistry and Physics*. doi: 10.1016/j.matchemphys.2004.06.043.

Zhang, Xing Xiang *et al.* (2004) 'Structure and thermal stability of microencapsulated phase-change materials', *Colloid and Polymer Science*. doi: 10.1007/s00396-003-0925-y.

Zhang, X. X. *et al.* (2005a) 'Crystallization and prevention of supercooling of microencapsulated n-alkanes', *Journal of Colloid and Interface Science*. doi: 10.1016/j.jcis.2004.08.046.

Zhang, X. X. *et al.* (2005b) 'Crystallization and prevention of supercooling of microencapsulated n-alkanes', *Journal of Colloid and Interface Science*, 281(2), pp. 299–306. doi: 10.1016/j.jcis.2004.08.046.

Zhang, Y., Zhang, Z., *et al.* (2019) 'Converting Capsules to Sensors for Nondestructive Analysis: From Cargo-Responsive Self-Sensing to Functional Characterization', *ACS Applied Materials and Interfaces*. doi: 10.1021/acsami.8b17679.

Zhang, Y., Baiocco, D., *et al.* (2019) 'Hydrocolloids: Nova materials assisting encapsulation of volatile phase change materials for cryogenic energy transport and storage', *Chemical Engineering Journal*. doi: 10.1016/j.cej.2019.123028.

Zhang Yan, Jiang Zhu, Zhang Zhibing, Ding Yulong, Yu Qinghua, L. Y. (2018) *Polysaccharide Assisted Microencapsulation for Volatile Phase Change Materials with a Fluorescent Retention Indicator*.

Zhang, Z., Saunders, R. and Thomas, C. R. (1999) 'Mechanical strength of single microcapsules determined by a novel micromanipulation technique', *Journal of Microencapsulation*. doi: 10.1080/026520499289365.

Zhao, A. *et al.* (2018) 'Microencapsulated phase change materials with composite titania-polyurea (TiO2-PUA) shell', *Applied Energy*. doi: 10.1016/j.apenergy.2018.02.057.

Zhou, W. *et al.* (2007) 'Fundamentals of scanning electron microscopy (SEM)', in *Scanning Microscopy for Nanotechnology: Techniques and Applications*. doi: 10.1007/978-0-387-39620-0_1.

Zhu, K. *et al.* (2012) 'Preparation and characterization of melamine-formaldehyde resin micro- and nanocapsules filled with n -dodecane', *Journal of Macromolecular Science, Part B: Physics*. doi: 10.1080/00222348.2012.661663.

Zou, D. *et al.* (2017) 'Experimental research of an air-source heat pump water heater using water-PCM for heat storage', *Applied Energy*. doi: 10.1016/j.apenergy.2017.08.209.

APPENDIX 1 – LIST OF MATERIALS

Material	Specification	Supplier
Heptane (24644, anhydrous)	99 %	Sigma-Aldrich (UK)
Urea (U5128, ACS reagent)	99.0 – 100.5 %	Sigma-Aldrich (UK)
Formaldehyde solution (47608, for molecular biology, BioReagent)	≥ 36.0 % in H2O	Sigma-Aldrich (UK)
Nile red (72485, for microscopy)	-	Sigma-Aldrich (UK)
Resorcinol (398047)	≥ 99.0 %	Sigma-Aldrich (UK)
Gelatin (04055, from porcine skin)	-	Sigma-Aldrich (UK)
Chitosan		Sigma-Aldrich (UK)
Xanthan gum (G1253, from Xanthomonas Campestris	-	Sigma-Aldrich (UK)
Gellan Gum (J63423, powder)	-	Alfa Aesar
Alginic Acid from Sodium Salt (180947)	-	Sigma-Aldrich (UK)
Methyl Cellulose (M0262)	Viscosity 400 cP	Sigma-Aldrich (UK)
Poly(ethylene-alt-maleic anhydride) (188050)	Average Mw 100,000~500,000	Sigma-Aldrich (UK)
Poly(ethylene glycol) (181986)	Average Mw 100,000 powder	Sigma-Aldrich (UK)
Polyacrylamide (749222)	Average Mn 150,000	Sigma-Aldrich (UK)
Polyethylenimine, branched (408727)	Average Mw ~25,000 by LS, average Mn ~10,000 by GPC)	Sigma-Aldrich (UK)
Poly(methyl vinyl ether) solution (182729)	50 wt. % in H2O	Sigma-Aldrich (UK)
Catechol (A10164.30)	99 %	Alfa Aesar
Hydroquinone (A11411.30)	99 %	Alfa Aesar
4-Aminoresorcinol hydrochloride (163171)	96 %	Sigma-Aldrich (UK)

Cis,cis-muconic acid (15992)	≥ 97.0% (HPLC)	Sigma-Aldrich (UK)
Glycerol (G9012)	≥ 99.5%	Sigma-Aldrich (UK)
Triethanolamine, reagent grade (T58300)	98 %	Sigma-Aldrich (UK)
Ammonium carbonate, extra pure (390290025)	MW = 96.09	ACROS Organics
Ammonium nitrate, ACS reagent (221244)	≥ 98 %	Sigma-Aldrich (UK)
Di(propylene glycol) butyl ether, mixture of isomers	99 %	Sigma-Aldrich (UK)
Copper (II) chloride dihydrate (307483)	≥ 99 %	Sigma-Aldrich (UK)
Dodecane, anhydrous (297879)	≥ 99 %	Sigma-Aldrich (UK)
Hexadecane (820633)	99 %	Sigma-Aldrich (UK)
Octadecanol (258768)	99 %	Sigma-Aldrich (UK)
Sodium borohydride (213462)	99 %	Sigma-Aldrich (UK)